Istituto Universitario di Studi Superiori di Pavia

PhD program in Biomolecular Science and Biotechnology

Biochemical aspects of Neurodegeneration:

an overview of Metal-Protein Interaction.

Chiara Bacchella

Tutor: Prof. Enrico Monzani

XXXIII CICLO – A.A. 2019-2020

Table of Contents

Introduction to Neurodegeneration

Neurodegenerative diseases are pathological conditions in which neuronal activities in specific subcortical and cerebral cortex areas are irreversibly compromised, leading to uncontrollable movements and to impairment of memory and cognitive capabilities.[1a] Although these conditions are usually associated to protein abnormalities, these disorders highlight some common mechanisms correlated to altered neuronal functions and extensive damage, such as alterations in autophagy pathway, neuronal death, oxidative stress and neuroinflammation.[1b]

The classification of neurodegenerative diseases, now estimated a few hundred, is primarily linked to the clinical and topographic manifestations of lesions (Figure 1) and the main three families collecting all neurodegenerative conditions are:

(i) Amyloidoses (Creutzfeldt-Jakob, Gerstmann-Straussler-Scheinker, Alzheimer's diseases and Familial British dementia)

(ii) Tauopathies (Chronic traumatic encephalopathy, Primary age-related tauopathy, Pick's disease, Progressive supranuclear palsy, Corticobasal degeneration, Argyrophilic grain disease, Aging-related tau astrogliopathy)

(iii) Synucleinopathies (Lewy body disorders and Multiple system atrophy)

(iv) TDP-43 Proteinopathies (Frontotemporal lobar degeneration, Amyotrophic sclerosis, Primary lateral sclerosis and Progressive muscular atrophy).

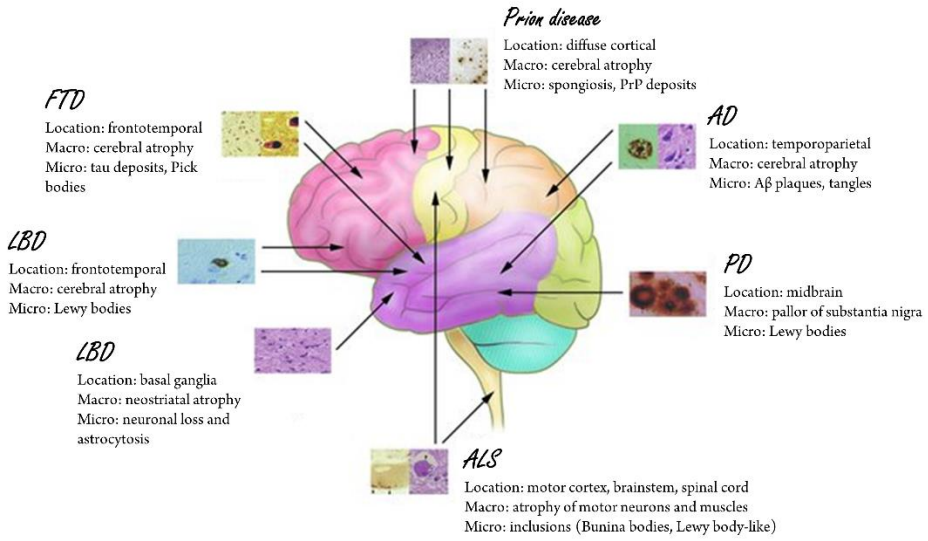

Figure 1. *Schematic progression of proteinaceous lesions in different neurodegenerative disorders over time obtained from post-mortem studies of brains. The cartoon shows the putative areas of damage onset.*[1c]

Amyloidoses are linked to the presence of insoluble aggregates of fibrous proteins generated upon the uncontrolled misfolding of protein scaffolds to give β-sheet rich secondary structures highly prone to give intermolecular stacking. The most common amyloidogenic deposits are generated from the amyloid precursor protein (APP) upon selective proteolytic cleavage. In particular, Aβ deposits in senile plaques together with the evidence of neuronal tau inclusions are the most relevant hallmarks of Alzheimer's disease, classified as the prevalent neuronal disease, accounting for 60%-80% of the total dementia cases worldwide.[1a] Other less common amyloidoses are correlated to the aggregation of prion proteins (PrP) in familial and sporadic Creutzfeldt–Jakob disease (CJD), characterized by an annual mortality rate of one on million people and spread in humans ae well as animals, such as sheep and bovines[2], and in Gerstmann-Straussler-Scheinker disease, a rare disorder due to the mutations in the *PRNP* gene and denoted by an autosomal

dominant inheritance.[3] Less known type of amyloidoses involves a high insoluble peptide ABri that generates perivascular plaques and tangles leading to cerebellar ataxia and pathological dementia called Familial British dementia.[4] Disorders associated with detection of tau protein deposits in neuronal tissues are known as Tauopathies and include several disorders, such as Alzheimer's, in which tau protein is subjected to massive posttranslational modifications, as phosphorylation, ubiquitination, nitration, acetylation etc., promoting the structural rearrangement of the protein and its partial inefficiency as microtubule stabilizer.[5a] A peculiar form of tauopathy is referred to the chronic traumatic encephalopathy (CTE), a disorder in which the deterioration of the behavioral and clinical functionalities is strongly influenced by the environmental factors and in particular by head damages and injuries connected to the practice of contact sports, as football.[5b] As shown in Figure 2, other rare tauopathies include: (i) Progressive supranuclear palsy, characterized by an irreversible neuronal deterioration, loss of balance and difficult control of voluntary muscles; (ii) Pick's disease also known as a frontotemporal lobar degeneration; (iii) Corticobasal degeneration that affects frontoparietal and basal ganglial regions through aphasia and ataxia condition, and (iv) Argyrophilic Grain Disease, a mild cognitive deficit tightly associated to the aging and showing a characteristic spindle-shaped morphology of lesions.[6]

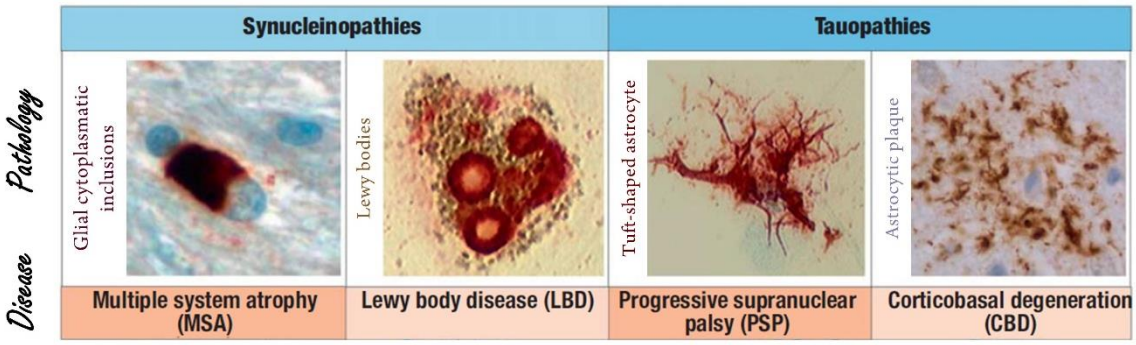

Figure 2. *Synucleinopathies or tauopathies are characterized by intracellular aggregates of alpha-synuclein or tau proteins that display several morphologies of the lesions; in particular, multiple system atrophy (MSA) is neuropathologically identified by the presence of glial cytoplasmatic inclusions, while Lewy's bodies are characteristic of some specific type of dementia. Tuft-shaped astrocytes and astrocytic plaques are detected in tauopathies, such as progressive supranuclear palsy (PSP) or corticobasal degeneration (CBD).*[7a]

Synucleinopathies correspond with the third heterogeneous class of neurodisorders and involve the deposition of a protein usually implicated in the vesicle trafficking, known as α-synuclein, in neuronal inclusions called Lewy bodies. Dementia and Parkinson's are the mainly-known pathological conditions linked to the presence of Lewy bodies, while Multiple system atrophy is a rare neurodegenerative disorder affecting the body's involuntary functions, as breathing or motor control, and is probably related to an overexpression of α-synuclein protein.[7b] The last heterogeneous class of neurodisorders corresponds to the proteinopathies induced by the generation of nuclear and cytoplasmatic inclusion bodies primarily composed by TDP-43, a 43-kDa protein normally involved in RNA transcription and maturation and recently detected in ALS and AD affected neuronal tissues.[8a] The two main diseases associated with TDP-43 pathology are Amyotrophic Lateral Sclerosis (ALS), characterized by motor cortex and spinal cord atrophy besides a wide neuronal loss, and frontotemporal dementia (FTLD-TDP), identified by frontal and temporal atrophy and evident *substantia nigra* depigmentation.[8b] The previous categorization provides an overview of the complexity of the neurodegeneration nature and justifies the great interest of the researchers on the clarification of the biochemical mechanisms implicated in the progression of these disorders. For instance, while Huntington disease is primarily a genetic condition, Parkinson's disorder is mainly sporadic and the amorphous deposition of alpha-synuclein and parkin

proteins plays a crucial role in the disease onset. The abnormal aggregation of proteins is now identified as common feature in all these disorders: while Alzheimer's sees the misfolding of amyloid-β protein (Aβ), acting as initializer of the disease, in ALS tissues an alteration of normal activity of superoxide dismutase-1 (SOD1) enzyme exacerbates this condition. The link between the onset of amyotrophic lateral sclerosis and the discovery of mutations in gene encoding SOD1 enzyme was proposed about 30 years ago, in which the dysregulation of its activity was detected an important enhancer of oxidative stress condition in neurons.[8c] If the superoxide dismutase activity is altered in several sub-cellular environments, its re-localization in nucleus was suggested to have a protective role against DNA damages, while it is still incomplete the comprehension of the mechanisms leading to aggregation and misfolding of this enzyme.[8d]
Mitochondrial dysfunction[9a] is another common hallmark of all these diseases: these organelles are normally involved in different functions, as ATP generation, homeostatic control of intracellular calcium ions, production of ROS and apoptotic signaling, and all these functions are essential in neuronal cells, where the energetic demand is particularly high. It was proposed a direct correlation between the misfolding of neuronal proteins, besides the mutation of specific regions in mtDNA, and the dysfunction of mitochondrial activity, where deficiency in the electron transport chain enhances the local concentrations of reactive oxygen species until neuronal necrosis. The inefficiency of the electron transport also decreases the production of ATP, which causes impairment of Ca^{2+} levels and further release of apoptotic signals, till neuronal death.[9b] The altered production of oxidative and nitrative species has been also suggested as a potential target for therapeutic interventions focused on the mitigation of these oxidative processes. These reactive species comprise hydrogen peroxide, superoxide anions, hydroxyl and monoxide radicals and nitric oxide, which are normally produced by the aerobic cellular metabolism via enzymatic and non-enzymatic reactions. At low concentrations, these species are biologically involved in cellular signaling system, influencing the rate of ATP synthesis and modulating the levels of transduction growth signals, besides their role in cellular structuring and in body's defense via their release by phagocytes as unspecific attach against pathogenic organisms.[9c] On the other hand, reactive oxygen and nitrogen intermediates can strongly modify several biological structures, such as oxidizing lipids, proteins and DNA and generating byproducts as peroxides, aldehydes, alcohols, ketones and cholesterol oxide.[10a,10b, 10c] This uncontrolled reactivity was widely assayed usually associated with the dysmetabolism of metal ions, as copper or iron, that culminates in Fenton or Haber-Weiss chemistry.[11a,11b] High contents of transition metal ions were found in amyloid plaques, in which the main component, the amyloid-β peptide, shows high affinity binding sites for copper(II) or iron(II) and the reactivity of the resulting complexes results in not negligible production of ROS. Like Alzheimer's, also Parkinson's is associated with the presence of intracellular and insoluble deposits, known as Lewy bodies, rich in α-synuclein protein and primarily detected in *substantia nigra*. On the other hand, if the interaction between αSyn and Cu or Fe ions modestly occurs, in *substantia nigra* the main metal chelator is the neurotransmitter dopamine, working as electron donor in the redox cycling of bound metals and leading to the generation of further insoluble bodies, called neuromelanins, in which oxidative products of catecholamines besides high amount of metals are accumulated.[11c]
In the following sections, a wide characterization of the more relevant neuronal proteins or fragments is performed in order to understand (i) their affinity toward active metals, (ii) their redox behavior upon the generation of the metallic adducts, (iii) their susceptibility toward oxidative modifications in several environmental conditions and (iv) their possible participation as promoters or scavengers in the generation of dangerous reactive species.

References

1. *(**a**) J.A. Lima and L. Hamerski, Chapter 8 - Alkaloids as Potential Multi-Target Drugs to Treat Alzheimer's Disease,* ***Studies in Natural Products Chemistry,*** 61, 301-334, 2019; *(**b**) B.N. Dugger and D.W. Dickson, Pathology of Neurodegenerative Diseases,* ***Cold Spring Harb Perspect Biol.,*** 9, 7, a028035, 2017; *(**c**) C. Foguem and B. Kamsu-Foguem Neurodegeneration in tauopathies and synucleinopathies,* ***Revue Neurologique,*** 172, 11, 709-714, 20166.
2. *L.G. Goldfarb, P. Brown, W.R. McCombie, D. Goldgaber, G.D. Swergold, P.R. Wills, L. Cervenakova, H. Baron, C.J. Gibb Jr. and D.C. Gajdusek, Transmissible familial Creutzfeldt-Jakob disease associated with five, seven, and eight extra octapeptide coding repeats in the PRNP gene,* ***Proc Natl Acad Sci U S A,*** 88, 23, 10926-10930, 1991
3. *K.K. Hsiao, C. Cass, G.D. Schellenberg, T. Bird, E. Devine-Gage, H. Wisniewski and S.B. Prusiner, A prion protein variant in a family with the telencephalic form of Gerstmann-Sträussler-Scheinker syndrome,* ***Neurology,*** 41, 5, 681-684, 1991.
4. *R. Vidal, T. Revesz, A. Rostagno, E. Kim, J.L. Holton, T. Bek, M. Bojsen-Moller, H. Braendgaard, G. Plant, J. Ghiso and and B. Frangione, A decamer duplication in the 3′ region of the BRI gene originates an amyloid peptide that is associated with dementia in a Danish kindred.* ***Proc Natl Acad Sci,*** 97, 4920 – 4925, 2000.
5. ***a**) L. Martin, X. Latypova and F. Terro, Post-translational Modifications of Tau Protein: Implications for Alzheimer's Disease,* ***Neurochemistry International,*** 58, 4, 458-71, 2011*; (**b**) A.C. McKee, R.C. Cantu, C.J. Nowinski, E.T. Hedley-Whyte, B.E. Gavett, A.E. Budson, V.E. Santini, H.S. Lee, C.A. Kubilus and R.A. Stern, Chronic traumatic encephalopathy in athletes: progressive tauopathy after repetitive head injury,* ***J Neuropathol Exp Neurol.,*** 68, 7, 709-35, 2009.
6. *R.D. Rodriguez and L.T. Grinberg, Argyrophilic grain disease: An underestimated tauopathy.* ***Dement Neuropsychol.,*** 9, 1, 2-8, *2015.*
7. *a) J. Levin, A. Kurz, T. Arzberger, A. Giese, and G.U. Höglinger, The Differential Diagnosis and Treatment of Atypical Parkinsonism,* ***Dtsch Arztebl Int****, 113, 61-9, 2016; (**b**) P.L. Lantos, The definition of multiple system atrophy: a review of recent developments,* ***J Neuropathol Exp Neurol.,*** 57, 12, 1099-111, 1998.
8. ***a**) M. Neumann, D.M. Sampathu, L.K. Kwong, A.C. Truax, M.C. Micsenyi, T.T. Chou, J. Bruce, T. Schuck, M. Grossman, C.M. Clark, L.F. McCluskey, B.L. Miller, E. Masliah, I.R. Mackenzie, H. Feldman, W. Feiden, H.A. Kretzschmar, J.Q. Trojanowski and V.M. Lee, Ubiquitinated TDP-43 in frontotemporal lobar degeneration and amyotrophic lateral sclerosis,* ***Science,*** 314, 5796, 130-3, 2006; *(**b**) N. Aoki, K. Tsuchiya, Z. Kobayashi, T. Arai, T. Togo, H. Miyazaki, H. Kondo, H. Ishizu, H. Uchikado, O. Katsuse, Y. Hirayasu and H. Akiyama, Progressive nonfluent aphasia: a rare clinical subtype of FTLD-TDP in Japan,* ***Neuropathology,*** 32, 3, 272-9, 2011; *(**c**) D.R. Rosen, T. Siddique, D. Patterson, D.A. Figlewicz, P. Sapp, A. Hentati, D. Donaldson, J. Goto, J.P. O'Regan, H.X. Deng, Z. Rahmani, A. Krizus, D. McKenna-Yasek, A. Cayabyab, S.M. Gaston, R. Berger, R.E. Tanzi, J.J. Halperin, B. Herzfeldt, R.Van den Bergh, W.-Y. Hung, T. Bird, G. Deng, D.W. Mulder, C. Smyth, N.G. Laing, E. Soriano, M.A. Pericak–Vance, J. Haines, G.A. Rouleau, J.S. Gusella, H.R. Horvitz and R.H. Brown Jr , Mutations in Cu/Zn superoxide dismutase gene are associated with familial amyotrophic lateral sclerosis,* ***Nature,*** 4,362, 6415, 59-62, 1993; *(**d**) O. Pansarasa, M. Bordoni, L. Diamanti, D. Sproviero, S. Gagliardi and C. Cereda, SOD1 in Amyotrophic Lateral Sclerosis: "Ambivalent" Behavior Connected to the Disease,* ***Int J Mol Sci.,*** 19, 5, 1345, 2018.
9. ***a**) A. Johri and M. F. Beal, Mitochondrial Dysfunction in Neurodegenerative Diseases,* ***J Pharmacol Exp Ther.,*** 342, 3, 619–630, 2012; *(**b**) E. Lezi and R.H. Swerdlow, Mitochondria in Neurodegeneration,* ***Adv Exp Med Biol.,*** 942, 269–286, 2012; *(**c**) B. Halliwell, Biochemistry of oxidative stress,* ***Biochem Soc Trans,*** 35, 5, 1147-1150, 2007.
10. *(**a**) A.H. Bhat, K.B. Dar, S. Anees, M.A. Zargar, A. Masood, M.A. Sofi, Showkat and A. Ganie, Oxidative stress, mitochondrial dysfunction and neurodegenerative diseases; a mechanistic insight,* ***Biomed. Pharmacother,*** 74, 101–110., 2015*; (**b**) D.M.A. Olivera and R.H. Reddy, Molecular basis of Alzheimer's disease: Focus on mitochondria,* ***J. Alzheimers Dis.,*** 72, S95–S116, 2019*; (**c**) X. Chen, C. Guo and J. Kong, Oxidative stress in neurodegenerative diseases,* ***Neural Regen Res.,*** 7, 5, 376–385, 2012.
11. *(**a**) T.K. Das, M.R. Wati and K. Fatima-Shad, Oxidative Stress Gated by Fenton and Haber Weiss Reactions and Its Association With Alzheimer's Disease,* ***Arch Neurosci****.* 2, 3, e20078, 2014; *(**b**) H. Ischiropoulos and J.S. Beckman, Oxidative stress and nitration in neurodegeneration: cause, effect, or association?,* ***J Clin Invest.*** 111, 2, 163-169, 2003; *(**c**) B. Uttara, A.V. Singh, P. Zamboni and R.T. Mahajan, Oxidative Stress and Neurodegenerative Diseases: A Review of Upstream and Downstream Antioxidant Therapeutic Options,* ***Curr Neuropharmacol.,*** 7, 1, 65–74, 2009.

Chapter 1

EFFECT OF MEMBRANE-LIKE ENVIRONMENT: REDOX CHEMISTRY OF COPPER BOUND TO NEURONAL PEPTIDES INVOLVED IN NEURODEGENERATIVE DISORDERS.

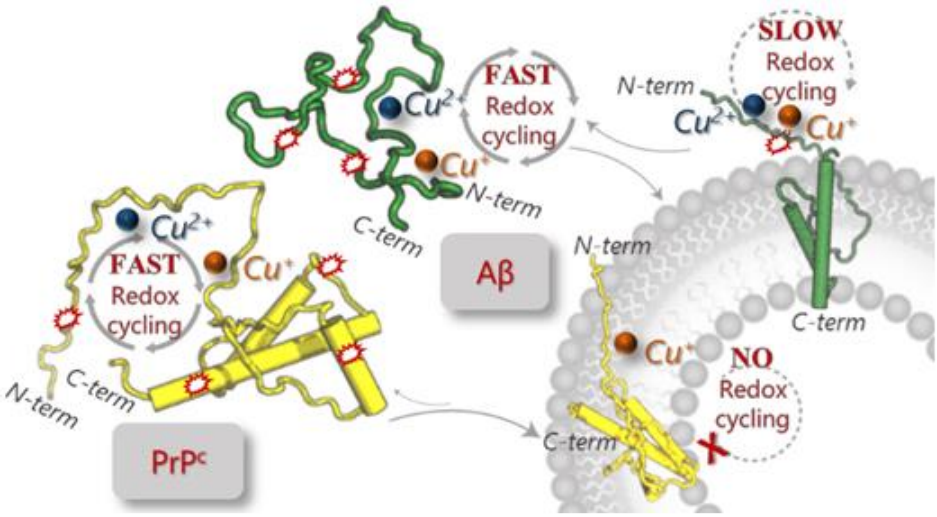

Ref. *Inorg. Chem., 59, 1, 900-912, 2020*

"Membrane Binding Strongly Affecting the Dopamine Reactivity Induced by Copper Prion and Copper/Amyloid-β (Aβ) Peptides. A Ternary Copper/Aβ/Prion Peptide Complex Stabilized and Solubilized in Sodium Dodecyl Sulfate Micelles"

C. Bacchella, S. Nicolis, S. Dell'Acqua, E. Rizzarelli, E. Monzani, L. Casella.

The tight interplay between neuronal proteins, metal ions and phospholipids

The dysregulation of tight homeostatic control of neurometals, such as copper, can play an important role in the development of several pathological conditions, including Alzheimer's, Parkinson's and prion diseases. The relevance of this interaction is linked to the capability of several proteins involved in neurodisorders to bind with high-affinity redox-active metal ions and undergo conformational changes of their scaffolds. In fact, the misfolding of well-known proteins, such as α-synuclein (αSyn), prion (PrP), amyloid-β (Aβ) etc., is a triggering factor in the protein aggregation and in the generation of insoluble deposits in various cerebral areas. Besides the key interaction with metal ions, several findings suggest that the primary target of amyloid and prion peptides is the neuronal cellular membrane: the neuronal bilayer could influence the oligomerization mechanism of proteins and the generation of dangerous fibrillary species. Prion protein is shown to act as unspecific receptor for αSyn, β-amyloid and tau proteins and this interaction is probably mediated by a confined region that partially includes the high-affinity copper binding site, although the role of the metal has not been clarified.[1a,1b,1c] The unspecific interaction between amyloid-β proteins and neuronal membranes can induce massive conformational changes into the protein structures, altering their degradative pathways and promoting the growth of pathological deposits. Moreover, another relevant implication of the interaction between lipid membranes and proteins is the possible change of the membrane lipids packing order.[1d] In addition, this pathological frame is exacerbated by the critical enhancement of reactive oxygen species and catecholamine oxidative products able to attach and strongly modify the protein backbone, playing as a modulator in the oligomerization. In particular, abnormal signaling and accumulation of catecholamine neurotransmitters increase the potential reactivity of these neurotransmitters induced by oxidative species and reactive metals in oxidative stress conditions, causing a huge production of free dangerous molecules.[1e] All these pathological mechanisms should be studied both in aqueous *medium* but also in the presence of membrane-mimicking models. For this reason, this section reports a comparative study on the oxidative reactivity toward catechols shown by copper complexes with β-amyloid and prion, selecting the fragments mainly involved into the metal binding, in aqueous and micellar *medium*. The aim of the work is to assess the influence of the membrane on the catalytic efficiency of complexes and on the modification pattern of protein backbone, focusing the attention on the potential covalent binding by oxidative species. A previous study shows that the membrane interaction induces a strong quenching of the redox reactivity of αSyn complexed with copper;[1f] similarly, the interplay between neuronal phospholipids and copper-Aβ and PrP peptides complexes probably affects the oxidative reactivity. Therefore, new investigations about the interplay between neuronal phospholipids and biological proteins are required.

Amyloid-β (Aβ) protein – an overview

Alzheimer's disease is a progressive neurodegenerative disease affecting more than 25 million people worldwide, characterized by depression, loss of intellectual faculties and brain degeneration. More than 100 years after its discovery, the primary origin of AD still remains unclear. The main reason lies in the hard path of diagnosis: subjects with severe cognitive decline may be unambiguously declared as AD patients only after post-mortem examination of their brains that normally display signs of apoptosis. Indeed, the presence of extracellular amyloid plaques and

intracellular neurofibrillary tangles (NFT) are the major pathological hallmarks. These neurofibrillary tangles are deposits of β-structured tau protein showing high percentage of phosphorylation and oxidative modifications. Amyloid plaques, or "senile plaques", are insoluble aggregates of amyloid-β (Aβ), a peptide with about 39-43 amino acids.[2a] Amyloid-β fragments, such as Aβ 1-40 and 1-42, are obtained though the proteolytic cleavage of *Amyloid precursor protein (APP)*, a large transmembrane glycoprotein (Figure 1). These peptides are the main components of extracellular amyloid plaques, but are also found as harmful soluble oligomers inside the cells and trans-membrane. Recent studies have suggested a strong correlation between the neuronal degeneration and synaptic dysfunction and the presence of small soluble β-sheet oligomers of Aβ, with respect to the less toxic amyloid fibrils. Anyway, the mechanism by which these potential synaptotoxins exert the neuronal damage is still controversial.[2b]

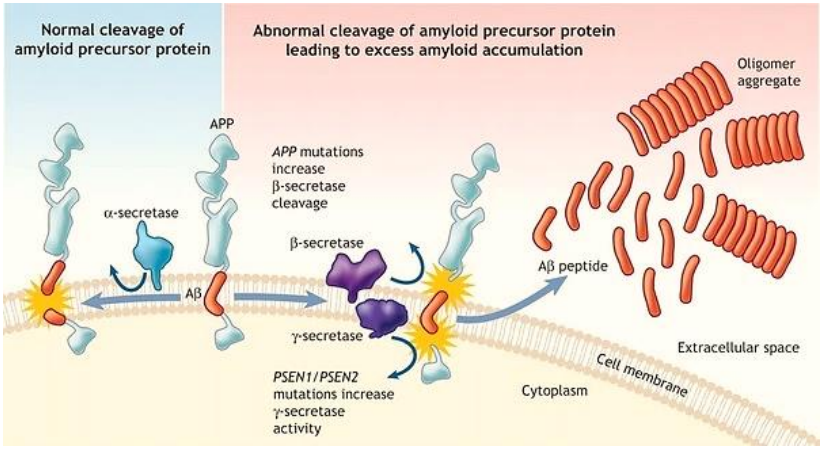

Figure 1. *APP processing can lead to not-amyloidgenic or amyloidgenic pathways: the combination of α- and γ-secretase cleavages produces harmless fragments, while β-secretase together with the activity of γ-secretase generate Aβ peptides that potentially form fibrillary aggregates.*

Together with the aggregation of tau and amyloid-β proteins, the dyshomeostasis of redox-active metals and the production of reactive oxygen species contribute to the development of Alzheimer's disorder. In particular, the detection of high copper concentration (400 μM), compared to the normal brain extracellular concentration of 0.2–1.7 μM, suggests that its complexation with amyloid-β can contribute to oxidative stress and neuronal damage.[3] A plethora of studies investigates the interaction of amyloid-β and transition metals in aqueous *medium*. Given the highly flexible nature of the peptide, copper(II) is known to interact with Aβ via various binding environments and the coordination sphere for these Aβ-Cu complexes is still now very controversial. At physiological pH, Aβ fragments are unstructured and the *N*-terminal region acts as the main binding site for copper(II) ions, via three histidines (H_6, H_{13} and H_{14}) together with a fourth residue that may be Ala_2, Glu_{11}, or *N*-terminal Asp_1. Two coordination spheres for copper(II) in equilibrium with each other are proposed:

(i) Component I is the major form at neutral pH, adopting a distorted-square planar geometry coordinated by Asp1 via the terminal amine, the adjacent CO from the Asp1-Ala2 peptide bond, a N-atom from imidazole ring of His6 and another one from His13 or His14 (Figure 2). To stabilize copper-peptide binding and to perform the catalytic cycle, copper has to be chelated by electron donor groups, such as NH_2 group of *N*-terminus, while electron-attractors as carboxyl groups only partially stabilize the metal coordination.

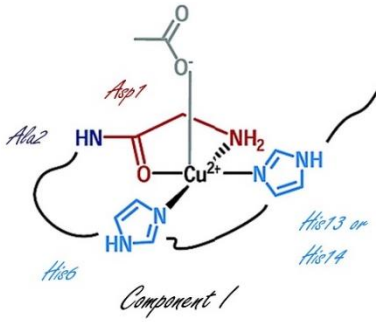

Figure 2. *Cu^{II} coordination sphere to amyloid-β peptide (Component I).*

(ii) Component II is the minor form consisting of the same coordination geometry mediated by *N*-terminal amine, the amidyl function from the Asp1-Ala2 peptide bond, the adjacent CO from the Ala2-Glu3 peptide bond, and one N-atom from the imidazole ring of one of the three His.

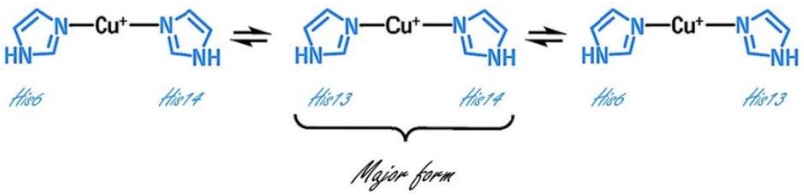

Figure 3. *Cu^{I} coordination sphere to amyloid-β peptide.*

Copper(I) binding site located in the *N*-terminus predominantly involves a linear coordination geometry through H_{13} and H_{14}, as shown in Figure 3.[4a] However, the interaction between amyloid peptides and copper ions is known to be highly dynamic to allow and promote an efficient catalytic cycling between Cu^{I} /Cu^{II} states. To explain copper-amyloid redox activity, a fast exchange between the two coordination environments would be required, while large structural rearrangement and too higher energetic barrier are evidenced between the two most populated states previously described. Therefore, recent studies are focused on the detection of a catalytic "in-between state";[4b] more detailed study is shown in the Chapter 4. On the other hand, the players contributing to the protein aggregation and neuronal damage are not confined between metal ions and radical species, but the interaction between membranes and amyloidogenic proteins may play an important role. Amyloid-β, such as other proteins as prion (PrP), α-synuclein (αSyn) etc., can strongly interact with neuronal membrane and the influence of lipids on the reactivity and on the metal binding affinity remains unclear. However, the presence of membranes can affect the affinity and availability of copper binding sites in protein sequences by influencing the structural rearrangement of proteins and the oxidative activity of metal-peptide complexes.[5a] For instance, *N*-terminal αSyn fragment (αSyn1-15) is able to bind both Cu^{2+} and Cu^{+} in micelle, quenching the oxidation reaction of an external substrate.[5b] This trend will also be confirmed by the experimental data obtained on full-length protein (showed below). It is generally accepted that the interaction between α-synuclein and neuronal phospholipids may induce fibrillation, involving the lipid interaction site in the *N*-terminal region of the protein.[5c] This environment can induce a structural rearrangement from a random-coil conformation to α-helix (Figure 4), allowing a stronger binding with copper and inhibiting the substrate oxidation.

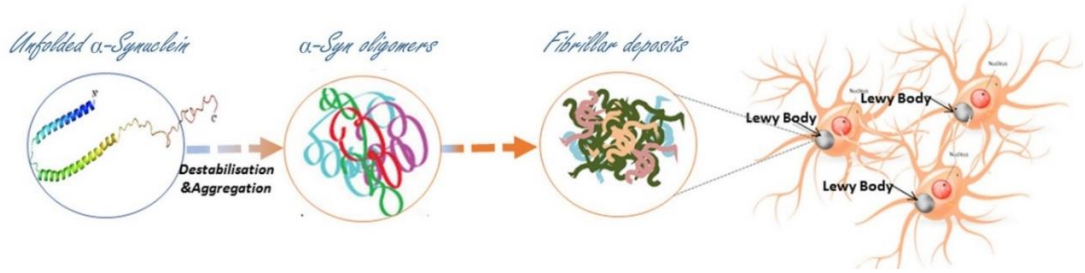

Figure 4. *Schematic illustration showing the origin of Lewy bodies and the mechanism of aggregation and toxicity.*

In regard to other amyloidogenic proteins, Aβ peptides are found both inside and outside cellular environments and also in membrane. Many studies have shown that $Aβ_{40}$ and $Aβ_{42}$ peptides interact with lipid layers, which can influence the oligomerization and the amyloid plaques generation *in vivo*.[6]

Indeed, the amyloid-β peptides contain a relatively hydrophilic *N*-terminal portion, while the *C*-terminal region contains mainly hydrophobic amino acid residues (Figure 5). The amphiphilic nature allows the interaction with several molecules, such as inorganic metal ions and organic ones such as polypeptides and lipids, which are potentially able to modulate the peptide aggregation tendency.[7]

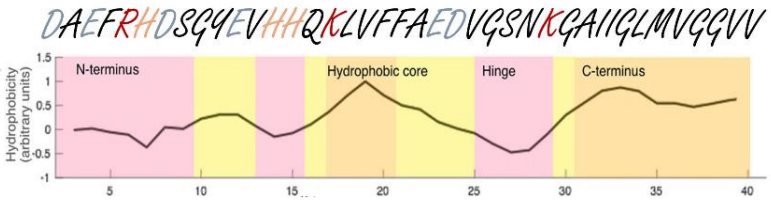

Figure 5. *Sequence of $A\beta_{40}$ with charged amino acid residues highlighted. The graphic below shows its theoretical hydrophobicity.*

In the biological context, the interaction between phospholipids and Aβ peptide can alter the permeability properties of neuronal membranes, playing a key role in brain degeneration. Aβ peptides act as Ca^{2+}-conducting nanopores, changing the cell membrane integrity and contributing to the neuronal toxicity. It was also supposed that biomembranes can work as nucleation sites for amyloid aggregation due to the electrostatic interaction between their surface and the side chains of amino acids, locally increasing the ionic strength.

In order to investigate the interaction between Aβ peptides and amphiphilic biomolecules, sodium dodecyl sulfate (SDS) (Figure 6) was utilized, in the present chapter, as simple membrane-like model. The chemical structure of a common surfactant shows a polar headgroup with specific chemical properties and a nonpolar hydrocarbon tail: SDS can easily self-assemble in aqueous environment to form micelles at above its critical micelle concentration (CMC of about 9 mM).

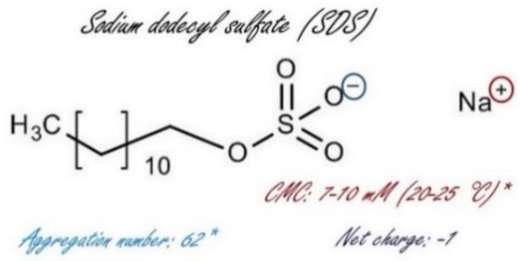

Figure 6. *Structure and properties of sodium dodecyl sulfate.*

The effect of anionic sodium dodecyl sulfate (SDS) surfactant toward the amyloid-β 1-40 and 1-42 structures is well-studied: CD spectra show a mainly disordered conformation in aqueous solution, while an α-helical one is adopted when SDS is added at the concentration above which micellar structures are spontaneously formed. In this membrane-mimicking system, the peptide adopts a "helix-loop-helix" structure with two helical segments (15-25 and 29-35) separated by an unstructured loop. In the presence of micelles, the first portion (1-28) of Aβ 1-40 and 1-42 is located outside lipid layers or on the surface, while the *C*-terminus occupies the transmembrane region. Since the localization of copper anchoring site is outside the transmembrane region, the metal binding would not have to be influenced by the presence of micelles. Moreover, some studies suggest the presence of copper(II) can alter the morphology of fibrils in the presence of synthetic liposomes and slow down the fibril formation and Aβ aggregation.[5a]

Prion (PrP) protein- an overview

Cellular prion protein is a cell-surface glycoprotein (254 amino acids, PM 33-35 kDa) consisting of a globular structured *C*-terminal domain that is linked to a flexible *N*-terminal region. It is ubiquitously expressed but is mainly found in neuronal tissue, predominantly on the cellular surface.[8a] It can undergo conformation change from normal cellular protein (PrP^{C}) to abnormal misfolded isoform (PrP^{Sc}) and this process has been recognized as the critical pathogenic event in transmissible spongiform encephalopathies, also known as Prion disorders. These disorders include Creutzfeldt-Jakob disease and *kuru* in humans, bovine spongiform encephalopathy, chronic wasting disease in deer and elk, and scrapie in goats and sheep.[8b]

The structural conversion gives rise to insoluble deposits and aggregates with elevated β-sheet content. As for other neurodegenerative disorders, the aggregates are the key factors contributing to the disease and in this case, abnormal

prion deposits rich in metals are commonly recognized as causative factor for the development of prion disorders. Although the role of this protein has been largely investigated, its cellular function is still debated. The identification of PrP as copper binding protein and the discovery that Cu^{II} and Zn^{II} stimulate its endocytosis can suggest an involvement in copper homeostasis.[8c] Other works support that PrP may be an antioxidant agent or it would be involved in signal transduction or cell-cell adhesion. [9]

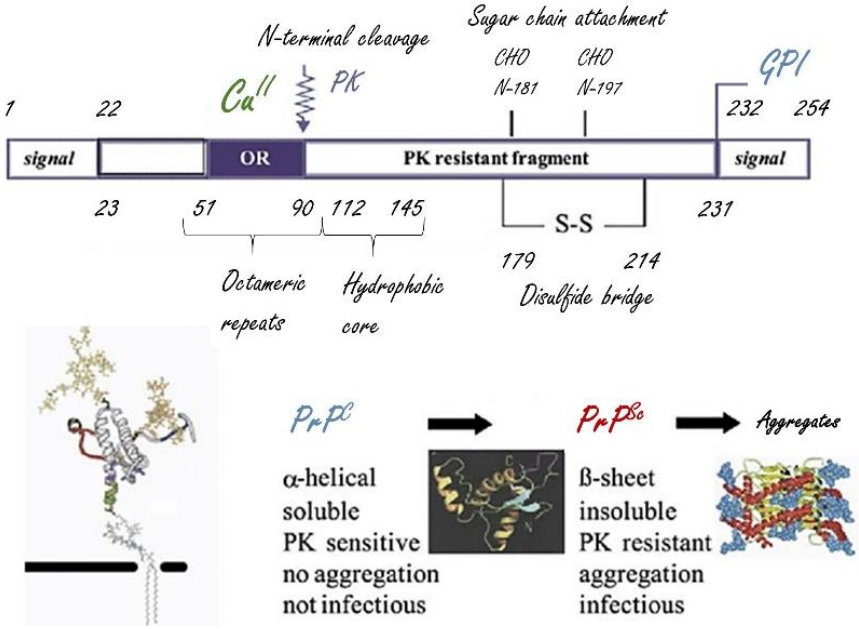

Figure 7. *Schematic illustration of human PrP^C protein. The N-terminal signal peptide is removed during the biosynthesis of the protein. The octarepeat region (OR) is the metal binding portion and the hydrophobic domain is highlighted. PrP consists of an unstructured N-terminal region and a globular C-terminal domain, containing two β-strands and three α-helices. The two glycosylation sites are also shown. A disulfide bond connects two α-helices. The C-terminal signal sequence is cleaved off and replaced with a GPI-anchor to the neuronal membrane.*

Anyway, the high binding affinity of *N*-terminal protein toward copper(II) is commonly accepted. Numerous studies report that the sensibility to proteinase K digestion of misfolded prion isoform is highly modulated by the addition of micromolar concentrations of copper, verifying the tight correlation with the metal.[10] The metal binding region of PrP resides in the unstructured *N*-terminal domain, comprising the large portion 60-90: this region is known as *octarepeat* due to the presence of four repeats of the highly conserved octapeptide PHGGGWGQ sequence followed by GGGTH (Figure 7). Close to this region, a hydrophobic segment, known as amyloidogenic portion, is highly conserved and it may influence the conformational change of PrP^C to PrP^{Sc}.

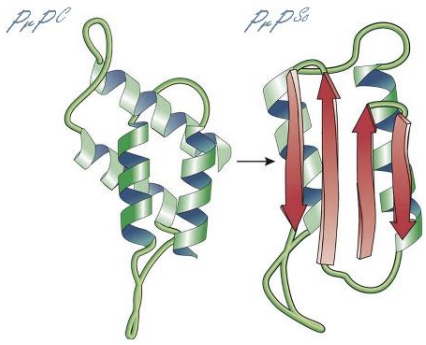

Figure 8. *Cartoon showing the conformation change from cellular PrP^c to misfolded PrP^{Sc}*

The misfolded isoform of PrP was identified via its protease resistance: the key event in the pathogenesis of prion diseases is the structural change of cellular PrP, predominantly composed by α-helix (47%), to a mainly β-conformation (43% β-sheet and 30% α-helix) (Figure 8).[17] Such as in other amyloidogenic disorders, PrP^{Sc} forms aggregates, but the peculiar feature of prion protein is the ability to catalyze self-propagating conversion, acting as a nucleation seed. Prion proteins are able to bind six copper(II) ions, four of them within the *octarepeat* and two, outside this region, via H_{96} and H_{111}. Histidine 111 is defined as the main copper ligand, showing the highest binding affinity for the metal.[11a] While

histidines are the preferred binding groups for copper(II), methionine side chains are generally required to stabilize the copper(I) interaction. Prion contains an interesting -M(X)$_n$M- motif able to bind copper(I) ions with a tetrahedral coordination geometry (2N2S) via H_{96}, M_{109}, H_{111} and M_{112} (Figure 9).[11]

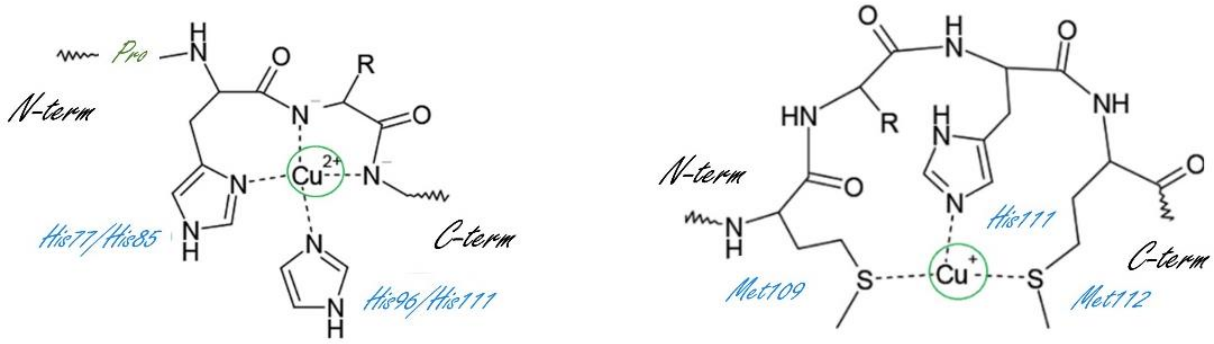

Figure 9. *Main structures of Cu^{II} and Cu^{I} coordination by prion peptides.*

Many studies reveal that metal binding to cellular form of prion protein strongly affects the aggregation process, but the mechanism is still debated: a possible inhibition of fibrillation mediated by the binding of copper ions to the amino acid side chains involved in the transition was also suggested.[5a] Metal binding is highly pH-dependent. Elevate levels of copper ions can induce endocytosis of the prion protein from extracellular space at pH 7.4 to the endosomal environment, that is characterized by an acidic *medium* at pH around 4-5. In the endosomes, the presence of biological reductants, such as NADH, may reduce prion-complexed copper(II) to copper(I). The reduced Cu^{I}-prion complex can then react with dioxygen, regenerating the oxidized complex but releasing some harmful reactive species as superoxide. In acid conditions, copper binding properties of histidine residues are drastically changed and the protonation of imidazole group results in its negligible contribution for the metal chelation, promoting the exclusive involvement of methionine in the copper(I) coordination. Therefore, the prion sequence is optimized to chelate both Cu^{II} and Cu^{I} in a wide range of biochemical environments and the same studies suggest that M(X)$_n$M motifs may also act as antioxidant agents, scavenging the reactive oxygen species via methionine sulfoxidation.[12a] Regarding the site and mechanism of structural conversion, it was reported that the unfolded PrP species are predominantly localized in the intracellular space, in endosomes, lysosomes, perhaps in lipid raft domains within these organelles. The lack of PrP^{Sc} deposits in cellular cultures where endosome formation was inhibited may indicate the endocytic organelles as plausible location for conversion.[12b] Some evidences suggest that a more acidic pH stimulates the conversion of PrP^{C} to an extended β-structure and insoluble conformer. Between pH 5 and 7.2 the CD spectra show an isoform with predominantly α-helical structure, while at a lower pH range, the double minimum at 222 and 208 nm is shifted to 215 nm, corresponding to β-structures. In particular, the *C*-terminal portion is almost totally insensitive to pH while pH-dependent structural changes are linked to the *N*-terminal region. [8a]

Prion is a glycoprotein normally anchored to the neuronal membranes via its *C*-terminal glycosyl phosphoinositol (GPI) tail; therefore, it is reasonable to assume that PrP may interact with phospholipids, but the type of interaction between prions, metal ions and membrane and its effect are still rather unknown. To perform a preliminary study about the influence of lipid layers on the copper-prion adduct, the anionic SDS was chosen as a good membrane-like system, being able to interact with positive charged Lys and Arg amino groups in the peptide sequence via its negative charged head groups. NMR and CD studies have shown that the prion hydrophobic or amyloidogenic domain (111-134 residues) adopts α-helical structure in SDS micelles, while it assumes random coil conformation in aqueous *medium*.[5a] This behavior may have a strong impact in the copper binding, influencing the *N*-terminal portion. Therefore, SDS micelles may include only the region outside the *octarepeat*, such as H_{96} and H_{111}, and may not influence the metal

binding to the *octarepeat* region (60-91 residues) that remains disordered and unstructured. This effect could strongly affect the metal coordination sphere and the catalytic properties of the complexes, in view of the following copper binding affinity order suggested above: $H_{111} > H_{96} >> H_{85} \approx H_{77}$

The ternary interaction between amyloid-β, prion and copper ions.

The interaction between prion protein and a wide range of proteins seems to be involved in the progression of dementia and particular attention was focused on the ability of prion *N*-terminus to selectively bind amyloid-β oligomers. This interaction influences the formation of amyloid plaques and the progression of the Alzheimer's disease, via alterations in the synaptic signaling.[13a] The neurotoxicity of amyloid-β species could be related to the interaction between prion, copper ions and *N*-methyl-D-aspartate receptors (NMDAR): the cellular prion protein is able to bind the NMDAR complex only upon the binding with copper and therefore, this interaction is generally compromised by the sequestration of the metal by Aβ, resulting in an alteration of signaling current and into the neuronal damage.[13b] Moreover, the prion protein may act as amyloid receptor on the neuronal surface, trapping oligomeric β-sheet structures with a dissociation constant around 70 nM and decreasing the fibrillation tendency. Finally, even if several evidences suggest that the prion protein acts as antagonist of the neurodegeneration, inhibiting the deposition of plaques, other works support a possible involvement of protein as a stabilizer of neurotoxic amyloid oligomers.[13c]
The aim of this section is to investigate whether the binding between amyloid-β and prion proteins occurs and whether this interaction is mediated or induced by copper in aqueous solution or micelle environment. The existence of two main binding sites in the *N*-terminus of prion protein for amyloid peptides has been suggested, the sequences 95-110 and 23-58 (or probably the shorter sequence 23-27) (Figure 10).[14] These two putative regions are characterized by high lysine-content, suggesting a probable electrostatic interaction between positive charges of the two sites and the negatively charged Aβ *N*-terminus; moreover, this domain is surrounded by histidine and methionine residues that are possibly involved in the metal binding. On the other hand, there is no evidence that the structured *C*-terminal region of prion protein, 113-231, is involved in the binding with oligomers: no changes in the generation and elongation of amyloid fibrils were observed in the samples containing $A\beta_{40}$ and this prion fragment.

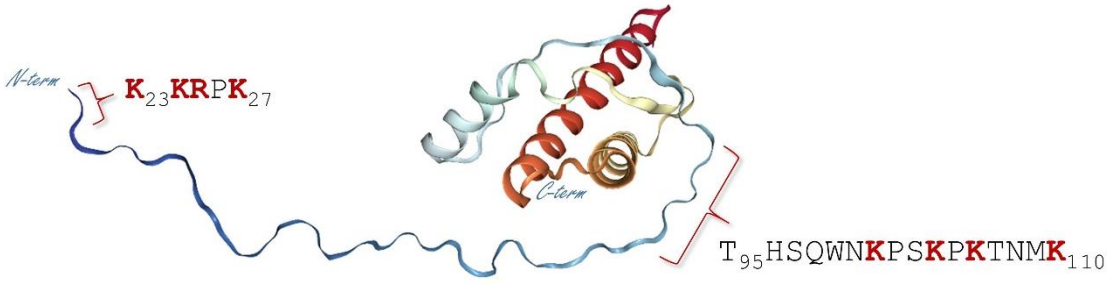

Figure 10. *Full-length prion cartoon showing the two regions mainly involved in the interaction with amyloid oligomers.*

However, no fibrillation and evident disassembly of preformed amyloid aggregates were obtained in the presence of the same amyloid fragment and the full-length prion including the *N*-terminus. Moreover, the amyloid oligomers and misfolded monomers seem to be bound both by PrP^C and by its β-sheet isoforms, supporting the possible involving of the flexible *N*-terminal regions both of prion and of Aβ proteins.[13c] Besides a possible electrostatic interaction between the opposite charged domains of the two proteins, another factor contributing to this binding could be the structural

rearrangement of backbones: *in vitro* studies indicate that cellular prions only bind β-sheet amyloid isoforms and not native monomers, while the misfolded prion could interact with monomers, inducing their oligomerization.[15a] Regarding the interaction site in the amyloid fibrils formed by 1-40 and 1-42 sequences, it might be evident that only the first 16 amino acids could be accessible to the interaction with the prion receptor, while it is known that the residues 16-21 and 30-40 are located in the hydrophobic core of oligomers and fibrils, hidden from any possible specific recognition. Furthermore, copper ions could induce the amyloid-prion interaction, acting as a bridge between the amyloid and prion *N*-termini and stabilizing their interaction. It was suggested a possible coordination sphere of the metal involving one histidine inside the prion *octarepeat* region and one outside the OR, a *N*-amide of the backbone and another histidine from the amyloid *N*-terminal domain.[15b] Anyway, the function of the interaction between the two proteins is still not totally characterized: prion protein could act as Aβ receptor to promote the transcytosis of amyloid monomers outside the blood-brain barrier or the binding between PrP and Aβ would inhibit the cascade of signals leading to the neuronal apoptosis, neutralizing and not allowing the identification of Aβ oligomers by the cell. While the inhibition of the interaction between prions and Aβ and of the following formation of toxic adducts seem to be a valid approach to contrast the disease, it will be important to clarify the cellular mechanisms and how they might be targeted pharmacologically. Therefore, the identification and the full characterization of the protein binding, besides the clarification on the role of this interaction in the alteration of specific physiological functions and in the promotion of several unregulated pathways, will be crucial to the design of new drugs.[15c]

Catalytic oxidation of MC by [Cu^{II}-peptide] in aqueous and membrane medium

Recently, notable oxidative reactivity of Cu-PrP_{76-114} complexes toward catecholic substrates such as the neurotransmitter dopamine was reported.[16] The catalytic oxidative ability of the adducts with respect to free copper ions was also verified toward a simple catechol, as 4-methylcatechol, that is subjected to faster oxidation rate and more stable quinonic product if compared to dopamine. In this chapter, the redox efficiency of copper-prion and amyloid fragment adducts was compared in aqueous *medium* and in a membrane-like environment: an anionic surfactant, the sodium dodecyl sulfate (SDS), was added to the reaction mixtures to generate micelles and to mimic a simple membrane layer.

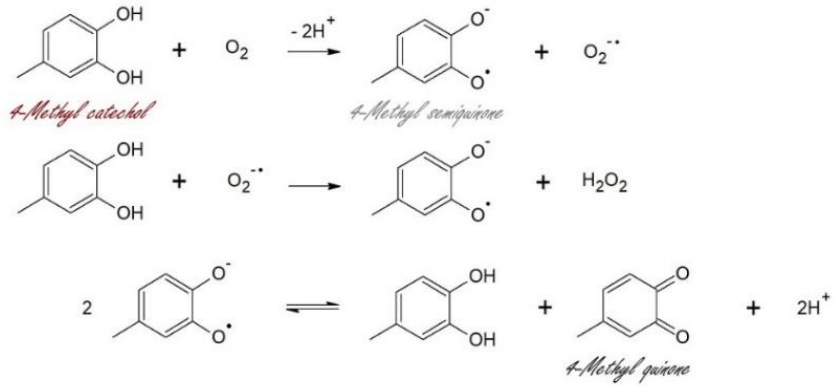

Figure 11. *Schematic reactions involved in the conversion of 4-methylcatechol into quinonic product. In cells, derivatives of catechols can undertake one- or two-electron redox cycling generating reactive oxygen species, such as superoxide and hydrogen peroxide via autoxidation or by catalysis of enzymes or transition metals, like Cu^{2+} or Fe^{3+}.*

The catalytic oxidation of 4-MC (3 mM) by copper(II) and its complexes was studied at 20 °C in 50 mM HEPES buffer at pH 7.4, saturated with atmospheric oxygen. The reaction was monitored by UV-visible spectroscopy following the 4-methyl-quinone band at 401 nm (ε = 1550 $M^{-1}cm^{-1}$) for a reaction time of 1800 s. Upon a quantitative accumulation of quinone in the initial phase of the reaction (Figure 11), the oxidative product undergoes a Michael addition on catechol, resulting in the accumulation of oligomeric species and red shift of the UV band. A similar but more complex

trend is assumed by DA oxidation (see below). The peptides ($A\beta_{1-16}$, $A\beta_{1-28}$, $A\beta_{1-40}$, $PrP_{106-114}$, PrP_{76-114}) were added at 0-50 μM concentrations, while copper(II) was kept constant at 25 μM. In the experiment with an excess of $PrP_{106-114}$, the peptide was added at 250 μM concentration to the solution of 4-MC (3 mM), followed by copper(II) nitrate (25 μM) as the last reagent. The different kinetic behaviors of Cu^{II}-peptide complexes in aqueous solution and in the presence of SDS (20 mM) were compared. Blank experiments on 4-MC oxidation under the same conditions but in the absence of the metal were also evaluated and then subtracted from kinetic profiles.

Copper reactivity when bound to Prion fragment (76-114)

As shown in Figure 12, the reactivity of free copper(II) remains unaltered, while the redox efficiency of Cu^{II}-PrP_{76-114} adduct upon the addition of SDS is drastically quenched. An opposite trend between the oxidative capability of the complex in buffer in comparison with the micellar *medium* is evidenced. When the oxidation of substrate is performed with only one equivalent of peptide, the reactivity is initially quenched, but then slowly takes place, while only in the presence of high peptide : metal ratio the total shutdown of the reactivity can be observed. As described in the Introduction, PrP_{76-114} peptide can bind more than one copper(II) ion, involving both the fragment encompassing the region 92-114 outside the *octarepeats*, showing a high affinity Cu site due to the presence of H_{96} and H_{111}, and two copper sites included in two of the four *octarepeats*.

Because of the existence of several copper coordination sites in prion protein, a similar experiment was also performed in the presence of 2 equiv. of copper and the Cu^{2+}-PrP_{76-114} complex at 2:1 molar ratio highlights higher oxidative ability than its 1:1 homologue in aqueous *medium*. When the adduct is bound to the micelle surface, stronger quenching of the reactivity promoted by the 2:1 complex is observed (Figure 13), compared to the decrease of the reaction rate induced by the presence of the complex at 1:1 ratio described above.

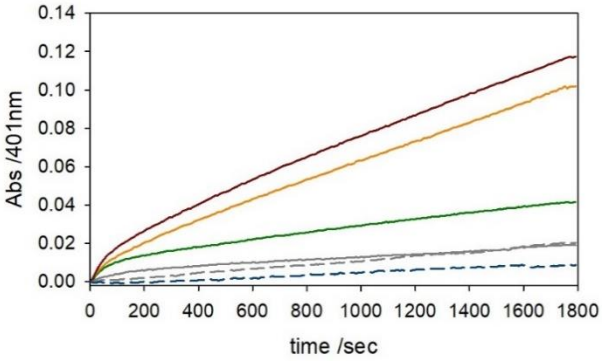

Figure 12. *Kinetic profiles of 4-MC (3 mM) oxidation with time in 50 mM HEPES buffer at pH 7.4 and 20 °C in the presence of Cu^{II} (25 μM) without SDS (solid green trace), and upon the addition of 1 equiv. PrP_{76-114} in the absence (solid orange)/ presence of SDS (20 mM, dashed grey), and 2 equiv. of prion peptide in the absence (solid brown)/ presence of SDS (dashed blue). Autoxidation of 4-MC is shown as solid grey trace.*

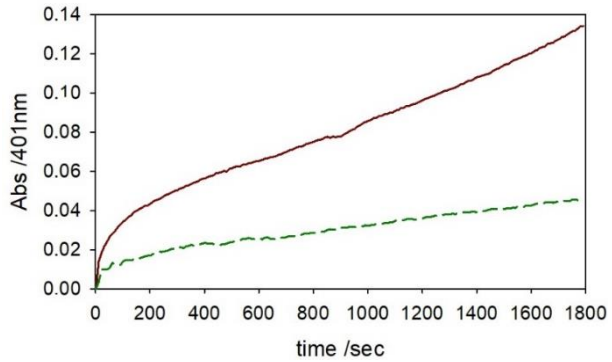

Figure 13. *Kinetic profiles of 4-MC (3 mM) oxidation with time in 50 mM HEPES buffer at pH 7.4 and 20 °C in the presence of PrP_{76-114} (25 μM) and 2 equiv. of copper(II) (50 μM) without SDS (solid brown trace) and with SDS (20 mM) (dashed green).*

Copper reactivity when bound to Prion fragment (106-114)

The shorter prion fragment with the sequence 106-114 corresponding to a small region located outside the *octarepeat* domain was also studied. $PrP_{106-114}$ includes only one histidine, His_{111}, and two methionines, Met_{109} and Met_{112}, that can partially stabilize copper(I) ions during the metal redox cycle. ESI-MS, UV-vis and EPR data have recently verified the initial generation of copper(II) : peptide complex (1:1) at pH 6, suggesting the involvement of imidazole group in the metal anchoring; the participation of peptide amides was also proposed to give a partially stable six-membered chelate-ring as possible coordination sphere for copper(II) (Figure 14). The poor catalytic environment around copper(II) does not allow catalytic efficiency,[17a,17b,17c] which differs from the redox cycling reported for copper(II)-prion (76-114) adduct. Indeed, our previous studies have suggested that for Cu-$PrP_{106-114}$ at 1:1 ratio a significant copper fraction is bound to the buffer, and only at 1:3 ratio most of Cu^{II} is bound to the peptide. The oxidative ability of Cu^{II}-$PrP_{106-114}$ complex in SDS micelles appears to be only reduced but not completely quenched at 1:2 molar ratio, due to the incomplete copper(II) complexation by the shorter prion (Figure 15A). Total quenching of the redox reactivity occurs at much higher $PrP_{106-114}$ concentration (Figure 15B).

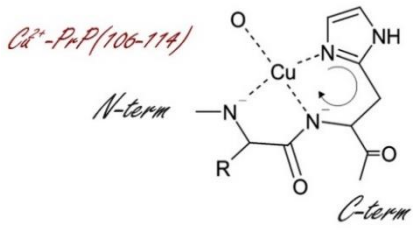

Figure 14. *Coordination structure of $PrP_{106-114}$ to Cu^{II}.*

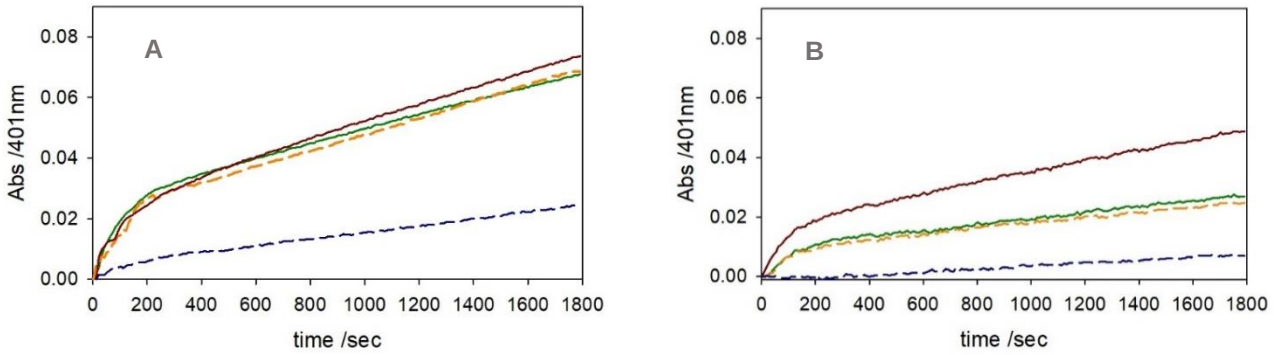

Figure 15. *Kinetic profiles of MC (3 mM) oxidation with time in 50 mM HEPES buffer at pH 7.4 and 20 °C in the presence of Cu^{II} (25 μM) alone (solid green trace) and with SDS (20 mM) (dashed orange); A) in the presence of Cu^{II} bound to $PrP_{106-114}$ (50 μM) without SDS (solid brown) and with SDS (20 mM) (dashed blue); B) in the presence of Cu^{II} bound to $PrP_{106-114}$ (250 μM) without SDS (solid brown) and with SDS (20 mM) (dashed blue).*

Copper reactivity when bound to Amyloid-β fragments (1-16), (1-28) and (1-40)

As previous works suggest, the redox capability of copper(II)-amyloid-β (1-16) and (1-28) is rather evident in physiological conditions but a peculiar trend is observed in membrane-like environment. The rates of 4-MC oxidation in the presence of copper and the longer prion fragment or the three amyloid-β peptides are similar. However, the situation is different in the presence of SDS because the catechol oxidation rate in the reaction mixture containing Cu^{II}, Aβ and substrate is only partially reduced, whereas the redox cycling of Cu^{II}-PrP_{76-114} is massively quenched in micelle (Figure 16).

We can conclude that copper ions, once reduced, are efficiently coordinated by PrP_{76-114} in redox-stable form in the SDS micelle, so that substrate oxidation is drastically quenched. Conversely, the reduced Cu^{I}-Aβ species are still reactive to dioxygen. This behavior can be explained by the evidence that the first region (1-16) of amyloid-β is located outside the transmembrane region, whereas only the *C*-terminus is bound to the membrane; therefore, copper binding and redox reactivity are not much affected by the binding with anionic micelles. Moreover, the oxidative trend in the presence of the amyloid peptide of different length ($Aβ_{16}$, $Aβ_{28}$ and $Aβ_{40}$) shows similar results.

Also in aqueous *medium* these three Aβ peptides show similar capability to increase the oxidative reactivity of copper toward catechols. The behavior of three amyloid fragments is almost totally superimposable each other when the reactivity is assayed toward dopamine, while slight changes in the oxidative reactivity are shown when the more reactive 4-methylcatechol is added (Figure 17). These results confirm that the portion (1-16) is the main region that mediates the binding with copper. Amyloid-β 1-28 and 1-40 peptides, in addition to the region where the binding between amyloid-β and copper occurs, include the *C*-terminal fragment devoid of any other binding site and characterized by high hydrophobicity. Based on the different extension of the amyloidogenic tail, $Aβ_{28}$ peptide shows reduced propensity to aggregate in solution compared with the longer $Aβ_{40}$.

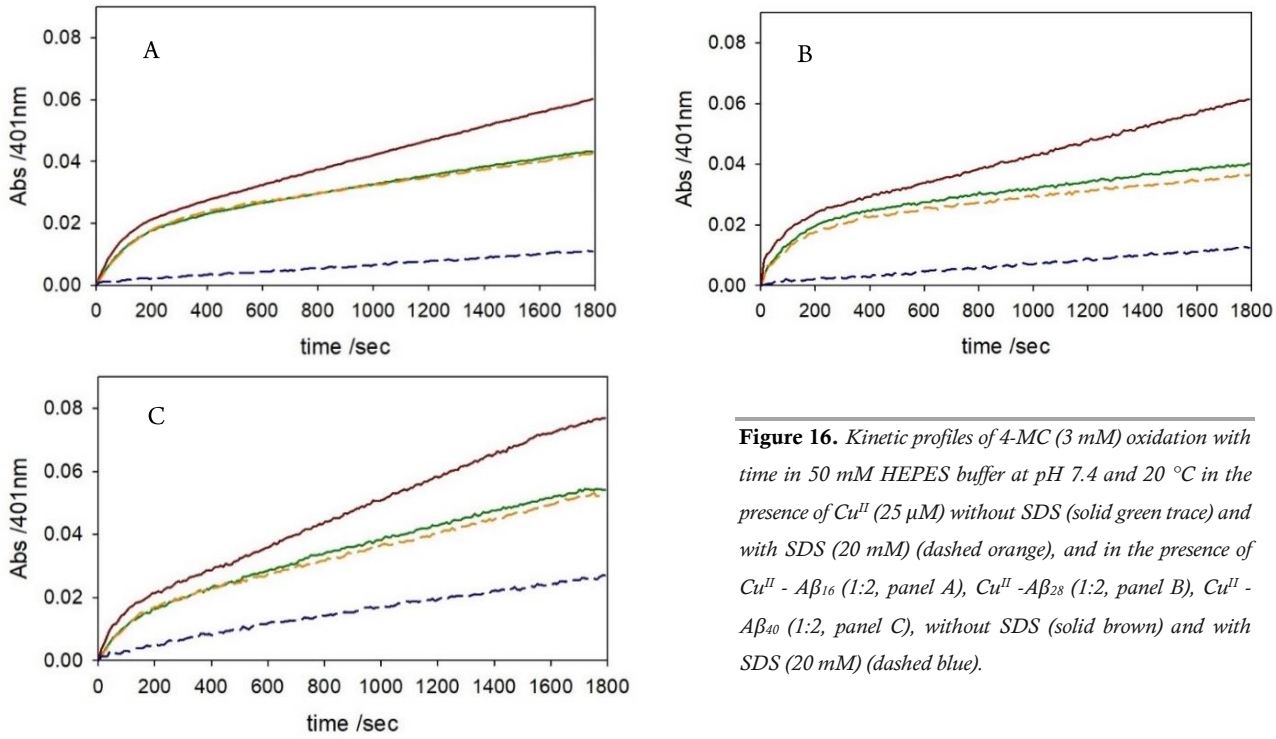

Figure 16. *Kinetic profiles of 4-MC (3 mM) oxidation with time in 50 mM HEPES buffer at pH 7.4 and 20 °C in the presence of Cu^{II} (25 μM) without SDS (solid green trace) and with SDS (20 mM) (dashed orange), and in the presence of Cu^{II} - $Aβ_{16}$ (1:2, panel A), Cu^{II} -$Aβ_{28}$ (1:2, panel B), Cu^{II} - $Aβ_{40}$ (1:2, panel C), without SDS (solid brown) and with SDS (20 mM) (dashed blue).*

Despite the consensus on Aβ structure, in literature a well-characterized localization of the peptide in lipid environment has still to be defined: some data suggest that the peptide can be located in the core of SDS micelles, while other studies support a superficial binding of the peptide on micelles or a partial insertion into the lipid bilayer.[5a]

As shown in Figure 18, the hydrophobic region of the peptide (residues 32–40) may be localized inside the micelle core, whereas the hydrophilic sequence (residues 1–16) remains unstructured near the anionic surface. In particular, the amyloid sequence (1–28) interacts with the hydrophilic heads of the membrane, while Aβ(25–40) portion is located in the hydrophobic lipid core. Indeed, the previous amino acidic fragment provides hydrophobic groups easily embeddable into the hydrophobic part of lipid membranes.[1d] The *N*-terminal hydrophilic portion 1-16 would be able to bind copper(II) ions with high affinity ($K_d=10^{-10}$-10^{-11} M) via three His residues (His_6, His_{13}, and His_{14}).[3]

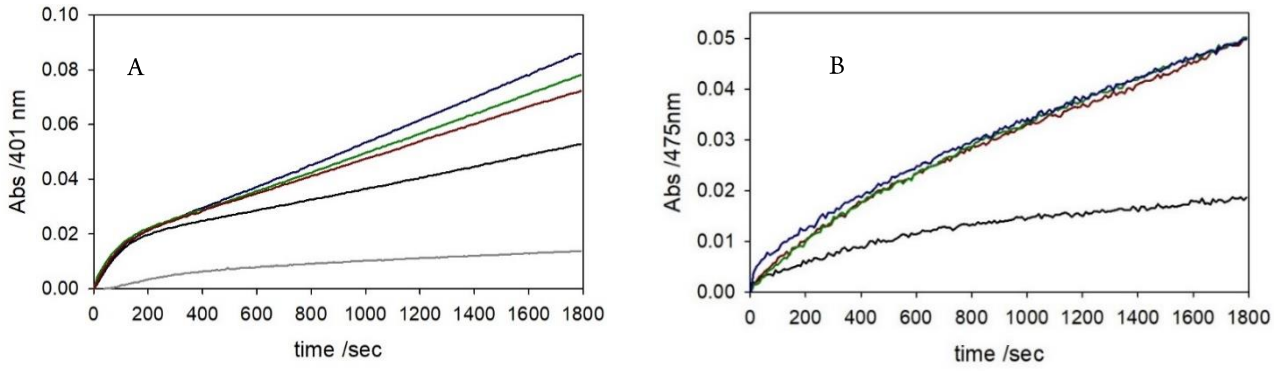

Figure 17. *Kinetic profiles of MC (panel A) and DA (panel B) (3 mM) oxidation with time in 50 mM- HEPES buffer at pH 7.4 and 20 °C in the presence of Cu^{II} (25 μM) (black trace) and $A\beta_{16}$ (brown), $A\beta_{28}$ (green) and $A\beta_{40}$ (blue) (50 μM).*

The kinetic data performed in the presence of sodium dodecyl sulfate show that the catechol oxidation catalyzed by [Cu-PrP_{76-114}] is characterized by visible reduction of the reaction rate and slow accumulation of methyl-quinone in solution. This trend can be explained by the stability of Cu^{I}-PrP_{76-114} complex in membrane. The reaction mechanism previously proposed for catechol oxidation by copper-peptide complexes as β-amyloid, α-synuclein and prions, is shown below:

$$Cu^{II} + \text{peptide} \rightleftarrows [Cu^{II}\text{-peptide}]$$
$$[Cu^{II}\text{-peptide}] + \text{catechol} \rightarrow [Cu^{I}\text{-peptide}] + \text{semiquinone}^{\bullet+}$$
$$[Cu^{I}\text{-peptide}] + \text{catechol} \rightleftarrows [Cu^{I}\text{-peptide-catechol}]$$
$$[Cu^{I}\text{-peptide-catechol}] + O_2 \rightarrow [\text{Cu-peptide-catechol-}O_2]$$
$$[\text{Cu-peptide-catechol-}O_2] \rightarrow\rightarrow [Cu^{II}\text{-peptide}] + \text{quinone}$$
$$2\ \text{semiquinone}^{\bullet+} \rightarrow \text{catechol} + \text{quinone}$$

This mechanism explains the dioxygen influence on the reaction rate and the role of copper(I), rather than Cu^{II}, as the key species for the catalytic efficiency. Prions and amyloid-β show different behaviors in membrane: upon reduction of copper(II), the reduced Cu^{I}-PrP_{76-114} species trapped in the membrane are unreactive to dioxygen and this mechanism determines the reactivity quenching observed in SDS. Instead, the reduced Cu^{I}-$A\beta_{40}$ species interacting with membrane only via *C*-terminus shows the *N*-terminal copper binding region not much affected by the effect of lipid monolayer. Therefore, the binding with anionic micelles only affects the central Aβ region, leaving the *N*-terminal sequence capable to bind metals in membrane-like conditions.

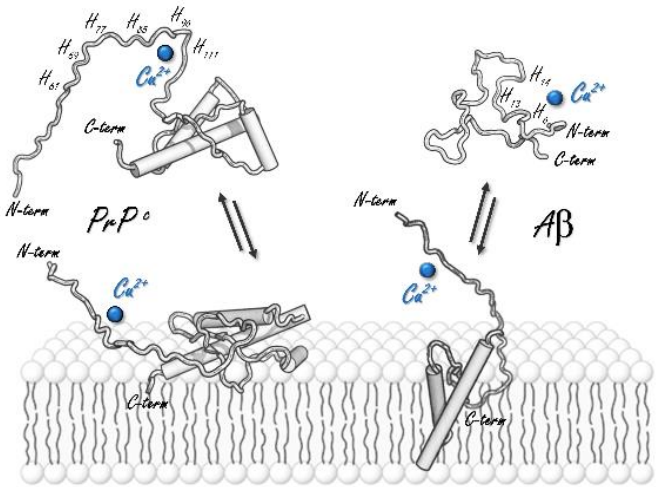

Figure 18. *Hypothetical representation of the interaction between phospholipids and the native prion protein (on the left) and the amyloid-β (1-40) peptide (on the right). The hydrophobic Aβ residues in the central region are directed toward the apolar phase, while the N-terminus appears to reside free and unstructured outside the membrane. N-terminal metal ion binding to Aβ is not much affected by the SDS micelles.*

The structures of Cu^{I}/Cu^{II} species bound to PrP peptides were characterized with various techniques: in physiological conditions the main Cu^{II} ligands are represented by three histidines, H_{96} and H_{111}, located outside the *octarepeat* region

and either H_{85} or H_{77} in the *octarepeat*. During the redox cycle of the metal ion, copper(I) can be bound by the prion fragment through two methionines and histidine 111.This last coordination geometry could be also assumed by the prion fragment 106-114, but the low efficiency in the copper(II) binding does not allow to promote an effective redox cycling of the metal, as shown by the previous kinetic data. Conversely, Cu^{I}-PrP_{76-114} species would involve large reorganization energy of the complex to switch from two redox metal states. On the other hand, the small fragment 106-114 does not show a totally silent redox activity, displaying an analogous behavior of PrP(91-126), both in terms of coordinative environment for the metal and of Cu^{II} K_d values of approximately 90 microM.[17d] To explain the metal coordination to amyloid-β peptides and their catalytic efficiency, a model inspired to the structural motif of some well-known copper enzymes, like the binuclear catechol oxidase, was proposed. A tetragonal distorted octahedral metal coordination sphere via three His side chains and some specific H-bonding interactions is mainly supported. Regarding to the longer amyloid fragment, the methionine located at position 35 can influence the oxidative stress process and may act as an electron donor for the reduction of copper(II) to Cu^{I}.

Moreover, it is known that methionine residues are easily oxidized to the sulfoxide under physiological conditions, suggesting a dual role of these residues: a pro-oxidant role, promoting the metal cycling, and an endogenous antioxidant one, as scavenger of reactive species. Studies on analogues of $A\beta_{28}$ fragment through mutation of each histidine or acetylation of the *N*-terminus have suggested that the *N*-terminus and histidine 13 are crucial for Cu^{II} binding and that His-6 and His-14 are also implicated at pH > 7.5, where substitution of the O-donor occurs.[10]

In membrane environment, the sequences (15-24) and (29-35) of β-amyloid protein can interact with SDS micelles and can undergo a structural change into α-helix. *N*-terminal region shows a random folding outside the membrane and maintains its metal coordination, as previously described. Although the high tendency to undergo aggregation in aqueous *medium*, the study on the catalytic behaviour of the longer amyloid-β 1-40 is essential to investigate the interaction with membrane in a biological context. To reduce the aggregation rate, a small amount of ammonia was added to dissolve the lyophilized peptide, previously treated with hexafluoro-2-propanol to obtain the monomeric form. Several controls were performed to verify that ammonia has negligible influence on the reactivity and on the following oxidative modification studies.

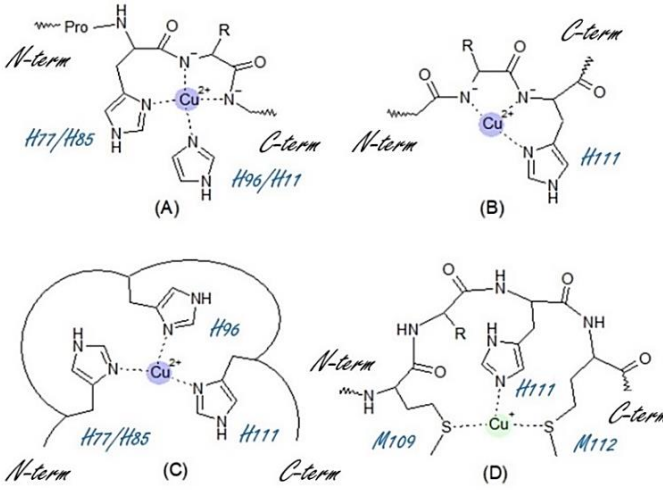

Figure 19. *Main Cu coordination spheres with prion peptide at 1:1 molar ratio at physiological pH (A, B, and C, for Cu^{II}, and D for Cu^{I})*

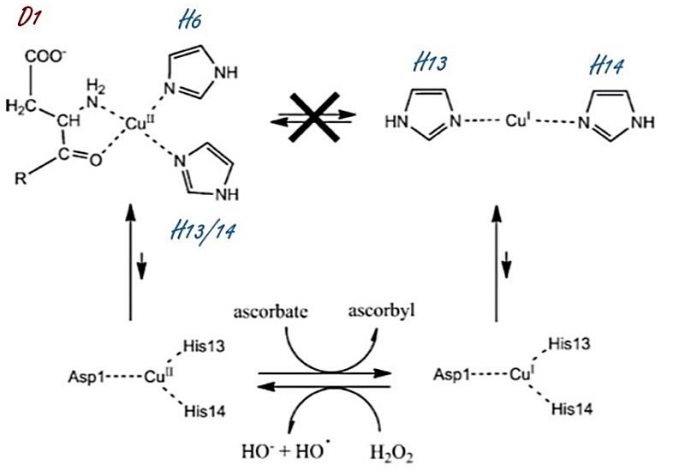

Figure 20. *Resting states are the main coordination spheres of copper(II) (left) and copper(I) (right); at the bottom, a possible redox mechanism not involving large reorganization energy to connect the two limit states is shown.*[18a]

Catalytic oxidation of DA by [Cu^{II}-peptide] in aqueous and membrane medium

The previous trend evidenced toward 4-methylcatechol was confirmed by the oxidation of dopamine, a biological catecholamine acting as neurotransmitter in neuronal cells characterized by a lower reaction rate but a more complex mixture of oligomeric products.

DA oxidation catalyzed by Cu^{II} was studied at 20 °C in 50 mM HEPES buffer at pH 7.4, saturated with atmospheric oxygen. The reaction was monitored by UV-visible spectroscopy through the development of dopaminochrome band at 475 nm. Both autoxidation of the substrate and its conversion to aminochrome by only copper were compared to the reactivity shown in the presence of the following peptides: $A\beta_{16}$, $A\beta_{28}$, $A\beta_{40}$, $PrP_{76\text{-}114}$ and $PrP_{106\text{-}114}$. The redox cycling of the metal alone or bound to the peptides was evaluated in aqueous and SDS environment (Figure 21 and Figure 22).

Copper reactivity when bound to Prion fragment (76-114) and (106-114)

Comparing the chemical structure of DA with 4-methylcatechol, the presence of NH_2-group allows the interaction of dopamine with anionic groups of SDS micelles, resulting in a higher reaction rate of substrate oxidation by only copper in aqueous *medium* if compared to the membrane environment. Indeed, the biological catecholamine shows a modest affinity for the interaction with the membrane surface and the redox chemistry of dopamine and related substrates is highly influenced by the affinity of the peptides for the lipid bilayers binding.

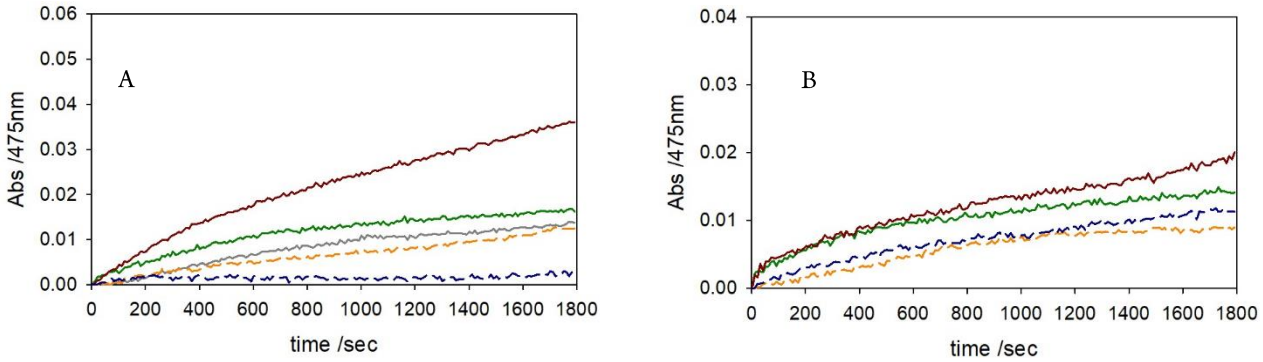

Figure 21. *Kinetic profiles of DA (3 mM) oxidation with time in 50 mM HEPES buffer at pH 7.4 and 20 °C (autoxidation, grey trace) in the presence of Cu^{II} (25 μM) without SDS (green) and with SDS (20 mM) (orange dashed), or with Cu^{II}-$PrP_{76\text{-}114}$ (1:2, panel A) and Cu^{II}-$PrP_{106\text{-}114}$ (1:2, panel B) without SDS (brown) and with SDS (20 mM) (blue dashed).*

Copper reactivity when bound to Amyloid-β fragments (1-16), (1-28) and (1-40)

The reaction mechanism is analogous to the one evidenced in the presence of the previous catechol and the DA-induced redox reactivity is almost totally prevented only for Cu-$PrP_{76\text{-}114}$ complex, as was evidenced by our group with Cu-αSyn complex.[5b] The common feature of these peptides is the presence of two adjacent methionines, ^{109}MKHM^{112} in PrP and ^{1}MDVFM^{5} in αSyn, that are optimal ligands for copper(I) and are able to stabilized the reduced form making unreactive to dioxygen.

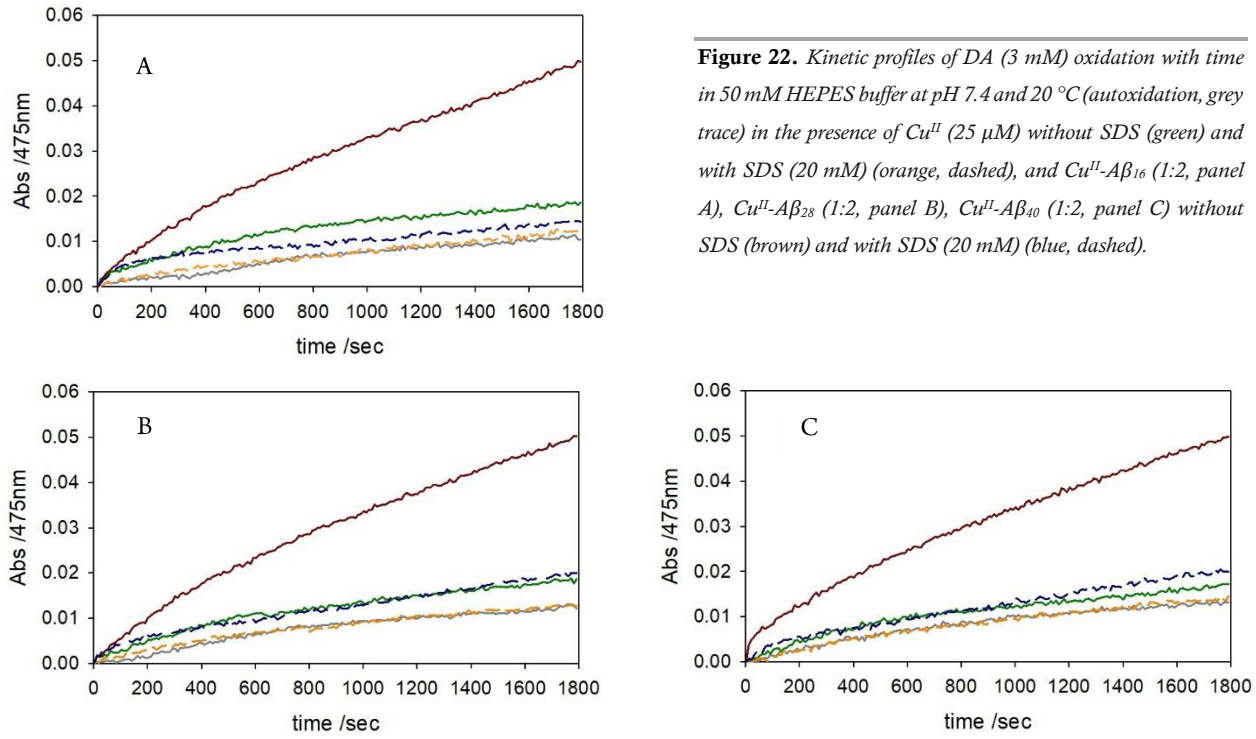

Figure 22. *Kinetic profiles of DA (3 mM) oxidation with time in 50 mM HEPES buffer at pH 7.4 and 20 °C (autoxidation, grey trace) in the presence of Cu^{II} (25 μM) without SDS (green) and with SDS (20 mM) (orange, dashed), and Cu^{II}-$A\beta_{16}$ (1:2, panel A), Cu^{II}-$A\beta_{28}$ (1:2, panel B), Cu^{II}-$A\beta_{40}$ (1:2, panel C) without SDS (brown) and with SDS (20 mM) (blue, dashed).*

Catalytic oxidation of DA and MC by ternary complex [Cu^{II}-amyloid-β-prion]

The interaction between prion and amyloid proteins has been highlighted in several reports, suggesting a possible involvement in the progression of Alzheimer's disease. A number of studies have suggested the possible implications of prion binding to beta-amyloid species as promoter of Aβ toxicity.[18b] In particular, prion protein was detected as the main ligand for amyloid-β in screening studies that have comprised around 200000 proteins, in which the deletion of the expression of the prion gene was linked to the immunity toward Alzheimer's disease and the absence of neurotoxicity of β-amyloid deposits.[19a] Anyway, opposite results were also published in which the connection between the presence of cellular prion and its binding with amyloid-β oligomers promotes alteration in the synaptic plasticity and deficiencies in axon signaling.[19b] Moreover, the deposition of insoluble plaques and the accumulation of Aβ oligomers modulate the trafficking and the endocytosis of cellular prion protein and at the same time, the presence of PrP seems to interfere with the post-translation modifications normally carried out on the amyloid precursor protein. Cellular prion protein is involved in the inhibition of fibrillation of β-amyloid monomers through the trapping of Aβ in antiparallel β-sheet-rich oligomers and the binding is primary located in the *N*-terminal region of prion. The stabilization of oligomers, that are commonly recognized as the most dangerous isoform of β-amyloid aggregates, could be connected with a potential harmful role of prion protein as enhancer of neurotoxicity of amyloid-β.[13c] In this chapter, a comparative study of the oxidative efficiency of the ternary complex Cu^{II}-Aβ-$PrP_{76\text{-}114}$ was performed, both in aqueous and in SDS environment to verify the role of the metal in the interaction between the two peptides. The kinetic data were obtained adding 1 equiv. of each peptide in the presence of 1 equiv. of copper(II) and following the oxidation of 4-methylcatechol (3 mM) at 401 nm, corresponding to the 4-methylquinone band (Figure 23) or dopamine at 475 nm, corresponding to the aminochrome (Figure 24).

The redox activity of the ternary complex in membrane environment results massively silenced while the oxidation of substrate is strongly increased in aqueous conditions if compared to the catalytic rate shown in the presence of the respective binary adducts.

The same trend is observed in the presence of all three amyloid-β peptides complexed to copper and prion 76-114, displaying a higher catalytic capability both in the first step of reaction that usually corresponds to the stoichiometric step in which the substrate is consumed to generate the reduced complex, and in the second step of the oxidative reaction linked to the re-oxidation of copper(I) to copper(II).

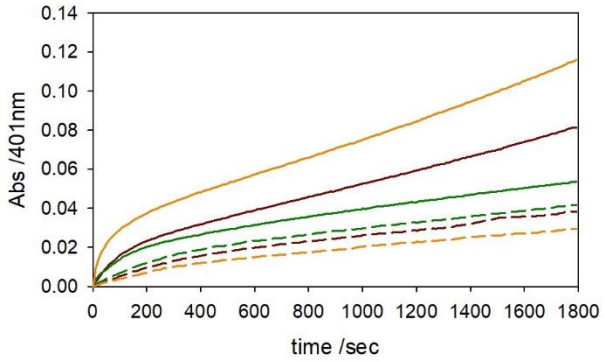

Figure 23. *Kinetic profiles of MC (3 mM) oxidation with time in 50 mM HEPES buffer at pH 7.4 and 20 °C in the presence of Cu^{II}-$A\beta_{40}$ (25 μM, 1:1) in absence (green solid)/ presence of SDS (20 mM, green dashed) or Cu^{II}-$PrP_{76\text{-}114}$ (25 μM, 1:1) without SDS (brown solid) and with SDS (20 mM) (brown dashed). The addition of the ternary complex, copper-amyloid-prion (1:1:1), is shown both in aqueous medium (orange solid) and in membrane environment (orange dashed).*

In order to explain this reactivity enhancement, we can propose a possible coordinative environment for copper that involves the participation of one histidine of amyloid-β besides the ligands usually involved in the prion sequence; the two methionines in prion peptide could bind copper(I) together with one amyloid-β histidine, allowing a more efficient oxidation by dioxygen.

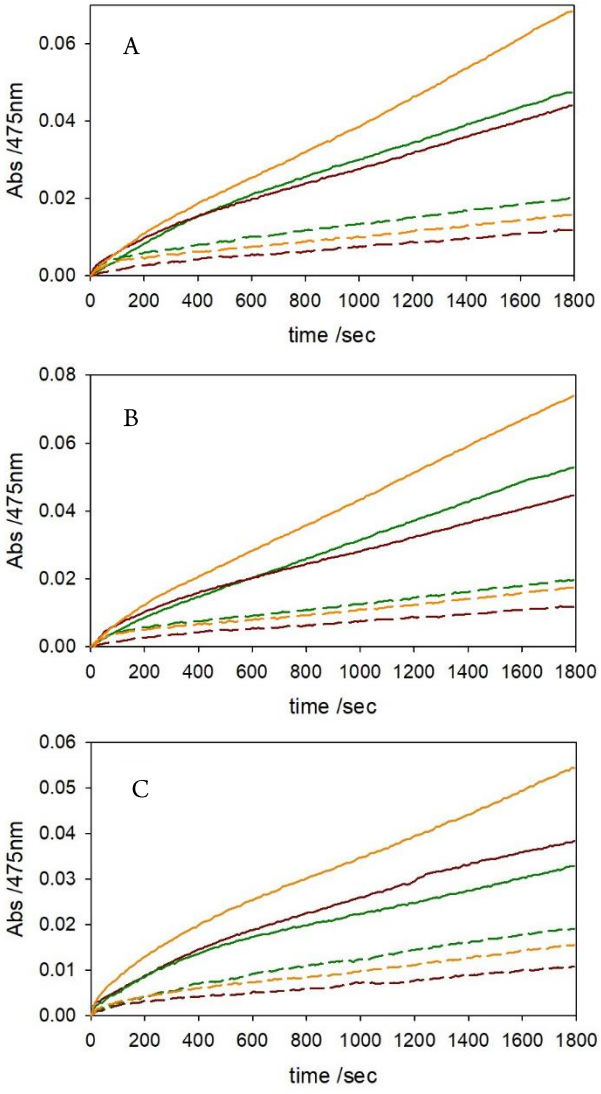

Figure 24. *Kinetic profiles of DA (3 mM) oxidation with time in 50 mM HEPES buffer at pH 7.4 and 20 °C A) in the presence of Cu^{II}- $A\beta_{40}$ (25 μM, 1:1) in absence (green solid)/ presence of SDS (20 mM, green dashed) and Cu^{II}-$PrP_{76\text{-}114}$ (25 μM, 1:1) without SDS (brown solid) and with SDS (20 mM) (brown dashed). The addition of the ternary complex, copper-amyloid- prion (1:1:1), is shown both in aqueous medium (orange solid) and in membrane environment (orange dashed); B) in the presence of Cu^{II}-$A\beta_{28}$ (25 μM, 1:1) in absence (green solid)/ presence of SDS (20 mM, green dashed) or Cu^{II}-$PrP_{76\text{-}114}$ (25 μM, 1:1) without SDS (brown solid) and with SDS (20 mM) (brown dashed). The addition of the ternary complex, copper- amyloid- prion (1:1:1), is shown both in aqueous medium (orange solid) and in membrane environment (orange dashed); C) in the presence of Cu^{II}-$A\beta_{16}$ (25 μM, 1:1) in absence (green solid)/ presence of SDS (20 mM, green dashed) or Cu^{II}-$PrP_{76\text{-}114}$ (25 μM, 1:1) without SDS (brown solid) and with SDS (20 mM) (brown dashed). The addition of the ternary complex, copper- amyloid- prion (1:1:1), is shown both in aqueous medium (orange solid) and in membrane environment (orange dashed).*

Catalytic oxidation of MC by [Cu^{I}-peptide] in aqueous and membrane medium

To confirm the proposed reaction mechanism, the oxidative reactivity in the presence of copper(I)-peptide complexes was assessed. The intracellular and extracellular *media* in neuronal cells are known to be reducing environments and therefore, the interaction between copper(I) with neuronal peptides such as amyloid or prion proteins plays a key role. The binding affinity of these peptides toward the metal ions can generate efficient catalysts that lead to the production of several oxidative species and ROS, via a fast redox cycling between Cu^{I} and Cu^{II} species. The electron-donation required for copper reduction can involve either internal amino acid side chains and an external reductant. To study the oxidation of 4-methylcatechol in the presence of cuprous ions in membrane *medium*, copper(I) was generated *in situ* by reaction of copper(II) nitrate (25 μM) and ascorbate (50 μM) in the presence of SDS (20 mM) in 50 mM HEPES buffer a pH 7.4. Upon several vacuum/argon cycles, the reduced complex was exposed to air, the substrate (3 mM) was added to the reaction mixture and the catechol oxidation was monitored by UV-visible spectroscopy through the development of the 4-methyl-quinone band at 401 nm. The same experiment was repeated in the presence of Cu^{I}-peptide complexes ($A\beta_{16}$, $A\beta_{28}$, $A\beta_{40}$, $PrP_{106\text{-}114}$, $PrP_{76\text{-}114}$; 50 μM). All kinetic traces are influenced by oxygen diffusion in the sample and by whole consumption of ascorbate added in excess.

Copper(I) reactivity when bound to Prion fragment (76-114)

Figure 25 shows that Cu^{I}-PrP complex is almost completely unreactive to dioxygen, whereas unbound Cu^{I} is still able to catalyze 4-MC oxidation. The data clearly suggest that the quenching of reactivity observed in SDS promoted by copper(II)-$PrP_{76\text{-}114}$ complex is linked to the stabilization of the reduced Cu^{I}-$PrP_{76\text{-}114}$ complex trapped in micelles upon the reduction of copper(II) that is unreactive to dioxygen. Previous data reported in literature suggest that the interaction between the peptide and micelles mainly involves the *C*-terminal residues; at the same time, this type of interaction may force the region encompassing histidine 111 to assume a more rigid conformation compared to the highly flexible one assumed in aqueous *medium*.

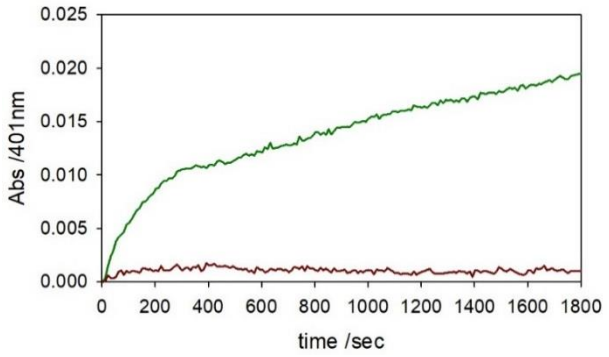

Figure 25. *Kinetic profiles of MC (3 mM) oxidation with time in 50 mM HEPES buffer at pH 7.4 and 20 °C containing SDS (20 mM) and in the presence of Cu^{I} (25 μM) alone (green trace) or Cu^{I} (25 μM) and $PrP_{76\text{-}114}$ (50 μM) (brown). Copper(I) is generated as previously described.*

Anyway, the presence of micelles can influence the copper binding affinity and the stability of the complex. This effect is clearly observed in the previous kinetics, although some works seem to indicate a low impact of SDS on Cu^{I}-PrP adduct, supporting a similar coordination sphere via Met_{109}, Met_{112}, His_{96} and His_{111}, rather stable both in water and in membrane.[5a]

Copper(I) reactivity when bound to Prion fragment (106-114)

Regarding to the behavior of [Cu^{I}-$PrP_{106-114}$] complex, Figure 26 shows a rather peculiar trend. The binding of metal ions to the shorter prion fragments is only partially stabilized by the presence of a single histidine residue, involved in the interaction with copper(II), and of two methionines that mediate the coordination with the reduced metal.

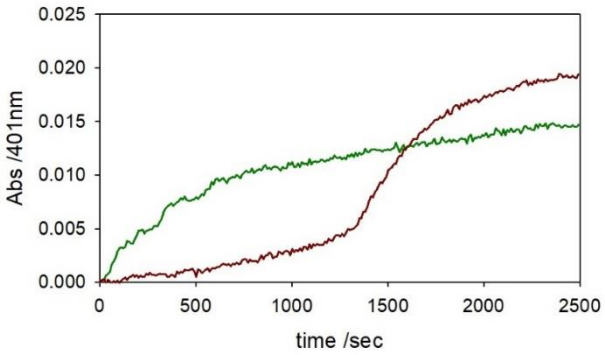

Figure 26. *Kinetic profiles of 4-MC (3 mM) oxidation with time in 50 mM HEPES buffer at pH 7.4 and 20 °C containing SDS (20 mM) and in the presence of Cu^{I} (25 μM) alone (green trace) or Cu^{I} (25 μM) and $PrP_{106-114}$ (50 μM) (brown trace). Copper(I) was generated in situ by reaction of copper(II) nitrate (25 μM) and ascorbate (50 μM) anaerobically prior to exposure of the solution to air.*

The biphasic oxidative trend shows a partial quenching of substrate oxidation only for a limited time interval and a marked increase of the reactivity after ~ 20 minutes. This initial inertness of the adduct toward the substrate oxidation can be influenced by the presence of a small excess of ascorbate, that was added to the reaction mixture at millimolar concentrations. Moreover, the time life of $PrP_{106-114}$is probably rather short and when the substrate oxidation starts, the peptide is extensively modified both by some reactive oxygen species generated in this oxidative environment and by covalent attaches from catechols and related products. Anyway, this data also supports an only modest capability of this fragment to bind the metal if compared to the longer prion peptide (76-114).

Copper(I) reactivity when bound to Amyloid-β fragments (1-16), (1-28) and (1-40)

As previously described, the coordination of metals, such as copper and zinc, to Aβ peptides is only marginally affected by the membrane or aqueous environments. The main effect of trapping of beta-amyloid monomers by SDS micelles is the induction of conformational changes and structural rearrangements of the *C*-terminal tail of peptide into α-helixes. Therefore, the interaction with neurolipids, the conformation transitions both to helical structures and to β-sheet ones, and the formation of oligomers and aggregated species may be partially independent from the generation of redox-active adducts complexed with metal. Figure 27 shows that, unlike copper(I)-PrP_{76-114} species that are stable to dioxygen and unable to promote 4-MC oxidation, Cu^{I}-amyloid adducts display a significant oxidative reactivity toward catechols. Therefore, given the oxidative behavior of prion complexes, SDS may force the prion backbone to assume a copper coordination mode with lower catalytic activity, while in the presence of amyloid-β peptides, the lipid micelles may not influence the metal binding confined in the free *N*-terminal region of the peptide. As asserted before, the *N*-terminal and hydrophilic portion of Aβ peptide is free to bind metal ions as copper(II) and copper(I) and to conserve its redox ability for an efficient redox cycling of the metal ion, while the more hydrophobic *C*-terminus penetrates into the negatively charged membrane, undergoing some structural transitions. The biological insertion into the lipid bilayers results in a decreased fluidity of the neuronal membranes and in the alteration of its permeability to small cations, thus leading to an uncontrolled intercellular signaling.

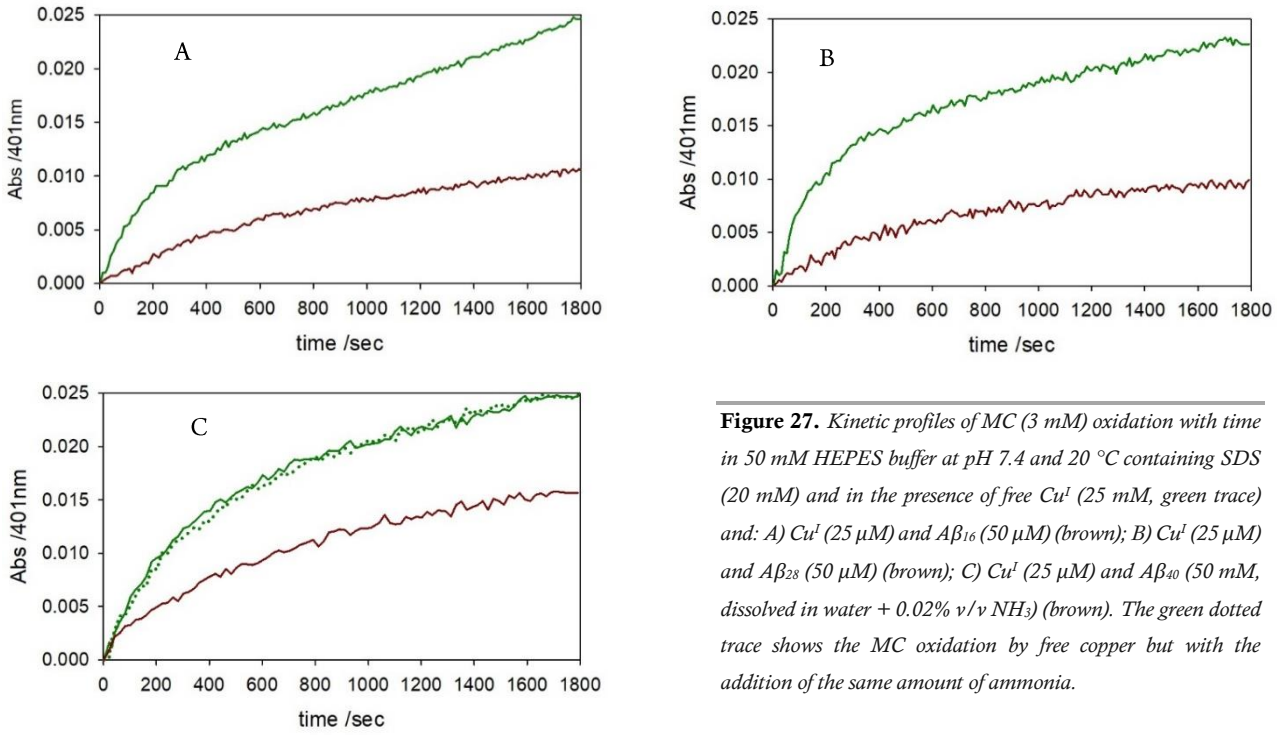

Figure 27. *Kinetic profiles of MC (3 mM) oxidation with time in 50 mM HEPES buffer at pH 7.4 and 20 °C containing SDS (20 mM) and in the presence of free Cu^{I} (25 mM, green trace) and: A) Cu^{I} (25 μM) and $A\beta_{16}$ (50 μM) (brown); B) Cu^{I} (25 μM) and $A\beta_{28}$ (50 μM) (brown); C) Cu^{I} (25 μM) and $A\beta_{40}$ (50 mM, dissolved in water + 0.02% v/v NH_3) (brown). The green dotted trace shows the MC oxidation by free copper but with the addition of the same amount of ammonia.*

Far-UV and Near-UV Circular Dichroism (CD) of binary complexes in membrane

In this section, the effect of sodium dodecyl sulfate and of the binding with copper ions on the peptide folding was analyzed. The use of sodium dodecyl sulfate as biological membrane model is explained through its chemical properties that allow the generation of negative-charged small micelles. Indeed, overpassing the critical micellar concentration (CMC, ~ 9 mM),[19c] the surfactant monomers are prone to assemble each other through the stacking between the hydrophobic chains and the resulting micelles show a net negatively-charged surface, provided by the anionic heads of SDS and mimicking the top of phospholipids, and a hydrophobic core, mimicking the inner region of lipid bilayers. The possible insertion of peptides in the lipid structures or the superficial interaction between the peptide and the cellular membrane directly influence the backbone conformation and the protein folding. The misfolding of neuronal proteins can modify their metal binding sites and the affinity constants, resulting in alterations of the redox ability of the complexes. The study of tertiary structures of each peptide is assayed both upon copper interaction in aqueous environment and when the metal-peptide adduct is trapped in micellar *medium*.

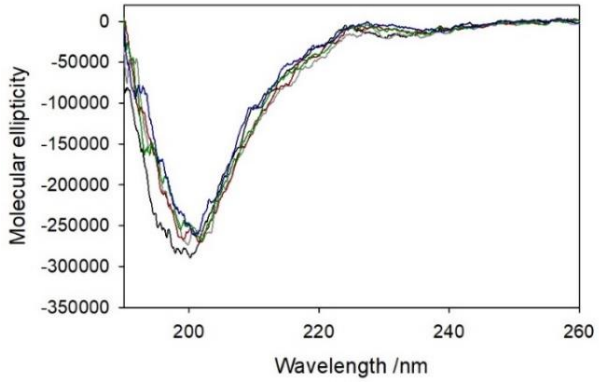

	α	β	Turn	Random
PrP_{76-114}	-	30%	15%	55%
+ SDS 5 mM	-	41%	9%	50%
+ SDS 10 mM	-	40%	9%	51%
+ SDS 20 mM	-	39%	10%	51%
+ Cu^{II}	-	38%	10%	52%

Figure 28. *Far-UV CD spectra recorded in 5 mM phosphate buffer solution pH 7.4 of PrP_{76-114} (63 μM) (black trace) and after the addition of 5 (grey), 10 (brown), and 20 mM SDS (green), and upon the addition of Cu^{II} (57 μM) (blue) to the final solution. (cell path 0.1 cm)*

The far-UV CD spectrum of PrP_{76-114} peptide upon the addition of copper(II) ions at 1:1 molar ratio and performed in 5 mM phosphate buffer solution at pH 7.4 was recorded (Figure 28). Firstly, the effect of the addition of surfactant (0-20 mM) and copper(II) (1 equiv.) to the solution of PrP_{76-114} (1.1 equiv.) was studied. The spectral changes upon the addition of SDS (20 mM) to the $[Cu^{II}\text{-}PrP_{76-114}]$ complex were also assessed. Human prion sequence consists in two main domains, the *N*-terminus that comprises the *octarepeat* region and is almost totally unstructured, and the *C*-terminus that is globular and shows a high content of α-helical structures.

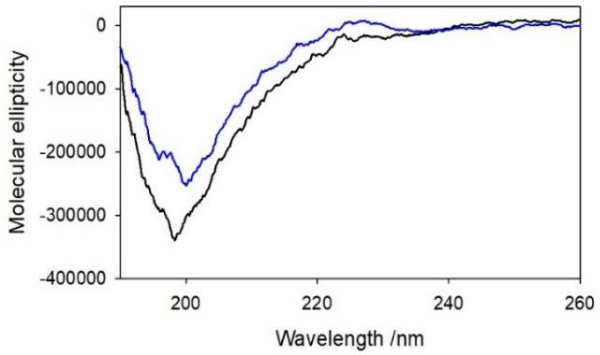

	α	β	Turn	Random
$[PrP_{76-114} - Cu^{II}]$	-	33%	15%	52%
+ SDS	-	31%	14%	55%

Figure 29. *Far-UV CD spectra recorded in 5 mM phosphate buffer solution pH 7.4 of PrP_{76-114} (50 μM) and Cu^{II} (45 μM) (black trace) and upon the addition of 20 mM SDS (blue trace) (cell path 0.1 cm).*

The CD spectra of PrP_{76-114} in aqueous environment and with the participation of copper binding highlight a random and unstructured conformation that is not strongly influenced by the presence of the micellar *medium*. The absence of the hydrophobic region encompassing the residues 115-127 does not allow to assume helical structures and the complexation between copper ions and prion fragments seems not considerably influenced by the interaction with lipids. To study the pure effect of the addition of SDS on the secondary structure of the complex, CD spectra of prion fragment complexed to copper(II) were assayed before and after the further addition of micelles (Figure 29).
CD spectra of Aβ peptides 1-16, 1-28 and 1-40 in aqueous *medium* confirm that these peptides assume disordered conformations, but the addition of sodium dodecyl sulfate to the solutions of β-amyloid fragments induces different effect on the peptide folding. While the presence of micelles induces only modest structural rearrangement of the shorter and more hydrophilic peptide 1-16 (Figure 30), the binding with SDS strongly affects the structures of longer peptides. As shown below, amyloid-β peptides 1-28 and 1-40 when are trapped by the micellar structures are subjected to an α-helical transition, resulting in only one helix for Aβ(1-28) and two vicinal helixes for the full-length peptide.

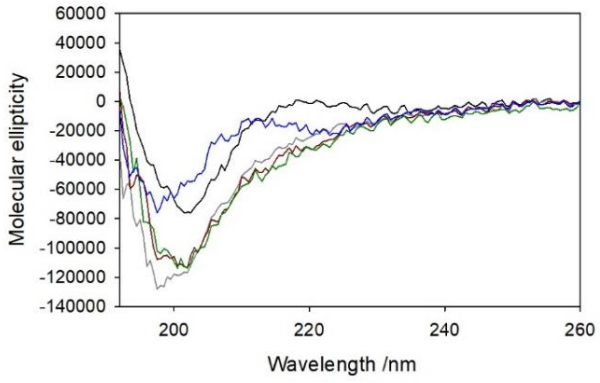

Figure 30. *CD spectra recorded in 5 mM phosphate buffer solution pH 7.4 of $Aβ_{16}$ (5.5 μM) (black trace) and after the addition of: 5 (grey), 10 (brown), and 20 mM SDS (green), and upon the binding with Cu^{II} (5 μM, blue). (cell path 1 cm)*

Figure 30 shows a characteristic profile with two minimal points at 208 and 222 nm that underlines a partial helical conformation: the length of hydrophobic *C*-terminus determines the extension of helical conversion, explaining the

different CD signal intensity of amyloid-β 1-28 and 1-40. The minor effect evidenced on the β-amyloid peptide (1-16) is due to its hydrophilic nature, corresponding to the extracellular *N*-terminal portion of the full-length peptide. This result suggests that only the presence of the hydrophobic *C*-terminal domain can drive the structural transition in Aβ. It is also clear that there is a negligible effect of the membrane environment on the copper-peptide binding affinity: *N*-terminal binding site is located outside the micelles and is therefore available to bind the metal through the previously described coordination sphere. As suggested by the reactivity of copper complexes with amyloid, prion and synuclein fragments in micellar *medium*, the redox activity is almost completely quenched only in the cases of Cu-PrP and Cu-αSyn (see below). Indeed, the high stability of copper(I) complex can be allowed through the binding of two vicinal methionines, M_{109} and M_{112}, that stabilizes the reduced form and prevents the interaction with dioxygen. Moreover, $PrP_{76\text{-}114}$ peptide is able to enrich its coordination sphere via one histidine comprised between the two Met residues, H_{111}. Several studies have suggested the imidazole group of histidine 111 as highest affinity residue for copper(II) binding. During the redox cycling of copper, the metal center is easily trapped by this strong ligand as soon as the reduced species is stabilized and the peptide does not require to undergo any significant conformational change. Far-UV CD spectra in the presence of either amyloid-β and prion peptides bound to copper(I) were also performed (Figure 31, 32, and 33). CD measurements of $Aβ_{1\text{-}28}$, $Aβ_{1\text{-}40}$ and $PrP_{76\text{-}114}$ (1.1 equiv.) peptides complexed with copper(I) (1 equiv.) and trapped in the micellar environment were obtained. At first, the spectrum of each peptide was recorded in only 5 mM phosphate buffer solution at pH 7.4 and in SDS (20 mM). CD curves in the presence of Cu^+ ions were anaerobically obtained by reduction of copper(II) nitrate (1 equiv.) by hydroxylamine (2 equiv.). In the experimental data obtained on $Aβ_{40,}$ Cu^I was re-oxidized to copper(II) through O_2 saturation. CD measurements were made with a 1 cm path-length cell, a scanning rate of 50 nm/min and at least 10 accumulations.

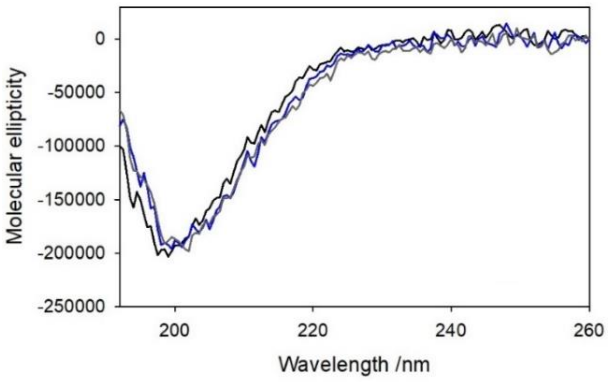

	α	β	Turn	Random
$PrP_{76\text{-}114}$	-	34%	-	66%
+ SDS	-	50%	-	50%
+ Cu^I	-	52%	-	43%

Figure 31. *CD spectra recorded in 5 mM phosphate buffer solution pH 7.4 of $PrP_{76\text{-}114}$ (5.5 μM, blue spectrum) after the addition of 20 mM SDS (blue) and Cu^I (5 μM) (grey). Copper(I) was generated in situ by reaction of copper(II) nitrate (5 μM) and hydroxylamine (10 μM) anaerobically. (cell path 1 cm)*

The *N*-terminal prion region is characterized by a flexible and disordered conformation in aqueous *medium* and almost any structural rearrangement is induced by anionic micelles. The interaction [Cu^I-$PrP_{76\text{-}114}$]-micelle and the quenching of Cu redox cycle may be associated with the restricted structural rearrangement of prion peptide that is required to bring copper ion to the main catalytic coordination sphere. Similar results were previously obtained with another prion fragment, $PrP_{91\text{-}115}$, adjacent to the α-helix structured region 115-127, in the presence of copper(II). Even with larger PrP fragment encompassing the α-helix, such as $PrP_{91\text{-}127}$, copper binding has no effect in the CD measurements, suggesting that the hydrophobic region is not affected by the metal coordination. At the same time, copper(I) binding site, comprised between Met_{109} and Met_{112}, is located in the disordered region outside the structured portion of the peptide and therefore, it is not influenced by the presence of lipid layers.

When the experimental data were collected on Aβ peptides 1-28 and 1-40, an evident structural change into α-helical conformation upon the interaction with SDS micelles is observed. In fact, it is commonly accepted that amyloid-β 1-40 adopts a disordered structure in aqueous solution, while two helical segments (15-25 and 29-35) separated by an unstructured loop are observed in the presence of surfactant. The CD spectrum of monomeric $Aβ_{40}$ in aqueous environment displays a typical random coil signal with a minimum around 198 nm, while in the presence of micellar structures, the amyloid transition into an α-helical conformation with characteristic minima around 208 and 222 nm is detected.[6]

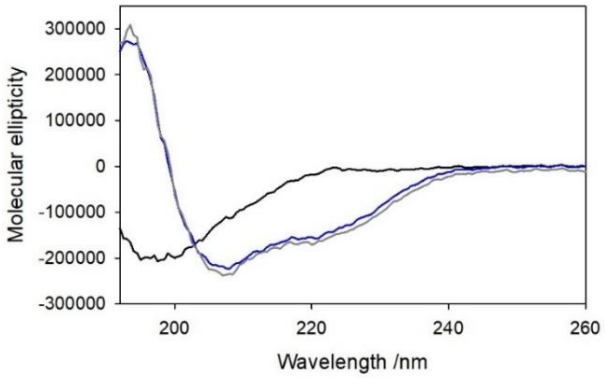

	α	β	Turn	Random
$Aβ_{28}$	-	35%	17%	47%
+ SDS	23%	49%	-	28%
+ Cu^{I}	26%	45%	-	29%

Figure 32. *CD spectra were recorded in 5 mM phosphate buffer solution pH 7.4 of $Aβ_{28}$ (5.5 μM) (black spectrum), after the addition of 20 mM SDS (blue) and Cu^{I} (5 μM) (grey). Copper(I) was generated as previously described.*

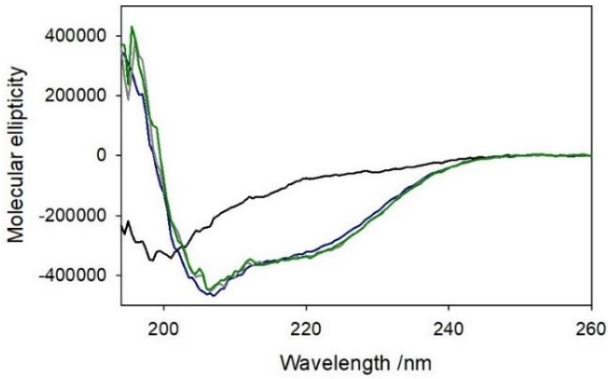

	α	β	Turn	Random
$Aβ_{40}$	-	45%	8%	47%
+ SDS	16%	54%	-	30%
+ Cu^{I}	18%	53%	-	29%
+ Cu^{II}	18%	54%	-	28%

Figure 33. *CD spectra were recorded in 5 mM phosphate buffer solution pH 7.4 of $Aβ_{40}$ (4.4 μM, dissolved in H_2O milliQ + 0.02% v/v NH_3) (black spectrum), after the addition of 16 mM SDS (blue), Cu^{I} (4 μM) (grey) and Cu^{II} (green). Copper(I) was oxidized to copper(II) by O_2 saturation.*

The CD profiles exhibited by the two longer peptides are similar, but, as expected, the CD intensity corresponding to the helical folding is higher for $Aβ_{40}$, since $Aβ_{28}$ only contains the first of the two helices. Therefore, $Aβ_{40}$ *C*-terminus is able to interact with lipid bilayers, influencing the permeability properties of neuronal membrane. The polar *N*-terminal region (1-16) is located outside the membrane-like environment and maintains the ability to interact with copper without destabilization of α-helical arrangement. CD spectra in Figure 33 confirm the CD signal of Cu^{I} and Cu^{II} complexes of $Aβ_{28}$ and $Aβ_{40}$ overlap the one of the corresponding free peptides. This is also verified by the same binding constants of $Aβ_{40}$ for Cu^{II} in absence and presence of SDS micelles (K_D ~ 0.6 μM). In conclusion, the binding of Aβ to neuronal membranes does not involve the *N*-terminal region and does not compromise the *N*-terminus's ability to bind metal ions or to generate ROS.[6]

Far-UV and Near-UV Circular Dichroism (CD) of ternary complexes in membrane

In this section, the structural characterization by CD spectroscopy of the interaction between prion and amyloid peptides was performed in order to fortify the results obtained by kinetic analysis. As discussed in the previous section, each peptide assumes an unstructured conformation in aqueous *medium* and the same behavior is maintained in the presence of both $PrP_{76\text{-}114}$ and $A\beta_{40}$ at 1:1 molar ratio. When copper(II) is added, a partial structuring of the complex generated by two peptides is observed, suggested by the reduced intensity of CD signal around 200 nm (Figure 34). Analogous result was obtained in micellar environment (Figure 35) but these slight conformational changes were not observed in the corresponding binary adducts. At the same time, an increase in the signal at 222 nm and a decrease in the peak around 208 nm are evidenced when copper ions are bound to PrP-Aβ adduct and this behavior is maintained in all experiments performed with the three different-length peptides, Aβ 1-16, 1-28 and 1-40. The CD spectra confirm that the structural rearrangement is independent from the conformation of the hydrophobic domain but is influenced by copper coordination environment. The binding with copper(II) ions and prion fragments 76-114 was well-characterized: this region is able to interact with 4 equiv. of copper(II) and each site can be described as an independent one. Imidazole is the main metal ligand besides the deprotonation and interaction with amide groups at physiological pH. Comparing with the data obtained on PrP(84-114), the potentiometric and visible data suggest the existence of a cooperative metal binding between histidines of the *octarepeat* region and the two His outside the OR, focusing the attention on the high affinity copper binding site located on histidine 111.[20a] The metal binding in Aβ peptide occurs in the *N*-terminal region and therefore, the small peptide 1-16 is usually assumed as an optimal model to study the metal binding in the full-length protein. Some studies suggest a possible competition between the binding of copper(II) ions mediated by His residues and the involvement of amino terminus.

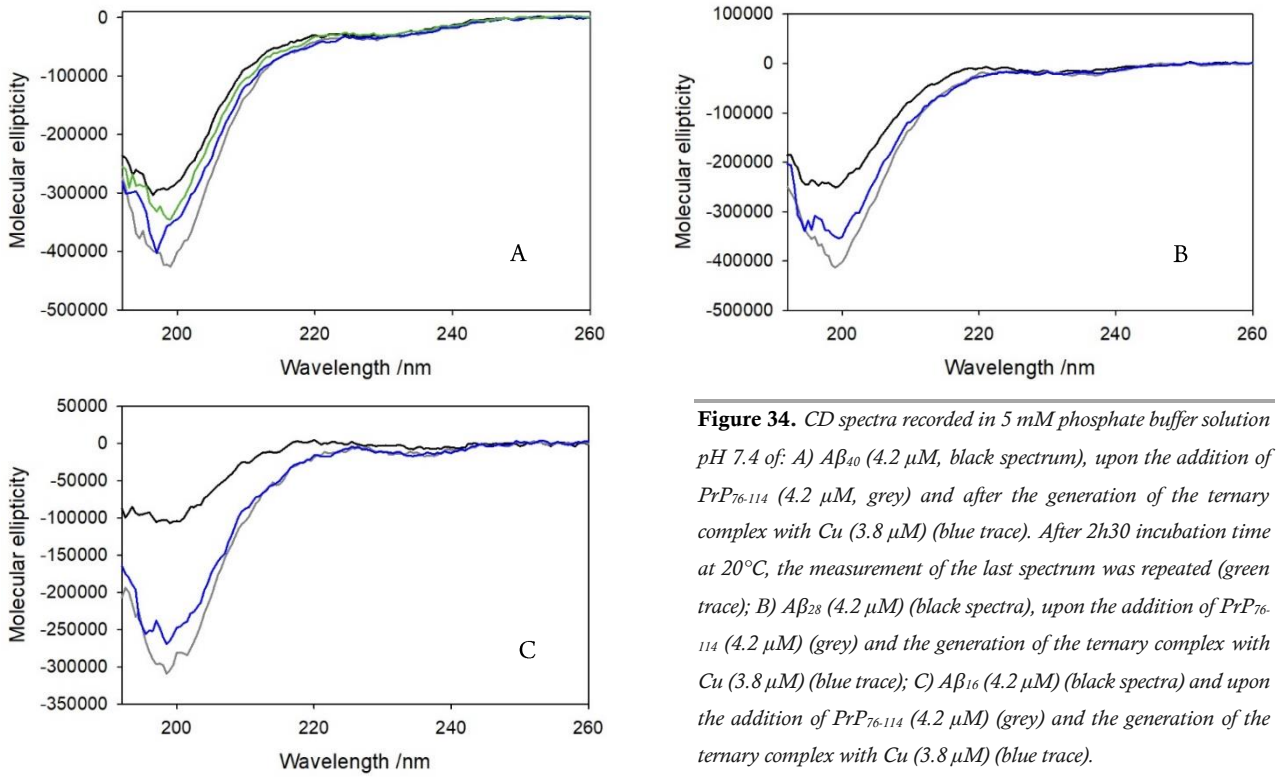

Figure 34. *CD spectra recorded in 5 mM phosphate buffer solution pH 7.4 of: A) $A\beta_{40}$ (4.2 μM, black spectrum), upon the addition of $PrP_{76\text{-}114}$ (4.2 μM, grey) and after the generation of the ternary complex with Cu (3.8 μM) (blue trace). After 2h30 incubation time at 20°C, the measurement of the last spectrum was repeated (green trace); B) $A\beta_{28}$ (4.2 μM) (black spectra), upon the addition of $PrP_{76\text{-}114}$ (4.2 μM) (grey) and the generation of the ternary complex with Cu (3.8 μM) (blue trace); C) $A\beta_{16}$ (4.2 μM) (black spectra) and upon the addition of $PrP_{76\text{-}114}$ (4.2 μM) (grey) and the generation of the ternary complex with Cu (3.8 μM) (blue trace).*

Anyway, although the binding affinities of copper(II) ions with prion and amyloid peptides are not clearly characterized, we can assume for Cu(II)-$A\beta_{16}$ a logK around 10.3[20b] and for Cu(II)-$PrP_{76\text{-}114}$ 14.3, suggesting the

involvement of prion as main coordinative environment for copper ions.

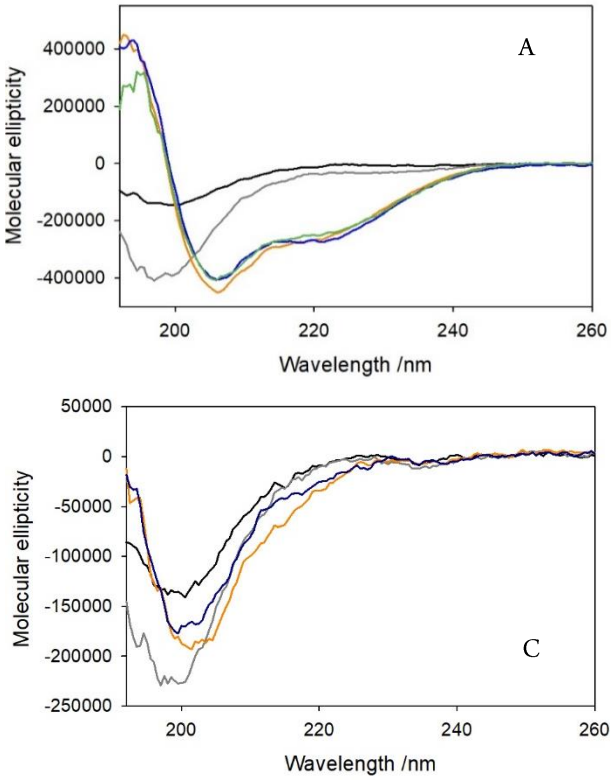

Figure 35. *CD spectra were recorded in 5 mM phosphate buffer solution pH 7.4 of: A) PrP_{76-114} (3.64 μM) (black spectra, 1.1 equiv.) and upon the addition of $Aβ_{40}$ (3.64 μM, 1.1 equiv.) (grey); B) PrP_{76-114} (4.2 μM, 1.1 equiv.) (black spectra) and upon the addition of $Aβ_{28}$ (4.2 μM, 1.1 equiv.) (grey); C) PrP_{76-114} (4.2 μM, 1.1 equiv.) (black spectra) and upon the addition of $Aβ_{16}$ (4.2 μM, 1.1 equiv.) (grey). SDS (20 mM, orange) and 1 equiv. of copper(II) (blue) was then added to the solutions. When in the presence of $Aβ_{40}$, the spectra after 2h30 at 20°C was also recorded (green trace).*

The halfway behavior of the ternary complex supports an interaction between the two peptides modulated by the coordination of copper, probably involving both peptides in the metal binding. The characterization of the coordination of metal ions in the ternary complex of Cu^{II}-$Aβ_{40}$-PrP_{76-114} was also investigated by CD spectroscopy in the near UV-vis region. It was necessary to keep rather high concentration of each peptide bound to copper(II) to allow a sufficient intensity of signals. Unfortunately, the scarcely soluble amyloid 1-40 peptide, at a concentration of 92.5 μM (1.1 equiv.) and in the presence of 1 equiv. of copper(II) forms a massive precipitate.

However, the further addition to the complex of SDS was able to dissolve the highly insoluble complex and on this mixture was registered the CD spectrum. The Figure 36 shows some peculiar features about the coordination of copper(II): a dichroic peak around 300-320 nm, shown as negative signal, would corresponds to the amide-Cu^{II} *ligand-to-metal charge-transfer bands* (LMCT). It was previously reported the same signal generated by the interaction between copper and smaller peptides, such as $Aβ_{16}$ and a prion fragment containing only one octarepeat, but with a positive orientation.[20c]

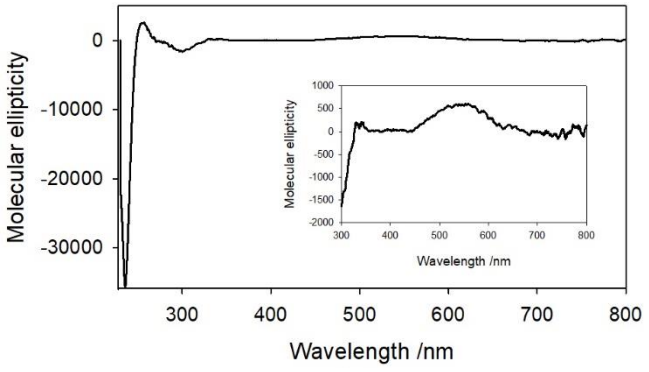

Figure 36. *CD spectrum in the near-UV/Vis region of the ternary complex Cu^{II}-$Aβ_{40}$-PrP_{76-114} in 5 mM phosphate buffer containing 20 mM SDS.*

The same signal is also visible as positive peak in the presence of binary complexes. Therefore, these data suggest a possible involvement in the copper coordination into the ternary adduct of the high affinity region outside the *octarepeat* sequence of prion, where three histidines of prion sequence and another one from amyloid peptide would bind copper ion.

Electron paramagnetic resonance (EPR) spectra of the ternary complex [Cu-Aβ$_{40}$-PrP$_{76-114}$]

The role of copper ions in the interaction between prion and amyloid-β was further analyzed by electron paramagnetic resonance experiment. The data were collected using a Bruker ECS106 spectrometer setting the microwave frequency at 9.28 GHz and a microwave power of 10.06 mW. All data were recorded with a sweep width of 1900 G and 20 scans were used to register each spectrum. The temperature was set at 132.8 K and the sample was prepared in 5 mM phosphate buffer solution pH 7.4 and glycerol (10% v/v) to avoid the expansion of SDS upon freezing. Firstly, the copper binding to amyloid sequence was investigated and Aβ$_{40}$ peptide (1.1 equiv., 0.41 mM) was added to the solution of copper(II) (1 equiv., 0.37 mM) (Figure 37, orange trace). Then, the addition of 1.1 equiv. of PrP(76-114) induces a shift of the EPR signal, providing a further evidence for the formation of the ternary adduct (Figure 37, blue trace). Finally, SDS (19 mM) was added to mimic the membrane *medium* (Figure 37, grey trace). The EPR parameters calculated for Cu^{II}-Aβ$_{40}$ are the following: $g_{\parallel} = 2.28(0)$, $A_{\parallel} = 170\times10^{-4}$ cm^{-1}, $g_{\perp} = 2.06$. These calculations are similar to the data reported in the literature, in which copper(II) ions are bound to the *N*-terminus of amyloid-β peptide. When PrP$_{76-114}$ is added to the mixture, the shift in these values supports a major contribution of prion ligands in the copper coordination environment ($g_{\parallel} = 2.27(0)$, $A_{\parallel} = 179\times10^{-4}$ cm^{-1}, $g_{\perp} = 2.06$). The data obtained in aqueous and micellar environment ($g_{\parallel} = 2.27(7)$, $A_{\parallel} = 175\times10^{-4}$ cm^{-1}, $g_{\perp} = 2.06$) suggest that the main coordinative ligands probably are histidine residues of prion peptide and there could be a participation of amyloid peptide via an additional histidine

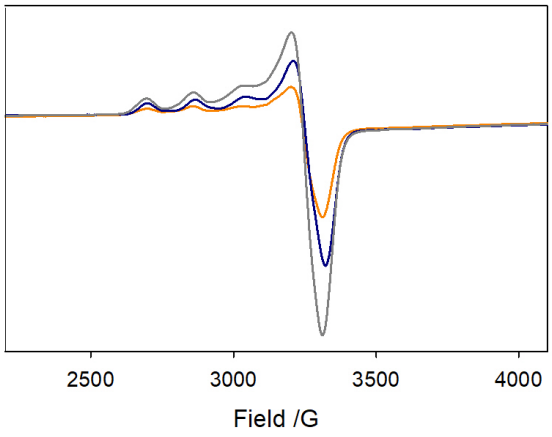

Figure 37. *EPR spectra recorded in 5 mM phosphate buffer solution pH 7.4 of the binary complex Cu (0.37 mM)-Aβ$_{40}$ (0.41 mM) (orange spectrum) and upon the addition of PrP$_{76-114}$ (0.41 mM) (blue). SDS (19 mM) was added to the ternary complex (grey).*

NMR quantification of 4-methylcatechol consumption

In order to assay the different behavior in the catalytic cycle of copper-peptide complexes in aqueous or membrane environment, the determination of the amount of reacted MC was also performed via Nuclear Magnetic Resonance (NMR). The experimental conditions were maintained like those used in the kinetic data: all spectra were recorded in 5 mM HEPES buffer at pH 7.4 and 20 °C, using the CH_2-group bound to sulfonic group as the standard signal to quantify the aromatic signals of catechol (Figure 38). The decrease in the intensity of 4-MC (3 mM) signals upon oxidation was studied in the presence of copper(II) nitrate (25 μM) in aqueous *medium* and SDS (20 mM) and upon the addition of the following fragments (25 μM): Aβ$_{16}$, Aβ$_{28}$, Aβ$_{40}$ and PrP$_{76-144}$. The spectrum corresponding to the *zero time* were obtained after 5 min from the mixing of the reactants, which is the time required to register the spectrum. The acquisition was repeated every 30 min until 150 min reaction time. In order to overcome the low availability of dioxygen in the NMR tube, the reaction was carried out in an open vial and transferred to the NMR tube prior to each spectral acquisition. All measurements were performed at least in duplicate.

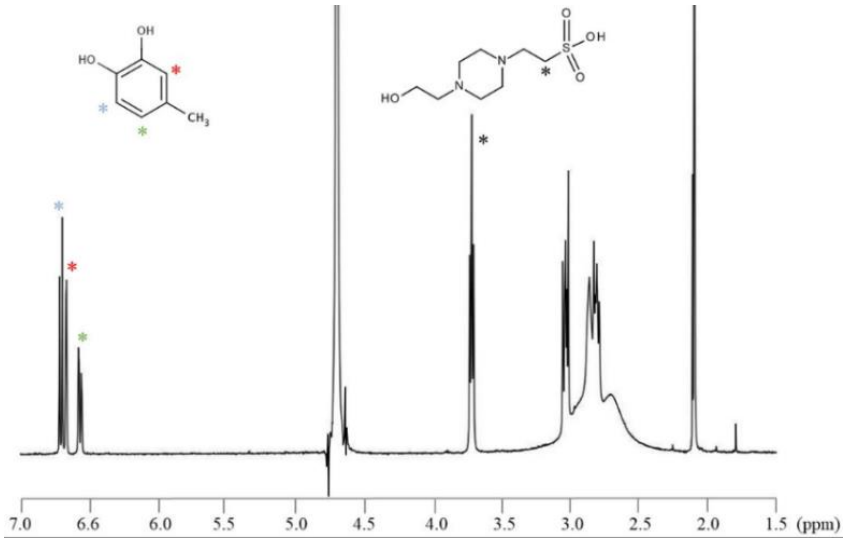

Figure 38. *Proton NMR spectrum of 4-MC (3 mM, dissolved in D_2O) in HEPES buffer (5 mM) pH 7.4 at 20 °C. The HEPES buffer signal of the CH_2–group bound to sulfonic acid group (*) was used as internal standard.*

Free copper(II), in aqueous and membrane environment

The reference data were obtained following the oxidation of methylcatechol catalyzed by copper(II) alone in the aqueous solution and in the presence of SDS. Also in this experiment, the addition of ammonia (10% v/v) was useful in order to dissolve $A\beta_{40}$ and to avoid its aggregation. MC consumption promoted by free copper alone and in the presence of ammonia follows the same trend (Table 1 and Table 2), confirming that the addition of base does not influence the reaction rate. It was also confirmed that the presence of sodium dodecyl sulfate in the mixture containing free copper(II) as catalyst does not influence the resulting reactivity.

Table 1. *NMR quantification of remaining catechol with time by copper(II) (25 μM) in only buffer and in the presence of SDS (20 mM). *Δ[MC] is concentration of consumed MC after 30 min or 2h30.*

Time	**Cu^{II} (mM)**	**Cu^{II}-SDS (mM)**	
t_0	3.000 ± 0.001	2.975 ± 0.025	
30 min	2.825 ± 0.005	2.800 ± 0.001	Δ[MC]* ↓6%
1h	2.655 ± 0.065	2.725 ± 0.015	
1h30	2.565 ± 0.055	2.540 ± 0.030	
2h	2.450 ± 0.040	2.455 ± 0.005	
2h30	2.375 ± 0.005	2.315 ± 0.035	Δ[MC]* ↓22%

Table 2. *NMR quantification of remaining MC with time by only copper(II) (25 μM) in buffer and SDS medium, upon the addition of NH_3 (10% v/v). *Δ[MC] is concentration of consumed MC after 30 min or 2h30.*

Time	**Cu^{II} /NH_3 (mM)**	**Cu^{II}/NH^3-SDS (mM)**	
t_0	3.000 ± 0.001	3.000 ± 0.001	
30 min	2.825 ± 0.025	2.910 ± 0.030	Δ[MC]* ↓4-5%
1h	2.735 ± 0.025	2.730 ± 0.001	
1h30	2.630 ± 0.040	2.590 ± 0.010	
2h	2.445 ± 0.035	2.420 ± 0.010	
2h30	2.333 ± 0.030	2.370 ± 0.010	Δ[MC]* ↓22%

Copper(II)-peptide complexes, in aqueous and membrane environment

The same experimental procedure was maintained for each quantification of consumed 4-methylcatechol catalyzed by copper(II)-peptide complexes and a comparative study between the redox reactivity evidenced in the kinetic data and in NMR spectra was performed and the results are reported in Table 3, 4, 5 and 6. The purpose of this study was to obtain additional information about the interaction and the consumption of substrate compared to the oxidative capability of the complexes and the modification susceptibility of the peptide chains.

Table 3. *NMR quantification of remaining catechol by Cu^{II}-PrP_{76-114} complex (25 μM) in buffer and upon the addition of SDS (20 mM). *Δ[MC] is concentration of consumed MC after 30 min or 2h30.*

Time	[**PrP_{76-114}-Cu^{II}**] (**mM**)		[**PrP_{76-114}-Cu^{II}**] **-SDS (mM)**	
t_0	2.553 ± 0.023		3.000 ± 0.001	
30 min	2.357 ± 0.063	Δ[MC]* ↓21%	2.930 ± 0.010	Δ[MC]* ↓2%
1h	2.170 ± 0.110		2.830 ± 0.030	
1h30	1.880 ± 0.030		2.730 ± 0.030	
2h	1.547 ± 0.077		2.670 ± 0.010	
2h30	1.330 ± 0.060	Δ[MC]* ↓56%	2.585 ± 0.015	Δ[MC]* ↓14%

Table 4. *NMR quantification of remaining catechol by Cu^{II}-$Aβ_{16}$ complex (25 μM) in buffer and upon the addition of SDS (20 mM). *Δ[MC] is concentration of consumed MC after 30 min or 2h30.*

Time	[**$Aβ_{16}$-Cu^{II}**] (**mM**)		[**$Aβ_{16}$-Cu^{II}**] **-SDS (mM)**	
t_0	2.985 ± 0.015		3.000 ± 0.001	
30 min	2.655 ± 0.015	Δ[MC]* ↓11%	2.960 ± 0.020	Δ[MC]* ↓1%
1h	2.510 ± 0.001		2.820 ± 0.050	
1h30	2.380 ± 0.001		2.660 ± 0.001	
2h	2.215 ± 0.035		2.500 ± 0.010	
2h30	1.975 ± 0.015	Δ[MC]* ↓34%	2.400 ± 0.010	Δ[MC]* ↓20%

Table 5. *NMR quantification of remaining catechol by Cu^{II}-$Aβ_{28}$ complex (25 μM) in buffer and upon the addition of SDS (20 mM). *Δ[MC] is concentration of consumed MC after 30 min or 2h30.*

Time	[**$Aβ_{28}$-Cu^{II}**] (**mM**)		[**$Aβ_{28}$-Cu^{II}**] **-SDS (mM)**	
t_0	2.965 ± 0.035		3.000 ± 0.001	
30 min	2.800 ± 0.070	Δ[MC]* ↓7%	2.940 ± 0.001	Δ[MC]* ↓2%
1h	2.595 ± 0.015		2.875 ± 0.015	
1h30	2.420 ± 0.010		2.795 ± 0.025	
2h	2.295 ± 0.035		2.660 ± 0.010	
2h30	2.075 ± 0.025	Δ[MC]* ↓31%	2.510 ± 0.010	Δ[MC]* ↓16%

Table 6. *NMR quantification of remaining catechol by Cu^{II}-$Aβ_{40}$ complex (25 μM) in buffer and upon the addition of SDS (20 mM). *Δ[MC] is concentration of consumed MC after 30 min or 2h30.*

Time	[**$Aβ_{40}$-Cu^{II}**]/**NH_3** (**mM**)		[**$Aβ_{40}$-Cu^{II}**]/**NH_3** **-SDS (mM)**	
t_0	3.000 ± 0.001		3.000 ± 0.001	
30 min	2.780 ± 0.020	Δ[MC]* ↓7%	2.955 ± 0.005	Δ[MC]* ↓1.5%
1h	2.700 ± 0.030		2.835 ± 0.005	
1h30	2.525 ± 0.005		2.720 ± 0.050	
2h	2.350 ± 0.001		2.605 ± 0.075	
2h30	2.160 ± 0.040	Δ[MC]* ↓28%	2.495 ± 0.055	Δ[MC]* ↓17%

Summarizing the NMR data (see Table 7 and Figure 39), the prion fragment 76-114 complexed with copper ions shows a rather high oxidative capability such as the catalysis observed in the presence of the smaller amyloid fragment. In particular, the redox reactivity of each amyloid fragment bound to the metal is tightly correlated to the peptide length and the order of catalytic capability in absence of micelles can be schematized as follows: Cu-Aβ_{16} ≥ Cu-Aβ_{28} ≥ Cu-Aβ_{40}. The opposite trend evidenced in the UV-visible studies is probably due to the absorption of all oxidation products that contribute to an increase of reaction rate and partially hide the growth of DAQ band. Anyway, the steric hindrance of the hydrophobic *C*-terminus of Aβ_{40} compared to the smaller Aβ_{16} disfavors the interaction [substrate-Cu-peptide] and decreases the efficiency of catalysis, as NMR data suggest.

Table 7. *Selected comparative data on MC oxidation, turnover number (TON), and molar ratio of oxidized catechol vs. modified endogenous peptide, by Cu^{II}-peptide complexes, after 30 and 90 min reaction time, in aqueous buffer and in SDS micelles. The expression Δ[MC]/Δ[peptide] represents the ratio between the number of molecules of catechol oxidized vs. the fraction of endogenous peptide undergoing chemical modification at the given time.*

	30 min reaction time			**90 min reaction time**		
Complex	Δ[MC] (mM)	TON	$\frac{\Delta[\boldsymbol{MC}]}{\Delta[\boldsymbol{peptide}]}$	Δ[MC] (mM)	TON	$\frac{\Delta[\boldsymbol{MC}]}{\Delta[\boldsymbol{peptide}]}$
Buffer						
Cu^{II}-Aβ_{16}	0.33	13	38	0.61	24	37
Cu^{II}-Aβ_{28}	0.17	7	17	0.55	22	28
Cu^{II}-Aβ_{40}	0.21	8	18	0.48	19	32
Cu^{II}-PrP_{76-114}	0.20	8	24	0.67	27	62
SDS micelles						
Cu^{II}-Aβ_{16}	0.04	2	17	0.34	14	68
Cu^{II}-Aβ_{28}	0.06	2	10	0.20	8	21
Cu^{II}-Aβ_{40}	0.05	2	-	0.28	11	-
Cu^{II}-PrP_{76-114}	0.07	3	13	0.27	11	37

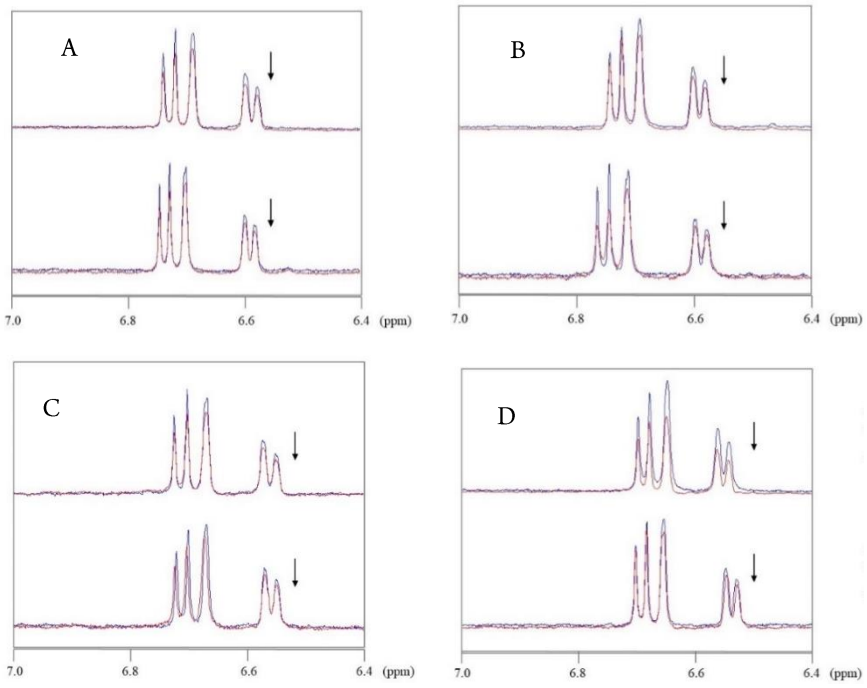

Figure 39. *Partial ^1H NMR spectra (7.0 to 6.4 ppm) of 4-MC aromatic region show catechol consumption with time (blue spectra, t_0, 3 mM) in 5 mM HEPES buffer pH 7.4 by the following complexes: [Cu^{II}-Aβ_{16}] (panel A), [Cu^{II}-Aβ_{28}] (panel B), [Cu^{II}-Aβ_{40}] (panel C) and [Cu^{II}-PrP_{76-114}] (panel D) (25 μM) in aqueous and SDS environment (20 mM). Red spectra correspond to 4-MC peaks after reaction time of 2h30.*

In the presence of sodium dodecyl sulfate above its CMC, a strong quenching of Cu-prion reactivity and a decrease of the reaction promoted by copper-amyloid adducts are observed. While the reactivity of free copper(II) remains unaltered, the cycling of Cu^{II}-PrP_{76-114} is almost totally quenched, although both UV-visible and NMR studies suggest a not totally unreactive system. Moreover, these data highlight a biphasic trend in the oxidative reaction, in which at short reaction time the oxidation of catechol proceeds with a higher rate but decreases with progress of time. This result is explained through oxidative modifications undergone by the peptide backbone, that alters the catalytic efficiency of the complex and also influences its stability in micelle.

Effect of membrane on the oxidative modification rate of neuronal peptides

Identification and characterization of modified peptides by HPLC-ESI/MS.

A wide variety of dangerous reactive species able to modify the normal cellular activity can be generated through the Fenton reaction by enzymatic or non-enzymatic activities, as the previously suggested redox activity of copper bound to neuronal proteins. The term "reactive species" is generically used to indicate a multitude of small molecules which can attach biological structures as lipids, DNA or proteins, resulting in massive structural or chemical modifications. Well-known reactive species are: reactive molecules that includes oxygen atoms (ROS), such as superoxide, hydrogen peroxide or hydroxyl radical, or reactive nitrogen molecules (RNS), as nitric oxide, dinitrogen trioxide, peroxynitrite, and nitroxyl anion.[20d] All these molecules are potentially able to attach some amino acids prone to be oxidized, as methionine and cysteine, due to the high reaction susceptibility of the sulfur group, but also histidine, tyrosine, tryptophan and phenylalanine. These modifications result in protein fragmentation or cross-linkage, structural modification of backbone and further aggregation, changed solubility or enhanced susceptibility to proteolysis, loss of the normal biological activity of the protein.

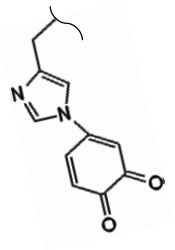

Figure 40. *Chemical structure of covalent adduct generated by the attach of quinone to the imidazole of a His residue.*

Moreover, the covalent oxidative modification of proteins can be mediated either by the direct reaction with the previously-described molecules or by an indirect reaction with secondary biological products obtained in oxidative stress condition. An example can be represented by the oxidative pathway on catecholamines that leads to the release of quinonic species and further oxidative products able to covalently bind nucleophilic amino acids in proteins to give the adduct shown in the Figure 40.

We used mass spectrometry coupled to high performance liquid chromatography (HPLC/MS) to investigate the competition between catechol oxidation and endogenous peptide modification.

Therefore, the modification patterns of β-amyloid and prion peptides in the aqueous and SDS environment were compared. For the samples containing sodium dodecyl sulfate, the removal of the surfactant is necessary in order to perform properly the LC-MS/MS analysis; the precipitation was induced by addition of excess KCl, then samples were immediately cooled for 30 min and centrifuged to separate the precipitated SDS. The modification patterns were studied in presence of both 4-MC and DA. Samples were prepared as follows: copper(II) nitrate (25 μM) or copper(I) (25 μM) were added at the last reagent to a solution containing $Aβ_{16}$/ $Aβ_{28}$ / $Aβ_{40}$/ PrP_{76-114} peptides (50 μM), methylcatechol or dopamine (3 mM) and SDS (0-20 mM) in 50 mM HEPES buffer at pH 7.4. Copper(I) was

generated as described in the UV-visible spectrophotometric kinetic studies. Sulfuric acid was added to quench the reaction (at pH~2) at different reaction times. LC-MS data in micellar environment, obtained by using a LCQ_ADV MAX ion-trap mass spectrometer, were compared with the corresponding analyses performed in aqueous *medium*. The elution was carried out by using 0.1% HCOOH in distilled water (solvent A) and 0.1% HCOOH in acetonitrile (solvent B), with a flow rate of 0.2 ml/min. Elution started with 98% solvent A for 5 min followed by a linear gradient from 98 to 55% A in 65 min. Elution of $A\beta_{40}$ samples was optimized through a linear gradient from 98 to 0% A in 65 min.

Competitive modifications of prion fragment (76-114)

The oxidative modifications and the generation of covalent adducts between the prion sequence and catecholic or quinonic products were studied at several reaction times in the presence of copper(II)/(I) as catalyst in aqueous and membrane-like environment. The main modifications evidenced on prion peptide were mass shifts of +16, +32 and +48 that correspond to the single, double and triple oxidation on His or Met residues, respectively; mass increment indicated as +Cat/+Q represents the covalent addition of catechol or quinone on an imidazole group (Figure 41).

Table 8. *Time-dependent modification of PrP_{76-114} peptide (50 μM) detected by LC/MS analysis upon reaction of Cu^{II} (25 μM)-PrP_{76-114} and 4-MC (3 mM) in HEPES buffer (50 mM) pH 7.4 at 20 °C. Reaction mixtures were quenched with sulfuric acid (pH~2).*

Time	**PrP_{76-114}**	**+16**	**+32**	**+48**	**+MQ**	**+MC**	**+MQ +16**	**+MQ+16 +16**
30 min	**66%**	8% 29min(M/H_{111}) 4%; 32min (H_{85}/H_{96}) 4%	3%	1%	8%	7%	4%	2%
Fragments		*S_{97}.QWNKPSKPKTNMKHM(+32).A_{113}*						*1%*
60 min	**57%**	9% 29min (M/H_{111}) 4%; 32min (H_{85}/H_{96}) 5%	3%	1%	8%	8%	6%	6%
Fragments		-						
90 min	**19%**	13% 29min (M/H_{111}) 3%; 32min (H_{85}/H_{96}) 10%	9%	6%	7%	6%	20%	19%
Fragments		*G.QGGGTH(+16)SQWNKPSKPKTNM(+16)KH(MC)M.A*						*1%*

Comparing the results resumed in Tables 8 and 9, the protective effect of the SDS environment is suggested by the slower modification rate of peptide. However, this effect confirms only partially the results obtained in the kinetic analysis because in that case a stronger quenching was observed. The copper-prion adducts is highly stabilized in the micelle but a small fraction is in an unbound state in equilibrium with the species interacting with SDS.

Table 9. *Time-dependent modification of PrP_{76-114} peptide detected by LC/MS analysis upon reaction of Cu^{II}-PrP_{76-114} and 4-MC in the presence of SDS micelles (20 mM). Reaction mixtures were quenched with sulfuric acid (pH~2). SDS was precipitated after addition of excess KCl and several centrifugation/cooling cycles.*

Time	**PrP_{76-114}**	**+16**	**+32**	**+48**	**+MQ**	**+MC**	**+MQ +16**	**+MQ+16 +16**
30 min	**79%**	9% 29min(M/H_{111}) 6%; 32min (H_{85}/H_{96}) 3%	3%	1%	2%	4%	1%	1%
Fragments		-						
60 min	**71%**	12% 29min (M/H_{111}) 8%; 32min (H_{85}/H_{96}) 3%	5%	2%	3%	4%	2%	1%
Fragments		-						

90 min	**67%**	12% 29min (M/H_{111}) 8%; 32min (H_{85}/H_{96}) 4%	7%	2%	3%	6%	2%	1%
Fragments		-						

Moreover, the stability of the complex is influenced by the percentage of peptide modification that assumes higher values when the peptide is more susceptible to the oxidation if located outside the membrane. In conclusion, the almost total quenching of the oxidative capability of the complex in micellar *medium* is maintained only for a modest timeframe but at long reaction time, the interaction between micelle and prion fragment gets weaker.

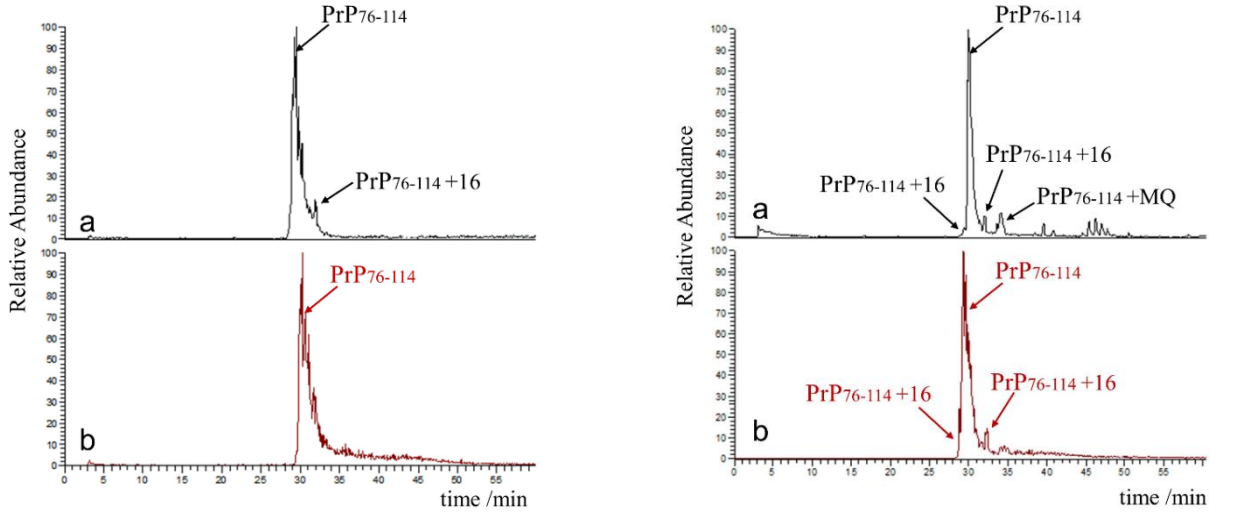

Figure 41. *Right panel) HPLC-MS elution profiles of PrP_{76-114} resulting from the oxidation of 4-MC (3 mM) in 50 mM HEPES buffer pH 7.4 after 30 min reaction time by: a) Cu^{II} (25 μM) and PrP_{76-114} (50 μM); b) Cu^{II} (25 μM) and PrP_{76-114} (50 μM) in presence of SDS (20 mM). Left panel) HPLC-MS elution profiles of PrP_{76-114} peptide resulting from oxidation of DA (3 mM) in 50 mM HEPES buffer pH 7.4 at 60 min reaction time by: a) Cu^{II} (25 μM) and PrP_{76-114} (50 μM); b) Cu^{II} (25 μM) and PrP_{76-114} (50 μM) in presence of SDS (20 mM).*

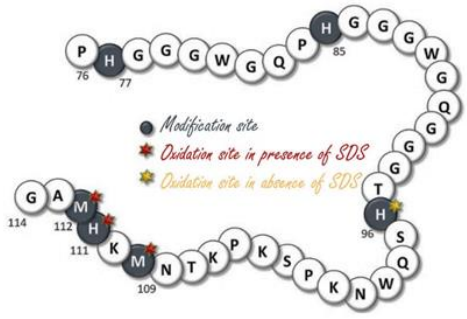

Figure 42. *Schematized chart showing the main modification sites on PrP(76-114) sequence in aqueous medium and in micelle.*

The different pattern of prion modifications is strongly influenced by the environment: a prevalence of *O*-atom insertion on His96 or His85 is observed in aqueous conditions, whereas the oxidation is mainly directed toward the *C*-terminal region of prion (His111, Met109 and Met112) in SDS (Figure 42). These data show the participation of two chemical environments for the coordination of the metal. Therefore, the surfactant acts as a shield toward the main binding site for copper ions, forcing the coordination toward a secondary binding site with low catalytic activity.

The covalent adducts on the peptide sequence are detected at low levels both in the presence of methylcatechol and dopamine. The following data show a similar modification pattern with both substrates (see Table 10 and 11), although the presence of the neurotransmitter dopamine leads to a more difficult interpretation of the chromatograms. Such as 4-methylcatechol, dopamine is a possible source of covalent modification on the peptide and several adducts can be generated. Both catechol and quinone can covalently bind histidine residues, such as the following products, indolequinone and dihydroxyindole. The oxidative pathway leading to the generation of the last chemical compounds follows a two-electron process to convert the catecholamine into quinonic species (see Figure 43). When the dopamine

is in a deprotonated form, the neurotransmitter can undergo a cyclization reaction via the Michael addition and it is converted into the leucodopaminochrome.

This chemical compound can be quickly oxidized respect with the starting catecholamine and a further step corresponding to a two-electron transfer leads to the dopaminochrome. The isomerization reaction of DC leads to 5,6-dihydroxyindole (DHI) and its following oxidation results in the generation of indolequinone (IQ). A disproportionation reaction as the last step produces the respective o-quinone and one molecule of regenerated dopamine.[20e]

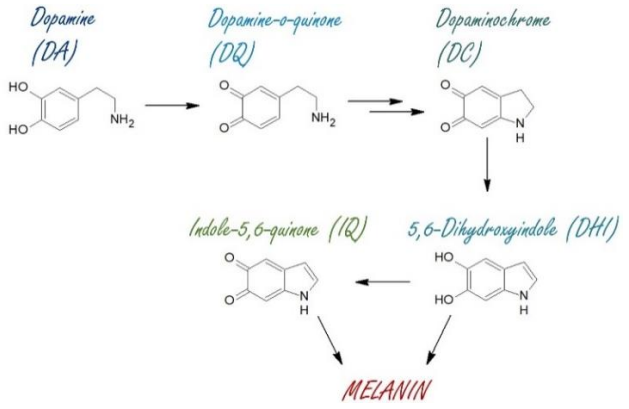

Figure 43. *Schematic oxidation pathway leading to melanins from catecholic substrate as the neurotransmitter dopamine and its relate oxidation products.*

Table 10. *Modification with time of PrP_{76-114} peptide detected by LC/MS analysis upon reaction of Cu^{II}-PrP_{76-114} and DA in HEPES buffer pH 7.4 at 20 °C. Reaction mixtures were quenched with sulfuric acid (pH~2).*

Time	**PrP_{76-114}**	**+16**	**+32**	**+48**	**+DQ**	**+DA**	**+DQ+16**
30 min	**81%**	10% 29min(M/H_{111}) 7%; 32min (H_{85}/H_{96}) 3%	2%	1%	1%	-	1%
		+DQ+32	**+IQ**		**+DHI**	**+IQ+ 16**	**+DHI+16**
		-	1%		-	1%	1%
Fragments	-						
		+16	**+32**	**+48**	**+DQ**	**+DA**	**+DQ+16**
60 min	**75%**	14% 29min (M/H_{111}) 9%; 32min (H_{85}/H_{96}) 5%	5%	2%	1%	1%	1%
		+DQ+32	**+IQ**		**+DHI**	**+IQ+16**	**+DHI+16**
		-	-		1%	-	-
Fragments	-						
		+16	**+32**	**+48**	**+DQ**	**+DA**	**+DQ+16**
90 min	**61%**	19% 29min (M/H_{111}) 10%; 32min (H_{85}/H_{96}) 9%	10%	4%	1%	2%	1%
		+DQ+32	**+IQ**		**+DHI**	**+IQ+16**	**+DHI+16**
		1%	-		1%	-	-
Fragments	-						

Table 11. *Modification with time of PrP_{76-114} peptide detected by LC/MS analysis upon reaction of Cu^{II}-PrP_{76-114} and DA in the same buffer but in presence of SDS micelles. Reaction mixtures were quenched with sulfuric acid (pH~2). Sodium dodecyl sulfate was precipitated after addition of excess KCl and same centrifugation/cooling cycles.*

Time	**PrP_{76-114}**	**+16**	**+32**	**+48**	**+DQ**	**+DA**	**+DQ+16**
30 min	**86%**	5%	3%	1%	-	-	1%
		+DQ+32	**+IQ**		**+DHI**	**+IQ+16**	**+DHI+ 16**
		-	1%		1%	1%	1%
Fragments	-						
		+16	**+32**	**+48**	**+DQ**	**+DA**	**+DQ+16**
60 min	**84%**	7%	2%	1%	1%	1%	1%
		+DQ+32	**+IQ**		**+DHI**	**+IQ+16**	**+DHI+16**
		-	1%		-	1%	1%
Fragments	-						
		+16	**+32**	**+48**	**+DQ**	**+DA**	**+DQ+16**
90 min	**73%**	16%	4%	4%	1%	1%	1%
		+DQ+32	**+IQ**		**+DHI**	**+IQ+16**	**+DHI+16**
		-	1%		1%	1%	-
Fragments	-						

Competitive modifications of amyloid-β fragment (1-16)

A plethora of studies indicates that the concentration of oxidative stress markers is strongly influenced and highly increased in AD-affected brains near Aβ aggregates and neurofibrillary tangles. Neurons show abnormally high amounts of oxidative damages toward proteins, lipids and DNA. Plaques and NFTs associated with the presence of redox-active metals, such as copper, seem to induce severe oxidative stress condition.[2] Therefore, besides the investigation of the redox chemistry and the generation of reactive oxygen species by amyloid-β peptide bound to copper ions, the possible modification of the peptide itself promoted by oxidizing species is also required.

Table 12. *Modification with time of $A\beta_{16}$ peptide detected by LC/MS analysis upon reaction of Cu^{II}-$A\beta_{16}$ and 4-MC in 50 mM HEPES buffer pH 7.4 at 20 °C. Reaction mixtures were quenched with sulfuric acid (pH~2).*

Time	**$A\beta_{16}$**	**+16**	**+32**	**+MQ**	**+MC**	**+MQ+16**
30 min	**65%**	12% 21min (H_6) 1%; 21.5min (Y) 2%; 24 (H_{14}/H_{13}) 9%	5%	6%	6%	4%
Fragments		*D.AEFRHDSGYEVHHQK.- (20-21min)* *-.DAEFRHDSGYEVH.H (27min)*				*1%* *1%*
90 min	**35%**	30% 21min (H_6) 6%; 21.5min (Y) 8%; 24min (H_{14}/H_{13}) 16%	16%	2%	12%	4%
Fragments		*-.DAEFRHDSGYEVH.H (27 min)*				*1%*
180 min	**25%**	37% 21min (H_6) 3%; 21.5min (Y) 22%; 24min (H_{14}/H_{13}) 12%	20%	3%	7%	7%
Fragments		*D.AEFRHDSGYEVHHQK.- (20-21 min)*				*1%*

LC-MS data obtained on Aβ(1-16) and (1-28) are carried out from the relative complexes with copper(II) and (I) in aqueous environment or upon trapping in micellar structures (Table 12, 13 and 14). The same experiments were performed in the presence of 4-methylcatechol and dopamine. The pattern of modification shows a general trend in which SDS plays a strong protective role as can be observed by the higher percentages of unmodified peptide compared to the lower intensity of the unmodified peptide peak in aqueous *medium* (see Figure 44).

Table 13. *Modification with time of $A\beta_{16}$ peptide detected by LC/MS analysis upon reaction of Cu^{II}-$A\beta_{16}$ and 4-MC in the same buffer but in presence of SDS micelles. Reaction mixtures were quenched with sulfuric acid (pH~2). Sodium dodecyl sulfate was precipitated after addition of excess KCl and several centrifugation/cooling cycles.*

Time	**$A\beta_{16}$**	**+16**	**+32**	**+MQ**	**+MC**	**+MQ+16**
30 min	**91%**	2%	1%	1%	1%	3%
Fragments		*D.AEFRHDSGYEVHHQK.- (20-21min)*				*1%*
90 min	**80%**	5% 21min (H_6) 1%; 21.5min (Y) 1%; 24min (H_{14}/H_{13}) 4%	5%	3%	2%	3%
Fragments		*D.AEFRHDSGYEVHHQK.- (20-21min)* *-.DAEFRHDSGYEVH.H (27min)*				*1%* *1%*
180 min	**60%**	13% 21min (H_6) 1%; 21.5min (Y) 3%; 24min (H_{14}/H_{13}) 9%	10%	4%	3%	5%
Fragments		*D.AEFRHDSGYEVHHQK.- (20-21min)* *-.DAEFRHDSGYEVH.H (27min)* *-.DAEFRHDSGYEVHHQ.K +MQ+16 (25min)*				*1%* *1%* *3%*

Table 14. *Modification with time of $A\beta_{16}$ peptide detected by LC/MS analysis upon reaction of Cu^{I}-$A\beta_{16}$ and 4-MC in the same buffer but in presence of SDS micelles. Cu^{I} was generated by reaction between sodium ascorbate (2 equiv.) and Cu^{II} (1 equiv.) anaerobically. Reaction mixtures were quenched with sulfuric acid (pH~2). Sodium dodecyl sulfate was precipitated after addition of excess KCl and several centrifugation/cooling cycles.*

Time	**$A\beta_{16}$**	**+16**	**+32**	**+MQ**	**+MC**	**+MQ+16**
30 min	**96%**	1%	1%	-	-	2%
Fragments		-				
90 min	**83%**	7% 21min (H_6) 1%; 21.5min (Y) 1%; 24min (H_{14}/H_{13}) 5%	3%	1%	2%	2%
Fragments		*-.DAEFRHDSGYEVH.H*				*1%*
		-.DAEFRHDSGYEVHHQ.K +MC+16				*1%*
180 min	**68%**	14% 21min (H_6) 1%; 21.5min (Y) 2%; 24min (H_{14}/H_{13}) 11%	6%	2%	3%	4%
Fragments		*-.DAEFRHDSGYEVHH.Q +MQ+MQ (27min)*				*1%*
		-.DAEFRHDSGYEVHH.Q +MC+MC (25min)				*1%*
		-.DAEFRHDSGYEVH.H				*1%*

The surfactant is able to reduce the modification susceptibility of the peptides toward the oxidative environment, suggesting an important role of neuronal membrane in the cascade of events leading to oxidative stress and to neurodegeneration. The incubation of amyloid peptides was also performed with 0.5 equiv. of reduced copper ions and the protective effect of SDS seems to be slightly more evident compared to the data obtained with copper(II). Moreover, the oxidative modification on amyloid peptide shows a modest rate and strong divergences in the oxidative patterns are visible only upon an appreciable incubation time of the order of half an hour.

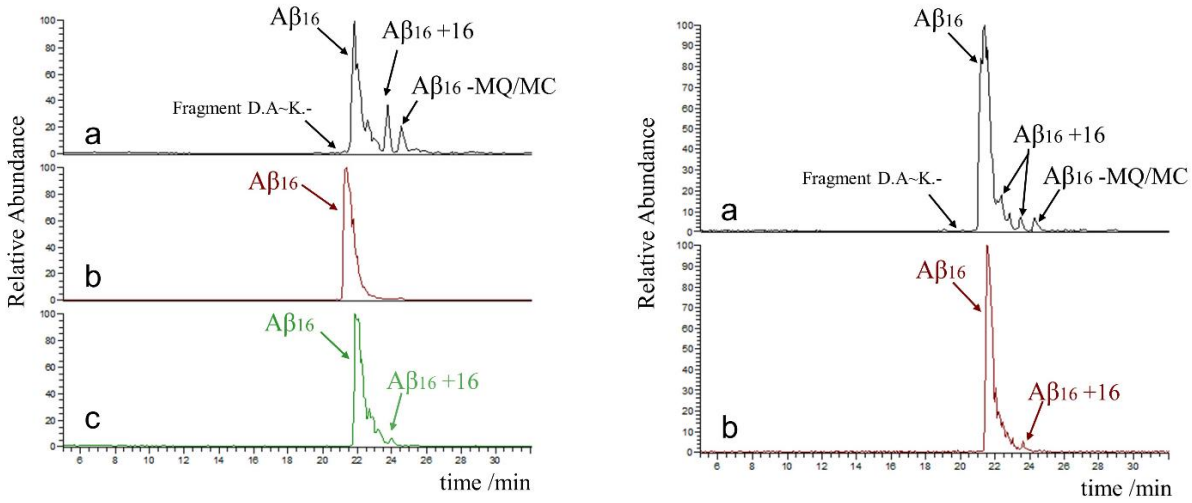

Figure 44. *At left) LC-MS elution profiles of $A\beta_{16}$ peptide resulting from oxidation of 4-MC (3 mM) in 50 mM HEPES buffer pH 7.4 at 30 min reaction time by: a) Cu^{II} (25 μM) and $A\beta_{16}$ (50 μM); b) Cu^{I} (25 μM) and $A\beta_{16}$ (50 μM) in presence of SDS; c) Cu^{II} (25 μM) and $A\beta_{16}$ (50 μM) in presence of SDS. At right) HPLC-MS elution profiles of $A\beta_{16}$ peptide resulting from oxidation of DA (3 mM) in 50 mM HEPES buffer pH 7.4 at 30 min reaction time by: a) Cu^{II} (25 μM) and $A\beta_{16}$ (50 μM); b) Cu^{II} (25 μM) and $A\beta_{16}$ (50 μM) in presence of SDS (20 mM).*

As shown in the kinetic data obtained from the oxidation of dopamine, the oxidation rate and the following generation of reactive species from dopamine is a slower process respect with the related 4-methylcatechol: therefore, the changes in the modification patterns in all conditions are not easy to analyze and longer reaction times are required to highlight the protective effect of SDS micelles (Table 15 and 16).

Table 15. *Modification with time of Aβ16 peptide detected by LC/MS analysis upon reaction of Cu^{II}-Aβ16 and DA in HEPES buffer pH 7.4 at 20 °C. Reaction mixtures were quenched with sulfuric acid (pH~2).*

Time	**$Aβ_{16}$**	**+16**	**+32**	**+48**	**+DQ**	**+DA**	**+DQ+16**
30 min	**73%**	12% 21min (H_6) 3%; 21.5min (Y) – 24min (H_{14}/H_{13}) 9%	5%	3%	-	1%	-
		+DQ+32	**+IQ**		**+DHI**	**+IQ+ 16**	**+DHI+16**
		1%	-		3%	-	-
Fragments		*D.AEFRHDSGYEVHHQK.-*		*2%*			
		+16	**+32**	**+48**	**+DQ**	**+DA**	**+DQ+16**
90 min	**65%**	19% 21min (H_6) 3% 21.5min (Y) 3% 24min (H_{14}/H_{13}) 13%	7%	3%	1%	1%	-
		+DQ+32	**+IQ**		**+DHI**	**+IQ+16**	**+DHI+16**
		2%	-		1%	-	-
Fragments		*D.AEFRHDSGYEVHHQK.-*		*1%*			
		+16	**+32**	**+48**	**+DQ**	**+DA**	**+DQ+16**
180 min	**52%**	20% 21min (H_6) 4%; 21.5min (Y) 4%; 24min (H_{14}/H_{13}) 12%	10%	5%	2%	2%	2%
		+DQ+32	**+IQ**		**+DHI**	**+IQ+16**	**+DHI+16**
		2%	1%		1%	-	-
Fragments		*D.AEFRHDSGYEVHHQK.-* *-.DAEFRHDSGYEVH.H* *-.DAEFRHDSGY(+16)EVH.H*		*1%* *1%* *1%*			

Table 16. *Modification with time of Aβ16 peptide detected by LC/MS analysis upon reaction of Cu^{II}-Aβ16 and DA in the same buffer but in presence of SDS micelles. Reaction mixtures were quenched with sulfuric acid (pH~2). Sodium dodecyl sulfate was precipitated after addition of excess KCl and several centrifugation/cooling cycles*

Time	**$Aβ_{16}$**	**+16**	**+32**	**+48**	**+DQ**	**+DA**	**+DQ+16**
30 min	**80%**	6% 21min (H_6) 1% 21.5min (Y) 2% 24min (H_{14}/H_{13}) 3%	1%	2%	1%	1%	-
		+DQ+32	**+IQ**		**+DHI**	**+IQ+16**	**+DHI+16**
		2%	-		3%	-	-
Fragments		*D.AEFRHDSGYEVHHQK.-* *D.AEFRHDSGYEVH.H +16* *-.DAEFRHDSGYEVH.H*		*1%* *1%* *1%*			
		+16	**+32**	**+48**	**+DQ**	**+DA**	**+DQ+16**
90 min	**70%**	13% 21min (H_6) 2% 21.5min (Y) 4% 24min (H_{14}/H_{13}) 7%	7%	4%	1%	1%	1%
		+DQ+32	**+IQ**		**+DHI**	**+IQ+16**	**+DHI+16**
		-	-		2%	-	-
Fragments		*D.AEFRHDSGYEVHHQK.-*		*1%*			
		+16	**+32**	**+48**	**+DQ**	**+DA**	**+DQ+16**
180 min	**58%**	22% 21min (H_6) 5%; 21.5min (Y) 6%; 24min (H_{14}/H_{13}) 11%	14%	4%	-	2%	-
		+DQ+32	**+IQ**		**+DHI**	**+IQ+16**	**+DHI+16**
		-	-		-	-	-
Fragments		-					

As described in the Introductive section, two histidines, His_6 and His_{13} (or His_{14}), the NH_2-terminus and the carboxyl group of Asp_1 fill the four equatorial positions in the coordination of copper(II) ions, while the Asp_1 side chain acts as axial ligand so as to offer a stable pyramidal coordination with a square planar base around the metal center. Several studies have used the simpler truncated peptide, $Aβ_{16}$, encompassing the first 16 amino acids as model of the full

protein: this highly soluble system is not subjected to aggregation and consists into the region commonly recognized as the main binding site for copper(II), therefore it is accepted as a reliable model of the full protein.

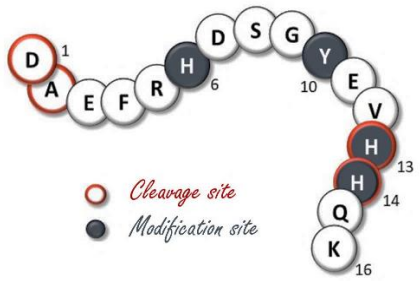

Figure 45. *Schematized chart showing the main modification sites on Aβ(1-16) sequence in aqueous medium and in micelle.*

Considering the copper coordination sphere, the modification pattern is shown in Figure 45. The trend of His_{13} and His_{14} oxidation looks quite similar, in which the residue 14 was hardly detected as the most susceptible to the conversion into 2-oxohistidine. A mass increment of 32 Da with a retention time of 25 minutes was detected and corresponds to the simultaneous oxidation of the two histidines, H_{13} and H_{14}. Negligible oxidation on His_6 is detected but the residue 6 is probably subjected to the covalent addiction of the catechol or quinone to the imidazole side chain.

These results are in agreement with the previous evidences in which His_6 is less prone to oxidation, whereas it is the main target of the reaction with quinones.[3] Anyway, the sites of modification are the same both in the presence and absence of micelles, confirming that the micellar *medium* does not influence the binding site for the metal and therefore, the differences in term of catalytic efficiency and susceptibility of that region to oxidation are not determined by SDS. Besides oxidation and generation of the covalent adduct, peptide sequences are also subjected to fragmentation, usually corresponding to the residues involved in copper coordination. The fragmentation of the amyloid-β 1-16 peptide shows a slightly reduced rate compared to the one of $Aβ_{28}$. Several cleavage sites were mapped in the presence of an oxidant environment and the most susceptible regions were identified as His-13/His-14 domain and the *N*-terminus (Asp-1/Ala-2).

Table 17. *Modification with time of $Aβ_{16}$ peptide detected by LC/MS analysis upon reaction of Cu^{II}-$Aβ_{16}$ and 4-MC in HEPES buffer pH 7.4 and 0.02% ammonia at 20 °C. Reaction mixtures were quenched with sulfuric acid (pH~2).*

Time	**$Aβ_{16}$**	**+16**	**+32**	**+MQ**	**+MC**	**+MQ +16**
30 min	**63%**	20%	6%	3%	5%	2%
Fragments			*D.AEFRHDSGYEVHHQK.-*			*1%*

At last, in order to verify the conditions used for the analysis in the presence of the longer peptide (1-40), it was also studied the effect of NH_3 addition on the peptide modification rate by adding a small percentage of ammonia (0.02% v/v) in the reaction mixture containing the usual concentrations of copper and peptide, which has confirmed no evident changes in the modification patterns (Table 17).

Competitive modification on amyloid-β(1-28) fragment

A similar modification pattern (Table 18, 19, 20 and Figure 46) results from the LC-MS analysis of the longer amyloid-β peptide (1-28) upon the same incubation conditions used for the analysis performed on $Aβ_{16}$. $Aβ_{28}$ peptide consists in a *N*-terminal region, corresponding to $Aβ_{16}$ sequence, that acts as the copper binding site and a more hydrophobic region that has only modest propensity to aggregate but does not mediate any type of relevant interaction with metal. Therefore, the kinetic behavior and the rate of oxidative modification of the peptide is primary determined by the first *N*-terminal region.

Table 18. *Modification with time of Aβ28 peptide detected by LC/MS analysis upon reaction of Cu^{II}-Aβ28 and 4-MC in HEPES buffer pH 7.4 at 20 °C. Reaction mixtures were quenched with sulfuric acid (pH~2).*

Time	**$Aβ_{28}$**	**+16**	**+32**	**+48**	**+MQ**	**+MC**	**+MQ+16**	**+MQ+32**
30m.	**62%**	12% 37.5min (Y) 3%; 38.5min(H_{13}) 2%; 39.5min (H_6) 1%; 40.5min (H_{14}) 6%	4%	3%	6%	5%	3%	1%
Fragments		*D.AEFRHDSGYEVHH(+16)QKLVFFAEDVGSNK.- (35min)*						*2%*
		D.AEFRH(+16)DSGYEVH(+MC)HQKLVFFAEDVGSNK.- (37min)						*2%*
90m.	**21%**	19%	7%	9%	9%	9%	9%	7%
Fragments		*D.AEFRHDSGYEVHHQKLVFFAEDVGSNK.-(+MQ) (42min)*						*3%*
		D.AEFRH(MQ)DSGY(+16)EVH(MQ)H(+16)QKLVFFAEDVGSN.K						*3%*
		Y.EVH(+16)H(+16)QKLVFFAEDVGSNK.- (36min)						*1%*
		D.AEFRHDSGYEVHHQKLVFFAEDVGSN.K (+MQ+MC+16)						*1%*
		-.DAEFRHDSGYEVHHQKLVFFA.E ($H_{13/14}$+16) (41min)						*1%*
		-.DAEFRH(+16)DSGYEVH(MQ)H(+16)QKLVF.F						*1%*
180m	**8%**	26%	13%	15%	7%	7%	8%	12%
Fragments		*H.HQKLVFFAEDVGSNK.- (35min)*						*1%*
		D.AEFRH(MC)DSGY(+16)EVH(MQ)H(MC)QKLVFFAEDVGSN.K						*3%*

Table 19. *Modification with time of Aβ28 peptide detected by LC/MS analysis upon reaction of Cu^{I}-Aβ28 and 4-MC in the same buffer but in presence of SDS micelles. Cu^{I} was generated by reaction between sodium ascorbate (2 equiv.) and Cu^{II} (1 equiv.) anaerobically. Reaction mixtures were quenched with sulfuric acid (pH~2). Sodium dodecyl sulfate was precipitated after addition of excess KCl and several centrifugation/cooling cycles.*

Time	**$Aβ_{28}$**	**+16**	**+32**	**+48**	**+MQ**	**+MC**	**+MQ+16**	**+MQ+32**
30 min	**82%**	3% 37.5min (Y) 2% 38.5min(H_{13}) - 39.5min (H_6) - 40.5min (H_{14}) 1%	3%	1%	2%	2%	2%	1%
Fragments		*D.AEFRHDSGY(+16)EVHHQKLVFFAEDVGSNK.- (35min)*						*2%*
		A.EFRH(+16)DSGYEVH(+16)H(MC)QKLVFFAEDVGSNK.- (36min)						*1%*
		-.DAEFRH(+16)DSGYEVH(MC)H(Q)QKLVF.F (41min)						*1%*
90 min	**70%**	6% 37.5min (Y) 2%; 38.5min(H_{13}) 1%; 39.5min (H_6) 1%; 40.5min (H_{14}) 2%	4%	2%	5%	3%	4%	2%
Fragments		*H.HQKLVFFAEDVGSNK.- (35min)*						*1%*
		-.DAEFRHDSGYEVH(MQ)H(+122).Q						*1%*
		A.EFRHDSGY(+16)EVH(+16)H(MC)QKLVFFAEDVGSNK.-						*1%*
		H.DSGY(+16)EVH(MQ)H(MC)QKLVFFAEDVGSNK.-						*1%*
180 min	**62%**	11% 37.5min (Y) 5%; 38.5min(H_{13}) 2%; 39.5min (H_6) 1%; 40.5min (H_{14}) 3%	4%	3%	5%	3%	4%	2%
Fragments		*H.HQKLVFFAEDVGSNK.- (35min)*						*1%*
		-.DAEFRHDSGYEVH(MQ)H(MC).Q (35min)						*2%*
		D.AEFRHDSGY(+16)EVHHQKLVFFAEDVGSNK.- (35min)						*2%*
		E.FRH(MC)DSGY(+16)EVH(+16)H(+16)QKLVFFAEDVGSNK.-						*1%*

Tables 21 and 22 show the quantification of oxidative and covalent modifications induced by the presence of dopamine, in which the slower oxidation rate of substrate reflects the reduced percentage of modification and fragmentation of peptide sequence. As observed on amyloid-β (1-16) fragment, His at positions 13 and 14 are the major sites undergoing *O*-atom insertion with a slight prevalence of oxidation at His-14 in aqueous *medium*. His-6 remains the main site for quinone/catechol addition. No evidence for the formation of Tyr–Tyr crosslinking has been found, which is in contrast with the LC-MS data obtained upon incubation of these peptides with hydrogen peroxide and heme.

Table 20. *Modification with time of $A\beta_{28}$ peptide detected by LC/MS analysis upon reaction of Cu^{II}-$A\beta_{28}$ and 4-MC in the same buffer but in presence of SDS micelles. Reaction mixtures were quenched with sulfuric acid (pH~2). Sodium dodecyl sulfate was precipitated after addition of excess KCl and several centrifugation/cooling cycles.*

Time	**$A\beta_{28}$**	**+16**	**+32**	**+48**	**+MQ**	**+MC**	**+MQ+16**	**+MQ+32**	
30 min	**77%**	5% (37.5min (Y) 3%)	4%	2%	2%	2%	2%	1%	
Fragments	*D.AEFRHDSGYEVHHQKLVFFAEDVGSNK.- +16 (35min)*								*2%*
	E.FRH(MQ)DSGY(+16)EVH(+16)H(+16)QKLVFFAEDVGSNK.-								*2%*
	D.AEFRHDSGYEVHHQKLVFFAEDVGSNK.-								*1%*
90 min	**62%**	10% 37.5min (Y) 4%; 38.5min(H_{13}) 2%; 39.5min (H_6) 2%; 40.5min (H_{14}) 2%	6%	3%	4%	2%	4%	3%	
Fragments	*-.DAEFRH(MQ)DSGY(+16)EVH(MC)H(+16)QKLVF.F (36min)*								*2%*
	D.AEFRHDSGY(+16)EVHHQKLVFFAEDVGSNK.- (35 min)								*3%*
	A.EFRH(+16)DSGYEVH(+16)H(MC)QKLVFFAEDVGSNK.-								*1%*
180 min	**35%**	10%	8%	9%	4%	3%	8%	6%	
Fragments	*H.HQKLVFFAEDVGSNK.- (35 min)*								*5%*
	A.EFRH(MQ)DSGY(+16)EVH(+16)H(MQ)QKLVFFAED.V								*4%*
	D.AEFRHDSGYEVHHQKLVFFAEDVGSNK.- (+MQ+MQ+MQ+16)								*3%*
	A.EFRHDSGYEVHHQKLVFFAEDVGSNK.- (+MQ+16+16)								*5%*

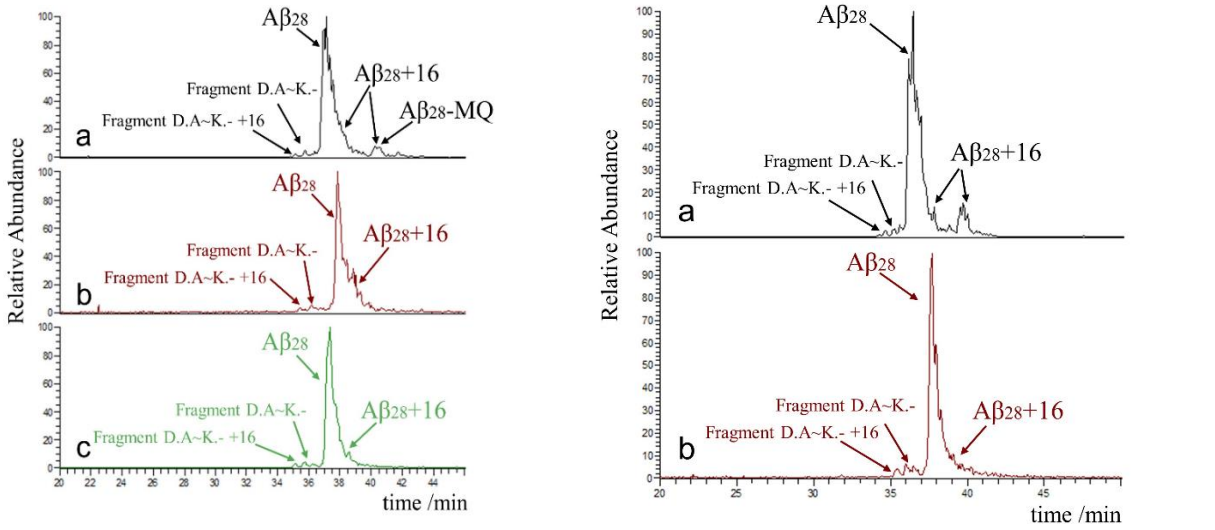

Figure 46. *Left panel) HPLC-MS elution profiles of $A\beta_{28}$ resulting from the oxidation of 4-MC (3 mM) in HEPES buffer (50 mM) pH 7.4 after 30 min reaction time by: a) Cu^{II} (25 μM) and $A\beta_{28}$ (50 μM); b) Cu^{I} (25 μM) and $A\beta_{16}$ (50 μM) in presence of SDS; c) Cu^{II} (25 μM) and $A\beta_{28}$ (50 μM) in presence of SDS (20 mM). Right panel) HPLC-MS elution profiles of $A\beta_{28}$ peptide resulting from oxidation of DA (3 mM) in HEPES buffer (50 mM) pH 7.4 at 90 min reaction time by: a) Cu^{II} (25 μM) and $A\beta_{28}$ (50 μM); b) Cu^{II} (25 μM) and $A\beta_{28}$ (50 μM) in presence of SDS (20 mM).*

Besides the usual types of modifications induced by copper and molecular oxygen, such as oxidation and hydroxylation, and covalent adducts with catechols or quinones, Aβ peptides are also subjected to the fragmentation in recurrent sites, usually corresponding to the metal binding sites. Indeed, specific hydrolysis between Asp1/Ala2 and His13/His14 are recurring. Amino acids have different susceptibility to the oxidative modification; for instance, aromatic residues, such as phenylalanine or tryptophan, are more susceptible than aliphatic ones. The cleavage between Phe19 and Phe20 is also reported, although the identification of the fragments was difficultly quantified (Figure 47).

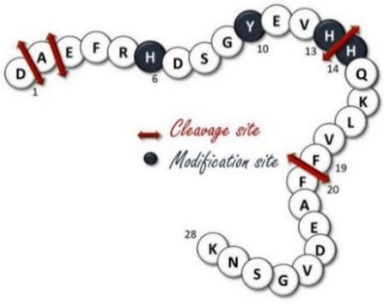

Figure 47. *Schematized chart showing the main modification sites on Aβ(1-28) sequence in aqueous medium and in micelle.*

Table 21. *Modification with time of $A\beta_{28}$ peptide detected by LC/MS analysis upon reaction of Cu^{II}-$A\beta_{28}$ and DA in HEPES buffer pH 7.4 at 20 °C. Reaction mixtures were quenched with sulfuric acid (pH~2).*

Time	**$A\beta_{28}$**	**+16**	**+32**	**+48**	**+DQ**	**+DA**	**+DQ+16**
30 min	**87%**	5% 37.5min (Y) 2% 38.5min(H_{13}) 1% 39.5min (H_6) - 40.5min (H_{14}) 2%	3%	1%	-	-	-
		+DQ+32	**+IQ**		**+DHI**	**+IQ+16**	**+DHI+16**
		-	-		-	-	-
Fragments	*D.AEFRHDSGYEVHHQKLVFFAEDVGSNK.- (36 min)*			*1%*			
	D.AEFRHDSGY(+16)EVHHQKLVFFAEDVGSNK.- (35 min)			*1%*			
	-.DAEFRHDSGYEVHHQKLVFFA.E			*1%*			
	D.AEFRHDSGYEVHH(+16)QKLVFF.A			*1%*			
		+16	**+32**	**+48**	**+DQ**	**+DA**	**+DQ+16**
90 min	**64%**	16% 37.5min (Y) 4% 38.5min(H_{13}) 3% 39.5min (H_6) 2% 40.5min (H_{14}) 7%	6%	3%	1%	1%	1%
		+DQ+32	**+IQ**		**+DHI**	**+IQ+16**	**+DHI+16**
		-	-		1%	-	-
Fragments	*-.DAEFRHDSGYEVHHQKLVFFA.E*			*3%*			
	D.AEFRH(+16)DSGYEVHHQKLVFFAEDVGSNK.- (35min)			*2%*			
	D.AEFRHDSGYEVHHQKLVFFAEDVGSNK.- (36 min)			*1%*			
	D.AEFRHDSGYEVHH(+16)QKLVFF.A (36 min)			*1%*			
		+16	**+32**	**+48**	**+DQ**	**+DA**	**+DQ+16**
180 min	**37%**	27% 37.5min (Y) 5%; 38.5min(H_{13}) 9%; 39.5min (H_6) 3%; 40.5min (H_{14}) 10%	8%	8%	2%	3%	2%
		+DQ+32	**+IQ**		**+DHI**	**+IQ+16**	**+DHI+16**
		2%	1%		2%	-	1%
Fragments	*D.AEFRH(+16)DSGYEVHHQKLVFFAEDVGSNK.- (35 min)*			*1%*			
	D.AEFRHDSGYEVHHQKLVFFAEDVGSNK.- (36 min)			*3%*			
	-.DAEFRHDSGYEVH(+16)HQKLVF.F			*3%*			

Table 22. *Modification with time of $A\beta_{28}$ peptide detected by LC/MS analysis upon reaction of Cu^{II}-$A\beta_{28}$ and DA in the presence of SDS micelles. Reaction mixtures were quenched with sulfuric acid (pH~2). SDS was precipitated after addition of excess KCl and several centrifugation/cooling cycles*

Time	**$A\beta_{28}$**	**+16**	**+32**	**+48**	**+DQ**	**+DA**	**+DQ+16**
30 min	**88%**	2%	3%	1%	1%	1%	-
		+DQ+32	**+IQ**		**+DHI**	**+IQ+ 16**	**+DHI+16**
		-	-		-	1%	-
Fragments	*D.AEFRHDSGYEVHHQKLVFFAEDVGSNK.- +16 (35 min)*			*1%*			
	D.AEFRHDSGYEVHHQKLVFFAEDVGSNK.- (36 min)			*1%*			
	Y.EVHH(+16)QKLVFFAEDVGSNK.- (36 min)			*1%*			
		+16	**+32**	**+48**	**+DQ**	**+DA**	**+DQ+16**
90 min	**76%**	6% 37.5min (Y) 2%; 38.5min(H_{13}) 1%; 39.5min (H_6) 1%; 40.5min (H_{14}) 2%	4%	2%	1%	2%	1%
		+DQ+32	**+IQ**		**+DHI**	**+IQ+16**	**+DHI+16**
		1%	-		1%	-	1%
Fragments	*D.AEFRHDSGYEVHHQKLVFFAEDVGSNK.- +16 (35min)*			*3%*			
	D.AEFRHDSGYEVHHQKLVFFAEDVGSNK.- (36 min)			*2%*			
		+16	**+32**	**+48**	**+DQ**	**+DA**	**+DQ+16**
180 min	**64%**	13%	5%	4%	2%	2%	1%
		+DQ+32	**+IQ**		**+DHI**	**+IQ+16**	**+DHI+16**
		2%	2%		2%	-	-
Fragments	*D.AEFRHDSGYEVHHQKLVFFAEDVGSNK.- +16 (35min)*			*2%*			
	H.HQKLVFFAEDVGSNK.- (35 min)			*1%*			

Competitive modification on amyloid-β (1-40) fragment

An almost total extraction of anionic surfactant was performed before each LC-MS analysis to avoid the interference of SDS with the stationary phase of column. Therefore, SDS was precipitated with the addition of solid KCl and by cooling the mixture; upon centrifugation of each sample, the supernatant was transferred into the vials for the injection in LC-MS. This protocol was efficient for all peptides previously analyzed, but in the case of $A\beta_{40}$, no reliable data were obtained.

Table 23. *Modification with time of $A\beta_{40}$ peptide detected by LC/MS analysis upon reaction of Cu^{II}-$A\beta_{40}$ and 4-MC in HEPES buffer pH 7.4 at 20 °C. Reaction mixtures were quenched with sulfuric acid (pH~2).*

Time	**$A\beta_{40}$**	**+16**	**+32**	**+48**	**+MQ**	**+MC**	**+MQ+16**	**+MQ+32**
30 min	**50%**	16%	10%	6%	4%	4%	4%	3%
		30min: M 6%						
Fragments	*F.RH(Q)DSGYEVHHQKLVFFAEDVGSNKGAIIGLM.V*							*1%*
	D.AEFRHDSGYEVHHQKLVFFAEDVGSNKGAIIGLMVGGVV.- (32min)							*2%*
90 min	**41%**	18%	11%	6%	6%	8%	5%	4%
		30min: M 4%						
Fragments	*D.AEFRHDSGYEVHHQKLVFFAEDVGSNKGAIIGLMVGGVV.-+16 (32min)*							*1%*
180 min	**32%**	18%	13%	9%	7%	8%	6%	5%
		30min: M 3%						
Fragments	*D.AEFRHDSGYEVHHQKLVFFAEDVGSNKGAIIGLMVGGVV.- (32min)*							*2%*

Probably, the organic phase binds the peptides in a stable form, interacting with the highly hydrophobic tail of the peptide, and the precipitation of micelles brings the amyloid peptide in the pellet phase. Only modification patterns of $A\beta_{40}$ in aqueous *medium* were obtained, showing a similar trend of oxidative and covalent modifications respect with the shorter peptides (Table 23 and 24; Figure 48).

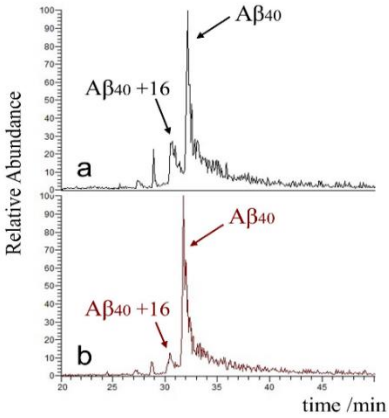

Figure 48. *HPLC-MS elution profiles of $A\beta_{40}$ peptide resulting from oxidation of MC (panel a) or DA (panel b) (3 mM) in HEPES buffer (50 mM) pH 7.4 at 30 min reaction time by Cu^{II} (25 μM) and $A\beta_{40}$ (50 μM).*

Table 24. *Modification with time of $A\beta_{40}$ peptide detected by LC/MS analysis upon reaction of Cu^{II}-$A\beta_{40}$ and DA in HEPES buffer pH 7.4 at 20 °C. Reaction mixtures were quenched with sulfuric acid (pH~2).*

Time	**$A\beta_{40}$**	**+16**	**+32**	**+48**	**+DQ**	**+DA**	**+DQ+16**
30 min	**65%**	11%	5%	3%	2%	2%	1%
		30min: M 3% 34min: H_{14} 4%					
		+DQ+32	**+IQ**		**+DHI**	**+IQ+ 16**	**+DHI + 16**
		1%	1%		2%	1%	1%
Fragments	*DAEFRHDSGYEVHHQKLVFFAEDVG.S (27min)*		*1%*				
	D.AEFRHDSGYEVHHQKLVFFAEDVGSNKGAIIGLMVGGVV.-(31min) 4%						
		+16	**+32**	**+48**	**+DQ**	**+DA**	**+DQ+16**
90 min	**58%**	15%	7%	4%	-	2%	1%
		30min: M 4%; 34min: H_{14} 5%					
		+DQ+32	**+IQ**		**+DHI**	**+IQ+16**	**+DHI+16**
		2%	2%		2%	2%	1%
Fragments	*D.AEFRHDSGYEVHHQKLVFFAEDVGSNKGAIIGLMVGGVV.- (31min) 4%*						
		+16	**+32**	**+48**	**+DQ**	**+DA**	**+DQ+16**
180 min	**52%**	16%	11%	6%	3%	3%	2%
		30min: M 6%; 34min: H_{14} 5%					
		+DQ+32	**+IQ**		**+DHI**	**+IQ+16**	**+DHI+16**
		1%	2%		3%	2%	1%
Fragments	*D.AEFRHDSGYEVHHQKLVFFAEDVGSNKGAIIGLMVGGVV.-*			*4%*			

Conclusions

The aim of this work was to investigate the redox chemistry promoted by the interaction of copper ions with neuronal peptides, such as prion and amyloid-β, in combination with a biological neurotransmitter, as dopamine. This catalytic behavior was assayed both in aqueous environment and in a simple model able to mimic the chemical properties of a neuronal membrane.

The impact of the presence of micelles of an anionic surfactant, as sodium dodecyl sulfate, was studied in term of redox capability to oxidize external substrates, as catechols, and of oxidative and covalent modifications directed toward the peptide sequences. Both prions and amyloid-β proteins present high affinity constant for copper ions and bear a strong binding affinity to micelles and, in the biological context, for membrane layers. At the same time, catecholamines show a weak tendency to interact with the surface of phospholipids due to the presence of a primary amine group, positively charged, able to mediate the interaction with the anionic layer. Therefore, membranes probably modulate the redox chemistry of copper-peptide complexes, creating over-populated regions on membrane surface rich in dopamine in which the metal-peptide complexes can be redox-activated or inactivated by the interaction with phospholipids. The association with SDS micelles almost totally quenches the oxidative reactivity of Cu-$PrP_{76\text{-}114}$, while only strongly reduces the redox capability of $A\beta_{40}$ adduct. Previous data show that the interaction between another important neuronal peptide, as α-synuclein fragment,[5b] and SDS inhibits the oxidative reactivity of copper ion. The same catalytic behavior of prion and α-synuclein indicates a similar binding coordination of the metal: both peptides contain a couple of methionine residues separated by 2-3 amino acids, ^{109}MKHM^{112} in PrP and ^{1}MDVFM^{5} in αSyn, that are able to stabilize copper(I) through the formation of a pseudo-linear coordination geometry that makes the copper-peptide complex unreactive to dioxygen.

Both the study performed on αSyn fragment either the current study on PrP fragments were focused on specific regions that probably mediate the interaction with neuronal membranes in a biological context. These fragments are involved in the direct and high affinity binding with metal ion and, when the metal binding domain is enclosed in the lipid phase, the interaction with copper and the reactivity of the resulting adduct are strongly modulated by the micelle. In conclusion, a possible neuroprotective role of prion can be assumed if the metal complex remains bound to the membrane, acting as a scavenger of reactive copper ions and preventing the production of ROS. In contrast, if prion is released in the extracellular *medium*, the binding with free copper ions and the high redox chemistry of the complex could promote wide damage toward several neuronal structures. On the other hand, a different behavior was suggested for Cu-Aβ adducts, where the reactivity of the complex decreases in the presence of micelles but without a massive quenching of the redox cycle of the bound metal.

Amyloid-β peptide can be divided in two principal regions: the *N*-terminal region is an unstructured and flexible portion with a strong affinity for the binding of copper in both oxidation states, while the *C*-terminus contains a rigid and hydrophobic portion that mediates the aggregation process but is lacking of any chelating site for the metal. The *C*-terminal tail interacts with the hydrophobic core of the SDS micelles but the more hydrophilic *N*-terminus remains essentially outside the membrane layers, maintaining the binding affinity for copper and its catalytic capability. Similar studies focused on the potential reactivity of free catecholamines and on the redox cycling of metals found dysregulated in some neuronal tissues can improve our understanding on the pathological role of prion proteins and on the chemical pathways leading to the deposition of amyloid plaques. Moreover, a potential interaction between copper, amyloid and prion fragments was assayed: several evidences suggest the link between the interaction of PrP with Aβ aggregates and the dysregulation of synapsis signaling and the progression of the neurodegenerative disorder.

In aqueous environment, the ternary complex shows a higher reactivity toward catecholic substrates but is strongly stabilized in SDS micelles, exhibiting a redox silencing of the metal cycling. On the other hand, further investigations are required to understand the exact coordination sphere of copper in the presence of both peptide and the biological properties of this adduct.

Peptide synthesis and purification

$PrP_{106-114}$	Ac-^{106}KTNMKHMAG^{114}-NH_2	mw 1057.5
PrP_{76-114}	Ac-^{76}PHGGGWGQPHGGWGQGGGTHSQWNKPSKPKTNMKHMAG^{114}-NH_2	mw 4074.45
$A\beta_{1-40}$	^{1}DAEFRHDSGYEVHHQKLVFFAEDVGSNKGAIIGLMVGGVV^{40}	mw 4329.9
$A\beta_{1-28}$	^{1}DAEFRHDSGYEVHHNKLVFFAEDVGSNK^{28}-NH_2	mw 3262.5
$A\beta_{1-16}$	^{1}DAEFRHDSGYEVHHNK^{16}-NH_2	mw 1955

PrP_{76-114} was provided by CNR-UniCt. $A\beta_{40}$ was purchased from Eurogentec (Liège, Belgium). $PrP_{106-114}$, $A\beta_{16}$ and $A\beta_{28}$ were synthesized through the fluorenyl methoxycarbonyl (Fmoc) solid-phase synthesis, using a Rink-amide resin (substitution 0.78 mmol/g) or a low loading Rink-amide resin (0.37 mmol/g) for $A\beta_{28}$ as solid support, which yielded the peptide amidated at the *C*-terminus. The removal of the Fmoc protecting groups during the synthesis was achieved by means of 20% piperidine solution in DMF. The coupling step was carried out for 35-45 min under a 2-fold excess of amino acid, *N*-hydroxybenzotriazole (HOBt), benzotriazol-1-yl-oxytripyrrolidinophosphonium hexafluorophosphate (PyBOP) and 4 equiv. of *N,N*-diisopropylethylamine (DIEA) at every cycle. In the synthesis of $A\beta_{28}$, amino acids were activated by above mentioned reagents for 10-15 minutes. The capping step was performed with acetic anhydride (4.7% v/v) and pyridine (4% v/v) in DMF. At the end of the synthesis, the protective groups on the amino acid side chains and the peptide release from the resin were performed in a solution of trifluoroacetic acid (95%), triisopropyl silane (2.5 %) and water (2.5 %). After stirring for 3 hours, cold diethyl ether was added to precipitate the peptide. The crude peptide was dissolved in water for the more soluble peptides or in acidic water (0.1% TFA) for the longer ones, and purified by HPLC, using a linear gradient of 0.1 % TFA in water to 0.1 % TFA in CH_3CN over 33 min (flow rate of 4 ml/min, loop 2 ml), as eluent. The purified peptide was lyophilized and stored at -20 °C until use.

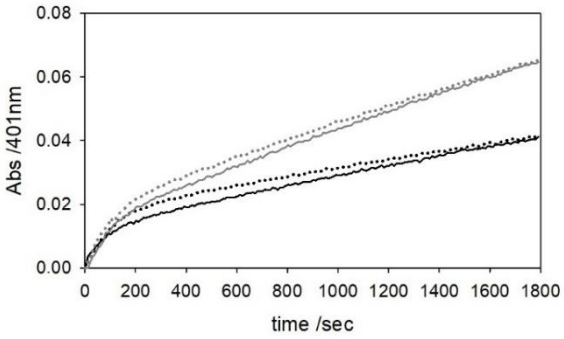

Figure 49. *Comparison of 4-MC (3 mM) oxidation kinetics in HEPES buffer (50 mM) pH 7.4 catalyzed by only copper(II) (25 μM) (black, dotted trace) and Cu^{II}-$A\beta_{16}$ (50 μM) complex (grey, dotted); the same experiment was performed in the presence of NH_3 (0.6 mM) in order to exclude any possible effect on the reactivity. Black solid and grey solid traces show catechol oxidation by Cu^{II} with NH_3 and Cu^{II}-$A\beta_{16}$ with NH_3, respectively.*

Regarding the treatment of the more hydrophobic peptide, prior to each experiment, $A\beta_{40}$ peptide was dissolved in hexafluoroisopropanol (HFIP) and incubated at room temperature for at least 4 h, to remove any preformed aggregates. HFIP was taken off by lyophilisation.[21] Dry $A\beta_{40}$ was then dissolved in H_2O milliQ with the addition of 0.02% (v/v) NH_3 ($1.6E^{-7}$ mol/200 μL) and the solutions were immediately used to avoid aggregation.[22] To verify the influence of NH_3 on the reactivity of copper-peptide complexes, the following experiment was performed in which the methylcatechol oxidation was assayed in the presence of copper-$A\beta_{16}$ in only HEPES buffer and upon the addition of ammonia in the reaction *medium*. Kinetic data are not influenced by the presence of ammonia and the solution pH remains unaltered (Figure 49).

Kinetic data of 4-methylcatechol oxidation

The catalytic oxidation of MC by Cu^{II} complexes was studied at 20 °C in 50 mM HEPES buffer at pH 7.4, saturated with atmospheric oxygen. The reaction was monitored by UV-visible spectroscopy following the 4-methyl-quinone band at 401 nm (ε = 1550 $M^{-1}cm^{-1}$) for a reaction time of 1800 s. The concentration of substrate was kept constant at 3 mM. The concentration of the peptides ($A\beta_{16}$, $A\beta_{28}$, $A\beta_{40}$, $PrP_{106\text{-}114}$, and $PrP_{76\text{-}114}$) was generally 50 μM, while copper(II) nitrate was maintained at 25 μM. In the experiment with excess $PrP_{106\text{-}114}$, the concentration of peptide was increased to 250 μM. The kinetic capability of Cu^{2+}-peptide complexes in only aqueous mixture and in the presence of SDS micelles (20 mM) was compared. Blank experiments of MC oxidation in the absence of Cu^{II} were carried out to compare the substrate autoxidation rates. All measurements were performed at least in duplicate. Moreover, the catalytic oxidation of MC by Cu^{I}, [Cu^{I}-PrP] and [Cu^{I}-Aβ] complexes and atmospheric O_2 in the lipid environment was studied. Cuprous ions were generated in *situ* by reaction of copper(II) nitrate (25 μM) and ascorbate (50 μM) with SDS (20 mM) in 50 mM HEPES buffer a pH 7.4 in anaerobic conditions. Then, MC (3 mM) was added to the solution, which was rapidly exposed to air. The same experiment was repeated in the presence of Cu^{I}-peptide complexes ($A\beta_{16}$, $A\beta_{28}$, $A\beta_{40}$, $PrP_{106\text{-}114}$, and $PrP_{76\text{-}114}$) using peptide concentration of 50 μM. All data are partially influenced by oxygen diffusion and whole consumption of sodium ascorbate. All measurements were performed at least in duplicate.

Kinetic data of dopamine oxidation

The catalytic oxidation of DA by Cu^{II} was studied at 20 °C in 50 mM HEPES buffer at pH 7.4, saturated with atmospheric oxygen. The reaction was monitored by UV-visible spectroscopy through the development of dopaminochrome band at 475 nm. The experiments were carried out by adding copper(II) nitrate (25 μM) to the solution containing DA (3 mM), in aqueous *medium* and in the presence of SDS (20 mM).

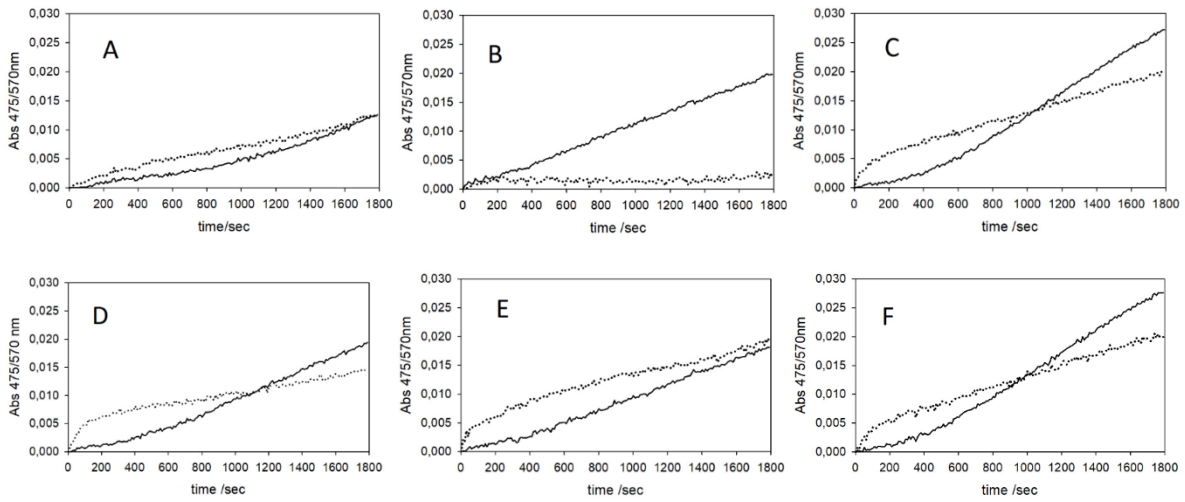

Figure 50. *Comparison of DA (3 mM) oxidation kinetics at 475 nm (DAQ, dotted traces) and 570 nm (unknown oligomers, solid traces) in the presence of: (A) Cu^{II} (25 μM) with SDS (20 mM) in HEPES buffer 50 mM pH 7.4; (B) Cu^{II} (25 μM) and $PrP_{76\text{-}114}$ (50 μM); (C) Cu^{II} (25 μM) and $A\beta_{28}$ (50 μM); (D) Cu^{II} (25 μM) and $A\beta_{16}$ (50 μM); (E) Cu^{II} (25 μM) and $PrP_{106\text{-}114}$ (50 μM); (F) Cu^{II} (25 μM) and $A\beta_{40}$ (50 μM).*

The kinetics were repeated in the presence of the copper(II)-peptide complexes (50 μM, $A\beta_{16}$, $A\beta_{28}$, $A\beta_{40}$, $PrP_{76\text{-}114}$ and $PrP_{106\text{-}114}$). DA (3 mM) autoxidation was recorded in the same conditions. All measurements were performed at least in duplicate. Performing the DA oxidation kinetics in the presence of only copper or copper-peptide complexes, an unusual band with the maximum absorption at 570 nm was observed (Figure 50 and 51). One of the possible natures of this absorption would correspond to the d-d transition of copper ion, that usually involves this spectral region but with lower intensity values. Therefore, the formation of one or some oligomers, generated from the oxidative pathway and highly stabilized by the membrane environment would be considered as a possible explanation.

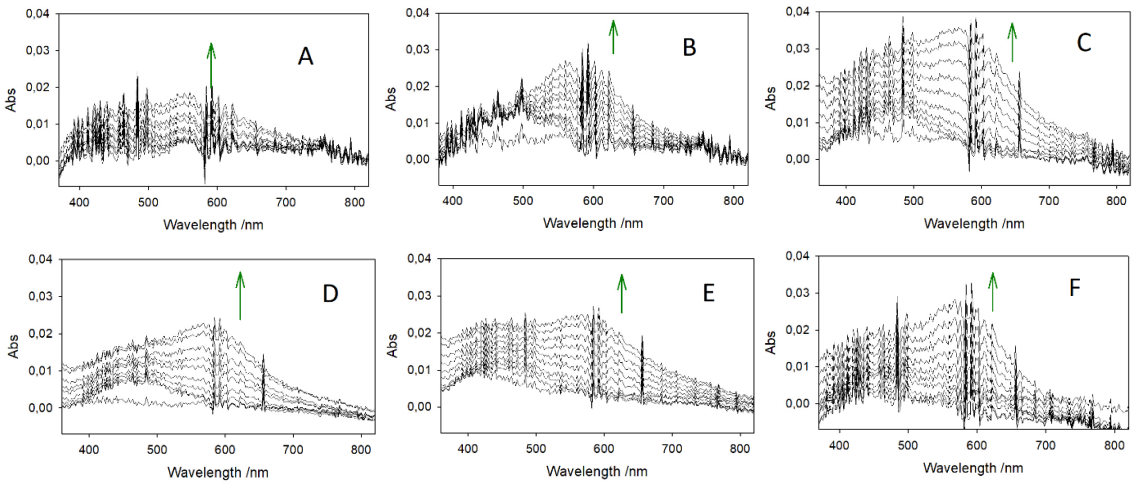

Figure 51. *Absorption bands of previous kinetic traces: DA (3 mM) oxidation spectra in SDS (20 mM) (A) in the presence of Cu^{II} (25 μM) and (B) $PrP_{76\text{-}114}$, (C) $A\beta_{28}$, (D) $A\beta_{16}$, (E) $PrP_{106\text{-}114}$ and (F) $A\beta_{40}$ (50 μM).*

To characterize these oligomeric products, the effect of the addition of ascorbate in excess to the reaction mixture containing copper(II) (25 μM) and dopamine (3 mM) in the micellar *medium* was assayed. Kinetic traces shown in Figure 52 suggest a fast production of dopaminochrome, converted with time into some undetectable intermediates, which then generate the observed oligomers; moreover, this oxidation mechanism seems to be accelerated by the interaction with lipids.

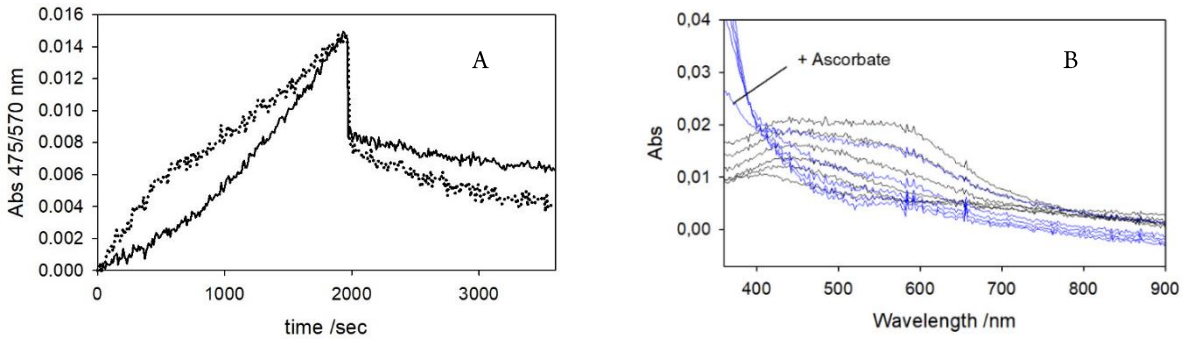

Figure 52. *A) Oxidation of DA (3 mM) in the presence of Cu^{II} (25 μM) and SDS (20 mM) following at 570 nm (solid trace) and 475 nm (dotted trace). B) Related spectra of DA oxidation/time (black lines) and upon the addition of sodium ascorbate after 35 min (blue lines).*

The addition of ascorbate induces a strong quenching at 570 nm, suggesting a correspondence between this absorption and some oligomers stabilized by the membrane-mimicking system and confirming the quinonic nature of these products. Moreover, the evaluation of the autoxidation traces obtained only in the presence of DA substrate in SDS *medium* indicates that the generation of these oligomers is tightly influenced by the presence of metal ions.

To obtain higher amount of oxidative products with the same concentrations of reagents, the dopamine oxidation in only buffer and in the presence of SDS was followed at several reaction times at 37 °C (Figure 53). The oxidation of dopamine in aqueous *medium* follows the usual oxidation mechanism, in which the initial accumulation of quinone and following polymerization to give several oxidative products are evidenced. In SDS micelles, a fast production of dopaquinone that quickly evolves to small oligomers with a strong absorption shifted to lower energy can be observed. To verify the link between the presence of SDS micelles and the generation of these oligomers and to understand how much strong their interaction could be, SDS was extracted from the mixture containing dopamine and copper in the micellar environment upon 30 min reaction at 37 °C and the Abs profiles were compared. Figure 54 shows a massive extraction of these oligomers and the residual absorption band at 475 nm corresponds to the accumulated dopaquinone. To have further indications about the reaction mechanism and the nature of the unknown band, the following experiment was performed (Figure 56).

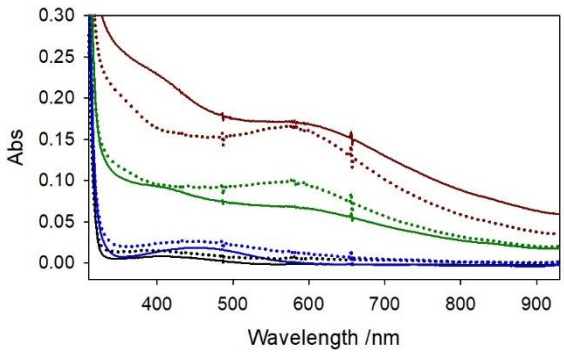

Figure 53. *Comparison of UV-vis spectra of DA (3 mM) oxidation with time at 37 °C catalyzed by Cu^{II} (25 μM) in absence/presence of SDS (20 mM). Solid lines show absorption bands in aqueous medium at following times: t_0 (black, solid line); t 5 minutes (blue, solid); t 30 minutes (green, solid) and t 1h (brown, solid). At the same reaction times, dotted lines show absorption bands in the presence of SDS.*

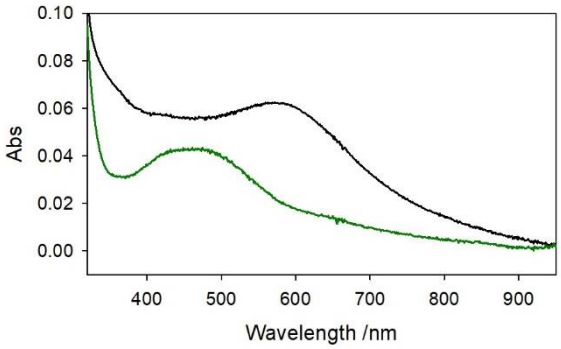

Figure 54. *Absorption bands of DA (3 mM) oxidation upon 30 min reaction at 37 °C in the presence of Cu^{II} (25 μM) before (black, solid line) and after (green, solid line) the extraction of SDS (20 mM).*

To exclude the correspondence between the band at 570 nm and the absorption band of superoxide, SOD enzyme was added to the usual reaction mixture to intercept some possible superoxide species released in the oxidative pathway. To enhance the accumulation of the unknown product, the oxidation of DA (3 mM) in SDS *medium* was catalyzed by copper-peptide complex.

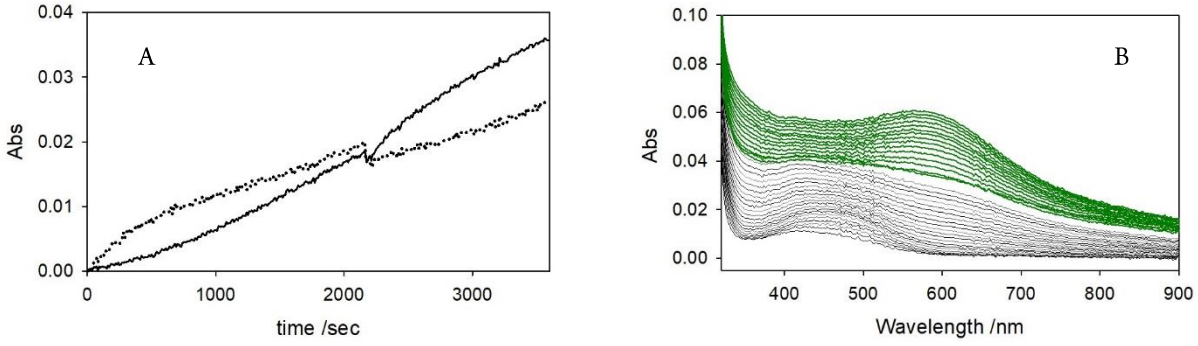

Figure 55. *A) Oxidation of dopamine (3 mM) at 475 nm (dotted trace) and at 570 nm (solid trace) in the presence of Cu^{II} (25 μM) before and after the addition of SDS (20 mM). B) Related spectra of DA oxidation/time (black lines) and upon the SDS addition (green lines).*

Kinetic profiles of DA oxidation in the presence of Cu^{II}-$A\beta_{16}$ show that the superoxide dismutase enzyme is able to reduce the quinone formation rate, suggesting the superoxide participation into the reaction mechanism. In the

presence of SDS, SOD enzyme could undergo denaturation of the catalytically-active folding and the inactivation of the catalytic site.

The reaction profiles with and without the enzyme in membrane *medium* show the same trend but, for the previous reason, it is not possible to completely exclude the correspondence between superoxide and the band evidenced at 570 nm. In the presence of KO_2 dissolved in DMSO and stabilized with 18-crown-6, the initial oxidation rate is drastically decreased by the exogenous superoxide acting as reducing agent; then, the reactivity re-starts. Finally, to exclude that the main responsible species of absorption at 570 nm would be the superoxide molecule, the UV-vis spectrum of KO_2 in 18-crown-6 in SDS environment was registered and the Figure 57 excludes any involvement of this species in the absorption encompassing the region between 500-700 nm.

In conclusion, further investigation would be required to characterized the exact oxidative mechanism and the mixture of products that are generated in both conditions. The possible stabilization of small oligomers respect with melaninic products via the interaction with SDS surface is now the better explanation of the peculiar absorption observed in this study but the isolation via chromatographic methods and a characterization via NMR spectroscopy will be the appropriate way to proceed.

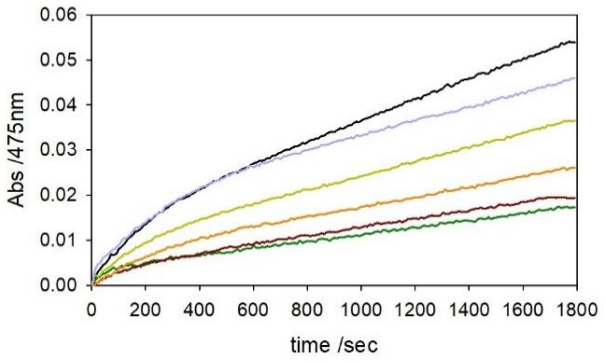

Figure 56. *Kinetic profiles of DA oxidation with time in HEPES buffer 50 mM pH 7.4 in the presence of copper(II) (25 μM) and $A\beta_{16}$ (50 μM) (black trace), and upon the addition of SDS (20 mM) (green). Orange and brown traces show the kinetic data upon the addition of ~ 960 units/1.6 μl SOD enzyme to the mixture in buffer alone or in SDS micelles, respectively. Light blue trace corresponds to the oxidation trace after denaturation at 100°C for 15 min of ~960 units SOD enzyme in the presence of peptide-copper adduct in only buffer. The addition of only 240 units/1.6 μl SOD enzyme is shown by the light green trace.*

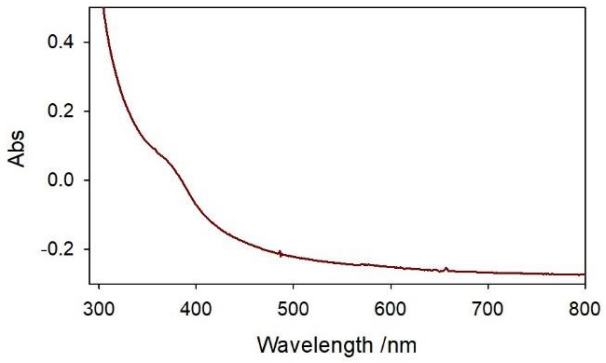

Figure 57. *Absorbance profile of KO_2 in 18-crown-6 ether (3 mM) in HEPES buffer 50 mM pH 7.4 and SDS (20 mM)*

Identification and characterization of modified peptides by HPLC-ESI/MS

The peptide modification was studied by HPLC-ESI/MS, performing experiments in the same conditions used for kinetic studies. Samples were prepared keeping constant the concentrations of the following reagents: copper(II)/(I) (25 μM), peptide ($A\beta_{16}$, $A\beta_{28}$, $A\beta_{40}$, or $PrP_{76\text{-}114}$) (50 μM), MC/DA (3 mM), in the presence and absence of SDS (20 mM) in HEPES buffer (50 mM) at pH 7.4. Copper(I) was generated as described above. Sulfuric acid was added to quench the reaction (pH~2) at different reaction times. Before LC-MS/MS analysis, SDS was precipitated by the addition of excess KCl. Upon cooling of the solution, samples were centrifuged (140 rpm, 2 min), and the supernatant was transferred into the vials for LC-MS analysis. The elution was carried out by using 0.1% HCOOH in distilled water (solvent A) and 0.1% HCOOH in acetonitrile (solvent B), with a flow rate of 0.2 ml/min. Elution started with 98% solvent A for 5 min followed by a linear gradient from 98 to 55% A in 65 min. Elution of $A\beta_{40}$ samples was optimized

through a linear gradient from 98 to 0% A in 65 min. To quantify the extraction of sodium dodecyl sulfate from the reaction mixtures, blue methylene assay was performed.[23] Methylene blue solution was prepared adding MB (3.75 mg), sodium sulfate (Na_2SO_4, 750 mg) and sulfuric acid (H_2SO_4,150 µl) in 15 mL H_2O. An aliquot of acidified samples (300 µl) was added to the same volume (300 µl) of MB solution and 1200 µl of chloroform were also mixed. Samples were vortexed and centrifuged for at least 1 min. Water (1.2 mL) was then added to the supernatant and the vortex/centrifugation procedure was repeated. Na_2SO_4 was used to remove the residual water from supernatant and the UV-vis quantification of SDS was performed by following at 651 nm.

Data were corrected with Abs value of pure chloroform. Calibration curve (see Figure 58) was drawn to quantify residual SDS after extraction. Several extraction procedures were tried to select the more efficient process: (1) addition of saturated KCl solution to the sample, following by centrifugation, cooling and centrifugation (3x); (2) addition of KCl solution (25 µl), following by cooling for 30 min, centrifugation for 15 min and addition of potassium chloride solution (150 µl); (3) addition of saturated K_2HPO_4 solution (150 µl), following by cooling of the mixture and extraction of SDS with a solution of EtOAc saturated H_2O; (4) addition of Sephadex and centrifugation; (5) addition of solid K_2HPO_4, following by cooling (2h) and extra addition of solid NaCl, further centrifugation, cooling and centrifugation (3x); (6) addition of solid KCl, following by cooling for 2h and centrifugation (5x).[24] The sixth procedure was chosen as the more efficient, leading to an almost total extraction of SDS micelles without any strong perturbation of the reaction conditions. Ninhydrin assay was also performed to quantify the removal of peptide during the procedure of extraction of SDS. Ninhydrin solution was prepared dissolving ninhydrin (100 mg) in 6 mL isopropanol and 4 mL acetate buffer (at pH 5.5, 100 mM); the solution was sonicated for at least 10 min. All precipitates obtained upon extraction of SDS from the reaction mixtures were dissolved in water (1 mL) and chloride acid (HCl, 1 M) was added to 1 mL of previous mixtures. The hydrolysis was performed O/N at 100 °C. The day after, ninhydrin solution (2 mL) was added to each sample for 15 min at 100 °C to allow the reaction between free amino acids and the indicator. Samples at room temperature were mixed with 1.5 mL ethanol (90%) and 1.5 mL H_2O and absorbance value at 570 nm was measured (cuvette 1 cm path, total volume 2000 µl). Results suggest that the peptide loss is negligible (around 1-3.7%). This assay is not quantitative but it is useful to estimate the removal of peptide after SDS extraction methods.

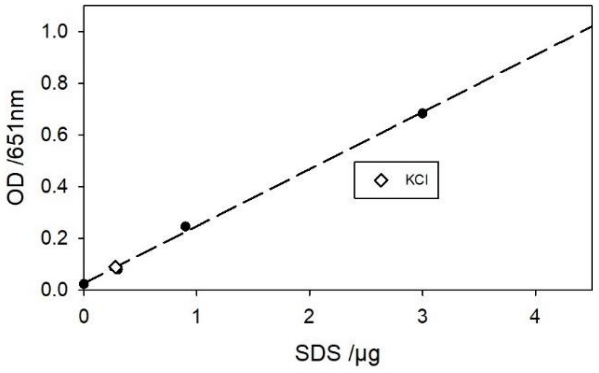

Figure 58. *Calibration curve for the quantification of removed sodium dodecyl sulfate from LC-MS samples.*

NMR quantification of oxidized catechol

The consumption of MC through ^{1}H-NMR spectroscopy was monitored as previously reported.[16] The spectra of reaction solutions containing MC were recorded in 5 mM deuterated HEPES buffer at pH 7.4 and 20 °C. The first reagent was MC (3 mM) and the reaction started upon the addition of copper(II) nitrate (25 µM), in the absence or presence of SDS (20 mM). The procedure was repeated in the presence of copper-peptide complexes ($A\beta_{16}$, $A\beta_{28}$, $A\beta_{40}$, and $PrP_{76\text{-}144}$; 25 µM). The initial data were obtained after 5 min, which is the time required to acquire the spectrum.

The acquisition was repeated every 30 min until 150 min reaction time, upon transfer of the reaction mixture from the NMR tube to an open vial in order to overcome the low availability of dioxygen. A blank experiment performed entirely in the NMR tube has confirmed that the reaction rate of MC oxidation was much slower due to slow diffusion of dioxygen to replace its consumption in the solution. All measurements were performed at least in duplicate.

Secondary structure of copper-peptide complexes determined via CD

The far-UV CD spectrum of Cu^{II}-PrP_{76-114} in 5 mM phosphate buffer solution at pH 7.4 was recorded with a 0.1 cm path-length cell, while all spectra of Cu^{II}-peptide complexes were obtained in anaerobic conditions using 1 cm path-length cells with Schlenk connections. For Cu^{II}-PrP_{76-114}, the dependence of SDS concentration (from 0 to 20 mM) was studied upon the addition of copper(II) (1 equiv.) to the solution of PrP_{76-114} (1.1 equiv.). CD spectra of $A\beta_{28}$, $A\beta_{40}$ and PrP_{76-114} (1.1 equiv.) in the presence of copper(I) (1 equiv.) were initially recorded in phosphate buffer solution (5 mM) at pH 7.4, and then after the addition of SDS (20 mM); Cu^{I} was generated by reduction of copper(II) nitrate (1 equiv.) by hydroxylamine (2 equiv.) anaerobically. In the case of $A\beta_{40}$, Cu^{I} was re-oxidized to copper(II) through O_2 saturation. CD measurements were routinely made with scanning rate of 50 nm/min and 10 accumulations. The CD spectra of ternary complexes were performed in the presence of PrP_{76-114} (1.1 equiv.) and 1.1 equiv. of Aβ fragments ($A\beta_{40}$, $A\beta_{28}$, or $A\beta_{16}$) in 5 mM phosphate buffer solution at pH 7.4, followed by the addition of Cu^{II} (1 equiv.). The same procedure was repeated in the presence of SDS. Optical spectra of solutions with the same ratio between $A\beta_{40}$/PrP_{76-114} and Cu^{II} were recorded using a 1 cm path-length cell for the near-UV and 10 cm cell for the visible region.

References

1. *(**a**) S. Chen, S. P. Yadav, W. K. Surewicz, Interaction between human prion protein and amyloid-β (Aβ) oligomers: role of N-terminal residues,* ***Journal of Biological Chemistry,*** 285, 34, 26377-26383, 2010; *(**b**) L. Urrea, I. Ferrer, R. Gavín, and J. A. del Ríoa, The cellular prion protein (PrP^C) as neuronal receptor for α-synuclein,* ***Prion,*** 11, 4, 226–233, 2017*; (**c**) E. De Cecco, L. Celauro, S. Vanni, M. Grandolfo, A. Aguzzi and G. Legname, The uptake of tau amyloid fibrils is facilitated by the cellular prion protein and hampers prion propagation in cultured cells,* ***Journal of Neurochemistry,*** doi: 10.1111/jnc.15040, 2020; *(**d**) M. Ionov, B. Klajnert, K. Gardikis, S. Hatziantoniou, B. Palecz, B. Salakhutdinov, J. Cladera, M. Zamaraeva, C. Demetzos, and M. Bryszewska, Effect of amyloid beta peptides $Aβ_{1–28}$ and $Aβ_{25–40}$ on model lipid membranes,* ***J Therm Anal Calorim,*** 99, 741-747, 2010*; (**e**) T. F. Beckhauser, J. Francis-Oliveira, and R. De Pasquale, Reactive Oxygen Species: Physiological and Physiopathological Effects on Synaptic Plasticity,* ***J Exp Neurosci,*** 10, 23–48, 2010; *(**f**) D. Valensin, S. Dell'Acqua, H. Kozlowski, and L. Casella, Coordination and Redox Properties of Copper Interaction With α-Synuclein,* ***J Inorg Biochem,*** 163, 292-300, 2016.

2. *(**a**) R. Giacovazzi, I. Ciofini, L. Rao, C. Amatorea and C. Adamo, Copper–amyloid-β complex may catalyze peroxynitrite production in brain: evidence from molecular modeling,* ***Phys. Chem. Chem. Phys.,*** 16, 10169-10174 , 2014; *(**b**) P. Cizas, R. Budvytyte, R. Morkuniene, R. Moldovan, M. Broccio, M. Lösche, G. Niaura, G. Valincius, and V. Borutaite, Size-dependent neurotoxicity of β-amyloid oligomers,* ***Archives of Biochemistry and Biophysics,*** 496, 2, 84-92, 2010.

3. *V. Pirota, S. Dell'Acqua, E. Monzani, S. Nicolis and L. Casella, Copper-Aβ Peptides and Oxidation of Catecholic Substrates: Reactivity and Endogenous Peptide Damage,* ***Chem. Eur. J.,*** 22, 16964 - 16973, 2016.

4. *(**a**) C. Cheignon, M. Jones, E. Atrián-Blasco, I. Kieffer, P. Faller, F. Collin, and C. Hureau, Identification of key structural features of the elusive Cu–Aβ complex that generates ROS in Alzheimer's disease,* ***Chem. Sci.,*** 8, 5107–5118, 2017; *(**b**) C. Cheignon, M. Tomas, D. Bonnefont-Rousselot, P. Faller, C. Hureau, and F. Collina, Oxidative stress and the amyloid beta peptide in Alzheimer's disease,* ***Redox Biol.,*** 450-464, 2018

5. *(**a**) A. Hecel, R. De Ricco and D. Valensin, Influence of membrane environments and copper ions on the structural features of amyloidogenic proteins correlated to neurodegeneration,* ***Coordination Chemistry Reviews,*** 8, 19, 327–328, 2016; *(**b**) S. Dell'Acqua, V. Pirota, E. Monzani, F. Camponeschi, R. De Ricco, D. Valensin, and L. Casella, Copper(I) Forms a Redox-Stable 1:2 Complex with α-Synuclein N-Terminal Peptide in a Membrane-Like Environment,* ***Inorg. Chem.,*** 55, 6100-6106, 2016; *(**5c**) N.P. Alza, P.A. Iglesias González, M.A. Conde, R.M. Uranga, and G.A. Salvador, Lipids at the Crossroad of α-Synuclein Function and Dysfunction: Biological and Pathological Implications,* ***Front Cell Neurosci.,*** 13, 175, 2019.

6. *A. Tiiman, J. Luo, C. Wallin, L. Olsson, J. Lindgren, J. Jarvet, R. Per, S.B. Sholts, S. Rahimipour, J.P. Abrahams, A.E. Karlström, A. Gräslund, S.K. Wärmländer, Specific binding of Cu(II) ions to amyloid-beta peptides bound to aggregation-inhibiting molecules or SDS micelles creates complexes that generate radical oxygen species,* ***Journal of Alzheimer's Disease,*** 54, 971–982, 2016.

7. *N. Österlund, Y.S. Kulkarni, A.D. Misiaszek, C. Wallin, D.M. Krüger, Q. Liao, F. Mashayekhy Rad, J. Jarvet, B. Strodel, S.K.T.S Wärmländer, L.L. Ilag, S.C.L. Kamerlin, and A. Gräslund, Affiliations expandAmyloid-β Peptide Interactions with Amphiphilic Surfactants: Electrostatic and Hydrophobic Effects,* ***Neurosci.,*** 9, 7, 1680–1692, 2018.

8. *(**a**) V. Lewis and N.M. Hooper, The role of lipid rafts in prion protein biology,* ***Frontiers in Bioscience,*** 16, 151-168, 2011; *(**b**) P.P. Liberski, Historical Overview of Prion Diseases: A View From Afar,* ***Folia Neuropathol.,*** 50, 1, 1-12, 2012*; (**c**) N. Watt and N.M. Hooper, The prion protein and neuronal zinc homeostasis,* ***Trends in Biochemical Sciences*** 28, 8, 406-410, 2003.

9. *A.G. Kenward, L.J. Bartolotti, and C.S. Burns, Copper and zinc promote interactions between membrane-anchored peptides of the metal binding domain of the prion protein,* ***Biochemistry,*** 46, 4261-4271, 2007.

10. *E. Gaggelli, H. Kozlowski, D. Valensin and G. Valensin, Copper Homeostasis and Neurodegenerative Disorders (Alzheimer's, Prion, and Parkinson's Diseases and Amyotrophic Lateral Sclerosis),* ***Chemical Reviews,*** 106, 6, 1995-2044, 2006.

11. *(**a**) G. Salzano, G. Giachin, and G. Legname, Structural Consequences of Copper Binding to the Prion Protein,* ***Cells.,*** 8, 8, 770, 2019*; (**b**) D. Valensin, E.M. Padula, A. Hecel, M. Luczkowski, and H. Kozlowski, Specific binding modes of Cu(I) and Ag(I) with neurotoxic domain of the human prion protein,* ***Journal of Inorganic Biochemistry,*** 155, 26-35, 2016.

12. *(**a**) M.L DeMarco and V. Daggett, Local environmental effects on the structure of the prion protein,* ***C. R. Biologies,*** 328, 847-862, 2005; *(**b**) Z. Marijanovic, A. Caputo, V. Campana, and C. Zurzolo, Identification of an Intracellular Site of Prion Conversion,* ***PLoS Pathog,*** 5,5, e1000426, 2009.

13. *(**a**) Y. Zhang, Y. Zhao, L. Zhang, W. Yu, Y. Wang and W. Chang, Cellular Prion Protein as a Receptor of Toxic Amyloid-β42 Oligomers Is Important for Alzheimer's Disease,* ***Front. Cell. Neurosci.,*** 13, 339, 2019; *(**b**) H. You, S. Tsutsui, S. Hameed, T.J. Kannanayakal, L. Chen, P. Xia, J.D.T. Engbers, S.A. Lipton, P.K. Stys, and G.W. Zamponi, Aβ Neurotoxicity Depends on Interactions Between Copper Ions, Prion Protein, and N-methyl-D-aspartate Receptors,* ***Natl Acad Sci U S A,*** 109, 5, 1737-1742, 2012; *(**c**) N.D. Younan, C.J. Sarell, P. Davies, D.R. Brown, and J.H. Viles, The cellular prion protein traps Alzheimer's Aβ in an oligomeric form and disassembles amyloid fibers,* ***FASEB J.,*** 27, 5, 1847-1858, 2013.

14. *B.R Fluharty, E. Biasini, M. Stravalaci, A. Sclip, L. Diomede, C. Balducci, P. La Vitola, M. Messa, L. Colombo, G. Forloni, T. Borsello, M. Gobbi, and D.A. Harris, An N-terminal Fragment of*

the Prion Protein Binds to Amyloid-β Oligomers and Inhibits Their Neurotoxicity in Vivo, ***The Journal of Biological Chemistry,*** 288, 11, 7857-7866, 2013.

15. ***(a)*** *A.A. Rubel, T.A. Ryzhova, K.S. Antonets, Y.O. Chernoff, and A. Galkin, Identification of PrP sequences essential for the interaction between the PrP polymers and Aβ peptide in a yeast-based assay,* ***Prion,*** 7, 6, 469-476, 2013; ***(b)*** *K. Ősz, Z. Nagy, G. Pappalardo, G. Di Natale, D. Sanna, G. Micera, E. Rizzarelli, and I. Sóvágó, Copper(II) Interaction with Prion Peptide Fragments Encompassing Histidine Residues Within and Outside the Octarepeat Domain: Speciation, Stability Constants and Binding Details,* ***Chemistry – A European Journal,*** 13, 25, 7129-7143, 2007; ***(c)*** *S.A. Purro, A.J. Nicoll and J. Collinge, Prion Protein as a Toxic Acceptor of Amyloid-β Oligomers,* ***Biological Psychiatry,*** 83, 4, 358-368, 2018.

16. *S. Dell'Acqua, C. Bacchella, E. Monzani, S. Nicolis, G. Di Natale, E. Rizzarelli, and L. Casella, Prion Peptides Are Extremely Sensitive to Copper Induced Oxidative Stress,* ***Inorg. Chem.,*** 56, 11317-11325, 2017.

17. ***(a)*** *M. Remelli, D. Valensin, L. Toso, E. Gralka, R. Guerrini, E. Marzola, and H. Kozłowski, Thermodynamic and spectroscopic investigation on the role of Met residues in Cu(II) binding to the non-octarepeat site of the human prion protein,* ***Metallomics,*** *4, 794-806, 2012;* ***(b)*** *G. Di Natale, G. Grasso, G. Impellizzeri, D. La Mendola, G. Micera, N. Mihala, Z. Nagy, K. Ősz, G. Pappalardo, V. Rigó, E. Rizzarelli, D. Sanna, and I. Sóvágó, Copper(II) Interaction with Unstructured Prion Domain Outside the Octarepeat Region: Speciation, Stability, and Binding Details of Copper(II) Complexes with PrP106–126 Peptides,* ***Inorg. Chem.,*** *44, 20, 7214–7225, 2005;* ***(c)*** *N. Russo, D.R. Salahub, M. Witko, Metal-Ligand Interactions: Molecular, Nano-, Micro-, and Macro-systems in Complex Environments,* ***Springer Science & Business Media,*** vol. 116, II, 2012; ***(d)*** *J. Shearer and P. Soh, The Copper(II) Adduct of the Unstructured Region of the Amyloidogenic Fragment Derived from the Human Prion Protein is Redox-Active at Physiological pH,* ***Inorganic Chemistry*** 46, 3, 710-709, 2007.

18. ***(a)*** *L.E. Cassagnes, V. Hervé, F. Nepveu, C. Hureau, P. Faller, and F. Collin, The catalytically active copper-amyloid-Beta state: coordination site responsible for reactive oxygen species production,* ***Angew. Chem. Int. Ed.,*** 52, 11110 –11113, 2013; ***(b)*** *D. Peretti, Is PrP^{C} a Mediator of Aβ Toxicity in Alzheimer's Disease?,* ***Journal of Neuroscience,*** 30, 36, 11883-11884, 2010.

19. ***(a)*** *J. Laurén, D.A. Gimbel, H.B. Nygaard, J.W. Gilbert, S.M. Strittmatter, Cellular prion protein mediates impairment of synaptic plasticity by amyloid-beta oligomers,* ***Nature,*** 457, 7233,1128-1132, 2009; ***(b)*** *C. Kong, H. Xie, Z. Gao, M. Shao, H. Li, R. Shi, L. Cai, S. Gao, T. Sun, and C. Li, Binding between Prion Protein and Aβ Oligomers Contributes to the Pathogenesis of Alzheimer's Disease,* ***Virologica Sinica,*** 34, 5, 475-488, 2019; ***(c)*** *O. Dössel and W.C. Schlegel,* ***World Congress on Medical Physics and Biomedical Engineering,*** 25, 50, 2009.

20. ***(a)*** *G. Di Natale, K. Ösz, Z. Nagy, D. Sanna, G. Micera, G. Pappalardo, I. Sóvágó and E. Rizzarelli, Interaction of Copper(II) with the Prion Peptide Fragment HuPrP(76–114) Encompassing Four Histidyl Residues within and outside the Octarepeat Domai,* ***Inorg. Chem.,*** 48, 9, 4239-4250, 2009; **(b)** *C.A. Damante, K. Ösz, Z. Nagy, G. Pappalardo, G. Grasso, G. Impellizzeri, E. Rizzarelli,, and I. Sóvágó, The Metal Loading Ability of β-Amyloid N-Terminus: A Combined Potentiometric and Spectroscopic Study of Copper(II) Complexes with β-Amyloid(1–16), Its Short or Mutated Peptide Fragments, and Its Polyethylene Glycol (PEG)-ylated Analogue,* ***Inorg. Chem.,*** 2008, 47, 20, 9669-9683; ***(c)*** *A. Magri, G. Di Natale, and E. Rizzarelli, Copper-assisted interaction between amyloid-β and prion: Ternary metal complexes with Aβ N-terminus and octarepeat,* ***Inorganica Chimica Acta,*** 472, 93–102, 2018; **(d)** *S.B. Wall, J-Y. Oh, A.R. Diers and A. Landar, Oxidative Modification of Proteins: An Emerging Mechanism of Cell Signaling,* ***Front Physiol.,*** 3, 369, 2012; **(e)** *Y.V. Il'ichev and J.D. Simon, Building Blocks of Eumelanin: Relative Stability and Excitation Energies of Tautomers of 5,6-Dihydroxyindole and 5,6-Indolequinone,* ***J. Phys. Chem. B,*** 107, 7162-7171, 2003.

21. *E. Flashner, U. Raviv, and A. Friedler, The effect of tachykinin neuropeptides on amyloid β aggregation,* ***Biochemical and Biophysical Research Communications,*** 407, 13-17, 2011.

22. *V. Tõugu, A. Karafin, and P. Palumaa, Affiliations expandBinding of zinc(II) and copper(II) to the full-length Alzheimer's amyloid-beta peptide,* ***J. Neurochem.,*** 104, 1249–1259, 2008.

23. *M. Arand, T. Friedberg, and F. Oesch, Colorimetric quantitation of trace amounts of sodium lauryl sulfate in the presence of nucleic acids and proteins,* ***Analytical biochemistry,*** 207, 73-75, 1992.

24. *D. G. Bishop, L. Rutberg, and B. Samuelsson, The Solubilization of the Cytoplasmic Membrane of Bacillus subtilis by Sodium Dodecyl Sulphate,* ***European J. Biochem.,*** 2, 454-459, 1967.

Chapter 2

EFFECT OF MEMBRANE MIMICKING SYSTEM: REDOX BEHAVIOR OF COPPER BOUND TO ALPHA-SYNUCLEIN.

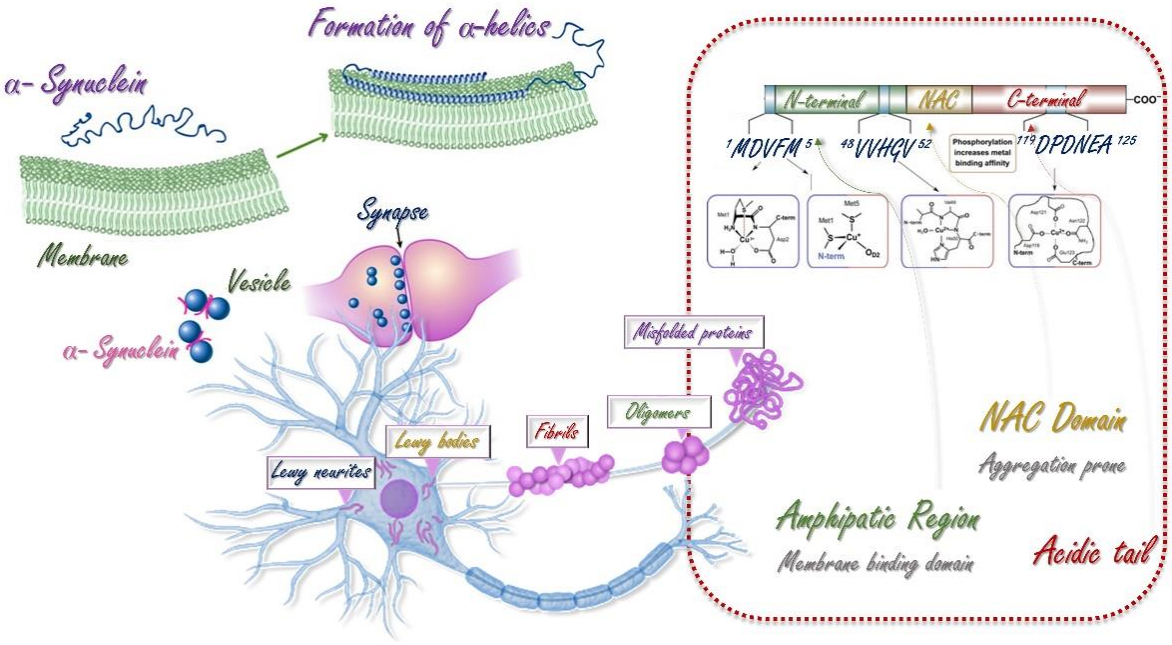

Ref. Data not yet published

Parkinson's disease is a common neurodegenerative disorder due to the loss of dopaminergic neurons and to the high levels of cytoplasmic inclusions called Lewy bodies, mainly containing α-synuclein protein. As previously described, the regulation of redox metal ions in neuronal tissues is an important factor able to influence the progression of neurodegenerative processes. The generation of insoluble aggregates and protein deposits is strongly promoted by the interaction between metals and neuroproteins, as α-synuclein, subjected to oligomerization and post-translation oxidative modifications, such as *N*-terminus acetylation, phosphorylation, ubiquitination, *C*-terminal truncation and nitration.[1a] Lewy's bodies are therefore the main hallmark of PD and correspond to proteinaceous fibrillary deposits showing high concentrations of 10-14 nm amyloid-like fibrils of α-synuclein.[1b] αSyn is an intrinsically disordered 14 kDa protein that comprises 140 amino acids, usually grouped into three main regions, as shown in Figure 1:

(i) An amphipathic *N*-terminus (residues 1-60), containing the membrane binding domain and some sites associated to common mutations linked to hereditary PD forms.

(ii) A highly hydrophobic self-aggregating sequence, called NAC domain (residues 61-95), comprising some essential residues (aa 71-82) that work as initializer of fibrillation.

(iii) An acidic *C*-terminal tail (residues 96-140), enriched in Asp and Glu residues that confer a negative net charge of -14 and allow an easy interaction with metal cations, regulating the oligomerization process. Moreover, this region contains the principal sites that can be subjected to nitration and phosphorylation.[2a]

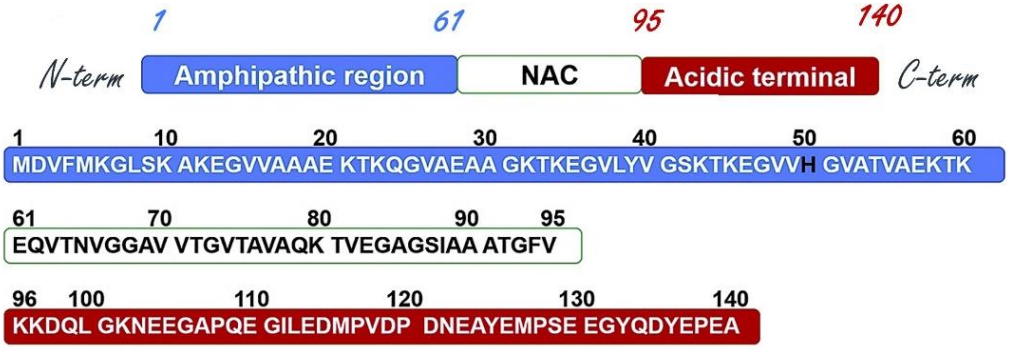

Figure 1. *Primary sequence of α-synuclein protein, highlighting the N-terminal, NAC and C-terminal regions in light blue, white and red, respectively.*

In the cytoplasmatic environment, αSyn can be detected in equilibrium between the unfolded and monomeric form and helical tetrameric species. Moreover, the protein can be associated with membrane via electrostatic interactions and undergoes some conformational changes from the unstructured state to an α-helical conformation in lipid environment.[2b] The structural change primary involves the *N*-terminal and NAC regions, where two helical domains 3-37 and 45-92 are defined, while *C*-terminal tail is unaffected by the presence of lipids.

In particular, the interaction between the protein and SUVs (Small Unilamellar Vesicles) reveals that:

(i) the region 6–25 is responsible of membrane anchoring;

(ii) the *C*-terminal region weakly interacts with vesicles;

(iii) the portion 26–98 influences the binding affinity for membrane.[3a]

Circular dichroism data indicate that when α-synuclein is in aqueous environment is highly unstructured, while upon the binding with lipid matrix, the protein undergoes an evident α-helical change from less than 3% to about 71%. The electrostatic nature of this interaction is verified by several studies that suggest a strong association with acidic

phospholipids, but not with neutral charged vesicles; moreover, the protein has a stronger tendency to association with vesicles of small diameter (20–25 nm) if compared to the larger (125 nm) ones. Biological evidences obtained from the experiments *in vivo* in the presence of a phosphorylated isoform of this protein, β-synuclein, show that post-translational modifications (Figure 2), as phosphorylation, could disrupt lipid binding, altering the net negative charges.[2b]

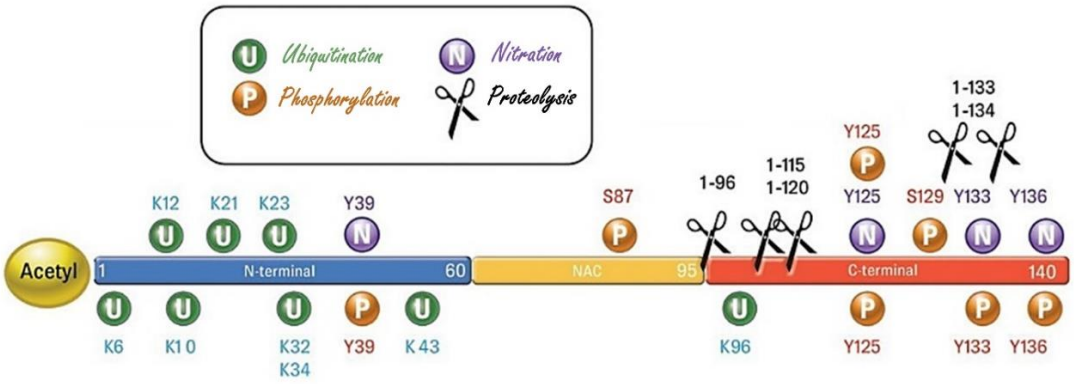

Figure 2. *Possible modifications of full-length α-Syn; the main sites of phosphorylation, ubiquitination, nitration, and cleavage are indicated. For example, α-synuclein trapped in the Lewy Bodies shows high percentage of phosphorylation on specific residues, as Ser87, Ser129, and Tyr125, and is massively ubiquitinated on Lys12, Lys21, or Lys23 while the tyrosine residues are very susceptible to oxidation. At the end, the C-terminal region is the preferential site for cleavage.*[3b]

A possible therapeutic approach could be the design of molecules able to stabilize the interaction protein-membrane: in the cytoplasm, the full-length protein can assume several aggregations states, but when it is anchored to the phospholipids is less susceptible to oligomerization and to the interaction with metals. Indeed, the protein can selectively interact with different metals and two *N*-terminal regions are known as binding sites for copper: the first Cu^{2+} ion interacts with the site 1 (^{1}MDVFMKGLS^{9}), while the second one occupies the lower affinity site (^{48}VVHGV^{52}) (Figure 3). The existence of two independent copper sites is now largely discussed and recent works suggest the involvement of only one rather stable species showing a square-planar or distorted-tetragonal geometry, or a dynamic equilibrium between this last coordination and the site 1.[4a]

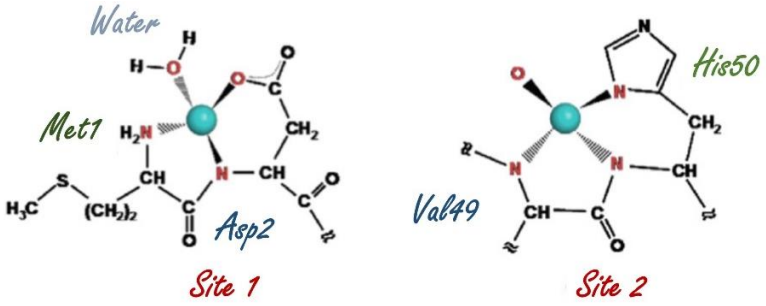

Figure 3. *Schematic representation of copper coordination structures, Site 1 and Site 2. Another C-terminal site associated with* Asp_{121} *could exist but with a weaker affinity toward the metal.*

Another metal with a high impact on the progression of oxidative stress condition is iron, that is the most abundant trace element in the human body and therefore, its homeostasis is tightly regulated to avoid uncontrolled redox reactions. The interaction between αSyn and Fe is still controversial, but some studies have revealed a moderate binding affinity of 50 μM between αSyn and Fe^{II} mainly involving the *C*-terminal region via Asp_{121}, Asn_{122}, and Glu_{123}.[4b] Furthermore, cellular lysates of PD's brains evidence high levels of Cu-saturated αSyn and these species may have some

ferrireductase-like activity, reducing Fe^{III} to Fe^{II} via NADH.[4c] The generation of oxidative species as hydrogen peroxide was also proposed upon the binding between Fe^{II}-αSyn and dioxygen. Anyway, the coordination chemistry of metals such as copper or iron is strongly influenced by the chemical properties of the *medium* and by the interaction with lipids. The coordination chemistry of Cu-αSyn is strongly modified by the interaction with membrane, where an important ligand as His-50 is trapped in the helical structure region, reducing its ability to bind the metal. Like the sequence of PrP, α-synuclein contains a conserved -$M(X)_nM$- motif, an optimal site for the binding and stabilization of copper(I) generated during the metal redox cycling. Because of the biological acetylation of *N*-terminus, a higher attention on the coordination of copper(I) to the methionines 1 and 5 respect to the redox role of copper(II) was paid and two main regions, 1-5 and 116-127, were suggested as efficient binding sites for copper(I) ions.[5a]

Regarding the mechanism of protein fibrillation, a structural change from unfolded αSyn monomers into fibrillary β-structures through several intermediates such as oligomers, pre-fibrils, annular and granular structures, is required (Figure 4).[5b] Moreover, this process can be triggered by the presence of metal ions as Al^{III}, Cu^{II}, Mn^{II} and Fe^{III}, as verified through circular dichroism (CD) spectroscopy and by the binding signatures of the fluorophore 1,1'-bis(4-anilino)naphthalene-5,5'-disulphonic acid (bis-ANS): the resulting data indicate that the protein adopts a partially folded state that is highly prone to aggregate.[4a]

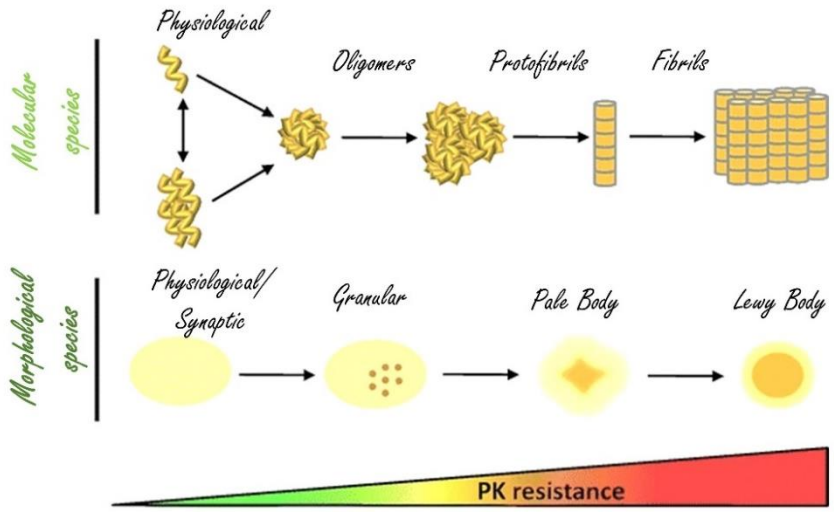

Figure 4. *Pathway of aggregation of αSyn from monomeric species to oligomers and fibrils. In PD-affected brains, several morphological species are detected: starting from the physiological protein located at synapses, other forms as granular species presenting small aggregates or larger insoluble Lewy bodies can be accumulated; pale bodies are similar deposits showing less compacted αSyn.*

Indeed, Cu depletion by specific chelators results in a redistribution of αSyn toward the membrane and reduces its aggregation rate, while supplementation with $CuCl_2$ restores its cytosolic localization and its propensity to generate insoluble fibrils.[6] The observed behavior is probably linked to the redox properties of copper and its involvement in the oxidative stress processes. Another factor that contributes to the oxidizing environment is the dysregulation of catecholamines, as dopamine, due to the high susceptibility of dopaminergic neurons to degeneration. The interaction between αSyn, DA and Cu can influence the protein structure, its aggregation propensity and can enhance the amount of harmful species in neuronal cells. Indeed, the fibrillation process of α-synunclein in the presence of Cu is enhanced by DOPAL, a direct metabolite of the neurotransmitter DA. However, the nature of this interaction and the related redox reactivity are not well characterized, although it is known that the metal-bound protein can promote Cu^{II}/Cu^{I} cycle, the generation of ROS and the post-translation modification, such as dityrosine cross-linking and methionine sulfoxidation.[6]

Reactivity of αSyn-copper complex and Oxidative modification of the full-length protein

αSyn is biologically located both as free species in solution and as membrane bound form and it probably works as regulator of metal redox activity; EPR and CD experiments have determined a coordination shell for copper bound to the protein in solution that identifies Met1, Asp2 and His50 as the primary metal ligands, suggesting a dissociation constant of 0.1 nM. When the protein is affected by the presence of membrane-like systems, it assumes a predominant helical conformation that does not allow a compatible coordination geometry that includes His-50. Interestingly, the affinity for copper(II) shown by free or micelle-anchored protein is similar, suggesting that the copper binding site is trapped in membrane.[7] Anyway, to better understand the redox cycling of the metal bound to the protein in solution and upon the interaction with membrane, the reactivity was assayed toward catechols, as 4-methylcatechol and dopamine. The oxidation of substrate (3 mM) promoted by copper was studied at 20 °C in 50 mM HEPES buffer at pH 7.4 and the metal was added at 25 μM concentration to the substrate solution in the presence of α-synuclein (0-50 μM). The catalytic behaviors of Cu-protein complex when it is free in solution or anchored to SDS micelle (0-20 mM) are compared. As shown in Figure 5, the redox activity of Cu-αSyn adduct bound to a membrane-like system is completely quenched. Such as prion peptide, αSyn contains a couple of close methionines in its sequence, ^{1}MDVFM^{5}, that act as efficient ligands for the stabilization of Cu^{I}. This coordinative environment for copper(I) leads to a partial unreactivity of the metal to dioxygen. However, a possible model for the coordination of copper to αSyn corresponds to the generation of a $Cu^{I}(αSyn)_2$ complex, with four Met residues belonging to the α-helices of two αSyn chains, whereas for Cu^{I}-$PrP_{76\text{-}114}$ the binding is intramolecular and the metal coordination sphere leads to the involvement of H_{111} residue besides the two methionines. The intermolecular coordination of the metal via two proteins is supported by an analogous experiment performed in the presence of copper: protein at 1:1 molar ratio, which shows a weaker metal binding by αSyn and a reactivity more comparable to the redox cycling of free copper. The interaction with SDS produces less drastic effects on the reaction efficiency probably due to the low stabilization of copper(I) complex.

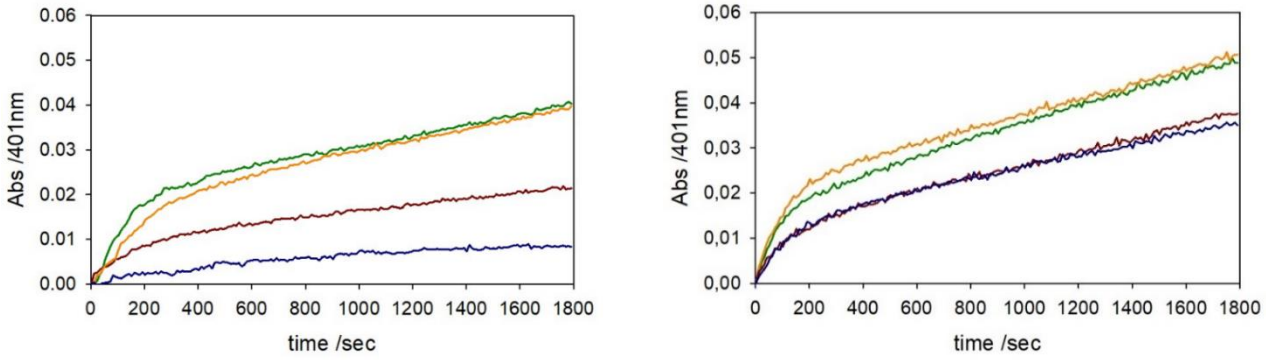

Figure 5. *Kinetic profiles of 4-MC (3 mM) oxidation with time in 50 mM HEPES buffer at pH 7.4 and 20 °C in the presence of Cu^{II} (25 μM) without SDS (green trace) and with SDS (20 mM) (orange), and with the addition of αSyn (50 μM, left panel and 25 μM, right panel) without SDS (brown) and with SDS (20 mM) (blue).*

An analogous behavior is observed when 4-MC is substituted by a catecholamine (Figure 6), suggesting that the reactivity of the complex bound to the micelle is quenched independently of the oxidative potential of the substrate. The minor effect evidenced in the presence of dopamine is linked to the chemical properties of substrate that is able to interact with the anionic surface of micelle through its amine group; therefore, the differential distribution of substrate between aqueous and micellar *medium* influences the resulting catalytic efficiency of copper-αSyn complex. Several investigations were performed in the last years about the coordination and redox chemistry of copper(II) bound to

αSyn and the results have suggested both the promotion of protein aggregation and precipitation and the catalytic generation of some reactive oxygen species. Otherwise, the role of Cu^{I}-αSyn intermediate for the redox cycling can also be considered; CD and NMR studies have proposed the existence of two independent and defined binding domains for copper(I) encompassing the regions (1-5) and (116-127) and characterized by similar values of metal binding constant.

Moreover, comparable coordination environments for Cu^{I} via two Met in a linear fashion have been identified.[7a] The coordination model has been determined in aqueous *medium* but the interaction with lipid structures and its effect on the folding and metal binding ability of the protein have to be considered. An easy binding of the full-length protein to vesicles containing at least 30% anionic phospholipids was suggested and the influence of this interaction on biological properties, as solubility and tendency to aggregate, was verified.[7b] Therefore, the redox behavior of the protein bound to copper(I) and trapped in the micellar environment was also studied and, as previously observed in the presence of Cu-PrP adduct,[7c] the reactivity of the resulting complex is totally quenched (Figure 7). Indeed, an analogous domain containing two vicinal Met allows to bind copper(I) and to generate a high stabile adduct, that prevents the re-oxygenation of the reduced species. As mentioned in the previous chapter, the redox chemistry of $Cu^{II/I}$ generates several oxidizing Cu/O_2 species and, unlike the specific activities of the enzymes, the resulting reactivity of these species is almost totally uncontrolled, promoting Fenton reactions, production of hydroxyl radicals or hydrogen peroxide, and other harmful species able to attach biological structures. The oxidative damage of protein is one of the possible biological alterations and, therefore, it was investigated *in vitro* through HPLC-MS analysis upon a proteolytic digestion of full-length protein catalyzed by the enzymatic activity of pepsin enzyme.

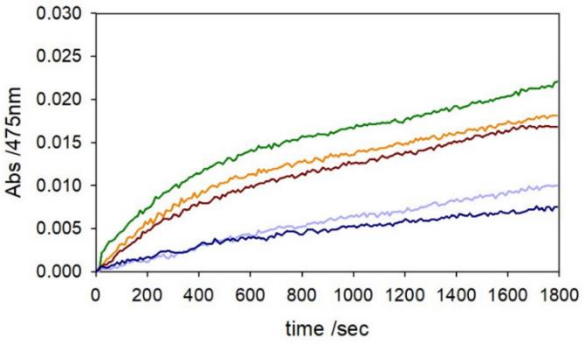

Figure 6. *Kinetic profiles of DA (3 mM) oxidation with time in 50 mM HEPES buffer at pH 7.4 and 20 °C (autoxidation, grey trace) in the presence of Cu^{II} (25 μM) (green) and upon the addition of αSyn 25 μM in aqueous (orange) or SDS medium (dashed light blue) or 50 μM in only buffer (brown) or in presence of SDS (blue dashed).*

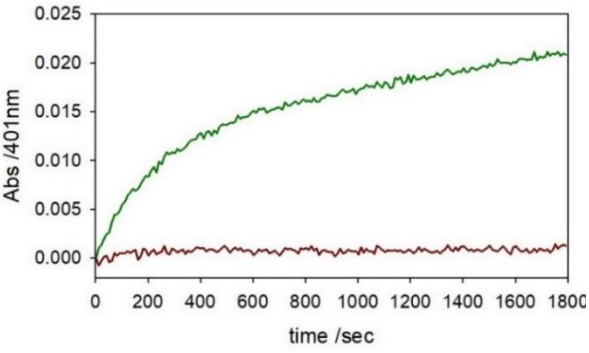

Figure 7. *Kinetic profiles of 4-MC (3 mM) oxidation with time in 50 mM HEPES buffer at pH 7.4 and 20 °C containing SDS (20 mM) and in the presence of Cu^{I} (25 μM) alone (green trace) or Cu^{I} (25 μM) and α-Syn (50 μM) (brown trace). Copper(I) was generated in situ by reaction of copper(II) nitrate (25 μM) and ascorbate (50 μM) anaerobically prior to exposure of the solution to air.*

This catalytic cleavage mediated by this enzyme is activated by acidic *medium* and is not specific for recurring sequences; therefore, the pH of all samples was kept around 1 because of the higher reproducibility of the enzymatic cleavage at pH < 2. As expected, the chromatograms show several peaks (data not shown), corresponding to the multitude of fragments generated upon the cleavage, that does not allow to perform a quantitative study of modification percentages. Anyway, the qualitative results suggest the most relevant modifications, where methionine 116 seems to be the most susceptible residues toward the oxidation, while methionine 127 has been found in the oxidized form with lower percentages. On the other hand, *N*-terminal Met-1 and -5 are less prone to undergo oxidative modifications, while histidines and lysines residues are negligibly affected by modification.

Conclusions

α-Synuclein is a neurological protein linked to the pathogenesis of Parkinson's disease, being a primary component of insoluble inclusions called Lewy bodies. The biological role of this protein is now debatable but recent works suggest that the normal physiological function could be reflect some involvement in the regulation and trafficking of vesicles or in the homeostasis of metals, such as copper. In fact, α-Syn can be detected both inside and outside of the neuronal cells and its mainly localized in some areas with an intense vesicle trafficking, as the presynaptic region of dopaminergic neurons.[8] Moreover, α-Syn is normally able to bind redox-active cations and several coordination spheres for copper(II) binding are identified when the protein is in solution or in membrane-mimicking models, such as SDS micelles or SUVs. In the presence of lipid vesicles, the full-length protein assumes a conserved structure showing two helical domains (3-37) and (45-92), that are connected by a short region 38-44, and ends with a long flexible tail, 93-140.[9a]

Besides the involvement of structural changes that promote the generation of neuronal deposits, the role of transition metals and of oxidative stress is commonly accepted; copper is able to interact with several neuronal proteins, such as prions, Aβ and α-Syn, and the resulting redox active complexes enhance the local concentrations of harmful reactive species and of insoluble aggregates. In particular, copper(II) can bind the protein in two main binding sites corresponding to the *N*-terminal region and the domain that comprises His-50. In particular, a correlation between the point mutation H_{50}→Q and the onset of familial PD, together with the alterations in copper binding affinities and in structural folding of the resulting protein, was recently suggested.[9b,9c] Since both redox states of the metal normally co-exist in the neuronal cells, participating in the ROS production and cellular damage,[9d] the interaction with the reduced metal form was also suggested, in which copper(I) shows high affinity for methionine residues and two regions, Met_1-Met_5 and Met_{116}-Met_{127}, are identified as good binding domains.

The ability to chelate both redox states of copper suggests a role of the protein in the promotion of oxidative stress condition. Anyway, when the protein interacts with vesicles or phospholipids, the conformational properties and the accessibility to the metal binding sites can be altered and the aim of this section is a preliminary study on the reactivity changes in aqueous and SDS *medium* shown by Cu-αSyn complex. The kinetic behavior of the complex suggests that the interaction with micelles induces a quenching of the redox ability of the adduct that is strongly evidenced when protein : copper(II) are at 2:1 molar ratio; moreover, the kinetic trace obtained from the oxidation of catechols starting from Cu^{I}-αSyn complex at 1:2 molar ratio shows an almost totally quenched profile. These data indicate that the key intermediate in the redox mechanism is the reduced form of the complex that is trapped by the interaction with membrane where its reoxygenation is not allowed. Furthermore, the reactivity changes are more visible when 2 equiv. of protein are bound to 1 equiv. metal, suggesting the involvement of a ternary adduct $Cu^{I}(\alpha Syn)_2$ in which 2 Met from each protein are used to chelated one Cu^{I} ion.

Obviously, these data are so ancestral and a huge effort will be required to characterize the redox mechanism of this complex in both environments. The *N*-terminal region is known to be the primary domain trapped into the membrane and the quenching of the reactivity observed in the presence of SDS is imputable to the generation of a ternary complex $Cu^{I}(\alpha Syn)_2$ in which two methionines located in the *N*-termini of each protein work as the main chelating groups for the metal. Therefore, one of the future prospects may correspond to the single point mutation of only one Met residue that would remove the Cu^{I} binding site and affect the resulting reactivity of copper-protein complexes. On the other hand, if several works are in agreement on the reduced redox ability of Cu^{II} when bound to αSyn and suggest a protective role of the protein in the control of metal homeostasis, the effects of membrane interaction on the reactivity

of the resulting complexes is still controversial. Since some recent studies affirm that these adducts when anchored to membrane-mimicking systems show an enhanced catechol oxidase activity if compared with the reactivity detected in aqueous *medium*[10] and these results are strongly incompatible with the present work, a deeper characterization of these adducts through several spectroscopic techniques and with more complex synthetic membrane will be performed.

Catalytic oxidation of 4-MC and Dopamine by Cu^{II}-αSyn

The catalytic oxidation of 4-methylcatechol and dopamine by copper(II) was studied at room temperature in 50 mM HEPES buffer at pH 7.4, saturated with atmospheric oxygen. The development of the relative quinone band at 401 nm for 4-MC and at 475 nm for DA was followed for 1800 s. In all kinetic data, the concentration of copper(II) nitrate and substrate was fixed at 25 μM and 3 mM, respectively. The autoxidation was also evaluated, performing the experiment in the presence of substrate in buffer solution. The different kinetic behaviors in the presence of copper–protein complexes were evaluated through the addition of 2:1 or 1:1 molar ratios relative to copper into the substrate solution (3 mM), followed by copper(II) nitrate as the last reagent. The same experiments were then performed in presence of SDS micelles (20 mM).

Catalytic oxidation of 4-MC by Cu^{I}-αSyn in aqueous and SDS environment

To study the catalytic oxidation of MC by Cu^{+} and [Cu^{+}-protein] in the membrane *medium*, copper(II) ions were anaerobically reduced to copper(I) (25 μM) by ascorbate (50 μM) in the presence of SDS (20 mM). Upon vacuum cycles, MC (3 mM) was added and the solution was rapidly exposed to air. As previously described, 4-methyl-quinone band at 401 nm was monitored to quantify the substrate oxidation rate. The same experiment was repeated in the presence of Cu^{I}-αSyn adduct with 1:2 molar ratio.

HPLC-ESI/MS analysis of protein modification

The solutions obtained from the kinetic data and incubated for different reaction times were quickly acidified and frozen. To analyze them via HPLC-MS, the 250 μL samples containing 50 μM αSyn ($1.25E^{-8}$ mol, 0.175 mg of protein) were centrifuged. The enzymatic digestion was performed in the presence of αSyn: pepsin at 50:1 w/w (0.175 mg αSyn: 0.0035 mg pepsin). After 2h30 incubation at 37 °C, all samples were analyzed by LC-MS. Each sample was prepared adding copper(II) nitrate (25 μM), αSyn (50 μM), 4-MC (3 mM) and SDS (0-20 mM) in 50 mM HEPES buffer at pH 7.4.

References

1. (a) N. González, T. Arcos-López, A. König, L. Quintanar, M.M. Márquez, T.F. Outeiro and C.O. Fernández, Effects of alpha-synuclein post-translational modifications on metal binding, **Journal of Neurochemistry**, 150, 5, 507-521, 2019; (b) E. Gaggelli, H. Kozlowski, D. Valensin and G. Valensin, Copper Homeostasis and Neurodegenerative Disorders (Alzheimer's, Prion, and Parkinson's Diseases and Amyotrophic Lateral Sclerosis), **Chemical Reviews**, 106, 6, 1995-2044, 2006.
2. (a) F. Longhena, G. Faustini, A. Bellucci, Study of alpha-synuclein fibrillation: state of the art and expectations, **Neural Regen Res**, 15, 59-60, 2020; (b) W.S. Davidson, A. Jonas, D.F. Clayton and J.M. George, **The Journal of Biological Chemistry**, 273, 9443-9449, 1998.
3. (a) A. Hecel, R. De Ricco and D. Valensin, Influence of membrane environments and copper ions on the structural features of amyloidogenic proteins correlated to neurodegeneration, **Coord Chem Reviews**, 327-328 , 8-19, 2016; (b) A.W. Schmid, B. Fauvet, M. Moniatte and H.A. Lashuel, Alpha-synuclein Post-translational Modifications as Potential Biomarkers for Parkinson Disease and Other Synucleinopathies, **Molecular & Cellular Proteomics,** 12, 12, 3543-3558, 2013.
4. (a) A. Binolfi, L. Quintanar, C.W. Bertoncini, C. Griesinger and C.O. Fernándezd, Bioinorganic chemistry of copper coordination to alpha-synuclein: Relevance to Parkinson's disease, **Coordination Chemistry Reviews,** 256, 19–20, 2188-2201, 2012; (b) E. Carboni and P. Lingor, Insights on the interaction of alpha-synuclein and metals in the pathophysiology of Parkinson's disease, **Metallomics**, 7, 395-404, 2015; (c) P. Davies, D. Moualla and D.R. Brown, α-Synuclein is a cellular ferrireductase, **PLoS ONE,** 6, 1, e15814, 2011.
5. (a) F. Camponeschi, D. Valensin, I. Tessari, L. Bubacco, S. Dell'Acqua, L. Casella, E. Monzani, E. Gaggelli and G. Valensin, Copper(I)-α-Synuclein Interaction: Structural Description of Two Independent and Competing Metal Binding Sites, **Inorg. Chem.**, 52, 3, 1358–1367, 2013; (b) N. Bengoa-Vergniory, R.F. Roberts, R. Wade-Martins and J. Alegre-Abarrategui, Alpha-synuclein oligomers: a new hope, **Acta Neuropathologica**, 134, 819 – 838, 2017.
6. E. Carboni and P. Lingor, Insights on the interaction of alpha-synuclein and metals in the pathophysiology of Parkinson's disease, **Metallomics**, 7, 395-404, 2015.
7. (a) L.S. Kau, D.J. Spira-Solomon, J.E. Penner-Hahn, K.O. Hodgson, and E.I. Solomon, X-Ray absorption edge determination of the oxidation state and coordination number of copper: application to the type 3 site in rhus vernicifera laccase and its reaction with oxygen, **J. Am. Chem. Soc.**, 109, 6433–6442, 1987; (b) W.S. Davidson, A. Jonas, D.F. Clayton and J.M. George, Stabilization of α-Synuclein Secondary Structure upon Binding to Synthetic Membranes, **The Journal of Biological Chemistry,** 273, 16, 9443–9449, 1998; (c) C. Bacchella, S. Nicolis, S. Dell'Acqua, E. Rizzarelli, E. Monzani and L. Casella, Membrane Binding Strongly Affecting the Dopamine Reactivity Induced by Copper Prion and Copper/Amyloid-β (Aβ) Peptides. A Ternary Copper/Aβ/Prion Peptide Complex Stabilized and Solubilized in Sodium Dodecyl Sulfate Micelles, **Inorg. Chem.**, 59, 1, 900-912, 2020.
8. C.G. Dudzik, E.D. Walter, B.S. Abrams, M.S. Jurica and G.L. Millhauser, Copper Coordination to the Membrane Bound Form of α-Synuclein, **Biochemistry**, 52, 1, 53–60, 2012;
9. (a) M. Bisaglia, A. Trolio, M. Bellanda, E. Bergantino, L. Bubacco and S. Mammi, Structure and topology of the non-amyloid-β component fragment of human α-synuclein bound to micelles: Implications for the aggregation process, **Protein Sci.**, 15, 6, 1408–1416, 2006; (b) C. Proukakis, C.G. Dudzik, T. Brier, D.S. MacKay, J.M. Cooper, G.L. Millhauser, H. Houlden and A.H. Schapira, A novel α-synuclein missense mutation in Parkinson disease, **Neurology**, 80, 11, 1062-1064, 2013; (c) A. Villar-Piqué, T. Lopes da Fonseca, R. Sant'Anna, E.M. Szegö, L. Fonseca-Ornelas, R. Pinho, A. Carija, E. Gerhardt, C. Masaracchia, E. Abad Gonzalez, G. Rossetti, P. Carloni, C.O. Fernández, D. Foguel, I. Milosevic, M. Zweckstetter, S. Ventura and T.F. Outeiro, Environmental and genetic factors support the dissociation between α-synuclein aggregation and toxicity, **Proc Natl Acad Sci U S A.,** 113, 42, E6506-E6515, 2016; (d) M.C. Miotto, E.E. Rodriguez, A.A. Valiente-Gabioud, V. Torres-Monserrat, A. Binolfi, L. Quintanar, M. Zweckstetter, C. Griesinger and C.O. Fernández, Site-specific copper-catalyzed oxidation of α-synuclein: tightening the link between metal binding and protein oxidative damage in Parkinson's disease, **Inorg Chem.**, 53, 9, 4350-4358, 2014.
10. J.S. Calvo, N.V. Mulpuri, A. Dao, N.K. Qazi and G. Meloni, Membrane insertion exacerbates the α-Synuclein-Cu(II) dopamine oxidase activity: Metallothionein-3 targets and silences all α-synuclein-Cu(II) complexes, **Free Radical Biology and Medicine**, 158, 149–161, 2020.

Chapter 3

REDOX REACTIVITY OF COPPER BOUND TO R1 AND R3 FRAGMENTS OF TAU PROTEIN.

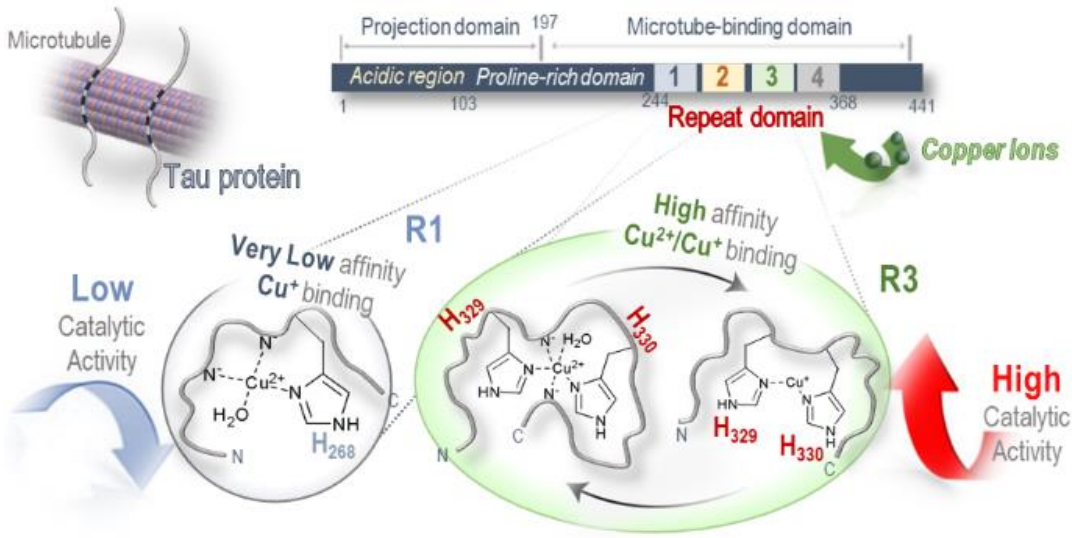

Ref. *Inorg. Chem. 59, 1, 274-286, 2020*
"Binding and Reactivity of Copper to R_1 and R_3 Fragments of tau Protein"
C. Bacchella, S. Gentili, D. Bellotti, E. Quartieri, S. Draghi, M. C. Baratto, M. Remelli, D. Valensin, E. Monzani, S. Nicolis, L. Casella, M. Tegoni, and S. Dell'Acqua

Alzheimer's disease is the most common neurodegenerative disorder, affecting ~10% of humans by age 65 and~50% by age 85. It is a progressive disorder that results in memory loss, unusual behavior, personality changes, and a decline in thinking ability. The actual pharmacological treatments available aim to enhance the cognitive impairments once the disease is diagnosed. Cholinesterase inhibitors and NMDA receptor antagonists are now commercialized and allow to alleviate the symptomatology, but they are far away to constitute an effective remedy to cure the disorder.[1a]

Its onset and development can be attributable to:

(i) According to the *amyloid cascade* hypothesis, the abnormal processing of the amyloid precursor protein (APP) and the generation of Aβ peptides, that are prone to aggregate and form insoluble deposits, are the causes of the disorder.

(ii) According to the *neuronal cytoskeletal degeneration* hypothesis, the hyperphosphorylation and aggregation of tau proteins related to cytoskeletal changes can lead to neuronal death processes.[1b]

Tau ("*Tubulin associated unit*") protein is a neuronal protein located within the axonal compartments and indispensable for the stabilization and the organization of microtubules.[1c] This protein is known to interact with several cytoskeleton proteins, first among all with tubulin, that is usually found in over 10-fold excess if compared with tau (~2 μM) in a mature neuronal cell.[1d] The involvement into the axonal transport and neuronal plasticity can explain the link between tau dysregulation and the onset of the disease. In neurodiseases in which the structure and the endogenous function of tau protein are affected, this protein can be also detected in the cell body and dendrites. Therefore, besides the commonly accepted role of tau in the stabilization of cytoskeleton scaffolds of neurons and in the cellular trafficking, other functions are recently emerging, such as its possible involvement in the mitochondrial function[1e] and in the alteration of controlled oxidative phosphorylation and apoptosis signalling.[1f]

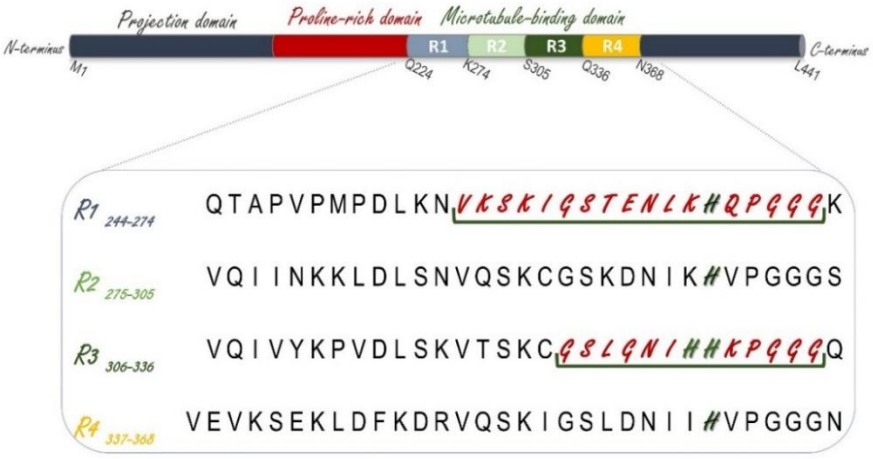

Figure 1. *Scheme of amino acid sequences of the four pseudorepeats in the full-length tau protein. The fragments used in this work are underlined (R1, Ac-^{256}VKSKIGSTENLKHQPGGG^{273}-NH$_2$ and R3, Ac-^{323}GSLGNIHHKPGGG^{335}-NH$_2$) and the main coordination sites for copper are evidenced in green.*

Tau gene is located on chromosome 17 and can encode several alternative splicing isoforms from 352 to 441 amino acids. The protein sequence shows an acid and variable *N*-terminal region, a proline-rich domain, a portion of three or four imperfect repeat motifs and a basic *C*-terminus (Figure 1). Each pseudorepeat consists of 31-34 amino acid residues containing a highly conserved octadecapeptide that begins with a valine residue and ends with a PGGG sequence. The four repeats, R1, R2, R3, and R4, have binding ability for copper(II), via a histidine and at least one

backbone amide group; it was reported that the octadecapeptides in R2 and R3 are able to coordinate copper ions and to generate hydrogen peroxide as product of the metal redox cycling.[2] A similar reactivity was also evidenced in the presence of R1 fragment. Further studies indicate that the interaction between metal ions, such as copper and zinc, and monomeric or oligomeric tau proteins, is a key factor in the pathogenic aggregation of protein and this binding occurs not only in the intracellular environment but also in the extracellular *medium*. Moreover, other metals are involved in the progression of the disease: abnormal zinc levels are accumulated in tau tangles in addition to high levels of ferric heme, released from hemoglobin and not detoxified by the endogenous protective systems.[3a]

The R1-R4 domains are also involved in the microtubule binding. The amino-terminal region together with the proline-rich domain is called as the "projection domain", being unstructured and able to interact with plasma membrane, microtubule surface and cytoskeletal proteins. Tau sequence can be considered as a dipole with two domains with opposite charge modulated by post-translational modifications or tau proteolysis.[3b]

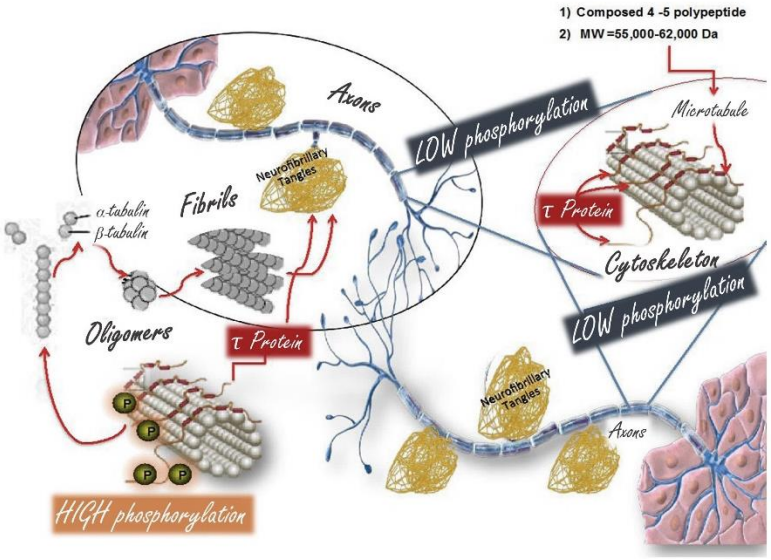

Figure 2. *Tau protein associated with microtubules forms the cytoskeleton. If the phosphorylated isoform increases, the disassembly of microtubules occurs; tubulin forms oligomeric structures bound to p-tau, that generates initial small fibrils and then, neurofibrillary tangles.*

$_{306}$VQIVYK$_{311}$ and $_{275}$VQIINK$_{280}$ sequences of R2 and R3 repeats promote protein aggregation by the generation of beta-structures. Moreover, abnormal post-translational modifications seem to influence tau function, stability and aggregation propensity. Almost 80 phosphorylation sites are mapped on the full-length protein and post-translational modifications can modulate the binding to tubulin and the cell localization of tau (Figure 2).[4,5a] Another significant modification is *O*-glycosylation or rather the addition of a sugar on serine or threonine residues close to the Pro-rich region. Some studies show the possible competition between glycosylation and phosphorylation, being directed toward the same domain of the protein. Furthermore, acetylation of tau protein could influence the microtubule interaction, the aggregation tendency and tau turnover *in vivo*.[5b] High amount of tau and phosphorylated tau (p-tau) is evidenced in cerebrospinal fluid in Alzheimer patients, making it a potential biomarker. Tau is widely distributed in the brain and it is normally involved in the microtubule assembly, while the abnormal intracellular accumulation of this protein in neurofibrillary tangles is considered as the characteristic hallmark of AD (Figure 3).[5c] These inclusions consist of aggregated tau in the form of twisted pairs or helical filaments, usually abnormally phosphorylated. Concentrations of total tau, p-tau and Aβ act as very sensitive and specific biomarkers for AD, because they are already

altered in patients with mild cognitive impairment;[6a] therefore, the levels of these proteins are excellent diagnostic tools for the identification of subjects who will subsequently evolve to AD.

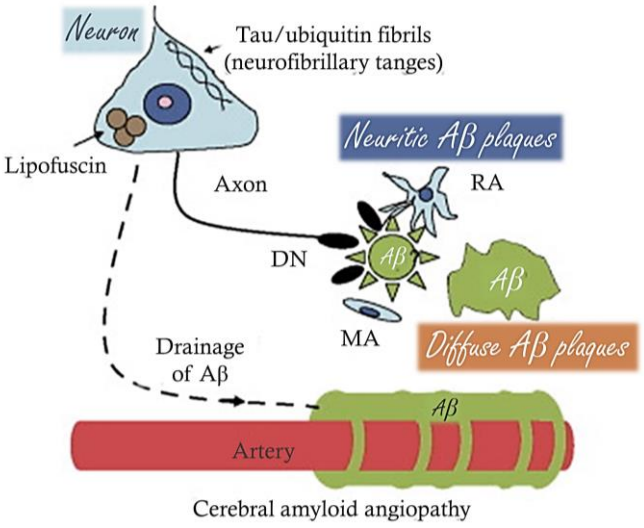

Figure 3. *Histopathological features of Alzheimer's disease are characterized by the accumulation of neurofibrillary tangles composed of tau and ubiquitin within neuronal cells, and by the deposition of amyloid-beta (Aβ) in brain parenchyma as amyloid plaques and in blood vessel walls as cerebral amyloid angiopathy. Aβ in amyloid plaques is associated with microglial activation (MA) and reactive astrocytosis (RA). Swollen dystrophic neurons (DN) containing tau are associated with many of the amyloid plaques (neuritic plaques).*[5c]

Moreover, tau protein forms copper adducts with one Cu^{II} ion bound to the monomeric peptide with 1:1 molar ratio and with a dissociation constant in a micromolar range. If some works suggest that the binding with the metal seems to inhibit the aggregation process in *vitro*,[6b] other studies *in vivo* obtained from the chronic exposure of copper in mice lines have determined an enhanced deposition of plaques and phosphorylation of tau protein.[6c] Furthermore, the treatment with use of chelating therapies, as clioquinol and several derivatives, has given promising effects in the improvement of the cognitive capabilities during the clinical trials.[6d] Previous studies also suggest a strong coordination of tau protein with metals such as aluminum and iron, in particular involving the repeat region of the protein.[6e] Anyway, if the coordination of several metal ions with amyloid-β and prions proteins has been properly investigated, the association of these cations with tau protein is incomplete and partially contradictory. The presence of metals, as copper, is a triggering factor in the deposition of toxic plaques and in the covalent modification of the protein,[6f] and therefore, a more detailed characterization of the metal binding is required. Tau protein shows an amino acidic sequence relatively rich in histidine residues, that usually work as primary binding sites for copper ions, besides several methionines located in different regions far from each other, therefore probably excluded from the participation in the metal binding. On the other hand, previous studies suggest the main involvement of the pseudorepeat region in the metal binding, where imidazolic groups besides amide-N ligands mediate the coordination sphere around the ion.[6g]
To elucidate the copper coordination site in the pseudorepeat domain, herein we report the redox reactivity of copper-adducts with tau fragments and the oxidative modifications of tau peptides when in presence of catecholic substrates. In future, further investigations will be required to understand the molecular bases of copper binding to the full-length protein, since an involvement of more histidines provided by each pseudorepeat has been proposed to generate a unique and highly-stabilized copper binding site in the native sequence.

Catalytic oxidation of catechols by Cu^{II}-tau complexes

Catecholamines, as dopamine, are evidenced in several brain regions, being involved in the signaling in neuronal network and the alteration of catecholamine metabolism is strongly involved in the development of neurodegenerative processes. Therefore, a comparative study about the oxidative capability of copper(II)-R1/R3 complexes toward these substrates was assayed respect with the catalytic efficiency of the unbound copper. The oxidation of dopamine and of related catechols characterized by a faster and easier polymerization mechanism, such as 4-methylcatechol, was performed in 50 mM HEPES buffer at pH 7.4 at 20 °C, following the development of the oxidative product at 401 nm, corresponding to the 4-methyl-quinone, and at 475 nm for the dopaminochrome.

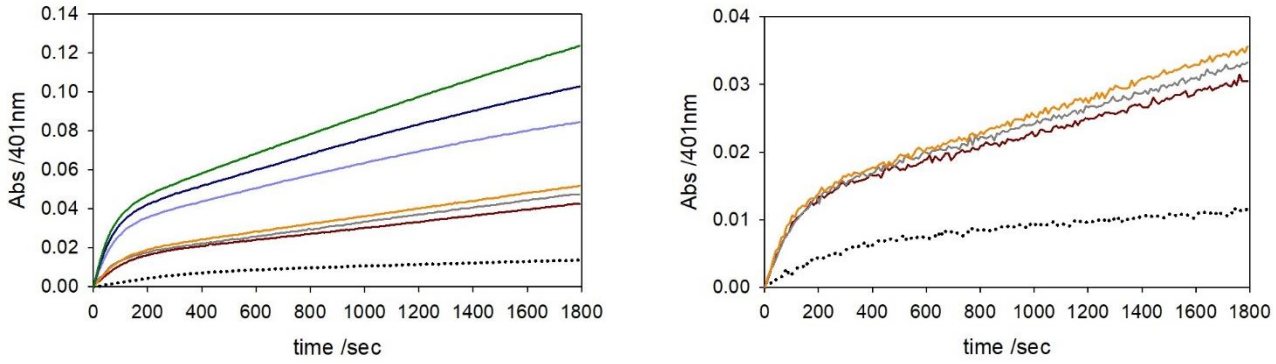

Figure 4. *Kinetic profiles of 4-MC (3 mM) oxidation with time in 50 mM HEPES buffer at pH 7.4 and 20 °C in the presence of only Cu^{II} (25 μM) (brown trace) and with 2 equiv. (grey), 4 equiv. (orange) of R1τ peptide or 1 equiv. (light blue), 2 equiv. (blue) and 4 equiv. of R3τ (green). Autoxidation of substrate is also shown (black dotted trace). At right, there is an enlargement of the oxidative trend of the R1 complexes.*

Oxidation of MC (3 mM) in the presence of copper(II) (25 μM) and with the addition till 4 equiv. of peptide was evaluated: the kinetic data show the strong catalytic capability of copper(II)-R3 complexes respect with the oxidation promoted by the R1 adduct. The increase of tau/copper ratio is proportional to the increase in the catalysis toward the catechol. Moreover, a biphasic behavior is clearly observed from the kinetic plots, in which a first and quantitative stage is quickly followed by a second linear step. A similar mechanism was evidenced for the oxidation pathway of dopamine, following the accumulation of dopaminochrome in the same reaction conditions; the additional bands at about 405 and 620 nm correspond to oligomeric and polymeric species, respectively, which can then generate high-molecular weight melanic products (data not shown). Therefore, the two-step mechanism described in Chapter 1 for 4-MC oxidation is less evident in the case of dopamine, due to the co-presence of several products with a similar wavelength absorption. In all data, the concentration of peptides influences both the first and the second step of the catalysis. The previously shown mechanism of oxidation of catechols by copper-peptide species can be extended to this work.[7,8] The first step corresponds to the complexation of Cu^{2+} with the high-affinity copper binding site in R1/R3 and the reaction rate is determined by the reduction of the metal complex through a mono-electronic oxidation of catechol. This quick step is only depending from the concentration of the substrate. The second stage shows the co-existence of several reactions: the reduced complex has to react with molecular oxygen and this interaction is usually described as the slow step of the full mechanism. A second molecule of substrate is then required to allow the transfer of a second electron from the bi-electronic reduction of O_2.

The copper(II)-peptide complex acts as a catalyst and the quinone is released. The higher catalysis promoted by copper(II)-R3 respect with R1 is probably due to the presence of tandem His-His site that is an excellent binding sequence for copper(I), enhancing the affinity for oxygen and the following re-oxidation of the complex.

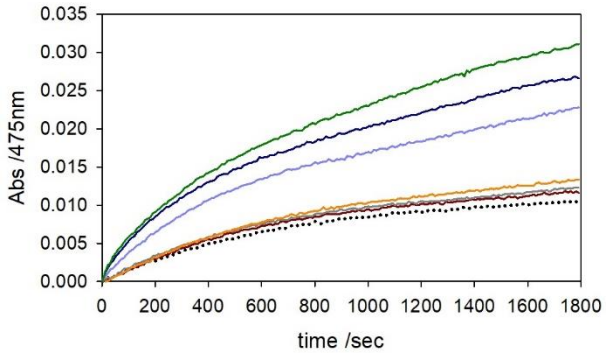

Figure 5. *Kinetic profiles of DA (3 mM) oxidation with time in 50 mM HEPES buffer at pH 7.4 and 20 °C in the presence of only Cu^{II} (25 μM) (brown trace) and with 2 equiv. (grey), 4 equiv. (orange) of R1τ peptide or 1 equiv. (light blue), 2 equiv. (blue) and 4 equiv. of R3τ (green). Autoxidation of substrate is also shown (black dotted trace).*

The low affinity of R1 for cuprous ions is related to the major concentration of unbound copper and the reactivity mainly corresponds to the catalytic behavior of the free copper.

Superoxide dismutase activity of copper(II)-tau complexes

The SOD-like activity was performed through the direct assay in which superoxide was generated by dissolution of potassium superoxide (28 mM) in a solution of 18-crown-6 (80 mM) in DMSO, previously prepared as anhydrous. The activity of [Cu^{2+}-R1/R3] complexes was compared to the behavior of free copper(II) ions and it was evaluated through the reaction between nitro blue tetrazolium (NBT) (1.25 mM) in phosphate buffer solution and superoxide to give methyl formazane (MF^+), that shows a strong absorption at 560 nm. Spectra were registered in 50 mM phosphate buffer solution at pH 7.4 and in the presence of NBT (0.2 mM), variable amounts of copper(II) (0-10 μM) and [Cu^{II}-tau] complex (0-10 μM, with a 1:1 ratio of Cu/peptide), 0.4 mM KO_2 from the 18-crown-6 ether solution in DMSO. Copper complexed to R1 and R3 shows the same activity of unbound copper; indeed, copper(II) ions are able to promote the dismutation of superoxide in hydrogen peroxide through the following reaction: $2\ O_2^- + 2\ H^+ \rightarrow H_2O_2 + O_2$. Anyway, the complexes do not show substantial differences in the catalysis of the SOD reaction leading to the conclusion that copper-tau adducts do not enhance SOD activity of the metal.

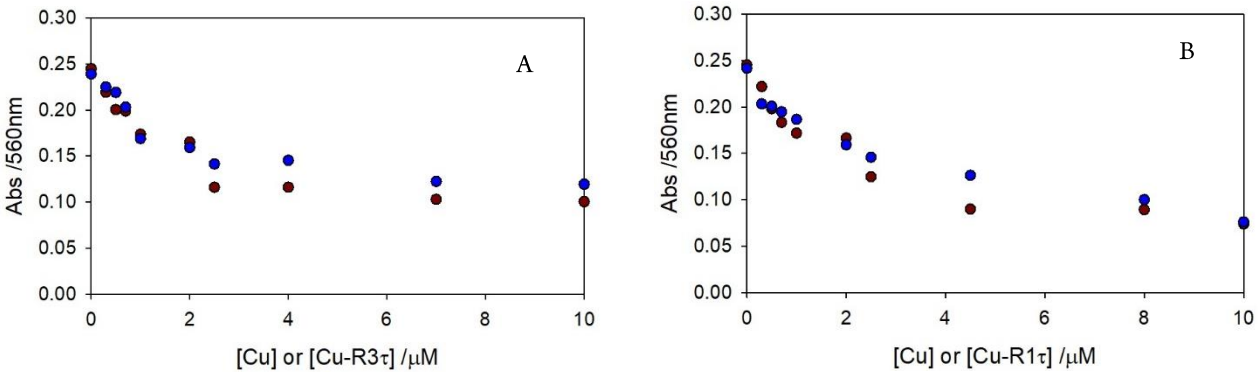

Figure 6. *Plots of UV-Vis absorbance at 560 nm for the NBT reduction to MF^+ by O_2^- in the presence of Cu^{II} (brown circles) and Cu^{II} complexed (blue circles) with A) R3τ and B) R1τ. Spectra were taken at 20 °C, in 50 mM phosphate buffer at pH 7.4.*

Oxidative modifications of tau peptides detected by HPLC-ESI/MS.

Radical oxygen species generated by copper redox cycling can attach both external substrate and peptide itself, since endogenous oxidative damage on peptides by metal-catalyzed oxidation (MCO) was largely suggested.[8] As explained in the Introduction, tau protein is also related to deficiencies in the mitochondrial activities and further fragmentation of these intracellular structures; this damage results in an unregulated production of reactive oxygen species, that are free to attach several cellular structures, such as proteins, leading to extensive post-translation modifications. The oxidative damage is due to the unselective oxidative activity of Cu/O_2 species and Fenton-like reactions that can have protein, lipids, nucleotides as modification targets.[9] The resulting damage on protein scaffolds can also affect the biological activity and the propensity to aggregate. The endogenous peptide modifications were studied by HPLC-ESI/MS, performing experiments in the same conditions used for kinetic studies. Reaction mixtures are prepared as follows: copper(II) nitrate (25 μM), R1τ or R3τ peptides (50 μM) and 4-MC (3 mM) were added in 50 mM HEPES buffer at pH 7.4. Samples are analyzed at different reaction times. Peptide modifications were also studied in the presence of dopamine (3 mM). The elution was carried out by using 0.1% HCOOH in distilled water (solvent A) and 0.1% HCOOH in acetonitrile (solvent B), with a flow rate of 0.2 ml/min. Elution started with 98% solvent A for 5 min followed by a linear gradient from 98 to 55% A in 65 min.

R1τ modification pattern

The experimental data collected in the presence of R1 fragment show that the peptide has a very modest susceptibility to the oxidative modification when incubated in the presence of MC and remains almost totally unmodified in the presence of dopamine. The main modification evidenced in these conditions was the covalent attach of catechol or quinone to histidine side chains, while the single insertion of oxygen was observed only upon long reaction time.

Table 1. *Modification with time of R1τ peptide detected by HPLC-MS upon reaction of Cu^{II} (25 μM), R1τ (50 μM) and 4-MC (3 mM) in 50 mM HEPES buffer at pH 7.4 and 20 °C.*

time	**R1τ**	**+16**	**+120**	**+122**	**+136**	**+138**
15 min	**95%**	-	3%	2%	-	-
30 min	**88%**	1%	6%	5%	-	-
90 min	**85%**	3%	5%	5%	1%	1%

Table 2. *Modification with time of R1τ peptide detected by HPLC-MS upon reaction of Cu^{II} (25 μM), R1τ (50 μM) and DA (3 mM) in 50 mM HEPES buffer at pH 7.4 and 20 °C.*

time	**R1τ**	**+16**	**+149**	**+151**	**+165**	**+167**
15 min	**100%**	-	-	-	-	-
30 min	**100%**	-	-	-	-	-
90 min	**100%**	-	-	-	-	-

The modification rate is tightly determined by the oxidative capability of the complex toward substrates and by the redox cycling rate of copper followed by the proportional generation of oxidative products in the reaction environment. The low redox ability of R1-adducts reflects the low oxidative environment and therefore, induces only partial modification of the peptide backbone.

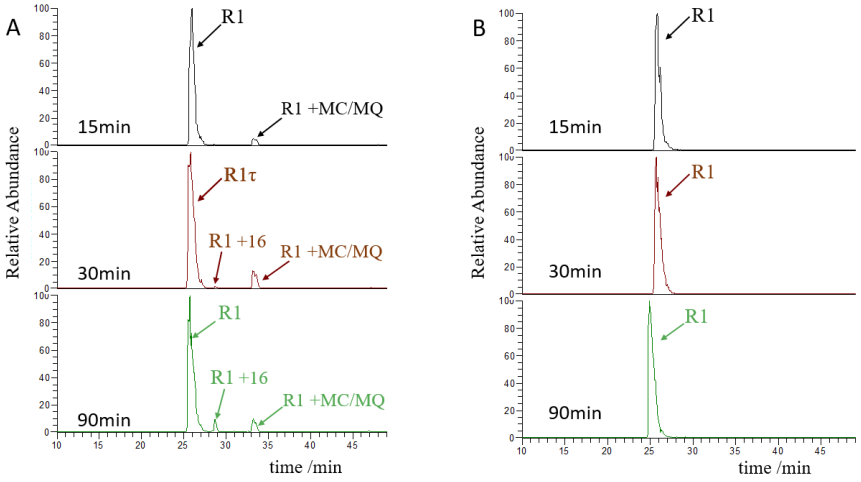

Figure 7. *HPLC-MS elution profiles of R1τ peptide (50 μM) resulting from oxidation of MC (panel A) or DA (panel B) (3 mM) in 50 mM HEPES buffer at pH 7.4 and at several reaction time by Cu^{II} (25 μM).*

R3τ modification pattern

The behavior of R3 tau peptide seems to be a quite divergent if compared with R1 fragment. Indeed, oxidative modifications on R3 are massive, resulting in a wide heterogeneity and in a visible extension of the modifications. The main modification is the addition of one atom of oxygen on the imidazole group of one histidine both in the presence of DA and MC, and after modest incubation time, the double insertion of oxygen is clearly observed. Minor modification consists in the formation of covalent adduct with catecholic or quinonic species, generated by the redox pathway. When MC is added to the solution, the pattern of modification is generally more complicated respect with DA and this behavior reflects the higher tendency of the catechol to be oxidized to give the respective quinone.

Table 3. *Modification with time of R1τ peptide detected by HPLC-MS upon reaction of Cu^{II} (25 μM), R3τ (50 μM) and DA (3 mM) in 50 mM HEPES buffer at pH 7.4 and 20 °C.*

time	**R3τ**	**-2**	**+16**	**+32**	**+120**	**+122**	**+136**	**+138**
15 min	**40%**	5%	27%	13%	1%	1%	6%	7%
30 min	**23%**	8%	36%	11%	1%	2%	7%	12%
90 min	**8%**	12%	36%	18%	1%	2%	7%	16%

Table 4. *Modification with time of R1τ peptide detected by HPLC-MS upon reaction of Cu^{II} (25 μM), R3τ (50 μM) and DA (3 mM) in 50 mM HEPES buffer at pH 7.4 and 20 °C.*

time	**R3τ**	**-2**	**+16**	**+32**	**+149**	**+151**	**+165**	**+167**
15 min	**97%**	-	3%	-	-	-	-	-
30 min	**86%**	-	11%	3%	-	-	-	-
90 min	**53%**	4%	29%	8%	1%	-	2%	2%

Therefore, Tables 3 and 4 highlight the following modifications: the *O*-atom insertion on histidine 329 and 330 (as +16 mass increment) or the insertion on both residues (+32), the covalent linkage with catechol (+122) or quinone (+120) and the coupled modification of covalent attach and oxidation of each histidine (+136/+138). A peculiar modification evidenced only in the presence of R3 is the oxidation of proline 332 to hydroxyproline, followed by dehydration and resulting in a total mass change of -2 units. The LC-MS analysis are in agreement with the kinetic data, that show a higher redox activity of R3 and therefore, the increased rate of modification is connected with the higher concentration of oxidative species in the incubation environment; on the other hand, R1 sequence is not a good ligand

for copper(I) and its copper complex is not redox competent, resulting in a slow reaction with oxygen and a lower local concentration of ROS, hence in a limited self modification.

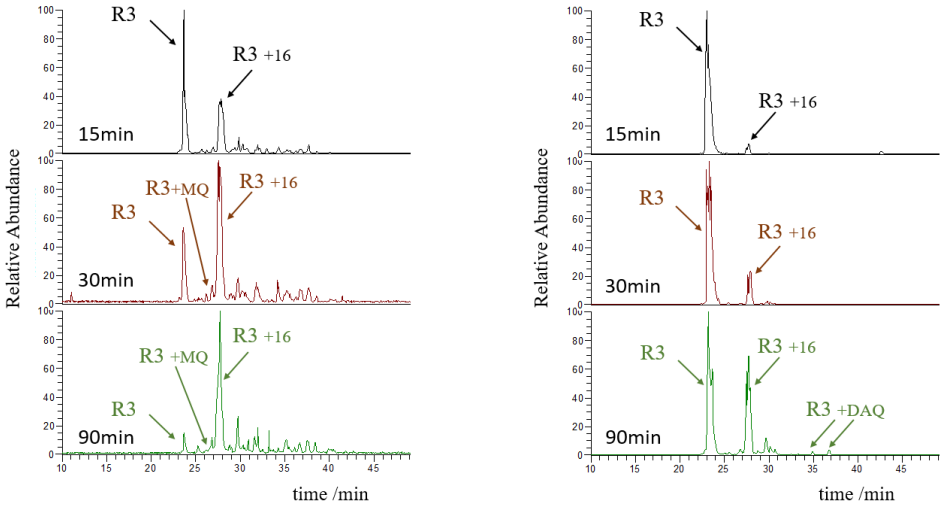

Figure 8. *HPLC-MS elution profiles of R3τ peptide (50 μM) resulting from oxidation of MC (left panel) or DA (right panel) (3 mM) in 50 mM HEPES buffer at pH 7.4 and at several reaction time by Cu^{II} (25 μM).*

Conclusions

All tauopathies, as Alzheimer's disease (AD), are associated with the abnormal deposition of misfolded tau proteins in neuronal and glial cells, destabilizing the microtubule apparatus. A correlation between the progression of these disorders and the loss of homeostatic control on redox active metals as copper has been verified, where the presence of metals in excess promotes the hyperphosphorylation of tau protein and its conversion into fibrillary structures. All these events contribute to the synaptic damage, cognitive impairment and neuronal death.[10] As previously described, the pseudorepeat domain in tau proteins plays an important role in the protein aggregation and, at the same time, corresponds to the region involved in copper coordination; the metal binding has been also correlated to evident conformational changes of the protein scaffold, altering the biological properties in the microtubule interaction. In particular, fragments encompassing the R1 and R4 repeats and incubated in the presence of copper(II) *in vitro* are prone to generate amorphous and insoluble structures, while β-sheets and fibrillary deposits were detected when R2 and R3 sequences are bound to the metal.[10] Several works have revealed strong affinity binding of copper(II) ions with full-length tau protein, mainly involving R2 and R3 repeats that are located in a region normally involved in the interaction with microtubules. Anyway, the characterization of metal complexation remains partially unknown if compared to other neuronal proteins, such as amyloid-β or α-synuclein, usually associated with the development of neurodegenerative disorders. In this chapter, the redox reactivity and the associated competitive modifications of two fragments, R1 and R3, were investigated, excluding in the third pseudorepeat the sequence encompassing the cysteine residue in order to avoid dimerization of the peptide and to increase the stability toward oxidation. The oxidative behavior of R3 indicates that the redox cycling of copper bound to the peptide is favored respect with free copper ions, since in this adduct the metal can assume an optimal coordination sphere that allows a fast exchange between the two metal redox states $Cu^{II/I}$. The divergent catalytic efficiency of R1 supports that the presence of only one histidine is not sufficient to ensure a fast redox cycling of copper, probably lacking of good ligands for the stabilization of copper(I). Studies performed in collaboration with other universities have confirmed through potentiometric and NMR studies that the redox capability of R3 is allowed by the presence of two vicinal His-His residues, as observed in amyloid-β, that are able to guarantee high affinity interaction with both oxidation states of the metal (K_d value of 71 nM and 0.08 nM for copper(II) and copper(I), respectively). Moreover, the catalytic reactivity of copper-R3 complex toward substrates as dopamine can exacerbate the inflammatory condition associated with neurodegenerative diseases via uncontrolled generation of oxidative and reactive species. ROS and similar molecules can unspecifically attach lipids, nucleotides or proteins, and therefore LC-MS studies were performed to clarify the possible competitive modification promoted by the oxidative environment and undergone by the protein backbone. R3 peptide is rapidly and extensively modified both in term of oxidative modification, as insertion of one atom of oxygen on imidazole side chains, and in term of covalent modification, as attach of catechol or quinone on histidine residues. The low redox capability of copper-R1 adduct reflects its low tendency to undergo modification respect with R3 and other neuronal peptides previously analyzed. Therefore, this short investigation confirms the relevance of the presence of bis-His domain in the interaction of copper ions with tau protein, ensuring an optimal binding site for both cupric and cuprous ions, while R1 sequence seems to be an exclusive binding sequence for copper(II), not allowing a good chelation of copper(I) and its further re-oxidation through the interaction with molecular oxygen. More detailed studies will be required to improve our knowledge about the copper coordination sphere with the other pseudorepeats and a further step will be the complexation of copper with the full-length protein and its characterization to verify the existence of only one copper binding site, thus involving the cooperation of several ligands supported by all pseudorepeats.

Synthesis of tau fragments

R1τ	Ac-^{256}VKSKIGSTENLKHQPGGG^{273}-NH_2	mw 1878
R3τ	Ac-^{323}GSLGNIHHKPGGG^{335}.-NH_2	mw 1271

The R1τ and R3τ peptides were synthesized on a solid-phase (Rink amide resin MBHA, substitution 0.78 mmol/g) using standard Fmoc-chemistry. The final products are amidated at the *C*-terminus while the *N*-terminus is acetylated. The usual steps of deprotection of Fmoc group, the coupling with amino acids and the capping of unreacted amino acids were performed as previously described. The crude peptides were purified by HPLC with a 0–100% linear gradient from 0.1% trifluoroacetic acid (TFA) in water to 0.1% TFA in CH_3CN over 30 min (flow rate of 3.5 mL min^{-1}), and characterized by ESI-MS: m/z 1879 $(R_1H)^+$, 940 $(R_1H_2)^{2+}$, 627 $(R_1H_3)^{3+}$; m/z 1272 $(R_3H)^+$, 636.5 $(R_3H_2)^{2+}$, 424.6 $(R_3H_3)^{3+}$.

Kinetic data of DA and MC oxidation

The catalytic oxidation of methylcatechol and dopamine by Cu^{2+} was studied at 20 °C in 50 mM HEPES buffer at pH 7.4, saturated with atmospheric oxygen. The reaction was monitored by UV-visible spectroscopy following the formation of methylquinone at 401 nm and dopaminochrome at 475 nm. Data obtained from autoxidation and from the catalysis in the presence of only copper(II) were compared with the kinetics promoted by copper-R1/R3 complexes, varying the equivalents of peptides respect with copper ions. These experiments were carried out by adding copper(II) nitrate (25 μM) as the last reagent to the solution containing MC or DA (3 mM) and R1 or R3 peptide (0-100 μM).

LC-MS modification pattern of R1 and R3

The peptide modification was studied by HPLC-ESI/MS, using a LCQ ADV MAX ion-trap mass spectrometer. All samples were prepared adding copper(II) nitrate (25 μM), R1 or R3 (50 μM) and MC (3 mM) in 50 mM HEPES buffer at pH 7.4 and the modification rate was obtained comparing the percentages of modification at several incubation points. The elution of R1 or R3 was carried out by using 0.1% HCOOH in distilled water (solvent A) and 0.1% HCOOH in acetonitrile (solvent B), with a flow rate of 0.2 ml/min; elution started with 98% solvent A for 5 min followed by a linear gradient from 98 to 55% A in 65 min.

Superoxide dismutase activity

The SOD-like activity of copper-peptide complexes was compared to the behavior of Cu^{2+} alone. The activity was evaluated through the direct assay in which O_2^- is directly added by dissolution of KO_2 salt (28 mM) in a solution of 18-crown-6 ether (80 mM) in anhydrous DMSO and detected by the reaction with nitro blue tetrazolium (NBT) (1.25 mM) in phosphate buffer. This last reagent forms an intermediate, the methyl formazane (MF^+), that is characterized by an intense absorption band at 560 nm. After sonication, the starting solution would become yellow-brown. UV-visible spectra were performed in 50 mM phosphate buffer at pH 7.4 with the following final concentrations: 0.2 mM NBT, variable amounts of copper(II) (0-10 µM) and [Cu^{2+}-R1/R3] complexes (0-10 µM, with a 1:1 ratio of Cu/peptide), 0.4 mM KO_2 from the 18-crown-6 ether solution in DMSO.

Recrystallization of partially oxidized 4-MC

To ensure a reproducibility of the catalytic data, 4-methylcatechol was purified before each data set. 4-MC (30 mg) was recrystallized in hexane : ethyl acetate mixture (10:1 ratio; 2 mL), heating until boiling in reflux apparatus. Boiling solution was filtered and dried through rotary evaporation. 4-MC was dissolved in diethyl ether (0.5-1 ml) and dried with vacuum pump. Impurities should be retained by the filter. This procedure was repeated twofold.

References

1. (a) B.E Glynn-Servedio and T.S. Ranola, AChE Inhibitors and NMDA Receptor Antagonists in Advanced Alzheimer's Disease, **Consult Pharm**, 32, 9, 511-518, 2017; (b) E. Gaggelli[1], H. Kozlowski, D. Valensin and G. Valensin, Copper Homeostasis and Neurodegenerative Disorders (Alzheimer's, Prion, and Parkinson's Diseases and Amyotrophic Lateral Sclerosis), **Chemical Reviews,** 106, 6, 2006; (c) M.D. Weingarten, A.H. Lockwood, S.Y. Hwo and M.W. Kirschner, A protein factor essential for microtubule assembly, **Proc Natl Acad Sci U S A**, 72, 5, 1858–1862, 1975; (d) D.F.V. Pîrşcoveanu, I. Pirici, V. Tudorică, T.A. Bălşeanu, V.C. Albu, S. Bondari, A.M. Bumbea and M. Pîrşcoveanu, Tau protein in neurodegenerative diseases – a review, **Rom J Morphol Embryol,** 58(4), 1141–1150, 2017; (e) B. Su, X. Wang, L. Zheng, G. Perry, M.A. Smith and X. Zhu, Abnormal mitochondrial dynamics and neurodegenerative diseases, **Biochim Biophys Acta**, 1802(1), 135–142, 2010; (f) C. Beharry, L.S Cohen, J. Di, K. Ibrahim, S. Briffa-Mirabella and A. del C Alonso, Tau-induced neurodegeneration: mechanisms and targets, **Neurosci Bull**, 30(2), 346–358, 2014.
2. A. Soragni, B. Zambelli, M.D. Mukrasch, J. Biernat, S. Jeganathan, C. Griesinger, S. Ciurli, E. Mandelkow and M. Zweckstetter, Structural Characterization of Binding of Cu(II) to Tau Protein, **Biochemistry**, 47 (41), 10841-10851, 2008.
3. (a) B. Shin and S. Saxena, Insight into Potential Cu(II)-Binding Motifs in the Four Pseudorepeats of Tau Protein, **J. Phys. Chem. B**, 115, 15067–15078, 2011; (b) M. Kolarova, F. García-Sierra, A. Bartos, J. Ricny and D. Ripova, Structure and Pathology of Tau Protein in Alzheimer Disease, **Int J Alzheimers Dis.**, 731526, 2012.
4. C.-X. Gong and K. Iqbal, Hyperphosphorylation of microtubule-associated protein tau: a promising therapeutic target for Alzheimer disease, **Curr Med Chem**, 15 (23), 2321-8, 2008.
5. (a) M.A. Brister, A.K. Pandey, A.A. Bielska and N.J. Zondlo, N-Acylation and Phosphorylation Have Opposing Structural Effects in tau: Phosphothreonine Induces Particular Conformational Order, **Journal of the American Chemical Society**, 136 (10), 3803-3816, 2014; (b) C. Kontaxi, P. Piccardo, and A.C. Gill, Lysine-Directed Post-translational Modifications of Tau Protein in Alzheimer's Disease and Related Tauopathies, **Front Mol Biosci**; 4: 56. 2017; (c) Amyloid: Vascular and Parenchymal, **Encyclopedia of Neuroscience,** 355-36, 2009.
6. (a) A. Anoop, P.K. Singh, R.S. Jacob and S.K. Maji, CSF Biomarkers for Alzheimer's Disease Diagnosis, **Int J Alzheimers Dis.,** 606802, 2010; (b) D. Kaden, A.I. Bush, R. Danzeisen, T.A. Bayer and G. Multhaup Disturbed Copper Bioavailability in Alzheimer's Disease, **International Journal of Alzheimer's Disease**, ID 345614, 5, 2011; (c) M. Kitazawa, D. Cheng and F.M. Laferla, Chronic copper exposure exacerbates both amyloid and tau pathology and selectively dysregulates cdk5 in a mouse model of AD, **J Neurochem**, 108, 6, 1550–1560, 2009; (d) C.W. Ritchie, A.I. Bush, A. Mackinnon, S. Macfarlane, M. Mastwyk, L. MacGregor, L. Kiers, R. Cherny, Q.X. Li, A. Tammer, D. Carrington, C. Mavros, I. Volitakis, M. Xilinas, D. Ames, S. Davis, K. Beyreuther, R.E. Tanzi and C.L. Masters, Metal protein attenuation with iodochlorhydroxyquin (clioquinol) targeting Abeta amyloid deposition and toxicity in Alzheimer disease: a pilot phase 2 clinical trial. **Arch Neurol,** 60, 12, 1685–1691, 2003; (e) A. De Benedictis, A. Vilella and A.M. Grabrucker, The Role of Trace Metals in Alzheimer's Disease, **Alzheimer's Disease,** 6, 2019; (f) S.S. Leal, H.M. Botelho and C.M. Gomes, Metal ions as modulators of protein conformation and misfolding in neurodegeneration, **Coordination Chemistry Reviews**, 256,19–20, 2253-2270, 2012; (g) Q.-F. Ma, Y.-M. Li, J.-T. Du, K. Kanazawa, T. Nemoto, H. Nakanishi and Y.-F. Zhao, Binding of copper(II) ion to an Alzheimer's tau peptide as revealed by MALDI-TOF MS, CD, and NMR, **Biopolymers**, 5, 79, 2, 74-85, 2005.
7. S. Dell'Acqua, C. Bacchella, E. Monzani, S. Nicolis, G. Di Natale, E. Rizzarelli and L. Casella, Prion Peptides Are Extremely Sensitive to Copper Induced Oxidative Stress., **Inorg Chem,** 56 (18), 11317-11325, 2017.
8. V. Pirota, S. Dell'Acqua, E. Monzani, S. Nicolis and L. Casella, Copper-Aβ Peptides and Oxidation of Catecholic Substrates: Reactivity and Endogenous Peptide Damage, **Chemistry – A European Journal**, 22 (47), 16964-16973, 2016.
9. S. Di Meo, T.T. Reed, P. Venditti and V.M. Victor, Role of ROS and RNS Sources in Physiological and Pathological Conditions, **Oxid Med Cell Longev**, 1245049, 2016.
10. (a) K. Zubčić, P.R. Hof, G. Šimić1 and M.J. Jembrek, The Role of Copper in Tau-Related Pathology in Alzheimer's Disease, **Front. Mol. Neurosci.,** 13, 174, 2020; (b) A.C. Kim, S. Lim and Y.K. Kim, Metal ion effects on Aβ and tau aggregation, **Int. J. Mol. Sci.,** 19, E128, 2018.

Chapter 4

COPPER REDOX CYCLING IN AMYLOID-β FRAGMENTS: THE CONTROVERSIAL ROLE OF *N*-TERMINAL AMINE.

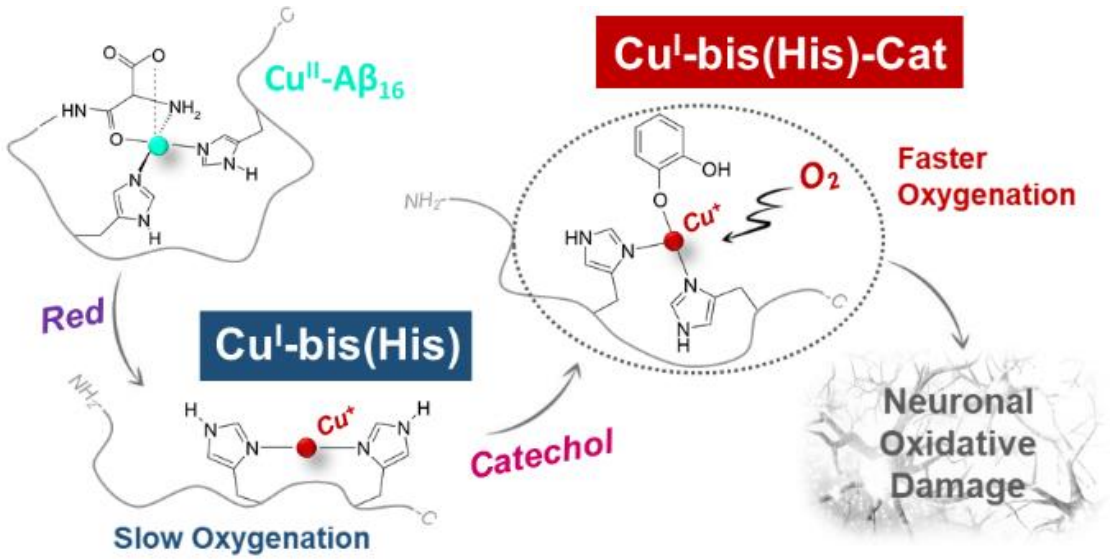

Ref. Inorg. Chem., 60, 2, 606–610, 2021
"A Cu-bis(imidazole) Substrate Intermediate Is the Catalytically Competent Center for Catechol Oxidase Activity of Copper Amyloid-β"
C. Bacchella, S. Dell'Acqua, S. Nicolis, E. Monzani and L. Casella

As described in the previous sections, neuronal extracts obtained from AD-affected brains show high levels of metal ions if compared to the normal biological contents. The dyshomeostasis of reactive metals, such as copper, can evolve in the uncontrolled redox reactivity and in the generation of harmful oxidative species, exacerbating the neurodegenerative disorder.[1a,1b] Alzheimer's disease is a neurodegenerative condition that is clinically recognized through some biological alterations, such as the deposition of extracellular insoluble plaques, mainly composed by aggregated amyloid-beta peptides, and of intracellular tangles showing fibrillary structures and containing high levels of tau protein.[2a,2b] In these deposits, both tau and β-amyloid proteins show abnormal folding of the amino acidic backbones linked to the extensive oxidative modification on recurrent susceptible amino acids. Amyloid plaques are therefore extracellular deposits of misfolded Aβ peptide that assumes β-folded secondary structure due to the stacking between parallel strands via hydrogen bonds. Besides these extracellular aggregates, intraneuronal fibrillary tangles resembling serpentine fibrils are also detected, in which significant content of high phosphorylated and helical structured tau protein is observed. In these dangerous context, the neuronal environment is strongly subjected to inflammatory processes and AD-affected brains show increased amounts of glial fibrillary acidic protein (GFAP) and activated microglia, that are the typical signals of the inflammatory response (Figure 1).[3]

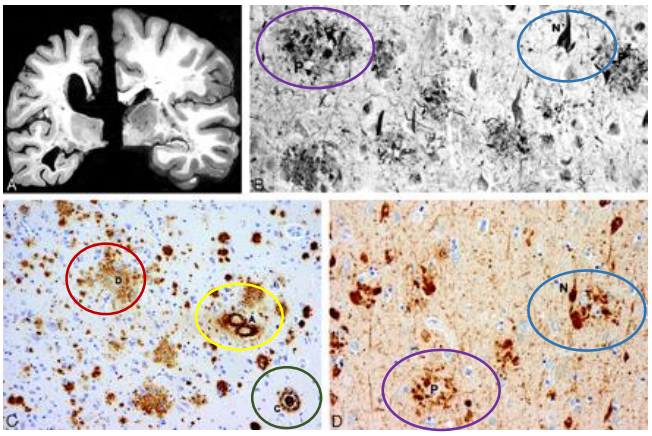

Figure 1. *A) Neuronal atrophy. On the left, the section of the hemibrain of AD patients and, on the right, a healthy control brain. The affected brain evidences marked atrophy, dilation of the lateral ventricle, and a reduced hippocampus. B) Neurofibrillary tangles (blue) and neuritic plaques (violet) in the hippocampus. C) β-amyloidosis in the frontal lobe, showing some diffuse plaques (red), a cored plaque (green), and cerebral amyloid angiopathy (yellow). D) Neurofibrillary tangles (blue) and neuritic plaques (violet) in the frontal lobe.*[3]

A multitude of studies suggest that the interaction of neuroproteins with metals strongly influences the progression of the disease. In particular, the binding between copper ions and amyloid-β peptides and the redox ability of the resulting complex has been studied extensively. Full-length β-amyloid sequence can be virtually divided in two regions, a *N*-terminal domain normally unstructured and with high affinity for copper(II)/(I) binding, and a *C*-terminal one, in which there is a prevalence of uncharged amino acids able to mediate the intermolecular crosslinking and to lead to fast aggregation of the protein. Although the interaction of metal ions such as copper with amyloid-β peptides is commonly accepted, the reaction mechanism whereby the redox-competent adduct works and its metal coordination sphere are still debated. Indeed, Cu^{I} and Cu^{II} species probably require distinct coordinative environments and different coordination geometries, but, at the same time, these binding modes would have to be easily exchangeable to ensure an efficient catalytic cycle of the metal center. In the last years, several works have confirmed the existence of a dynamic equilibrium between two coexisting binding modes of copper(II) at physiological pH, called *component I* and *II*,

showing a distorted square-planar geometry. The principal *component I* is described as a copper(II) core anchored to the *N*-amine group, a carboxyl group of Asp-1 and two histidines, His-6 and His-13/14; the secondary *component II* would involve the coordination of the primary amine, an amide group of Asp-1, the C=O group of Ala-2 and only one histidine.[4a]

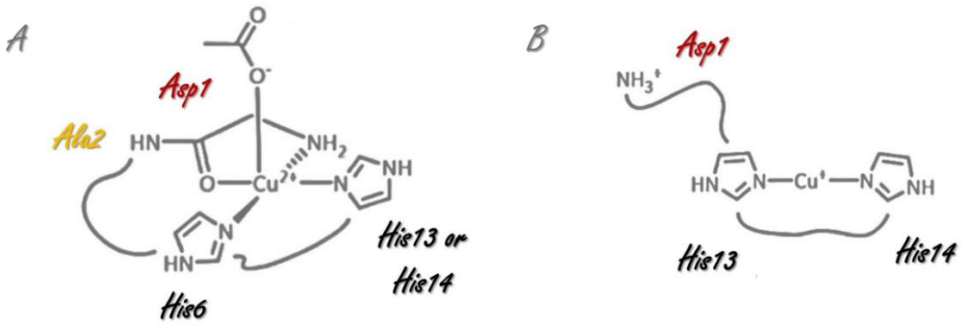

Figure 2. *A) Main copper(II) coordination geometry and B) Most stable coordination sphere for Cu^{I} upon the binding with amyloid-β peptides.*

Regarding the interaction between cuprous ions and amyloid-β peptides, a linear geometry mediated by only two histidine residues seems to be the most probable coordination, or, at least, the most stable geometry (Figure 2).[4b]

A minimal reorganization energy and a limited geometric rearrangement to connect the two *resting states* are required in order to ensure an efficient redox chemistry of the complex. Therefore, the existence of a catalytic "in-between state" (IBS) was suggested[5a, 5b] to justify the energetic gap that divides the two redox species. This intermediate could minimize the structural modification between the two resting states and may act as the redox-competent transient species. Faller et al.[5b] suggest the coordination sphere of the redox-competent intermediate shown in Figure 3, in which the anchoring ligands correspond to the *N*-terminal amine, the side chain of Asp_1 and the side chain of one Histidine (probably His-6).

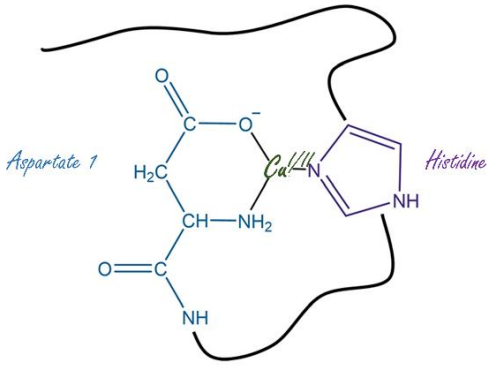

Figure 3. *Proposed copper coordination sphere, known as "in-between state", by amyloid-β peptides.*

The previous assertion would be motived by the high percentage of modification, such as decarboxylation and deamination, evidenced on aspartate at 1 position, suggesting the residue 1 as one of the main sites targeted by ROS and a possible ligand in the hypothetical transient state.[6a] Moreover, the protection or the deletion of *N*-terminal Asp_1 induce not negligible changes in the levels of ROS production, suggesting the involvement of this residue in copper redox cycle during the catalytic ascorbate oxidation. Therefore, this section has the aim to verify the role of *N*-terminal coordination site in the reaction efficiency and the participation of some IBS intermediate when a catecholic substrate, instead of ascorbate, is used as reducing agent. Among the high levels of free metals and the possible interaction with some neuronal proteins, the trafficking and the biological role of catecholamines have to be considered. Dopamine is a neurotransmitter normally involved in the signaling of neuronal pulses in the axons of cerebellar cells and its catecholic group shows a modest affinity for the binding of metal ions, as copper. Furthermore, the reactivity of this molecules toward redox active metals has been largely discussed and the possible generation of reactive oxidative products highlights the potential dangerous role of the neurotransmitter that is able to attach biological structures, such as proteins and lipids, exacerbating the neuronal damage.[6b] To this end, a comparative study was performed in terms of catalytic efficiency of copper(II)/(I) bound to the endogenous and point-mutated $A\beta_{1\text{-}16}$, and $A\beta_{1\text{-}9}$ peptides in both unprotected (NH_2-Aβ) and *N*-acetylated (Ac-Aβ) forms.

At first, an initial investigation of the catalytic behavior toward 4-methyl catechol and dopamine promoted by [Cu^{II}-NH_2-$A\beta_{16}$] and [Cu^{II}-Ac-$A\beta_{16}$] complexes was performed, working at saturating concentration of substrate (3 mM). The catalytic oxidation of the two catecholic substrates by Cu^{II} was studied at 20 °C in 50 mM HEPES buffer at pH 7.4. The reaction was monitored by UV-visible spectroscopy through the development of dopaminochrome band at 475 nm for dopamine, or 4-methylquinone band at 401 nm for 4-MC. All experiments were carried out by adding copper(II) nitrate (25 μM) to the substrate (3 mM) and the same conditions were maintained in presence of $A\beta_{16}$, and Ac-$A\beta_{16}$peptides (50 μM).

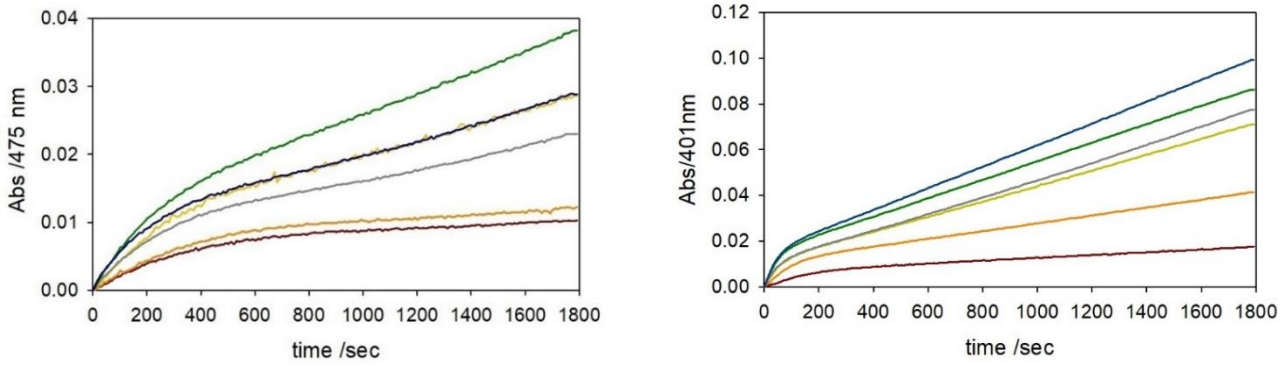

Figure 4. *Kinetic profiles of DA (3 mM, left panel) and MC (3 mM, right panel) oxidation with time in 50 mM HEPES buffer at pH 7.4 and 20 °C (autoxidation, brown trace) in the presence of Cu^{II} (25 μM) (orange) and with 1 eq. $A\beta_{16}$ (light green), 2 eq. $A\beta_{16}$ (green), or 1 eq. Ac-$A\beta_{16}$ (grey) and 2 eq. Ac-$A\beta_{16}$ (blue).*

In Figure 4, contradictory results can be observed. Dopamine at saturating concentration seems to be more easily oxidized by the copper(II)-acetylated peptide complex, suggesting that the redox efficiency of this adduct (1:1) is comparable to the catalysis promoted by 2 equiv. of the unprotected *N*-terminal peptide.

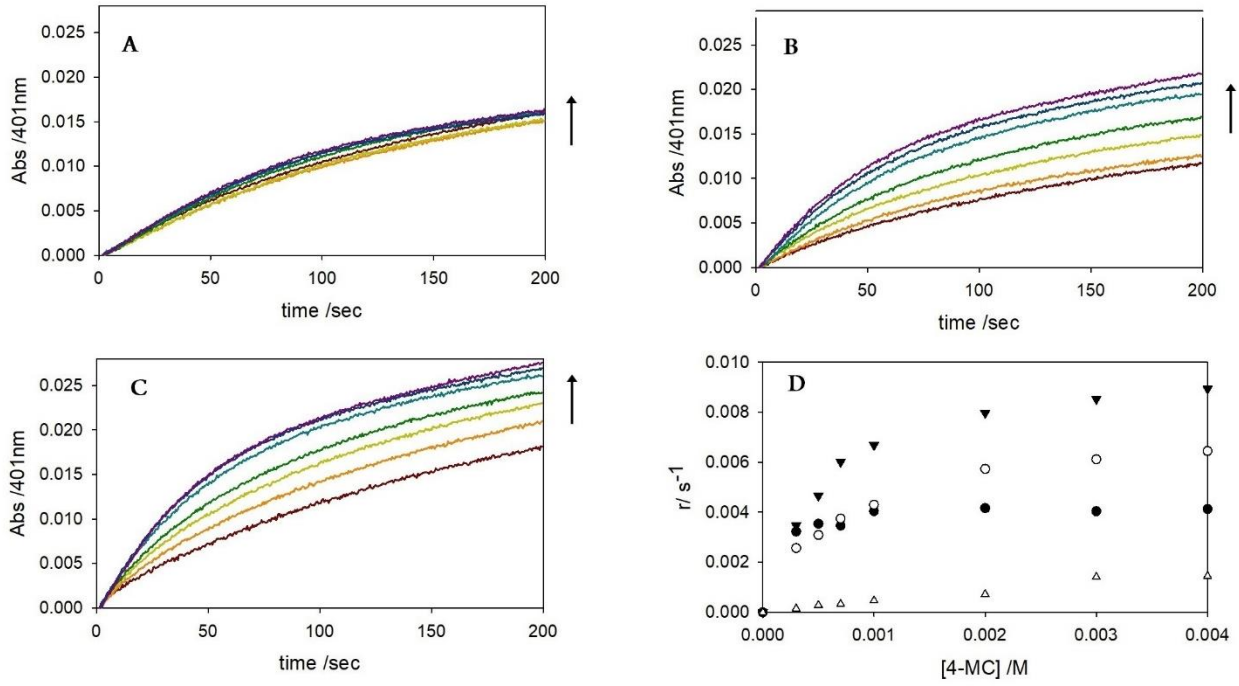

Figure 5. *Kinetics traces of 4MC oxidation in the presence of Cu alone (panel A) or Cu-peptide complex in 1:1 molar ratio, 25 μM: copper-$A\beta_{16}$ (panel B) and copper-Ac-$A\beta_{16}$ (panel C). The concentration of substrate varies from 0.3 to 4.0 mM. Panel D: Dependence on [MC] of the initial oxidation rates*

(indicated as r = rates/[catalyst]). The substrate oxidation is performed in only buffer (white triangles) and in the presence of copper alone (black circles), copper-Aβ16 (white circles) and Ac-Aβ16 (black triangles). The data for the not-catalytic oxidation were obtained assuming a Cu concentration of 25 μM.

On the other hand, this trend is not confirmed by the kinetics done in the presence of a more reactive, but neutral-charged substrate, 4-methylcatechol. Regarding the coordination sphere of copper ions, the results could suggest a possible involvement of the *N*-terminal amine as binding site of copper and therefore, the absence of the primary amine could influence the catalytic cycle efficiency. To understand the reaction mechanism and the different catalytic behavior of the two complexes, the substrate-dependence was investigated varying the concentration of 4-methylcatechol (Figure 5) or dopamine (Figure 6) from 0.3 to 4 mM and fixing the equivalents of copper and peptide (25 μM, 1:1). Only in the experiment with 4-MC the initial rates were plotted against the substrate concentration and the rate constants k_r and K_B were obtained through the interpolation with Michaelis-Menten-like equation (see the Experimental Notions). K_B corresponds to the substrate binding constant to the active species, while k_r is the rate parameter for the oxygen binding of the substrate-complex adduct. The initial rates of dopamine oxidation show a not hyperbolic behavior and therefore, no kinetic parameters have been calculated.

Table 1. *Kinetic constants calculated via the interpolation of the data shown in Figure 5D through Michaelis-Menten-like equation.*

	k_r /sec^{-1}	SE	K_B /M^{-1}	SE
Cu-Aβ16	5.68E^{-3}	±1.98E^{-4}	2220	±280
Cu-Ac-Aβ16	8.45E^{-3}	±2.67E^{-4}	2440	±290

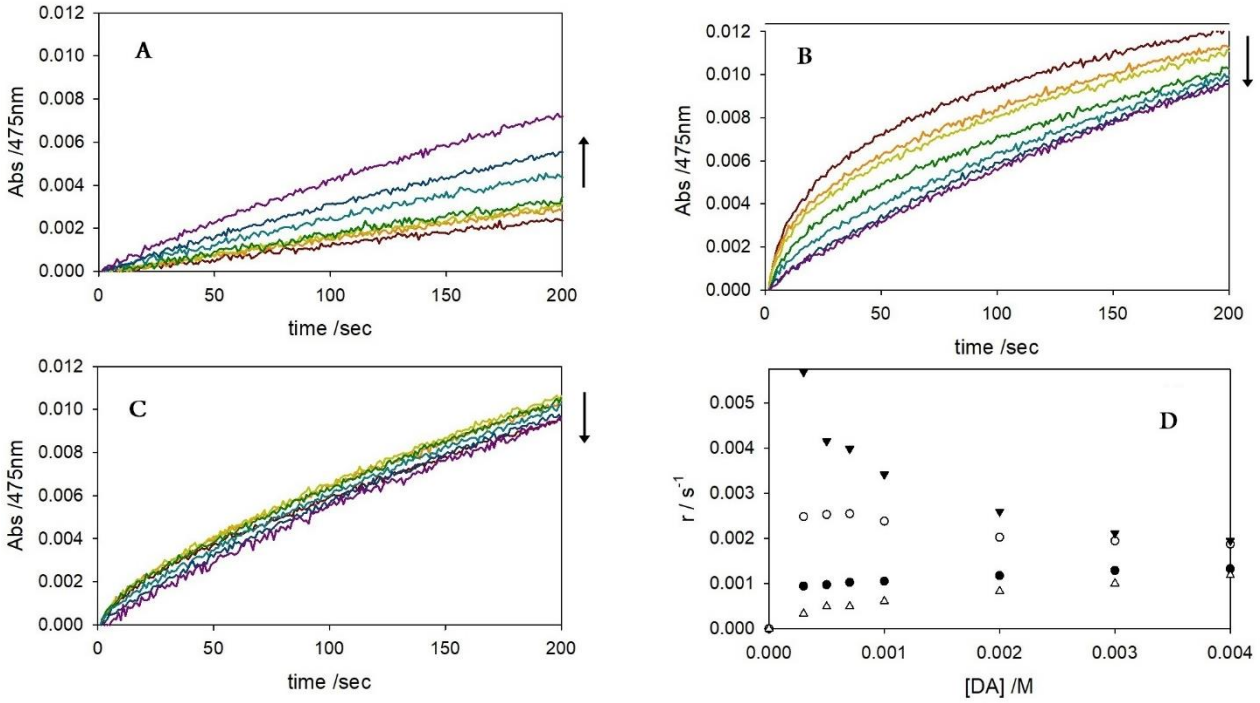

Figure 6. *Kinetics traces of DA oxidation in the presence of Cu alone (panel A) or Cu-peptide complex in 1:1 molar ratio, 25 μM: copper-Ac-Aβ16 (panel B) and copper-Aβ16 (panel C). The concentration of substrate varies from 0.3 to 4.0 mM. Panel D: Dependence on [DA] of the initial oxidation rates (indicated as r = rates/[catalyst]). The substrate oxidation is performed in only buffer (white triangles) and in the presence of copper alone (black circles), copper-Aβ16 (white circles) and Ac-Aβ16 (black triangles). The data for the not-catalytic oxidation were obtained assuming a Cu concentration of 25 μM.*

The initial rates, as ΔAbs/time, were converted into v(sec^{-1}) dividing the values with the product of catalyst concentration (copper or the copper-peptide complex, 25 μM) and the epsilon of the 4-methylquinone (1550 cm^{-1} M^{-}

[1]). For 4-methylcatechol, the constant parameters highlight the higher catalytic efficiency of copper complexed with the *N*-acetylated peptide, while in the case of dopamine, a convergence between the initial oxidation rates was observed when the substrate concentration reaches saturating values. In particular, when the dopamine concentration is maintained at sub-saturating values, the divergence from the initial rates obtained in the presence of the two complexes is larger, suggesting the higher catalytic potential of Cu^{II} bound to *N*-acetylated peptide. These preliminary data do not allow to determine a precise oxidative mechanism or an intermediate involved in the reaction, but they can suggest that the catalytic differences of the two adducts can be related to some different binding geometry of copper(II) when interacts with each peptide, and probably the lacking of the *N*-terminal amine as binding ligand may shift copper(II) toward a coordination mediated by at least two histidines. To better understand the reason of the divergent reactivity of the two substrates and hypothesizing a possible electrostatic interaction of the NH_2-group of dopamine with some negatively-charged amino acids, such as Asp1 and Glu3, located in the *N*-terminal domain, dopamine was NH_2-protected via acetylation and similar kinetic studies were performed. *N*-acetyl-dopamine was synthesized as shown in the Experimental section and was studied in term of oxidation to quinone, following the absorption band at 400 nm. Comparing the reactivity previously observed toward 4-MC or DA promoted by copper complexes, a parallel trend to that observed with 4-methylcatechol was obtained (Figure 7).

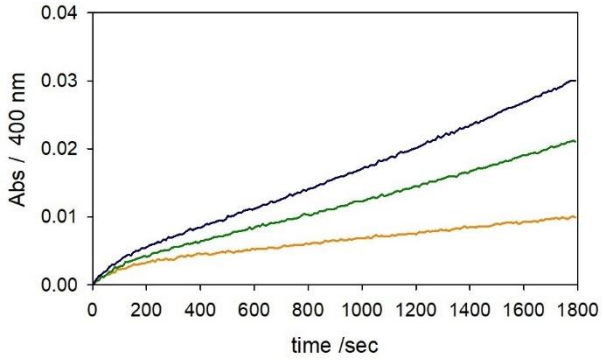

Figure 7. *Kinetic profiles of N-acetyl-dopamine (3 mM) oxidation with time in 50 mM HEPES buffer at pH 7.4 and 20 °C in the presence of Cu^{II} (25 μM) (orange) and with 2 eq. $A\beta_{16}$ (green) or 2 eq. Ac-$A\beta_{16}$ (blue).*

The copper(II)-Ac-$A\beta_{16}$ adduct shows a higher catalytic efficiency to generate the dopaquinone if compared to the *N*-unprotected peptide, suggesting an effective involvement of the side chain of dopamine in the reaction mechanism. Moreover, dopamine at saturating concentration is a competitive ligand for copper(II) (with a binding constant, K_b, of $5\times10^6\ M^{-1}$)[7a] and is probably able to compete with Ac-$A\beta_{16}$ ($K_b \sim10^8\ M^{-1}$),[7b] while no competition would be observed with NH_2-$A\beta_{16}$ ($K_b \sim10^{10}\ M^{-1}$).[7c]

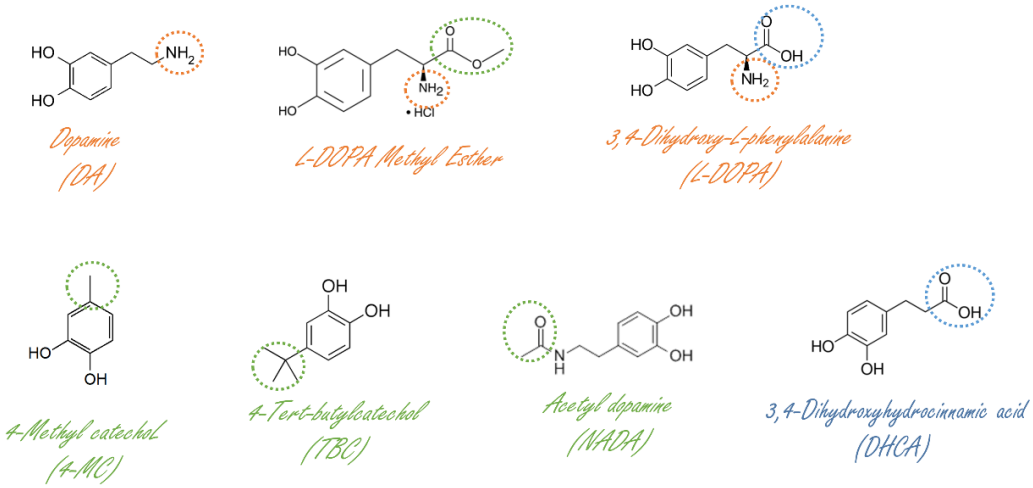

Figure 8. *Chemical structures of all catecholic substrates used in the following experiments, highlighting the different chemical properties.*

The calculation of the binding properties obtained from the equations shown in the Experimental section indicates that at 3 mM DA only 22% of Cu^{II} is sequestered by Ac-$A\beta_{16}$, while NH_2-$A\beta_{16}$ can bind approximately 96% of free metal. To assay the effective higher catalytic potential of Cu-Ac-$A\beta_{16}$ and the effect of the presence of an amine group in the substrate, the oxidation mechanism toward other catechols was investigated (Figure 8). The catechols used for these studies have been selected with different chemical properties, such as the presence of an amine side-chain in 3,4-dihydroxy-L-phenylalanine, or not-charged groups with different grades of steric hindrance, as 4-tert-butylcatechol, or carboxyl groups as 3,4-dihydroxyhydrocinnamin acid, to highlight some catalytic trend commonly observed on chemically similar substrates. All substrates were used at sub-saturating concentration (0.3 mM), previously dissolved in acetate buffer solution at pH 4 and the kinetics were performed in 50 mM HEPES buffer at pH 7.4 in the presence of copper-peptide complexes (25 μM) (Figure 9).

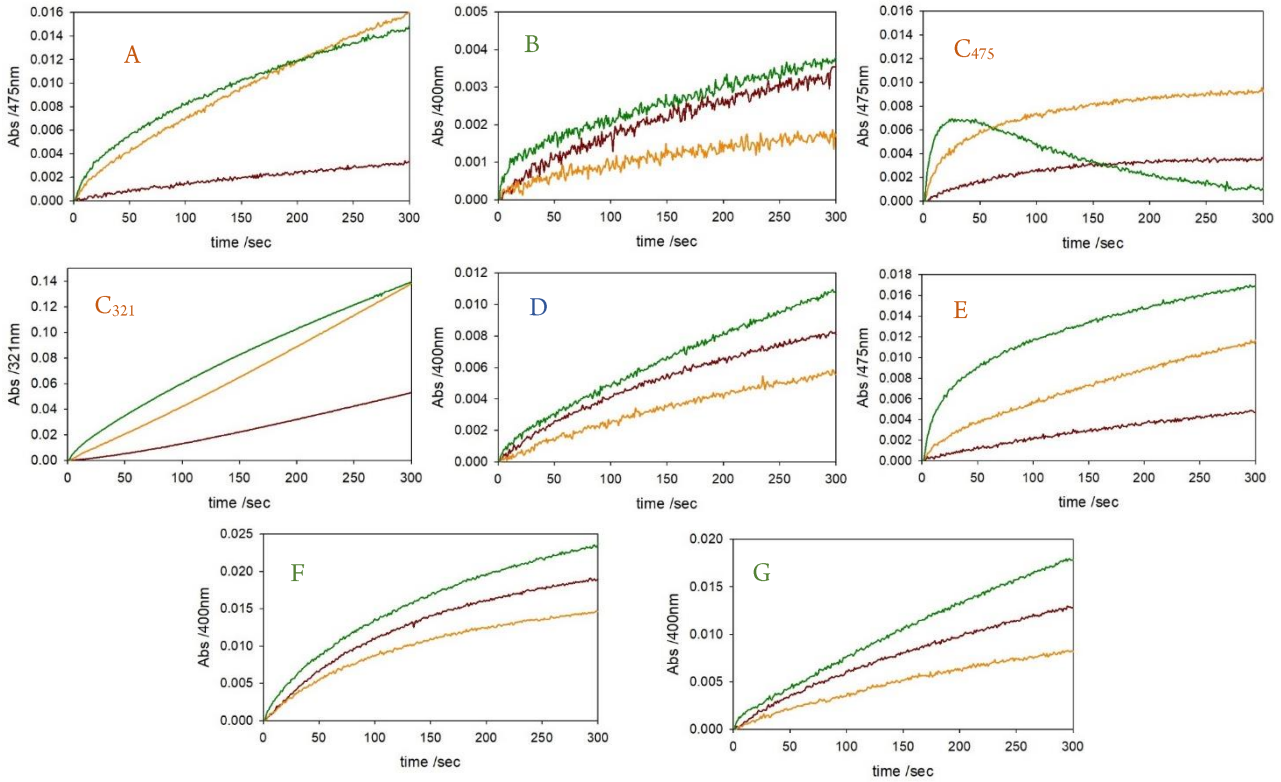

Figure 9. *Kinetic profiles of oxidation of several catecholic substrates (0.3 mM) with time in 50 mM HEPES buffer at pH 7.4 and 20 °C in the presence of Cu^{II} (25 μM) (brown trace) and with 1 eq. $A\beta_{16}$ (orange) or 1 eq. Ac-$A\beta_{16}$ (green): A) L-DOPA; B) N-acetyldopamine; C) L-DOPA methyl ester, followed at 475 nm and 321 nm; D) 3,4-dihydroxyhydrocinnamic acid; E) dopamine; F) 4-methylcatechol; G) 4-tert-butylcatechol*

All previous kinetics evidence a biphasic behavior in which the first fast step corresponds to the redox reaction between 2 equiv. copper(II) and a molecule of substrate to release the quinonic product and 2 reduced metal ions, as shown in the equation 1

eq. 1) $$\mathbf{2\ Cu^{2+} + Catechol \rightarrow 2\ Cu^{+} + Q}$$

As suggested by the data previously proposed,[8a,8b] this reaction is not stoichiometric and indeed, a lower initial reaction rate if compared to the expected absorbance values was obtained. The quickly generated dopaminochrome is just as fast degraded to promote the generation of oligomeric species, as evidenced by the absorption around 300 nm. Furthermore, the initial step is independent from the dioxygen binding to the complex: the first phase of the oxidative reaction toward dopamine proceeds without any reliable change both under air oxygen and upon the saturation of HEPES buffer with pure oxygen (1 atm) (Figure 10). The oxidative behavior in the first seconds of reaction shown by

Cu^{II}-Ac-Aβ$_{16}$ is in agreement with its higher redox potential (E°' +0.277 mV) if compared to Cu^{II}-Aβ$_{16}$ (E°' +0.178 mV).[9a]

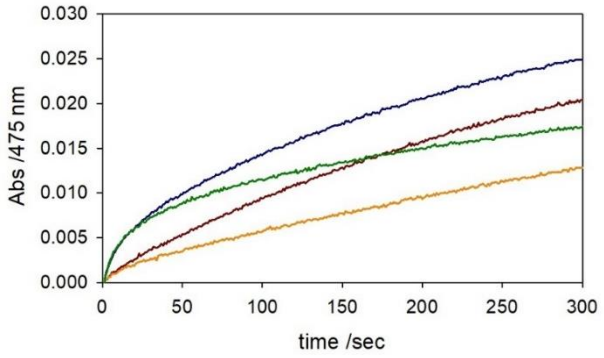

Figure 10. *Kinetic profiles of dopamine (0.3 mM) oxidation with time in 50 mM HEPES buffer at pH 7.4 and 20 °C in the presence of [Cu^{II}-Aβ$_{16}$] (25 μM) (orange trace) and [Cu^{II}-Ac-Aβ$_{16}$] (green). The same experiment was performed upon saturation of buffer solution with pure oxygen (brown, [Cu^{II}-Aβ$_{16}$] and blue, [Cu^{II}-Ac-Aβ$_{16}$])*

From the observation of the catalytic behavior of *N*-acetylated peptide bound to copper(II), two divergent slopes in the biphasic traces can be clearly distinguished, while the kinetic traces in the presence of free *N*-terminal peptide assume a straighter trend, in which the two steps seem to be interpenetrated. The dioxygen pre-saturation induces some changes limited to the second step of the catalysis, while the first reaction is not influenced by the amount of molecular oxygen. Increasing the local concentration of dopamine, the separation between the two reactions becomes less evident and the fast DAC decay is masked if the substrate oxidation is promoted by a good catalyst. Upon the quick reduction of copper(II) adduct to copper(I) in the first catalytic step, a second step involves the oxygenation of the complex and the re-oxidation of Cu^{I}-adduct to Cu^{II} after the O_2 binding acts as the limiting step of the reaction:

eq. 2) $$[\mathbf{Cu^{+}\text{-}peptide}] + \mathbf{O_2} \rightarrow [\mathbf{Cu^{+}\text{-}peptide\text{-}O_2}] \rightarrow\rightarrow [\mathbf{Cu^{2+}\text{-}peptide}]$$

The oxidation of catecholamines such as L-DOPA or dopamine shows a fast first step not influenced by oxygen and promoted by Cu-Ac-Aβ$_{1\text{-}16}$ complex, while the rate of the second step catalyzed by copper-peptide adduct is appreciably decreased. This effect is considerable in Figure 9C, in which a reactivity shutdown is observed when L-DOPA methyl ester is used as internal substrate. Therefore, the full oxidative process is characterized by a first step in which there is a fast accumulation of dopachrome following by its degradation and accumulation of small oligomers. The slowness of the second step does not allow to generate high-molecular weight polymers and induces the partial quenching of the reaction. On the other hand, copper-Aβ$_{16}$ adduct is not so efficient to induce a similar increase of the NH_2-catechol oxidation, showing a lower reaction rate in the stoichiometric step. Moreover, the reaction toward substrates lacking of the amine group and catalyzed by the free *N*-terminal peptide is partially depressed. All these observations lead to conclude that the amine group of substrate plays an effective role in the catalytic efficiency of the full process and it can affect the redox activity of the two copper-peptide complexes.

As first hypothesis, the primary amine of the substrate could interact with some negative-charged amino acids, such as the aspartate at 1 position. This residue has been recently suggested as a possible binding site for copper, in which the carboxyl side chain can stabilize the metal interaction acting as axial ligand. The proximity of carboxylate to the metal site also suggests an interaction with the incoming catechol mediated by electrostatic interaction with a positive-charged group as the primary amine of the substrate. Although the catalytic mechanism observed in the previous data may be explained through some direct binding between the amine of dopamine and copper(II) in mono-dentate fashion, that would result in a reduction of the electron-transfer efficiency, this coordination geometry is unlikely. This type of coordination sphere could explain the catalytic ability of the adduct in the first reaction step and would limit the interaction between oxygen and copper(I), being the metal center not enough electron-rich to bind O_2, but this peculiar coordination structure would exist only upon a strong twist of the chromophore and an unrealistic distortion

of the complex. On the other hand, the catalytic data could also suggest the presence of additional catalytic centers in the amyloid-β sequence: the *N*-terminal negatively charged residues, such as Asp-1, could be involved in an electrostatic attraction of dopamine and the low redox potential of copper(II) trapped into the *N*-terminal coordination sphere could lead to a decrease in the oxidative efficiency. Therefore, the catecholamine mainly localized in the *N*-terminal region could mask the metal catalysis promoted by the main redox-competent site, while in the presence of a not-charged substrate as 4-methylcatechol, copper is equally distributed between several coordination environments and the oxidation profiles reflect the involvement of the main redox center. The different catalysis promoted by the two peptides toward 4-methylcatechol can be explained by the redox activity of both *N*-terminal site and a competent site probably involving the His-tandem site, that are only viable for Cu-NH_2-Aβ_{16}. When the *N*-terminus is acetylated, the *N*-terminal binding site for Cu^{II} is not available and the metal bound to the *C*-terminal domain can efficiently promote the substrate oxidation, resulting in the enhancement of the catalytic profiles. To verify the proposed mechanism, a further experiment was performed following the oxidation of dopamine by copper(I)-peptide complex; in this way, the first catalytic step is overpassed and the oxidation of Cu^{I} bound to NH_2-Aβ_{16} and Ac-Aβ_{16} fragments upon the interaction with atmospheric molecular oxygen can be followed. To this end, tetrakis(acetonitrile)copper(I) hexafluorophosphate (25 μM) was previously dissolved in pure acetonitrile and, upon five vacuum/argon cycles, was added to the reaction mixture containing dopamine (0.3 mM) and each peptide (25 μM) in 50 mM HEPES buffer at pH 7.4. The data confirm that the O_2-dependent reaction is slower in the presence of copper(I) bound to the *N*-acetylated fragment if compared to the free *N*-terminal peptide, where the binding with molecular oxygen is promoted.

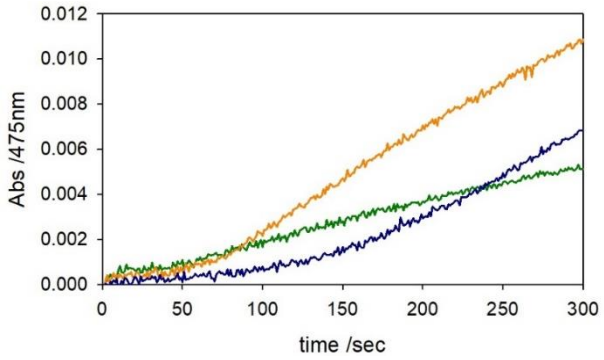

Figure 11. *Kinetic profiles of dopamine (0.3 mM) oxidation with time in 50 mM HEPES buffer at pH 7.4 and 20 °C in the presence of Cu^{I} (25 μM, green trace), [Cu^{I}-Aβ_{16}] (25 μM, orange) and [Cu^{I}-Ac-Aβ_{16}] (blue)*

Figure 11 suggests that the protracted shutdown of substrate oxidation upon the addition of copper(I) bound to *N*-acetylated peptide can be linked to a pseudo-linear coordination of the metal between the two vicinal histidines, thus preventing an efficient oxygenation of the complex. Otherwise, NH_2-Aβ_{16} interacts with Cu^{I} both through the His-tandem site and via the *N*-terminal coordination sphere: the last geometry would not provide a sufficient stable Cu^{I}-complex, resulting in a shorter lag-phase compared to the kinetic behavior observed in the presence of Cu^{I}-Ac-Aβ_{16}. Moreover, the metal redox cycling increases the local concentration of reactive species, which can attach both the substrate and the peptide sequence: the lag phase is therefore influenced by the oxidative modification and fragmentation of the peptide that decrease the stability of Cu^{I}-complex. To assess the existence of a catalytic IBS intermediate and to verify the existence of two distinct copper sites in amyloid-β sequence, corresponding to the low competent *N*-terminal site and the *C*-terminal His-tandem, a smaller peptide encompassing the region 1-9[9b] excluding His-13 and His-14, in both unprotected and *N*-acetylated form was synthesized. The results shown in Figure 12 suggest a lower oxidase activity of the *N*-unprotected peptide 1-9 if compared to the reactivity evidenced in the presence of Cu-Ac-Aβ_{16} and Cu-NH_2-Aβ_{16}. These observations indicate that the *N*-terminal acetylation does not induce a

reorganization of the *N*-terminal binding site but shifts the metal toward the His-tandem site, probably more competent for faster redox cycling. This secondary site is obviously suitable for the longer amyloid-β (1-16), while it is precluded for the shorter peptides, resulting in the decreased oxidative ability of the complexes.

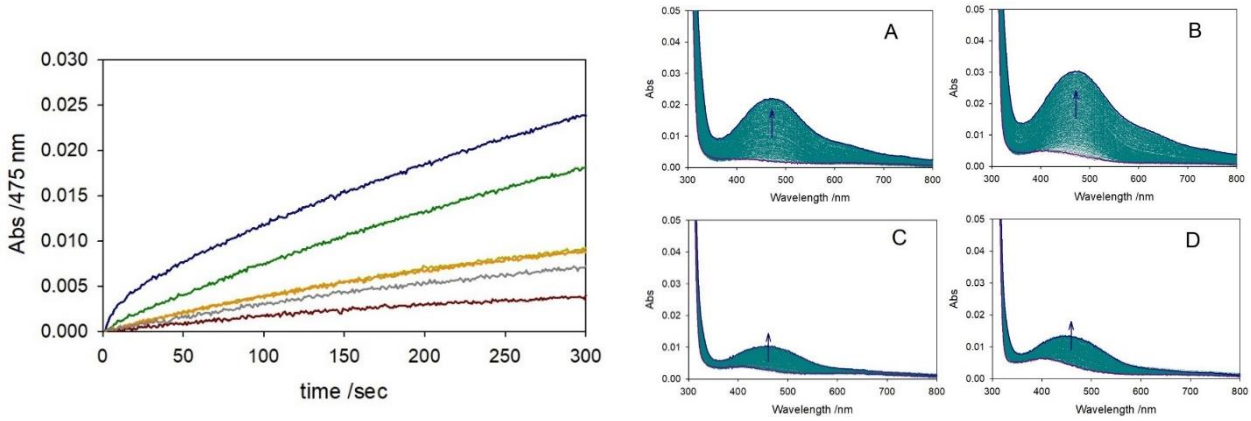

Figure 12. *Kinetic profiles of DA (0.3 mM) oxidation with time in 50 mM HEPES buffer at pH 7.4 and 20 °C in the presence of copper(II) (25 μM) alone (orange trace), and the following complexes (25 μM): Cu^{II}-NH_2-Aβ$_{16}$ (green and panel A), Cu^{II}-Ac-Aβ$_{16}$ (blue and panel B), Cu^{II}-Ac-Aβ$_9$ (light green and panel C) and Cu^{II}-NH_2-Aβ$_9$ (grey and panel D). The autoxidation of DA is shown as brown trace.*

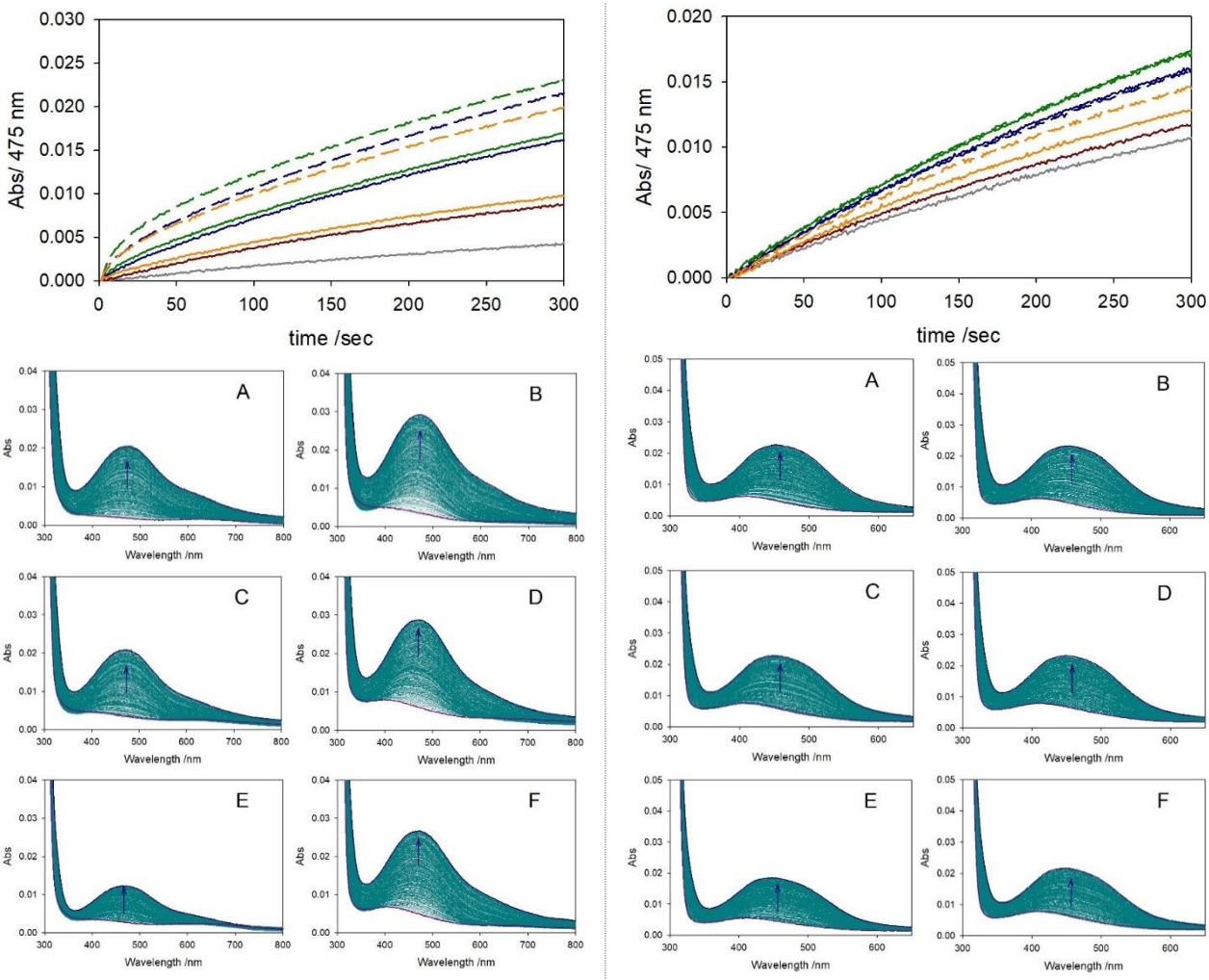

Figure 13. *Absorbance changes with time during DA (0.3 mM, at the left and 0.3 mM, at the right) oxidation in 50 mM HEPES buffer at pH 7.4 and 20 °C in the presence of copper(II) (25 μM) alone (brown trace), and the following complexes (25 μM): Cu^{II}-NH_2-Aβ$_{16}$ (solid green, and spectrum A), Cu^{II}-Ac-Aβ$_{16}$ (dashed green, and spectrum B), Cu^{II}-NH_2-Aβ$_{16}$ [H_6A] (solid blue, and spectrum C), Cu^{II}-Ac-Aβ$_{16}$ [H_6A] (dashed blue, and spectrum D),*

Cu^{II}-NH_2-Aβ$_{16}$ [H_{13}A] (solid orange, and spectrum E) and Cu^{II}-Ac-Aβ$_{16}$ [H_{13}A] (dashed orange, and spectrum F). The autoxidation of DA is shown as grey trace.

Another purpose of this study was to assay the nature of the catalytic intermediate when the copper binding is mainly located in the *C*-terminal region. In particular, a possible coordination mediated by all three histidines, that could allow a better redox environment for the metal, or by only two His, that could confirm the Cu^{I} stability and its partial redox inertia observed in the previous traces, was evaluated. The isoforms of Aβ$_{16}$ with two point mutations, H_{13}→A and H_6→A, both in *N*-unprotected or *N*-acetylated forms, were synthesized and the oxidation of dopamine and 4-methylcatechol was monitored as previously described via spectrophotometric but also chromatographic quantification. The kinetic traces were obtained from oxidation of substrates both at sub-saturation (0.3 mM) and saturating concentrations (3 mM) (Figure 13 and 14) and catalyzed by the following adducts: Cu^{II}-Aβ$_{16}$[H_6A], Cu^{II}-Ac-Aβ$_{16}$[H_6A], Cu^{II}-Aβ$_{16}$[H_{13}A], and Cu^{II}-Ac-Aβ$_{16}$[H_{13}A] (25 μM). To elucidate the reactivity of these complexes, MC oxidation (0.3 mM) was also followed through HPLC separation to quantify the substrate consumption during the redox reaction and to evaluate the mixture of oxidative products (see Experimental Section).

The data obtained from the copper-complexes with each mutant are in agreement with the higher catalytic efficiency of *N*-acetylated isoforms in both phases of the oxidative reaction, suggesting that the absence of the *N*-terminal amine coordination results in a lower stability of copper(II) adduct and therefore, enhances the reduction rate to Cu^{I}.

Table 1. *HPLC quantification of consumed MC (0.3 mM) obtained from oxidation by copper alone (25 μM), Cu^{II}-NH_2-Aβ$_{16}$, Cu^{II}-Ac-Aβ$_{16}$, Cu^{II}-NH_2-Aβ$_{16}$[H_{13}A], Cu^{II}-Ac-Aβ$_{16}$[H_{13}A], Cu^{II}-NH_2-Aβ$_{16}$[H_6A] and Cu^{II}-Ac-Aβ$_{16}$[H_6A] complexes (25 μM, 1:1) in 50 mM HEPES buffer at pH 7.4 and 25 °C.*

Reaction time	**Cu alone**	[**Cu-Aβ$_{16}$**]	[**Cu-Ac-Aβ$_{16}$**]	[**Cu-Aβ$_{16}$(H_6A)**]	[**Cu-Ac-Aβ$_{16}$(H_6A)**]	[**Cu-Aβ$_{16}$(H_{13}A)**]	[**Cu-Ac-Aβ$_{16}$(H_{13}A)**]
5 min	14%	17%	21%	12%	27%	5%	20%
30 min	40%	29%	47%	26%	54%	14%	49%

Surprisingly, the point mutation of one histidine in NH_2-peptides seems to increase the reaction rate, promoting the second step of reaction and therefore, influencing the oxygenation efficiency of the complexes. Together with the data obtained from HPLC quantification (see Table 1), it can be concluded that the catalytic intermediate requires the coordination to the metal of at least two histidines, probably involving the two vicinal histidines, H_{13} and H_{14}, while His-6 can work as an accessory ligand. In fact, the point mutation H_{13}→A, and probably a similar effect could be found upon the mutation of H_{14}, strongly affects the efficiency of substrate oxidation while the substitution of His-6 seems not to induce so marked effects.

Anyway, the existence of some transient and minor species showing a tris-His coordination can not be completely excluded. Moreover, the coordination sphere for copper(I) mediated by only two imidazolic groups in a linear fashion mode, that would not allow an efficient interaction with dioxygen, does not match with the suggested reactivity of the complexes. Therefore, the redox cycling of copper, and especially of copper(I), occurs upon the additional binding of substrate that warps the linear geometry and allows the oxygenation of the reduced complex. The active role of substrate is tightly associated to the oxidative mechanism of reaction and to the catalytic intermediate principally involved in the metal redox cycling: IBS intermediate proposed as the main catalytic species contributing to the redox cycling of Cu bound to amyloid-β peptide is made possible by the choice of a particular substrate as ascorbate.

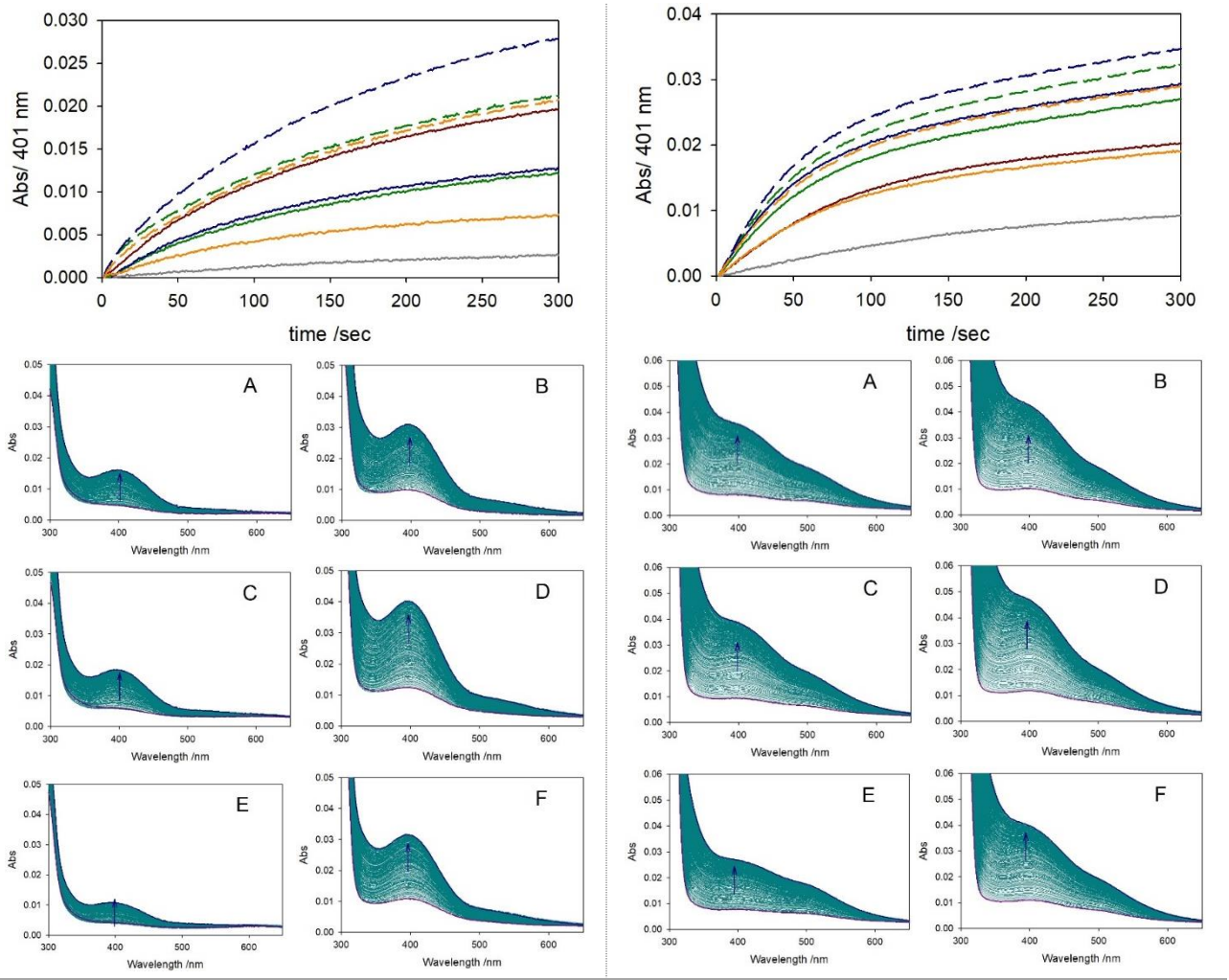

Figure 14. *Absorbance changes with time during MC (3 mM) oxidation in HEPES buffer (50 mM) at pH 7.4 and 20 °C in the presence of copper(II) (25 μM) alone (brown trace), and the following complexes (25 μM): Cu^{II}-NH_2-$A\beta_{16}$ (solid green, and spectrum A), Cu^{II}-Ac-$A\beta_{16}$ (dashed green, and spectrum B), Cu^{II}-NH_2-$A\beta_{16}$ [H_6A] (solid blue, and spectrum C), Cu^{II}-Ac-$A\beta_{16}$ [H_6A] (dashed blue, and spectrum D), Cu^{II}-NH_2-$A\beta_{16}$ [$H_{13}A$] (solid orange, and spectrum E) and Cu^{II}-Ac-$A\beta_{16}$ [$H_{13}A$] (dashed orange, and spectrum F). The autoxidation of DA is shown as grey trace.*

The catalytic oxidation of ascorbate is ruled by the rate determining step of the reaction that is represented by the reduction from Cu^{II} to Cu^{I}, while the low phase in the catechol oxidation corresponds to the second step, or the re-oxygenation of Cu^{I} adduct. Therefore, the different catalytic pathway due to the presence of two different substrates leads to the generation of distinct competent intermediates and, in these study, a ternary complex Cu^{I}-peptide-substrate can be assigned as the more relevant species involved in the catechol oxidation. This divergent result is in agreement with the recent and contrasting literature, in which a multitude of Cu binding modes have been proposed, influenced by different experimental conditions, such as ionic strength, acidity of the *medium* and temperature.[9c,10a,10b,11a]

In order to detect the ternary intermediate, we have tried to increase the lifetime of Cu^{I}-peptide-substrate adduct using a less reactive catechol as substrate, 4-chlorocatechol, and decreasing the temperature at 6 °C, that is the lowest viable temperature working in aqueous *medium* without the addition of further solvents, as methanol. At first, Cu^{I}-Ac-$A\beta_{16}$ complex (25 μM, 1:1) was generated adding tetrakis(acetonitrile)copper(I) hexafluorophosphate to the peptide in 50 mM phosphate buffer solution at pH 7.4 in anaerobic conditions; the substrate (0.3 mM) was then added in Argon atmosphere and the reaction was followed for 15 minutes in aerobic conditions (Figure 15).

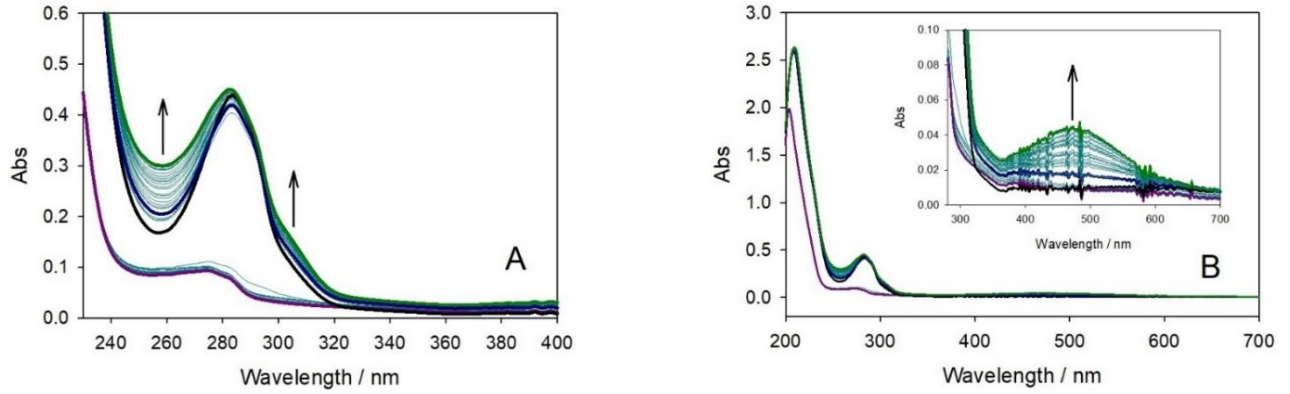

Figure 15. *Abs changes with time of Cu^{I}-Ac-Aβ_{16} complex (1:1, 25 μM) generated upon vacuum/Argon cycles and the addition of tetrakis (acetonitrile)copper(I) hexafluorophosphate (starting point as violet spectrum). 4-cholorocatechol (0.3 mM) was then added in Argon atmosphere (black spectrum) and then the solution was exposed to oxygen (blue spectrum, t0 and green spectrum (t15min). Panel A shows the region 230-400 nm while panel B corresponds to the full spectrum with and enlargement of the spectral region in which oxidative products are detected.*

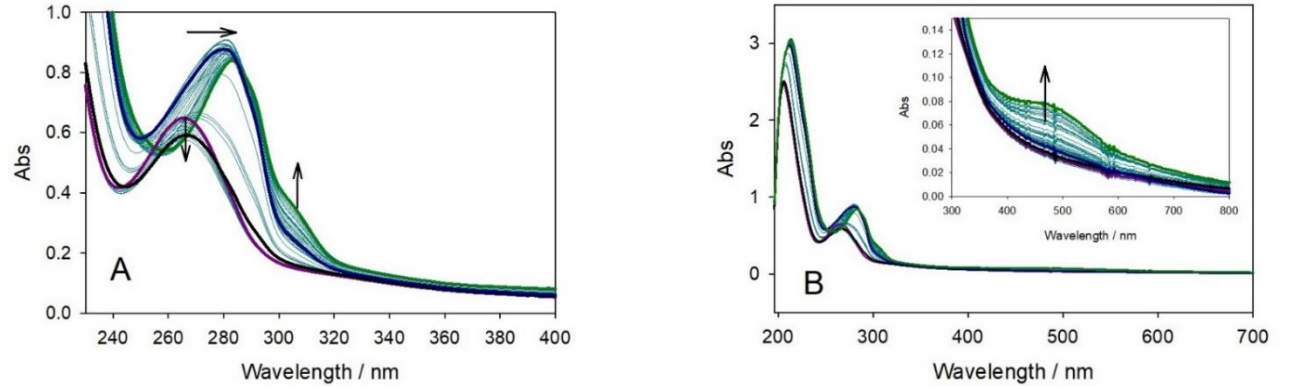

Figure 16. *Abs changes with time of Cu^{I}-Ac-Aβ_{16} complex (1:1, 25 μM) generated upon vacuum/Argon cycles and the addition of ascorbate (2 equiv, 50 μM) (starting point as violet spectrum). 4-cholorocatechol (0.3 mM) was then added in Argon atmosphere (black spectrum) and then the solution was exposed to oxygen (blue spectrum, t0 and green spectrum (t15min). Panel A shows the region 230-400 nm while panel B corresponds to the full spectrum with and enlargement of the spectral region in which oxidative products are detected.*

A similar procedure was followed for an analogous experiment in which copper(I) was produced *in situ* by the addition of 2 equiv. ascorbate (50 μM) before the addition of substrate (Figure 16). The results do not show any contribution attributable to some Cu^{I}-ternary adduct bound to oxygen, verifying the very short lifetime of these species that are not accumulated in the reaction mixture but they are consumed as fast as are produced.

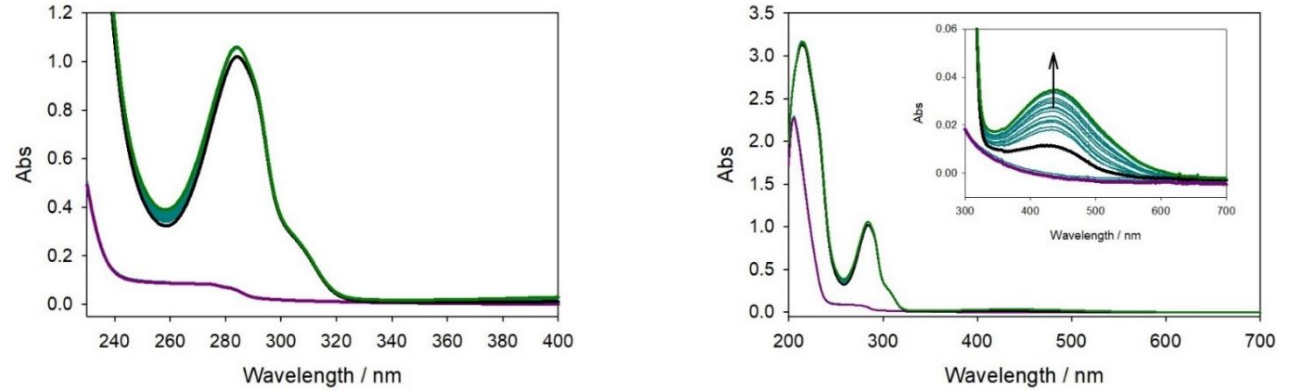

Figure 17. *Abs changes with time of Cu^{II}-Ac-Aβ_{16} complex (1:1, 25 μM, violet spectrum) and upon the addition of 4-cholorocatechol (0.3 mM, black spectrum, t0 and green spectrum, t 15min)*

Further control experiment was performed using the same concentration of the previous experiment shown in Figure 15 but working in aerobic conditions and starting from copper(II) nitrate; any additional spectral contributions were detected if compared to the previous data (Figure 17). The existence of a similar species could be confirmed through use of lower temperature and aqueous/alcoholic mixture, but the choice of a different *medium* would lead to several changes in the reaction mechanism and in the oxidative products followed so far. Moreover, when the reaction toward catechol is promoted by these complexes, the redox cycling of the metal is also driven by the generation of several ROS that are directly involved in the substrate oxidation.

Therefore, to understand the role of these reactive species in the reaction mechanism and to study their chemical nature, some scavengers were added to the reaction mixtures and changes in the oxidation rates were assayed.[11b,11c] At first, about 1% (v/v) DMSO was used to detect hydroxyl radicals generated by the oxidation of sub-saturating amounts of dopamine (0.3 mM) and promoted by [Cu-Ac-Aβ$_{16}$] and [Cu-NH$_2$-Aβ$_{16}$] adducts (25 μM). The results shown in Figure 18 suggest an evident shutdown of the reactivity obtained both in the presence of the adducts and with copper alone, which could be linked to the capture of free hydroxyl radical species but also to the partial chelation of copper(I), sequestering the catalyst.

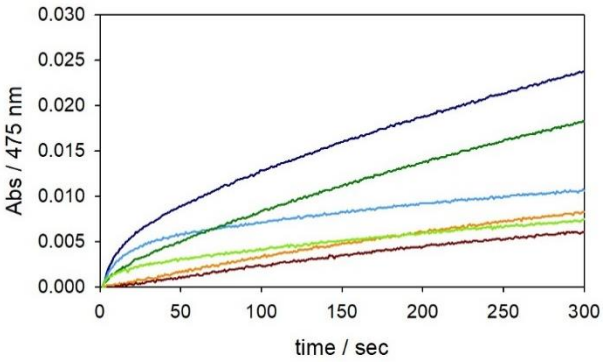

Figure 18. *Kinetic profiles of DA (0.3 mM) oxidation with time in 50 mM HEPES buffer at pH 7.4 and 20 °C in presence of Cu^{II} (25 μM) alone (orange and, upon the addition of 20 μl DMSO, shown as brown trace) and with 1 equiv. NH$_2$-Aβ$_{16}$ (green and, with DMSO, light green) and 1 equiv. Ac-Aβ$_{16}$ (blue and, with DMSO, light blue).*

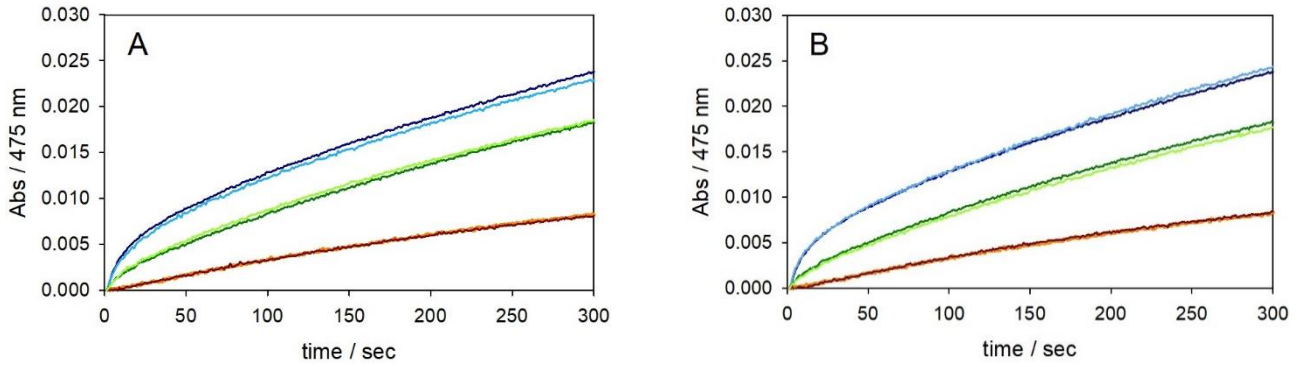

Figure 19. *Kinetic profiles of DA (0.3 mM) oxidation with time in 50 mM HEPES buffer at pH 7.4 and 20 °C performed as follows and studied in the presence of sodium azide (0.1 mM, panel A) or KI (0.1 mM, panel B). The catalysis is promoted by Cu^{II} (25 μM) alone (orange and, upon the addition of NaN$_3$ or KI, shown as brown trace) and with 1 equiv. NH$_2$-Aβ$_{16}$ (green and, upon the addition of NaN$_3$ or KI, light green) and 1 equiv. Ac-Aβ$_{16}$ (blue and, upon the addition of NaN$_3$ or KI, light blue).*

Analogous experiments were performed in the presence of sodium azide (0.1 mM) to exclude any involvement of singlet oxygen species (Figure 19A) and potassium iodide (0.1 mM) to assay the involvement of hydrogen peroxide in the reaction *medium* (Figure 19B). Negligible effects were observed in both studies but the use of KI is strongly limited by the high absorption of the products able to hide the oxidative products of substrate and therefore, a modest concentration of reagent was added to the reaction mixture, probably not sufficient to obtain useful results. In order to clarify the participation of hydrogen peroxide in the reaction, catalase enzyme was added to the reaction *medium* leading to a modest but not negligible decrease of DA oxidation rates and confirming the generation of H_2O_2 during the metal redox cycling (Figure 20).

Similarly, the study was repeated using another enzyme able to detect superoxide anions, as the superoxide dismutase (SOD) and the kinetic profiles shown in Figure 21 indicate an evident contribution of these species to DA oxidation, since the presence of SOD enzyme affects the reaction rates leading to a moderate slowdown. Moreover, the addition of denatured enzymes, inactivated through heating, does not influence the kinetics, excluding any indirect activity from the enzymes as metal sequesters. To further investigate the role of hydrogen peroxide in the oxidative reaction promoted by these copper-peptide adducts and to assess the existence of some hydroperoxo-intermediate, Cu^{I}-Ac-Aβ_{16} complex (25 μM) was again generated as previously described, working in anaerobic conditions and at 6 °C and keeping the mixture in Argon atmosphere, and reactive substrates as 4-methylcatechol or dopamine were added at sub-saturating concentration (0.3 mM). All experiment was performed in a close Schlenk apparatus avoiding the reaction with atmospheric oxygen and in these conditions, 10 equiv. H_2O_2 were added; Figure 22 and 23 does not highlight any relevant band traceable to some Cu^{I}-intermediate, but verifying that the addition of H_2O_2 promotes the substrate oxidation, as shown by blue spectra.

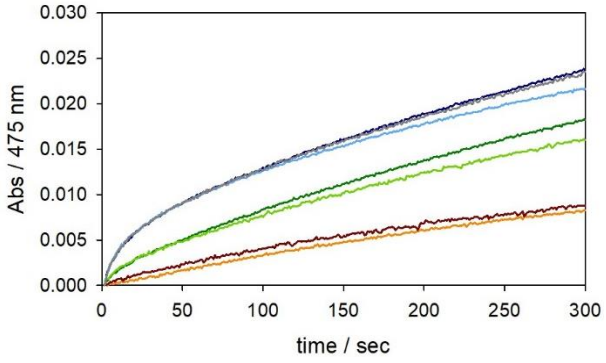

Figure 20. *Kinetic profiles of DA (0.3 mM) oxidation with time in 50 mM HEPES buffer at pH 7.4 and 20 °C in the presence of Cu^{II} (25 μM) alone (orange and, upon the addition of catalase enzyme (500 units/1.6 mL), shown as brown trace) and with 1 equiv. NH_2-Aβ_{16} (green and, upon the addition of catalase, light green) and 1 equiv. Ac-Aβ_{16} (blue and, upon the addition of active enzyme, light blue or denatured enzyme, grey).*

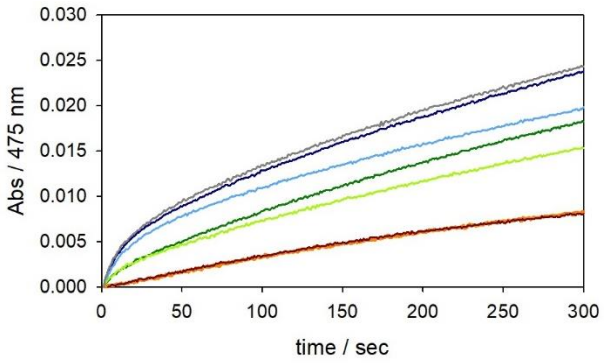

Figure 21. *Kinetic profiles of DA (0.3 mM) oxidation with time in 50 mM HEPES buffer at pH 7.4 and 20 °C in the presence of Cu^{II} (25 μM) alone (orange and, upon the addition of SOD enzyme (500 units/1.6 mL), shown as brown trace) and with 1 equiv. NH_2-Aβ_{16} (green and, with SOD, light green) and 1 equiv. Ac-Aβ_{16} (blue and, upon the addition of active enzyme, light blue or denatured enzyme, grey).*

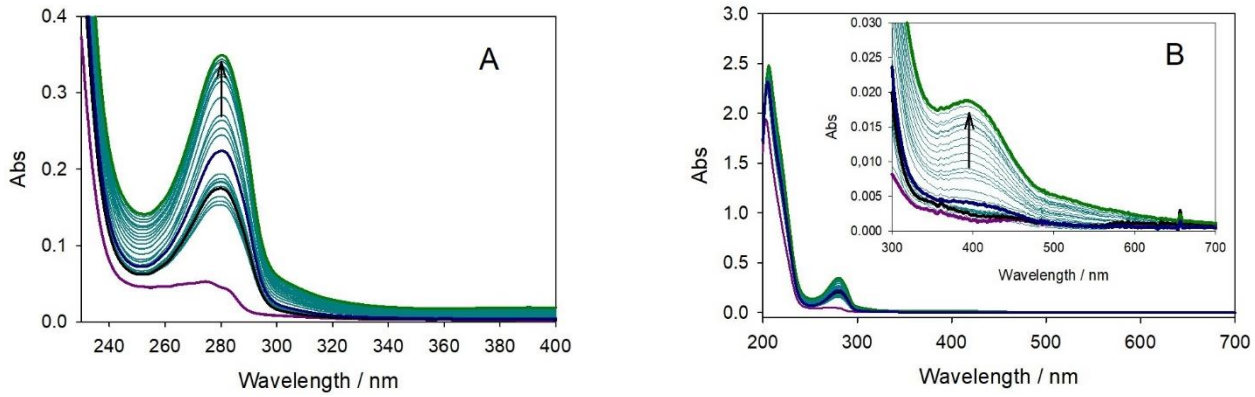

Figure 22. *Abs changes with time of Cu^{I}-Ac-Aβ_{16} complex (1:1, 25 μM) generated upon vacuum/Argon cycles and addition of tetrakis (acetonitrile)copper(I) hexafluorophosphate (starting point as violet spectrum). 4-methylcatechol (0.3 mM, black spectrum) and then H_2O_2 (0.25 mM, blue spectrum) were added in Argon atmosphere (black spectrum). The reaction was followed for 15 min in anaerobic conditions (final spectrum shown in green).*

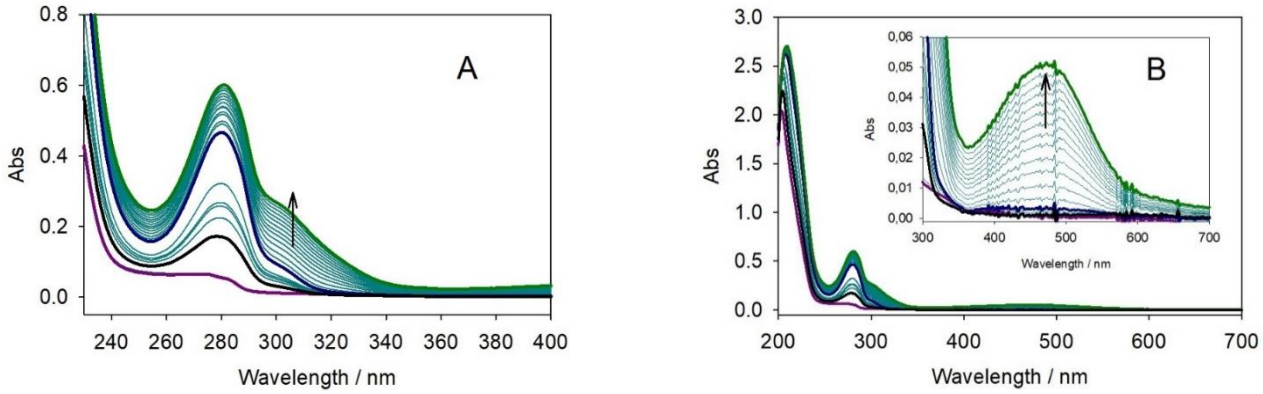

Figure 23. *Abs changes with time of Cu^{I}-Ac-Aβ$_{16}$ complex (1:1, 25 μM) generated upon vacuum/Argon cycles and addition of tetrakis (acetonitrile)copper(I) hexafluorophosphate (starting point as violet spectrum). Dopamine (0.3 mM, black spectrum) and then H_2O_2 (0.25 mM, blue spectrum) were added in Argon atmosphere (black spectrum). The reaction was followed for 15 min in anaerobic conditions (final spectrum shown in green). Panel A shows the region 230-400 nm while panel B corresponds to the full spectrum with and enlargement of the spectral region in which oxidative products are detected.*

The same conclusion can be obtained from the kinetic data shown in Figure 24, in which the reactivity of copper(II)-Ac-Aβ$_{16}$ adduct toward dopamine (0.3 mM) is strongly increased when large excess of H_2O_2 is added. In particular, the first step of the reaction, corresponding to the reduction of the metal via substrate reaction, does not be influenced by the presence of hydrogen peroxide, while the second phase is partially quenched, suggesting a direct reaction between H_2O_2 and Cu^{I}-species.

Therefore, H_2O_2, superoxide and probably hydroxyl radicals are produced in the metal redox cycling and their accumulation in solutions assists the substrate oxidation. As general conclusion we can assert that the *N*-acetylation of amyloid-β sequence (1-16) induces a deprivation of a high-affinity ligand for copper(II) but, at the same time, promotes the redox activity of a more competent site probably corresponding to a coordinative environment encompassing the two vicinal His residues. Resuming the catalytic cycling of Cu-Aβ species, we can affirm that the initial coordination for copper(II) matches with the *resting state* form, where the metal binding sphere directly involves two imidazolic side chains of His residues, one amide group of the first amino acid, the *N*-terminal amine and an axial coordination via the carboxyl group of Asp-1 as ligands.

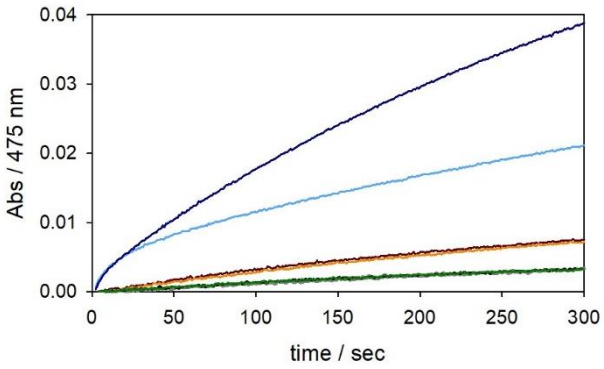

Figure 24. *Kinetic profiles of DA (0.3 mM) oxidation with time in 50 mM HEPES buffer at pH 7.4 and 20 °C in presence of Cu^{II} (25 μM) alone (orange trace), H_2O_2 alone (0.25 mM, black) and in the presence of both reagents (brown), while the catalysis obtained in the presence of 1 equiv. Ac-Aβ$_{16}$ bound to copper alone, copper and peroxide, or hydrogen peroxide alone are shown as light blue, blue and grey traces, respectively. The autoxidation of substrate is shown as green trace. Green, grey and black profiles are overlapped.*

The reduction of the complex leads to the shift of metal to a Cu^{I} coordination between the two vicinal histidines, H_{13} and H_{14}, that was suggested by several works as the most stable species for copper(I), but probably the low efficient species for the oxygenation of the complex. Therefore, the catecholic substrate shows an active role through its binding to the linear adduct, inducing a twist of the geometry and promoting a faster metal cycling via O_2-interaction. Given the existence of several metal binding sites, the flexible nature of the peptide and the strong influence of the chemical context, more efforts will be required to find a commonly accepted pathway to describe the oxidative damage due to the presence of copper-amyloid-β complexes.

Conclusions

The aim of the present work was to verify the existence and the involvement of a catalytic "in-between" state in the redox cycling of copper(II)-amyloid-β complexes, focusing the attention on the role of *N*-terminal amine as the key coordination group for the metal binding. We have chosen to study the redox-cycle of copper bound to amyloid-β fragments toward biological substrates, as the neurotransmitter dopamine, and other catechols showing different chemical proprieties. The catalytic activity of free *N*-terminal peptide and of the *N*-acetylated isoform complexed with Cu^{II}/Cu^{I} was compared. Surprisingly, the protection of *N*-terminus alters the redox capability of the resulting complexes but it does not quench the substrate oxidation, and these results were not in agreement with its possible involvement as binding site in the catalytically active state.

The data suggest that both the amount of dioxygen and the substrate concentration strongly influence the rate of catechol oxidase reaction promoted by the adducts; the kinetic traces also show a divergent oxidative reactivity between the two complexes, evincing the lower activity of Cu^{II}-NH_2-$A\beta_{16}$ if compared to the *N*-acetylated peptide bound to copper(II). This catalytic trend is tightly linked to the existence of a distribution of binding modes for copper(II) and copper(I) in the free *N*-terminal peptide, in which the metal coordination is mainly distributed between two sites, a *N*-terminal one probably assuming a coordination environment resembling the "in-between" intermediate and a *C*-terminal site that corresponds to the His-tandem domain. When the *N*-terminal site is acetylated and it is not available for the metal interaction, copper(II) is shifted toward the *C*-terminal coordination, generating a lower-stability adduct. For an efficient redox cycling of copper, the coordination spheres for Cu^{II} and Cu^{I} have to assume a modest structural reorganization associated to low energetic barrier in order to promote the fast interchange between the redox active states.[10b,11a] In the catalytic oxidation of ascorbate, an "in-between" model, showing the carboxylate of Asp-1, an amide group, one histidine and the *N*-terminal amine as ligands for the metal, was proposed[12] but this coordinative arrangement can not represent a satisfying model to ensure an efficient binding and further activation of dioxygen in the catechol oxidative pathway. As all previous data suggest, the key feature in the reaction mechanism toward catechols is a dynamic equilibrium between a highly stable coordination sphere for copper(I) in a pseudo-linear geometry via H_{13} and H_{14} and a reactive species in which the additional binding with the substrate induces a warping of Cu^{I}-bis(His) and allows the interaction with dioxygen. Anyway, some transient copper(I) intermediate corresponding to a tris(His) adduct can not be completely excluded because it could decrease the energetic barrier required for the redox cycling being able to stabilize both redox metal states; additionally, a similar intermediate would be biologically and chemically reasonable, since it resembles the catalytic sites of some enzyme, as copper amine oxidase[13] and quercetin 2,3-dioxygenase[14]. Anyway, when the catalytic efficiency is studied toward ascorbate, copper(II) alone shows the higher catalytic ability to consume the substrate while the presence of some chelating agent for the metal induces a decrease of the consumption rate, probably stabilizing the metal ion and influencing the redox cycling rate. In this context, the full mechanism is mainly ruled by the reduction from Cu^{II} to Cu^{I} that corresponds to the limiting step of the reaction, while, when the reactivity is assayed in term of catechol conversion to quinone, the slow step of the redox reaction coincides with the formation of the ternary adduct between copper(I), oxygen and the substrate[15]. The different intermediates generated during the oxidative reaction toward the two substrates are tightly linked to the lower reduction potential of ascorbate, to the higher catalytic efficiency of the metal if the redox cycling is promoted by ascorbate and to the generation of distinct reactive intermediates corresponding to the ternary complexes [copper-peptide-substrate].

To conclude this work, it can be assumed that the *N*-terminal site particularly stabilizes Cu^{II} ions, that is partially unreactive, while *N*-acetylation removes a strong binding ligand for copper(II), thus enhancing its reduction rate. The existence of several coordination domains for copper(II) emerges from the higher catechol oxidase activity of [Cu^{II}-Ac-$A\beta_{16}$] in which there is not competition for the metal binding that is mainly located in the *C*-terminal site; when the copper binding occurs on NH_2-$A\beta_{16}$, the metal is partially trapped into the lower activity *N*-terminal site and the resulting reactivity is decreased.

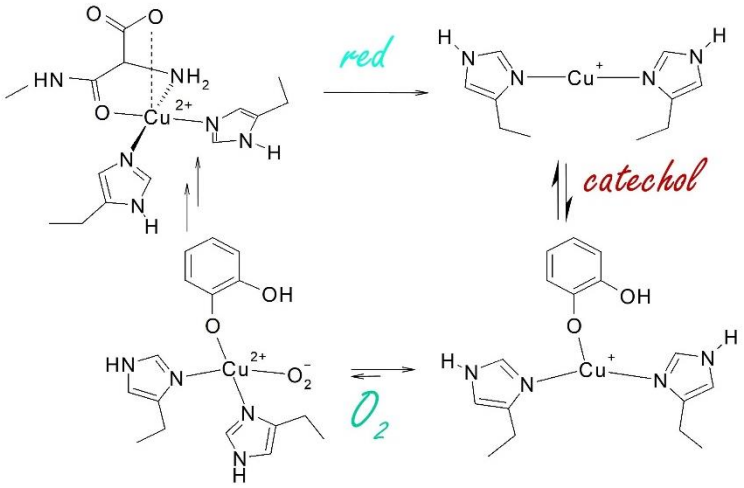

Figure 25. *Schematic pathway of Cu^{II}-Aβ complex showing the formation of a Cu^{I}-bis(histidine) species involved in the interaction with dioxygen only upon the binding with catechol. The linear, two-coordinate Cu^{I} species is unreactive to O_2 and requires the interaction with substrate to promote the oxidase reaction.*

Upon the reduction of copper bound to the amyloid-beta peptides and its coordinative shift toward a *C*-terminal site, probably corresponding to the His-tandem, Cu^{I}-bis(His) is the primary intermediate characterized by the high stability of copper(I) and therefore, it is almost totally unreactive (Figure 25). Moreover, the efficiency of the redox cycling is influenced by the presence of dioxygen and by the concentration of substrate. Once Cu^{I} ion is probably bound between the two vicinal histidines, His-13 and His-14, although His-6 can not be excluded acting as an accessory binding site, the metal center can be attached by the catecholic substrate and this interaction promotes the further oxygenation of the complex. The saturation with catechol of Cu^{I}-bis(His) adduct is therefore the main factor that controls the efficiency of the oxidative cycle.

Anyway, a detailed description of the coordination chemistry of the complex and a characterization of the intermediates with and without the catecholic substrate are required to understand the possible biological implications of this mutable behavior of the amyloid-β species.

Peptide synthesis and purification

Aβ16	$_1$DAEFRHDSGYEVHHNK$_{16}$-NH_2	**Ac-Aβ9**	Ac-$_1$DAEFRHDSG$_9$-NH_2
Ac-Aβ16	Ac-$_1$DAEFRHDSGYEVHHNK$_{16}$-NH_2	**Aβ16 [H6A]**	$_1$DAEFRADSGYEVHHNK$_{16}$-NH_2
Aβ28	$_1$DAEFRHDSGYEVHHNKLVFFAEDVGSNK$_{28}$-NH_2	**Ac-Aβ16 [H6A]**	Ac-$_1$DAEFRADSGYEVHHNK$_{16}$-NH_2
Ac-Aβ28	Ac-$_1$DAEFRHDSGYEVHHNKLVFFAEDVGSNK$_{28}$-NH_2	**Aβ16 [H13A]**	$_1$DAEFRHDSGYEVAHNK$_{16}$-NH_2
Aβ9	$_1$DAEFRHDSG$_9$-NH_2	**Ac-Aβ16 [H13A]**	Ac-$_1$DAEFRHDSGYEVAHNK$_{16}$-NH_2

All amyloid-β fragments were synthesized using the Fmoc solid-phase synthesis[16,17] in DMF, as previously reported. Rink-amide MBHA resin was used as solid support to obtain an amidated *C*-terminal product. For the longer peptides, a low loading Rink-amide resin (substitution 0.36 mmol/g) was preferred. The standard synthesis procedure can be divided in four repeated steps: 1) Deprotection (3+7 min) of the resin with 20 mL of 20% (v/v) piperidine in DMF; 2) and 3) Coupling and Recoupling of the amino acid (2 equiv. vs. resin sites) in the presence of 2 equiv. of HOBt, 2 equiv. of PyBOP, and 4 equiv. of DIPEA. After 45 min, the same coupling procedure is repeated. At fourth reaction, capping is performed using 20 mL of 4.7% acetic anhydride and 4% of pyridine in DMF. At the end of the synthesis, the deprotection of the side chains and the peptide release from the resin are performed through a solution of 95% TFA, TIS (2.5 %), and water (2.5 %). Cold diethyl ether was added to precipitate the peptide. The mixture was filtered and the precipitate was purified by HPLC, using a 0–100% linear gradient of 0.1% TFA in water to 0.1% TFA in CH_3CN over 50 min (flow rate of 4 ml/min, loop 2 ml), as eluent. The product was lyophilized and then characterized by direct injection in mass spectrometry, obtaining the following ESI-MS data:

Aβ16	m/z 1955 $^{(+)}$; 978 $^{(2+)}$; 652 $^{(3+)}$; 489 $^{(4+)}$	**Ac-Aβ9**	m/z 1075 $^{(+)}$; 538 $^{(2+)}$; 359 $^{(3+)}$
Ac-Aβ16	m/z 1997 $^{(+)}$; 999 $^{(2+)}$; 666 $^{(3+)}$; 500 $^{(4+)}$	**Aβ16 [H6A]**	m/z 1889 $^{(+)}$; 945 $^{(2+)}$; 630 $^{(3+)}$; 473 $^{(3+)}$
Aβ28	m/z 1631 $^{(2+)}$; 1088 $^{(3+)}$; 816 $^{(4+)}$; 653 $^{(5+)}$	**Ac-Aβ16 [H6A]**	m/z 1931 $^{(+)}$; 966 $^{(2+)}$; 644 $^{(3+)}$; 483.5 $^{(3+)}$
Ac-Aβ28	m/z 1652 $^{(2+)}$; 1101.5 $^{(3+)}$; 826.5 $^{(4+)}$; 641.5 $^{(5+)}$	**Aβ16 [H13A]**	m/z 1889 $^{(+)}$; 945 $^{(2+)}$; 630 $^{(3+)}$; 473 $^{(3+)}$
Aβ9	m/z 1033 $^{(+)}$; 517 $^{(2+)}$; 345 $^{(3+)}$	**Ac-Aβ16 [H13A]**	m/z 1931 $^{(+)}$; 966 $^{(2+)}$; 644 $^{(3+)}$; 483.5 $^{(3+)}$

Oxidation kinetics at sub-saturating and saturating concentration of substrate.

The catechol oxidation promoted by copper(II) was studied at room temperature for 300 s or 1800 sec in 50 mM HEPES buffer at pH 7.4. The reaction was monitored by UV-visible spectroscopy through the development of dopaminochrome band at 475 nm for dopamine and the quinone band at around 400 nm for 4-methylcatechol and *N*-acetyl-dopamine. The autoxidation of substrates at sub-saturating (0.3 mM) and saturating (3 mM) concentrations was also evaluated. All experiments were carried out by adding copper(II) nitrate (25 μM) and amyloid-β fragments at 1:1 (25 μM) or 1:2 molar ratios (50 μM) to the substrate solution. Quantification of peptide solution was obtained by UV-Visible absorption at 280 nm corresponding to the tyrosine band (epsilon 1480 M^{-1} cm^{-1})[18], while with the shorter NH_2-Aβ$_9$ and Ac-Aβ$_9$ peptides the quantification was made by weighing the pure product obtained from the synthesis. To exclude any possible buffer involvement in the oxidation mechanism and on the catalytic efficiencies of the complexes, control experiment in 50 mM phosphate buffer solution at pH 7.4 was performed and, as shown in Figure 26, the effect of *medium* can be excluded. All measurements were performed at least in duplicate.

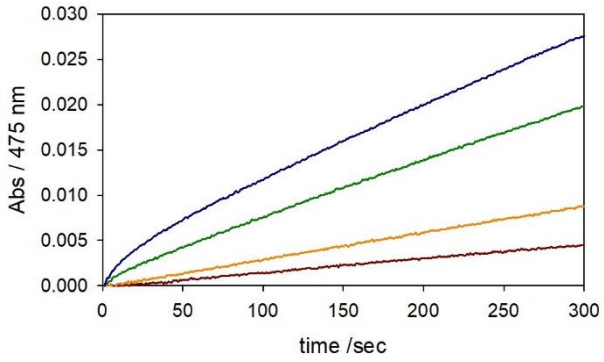

Figure 26. *Kinetic profiles of DA (0.3 mM) oxidation with time in phosphate buffer solution (50 mM) at pH 7.4 and 20 °C in the presence of copper(II) (25 μM) alone (orange trace), and the following complexes (25 μM): Cu^{II}-NH_2-$A\beta_{16}$ (green) and Cu^{II}-Ac-$A\beta_{16}$ (blue). The autoxidation of DA is shown as brown trace.*

To assay the possible generation of some bis-DA-adduct as intermediate in the oxidative reaction, additional kinetic data were collected. It is known that the rate-determining step of the full redox mechanism involves the reaction between the reduced [Cu^{I}-peptide] complex bound to a molecule of substrate and the dioxygen. In some preliminary studies, it has been observed that high levels of substrates affect in different ways the reaction rates promoted by copper bound to the free *N*-terminal or *N*-acetylated peptides and a substrate-dependence was also evidenced. The kinetic data may suggest two potential coordinative models for the two substrates. Since saturating concentration of DA quenches the reactivity of the copper(II)-*N*-acetylated peptide complex, at first, a bidentate binding mediated by two molecules of substrate to the copper ion was proposed. Copper(II) bound to *N*-acetylated amyloid-β fragment could accept two molecules of dopamine, being more coordinative suitable for the lacking of the *N*-terminal amine binding, while copper bound to $A\beta_{16}$ would be trapped in a chemical environment with higher steric hindrance, not allowing the interaction with an additional molecule of substrate. The bis-adduct might influence the accessibility to the metal site for the molecular oxygen, reducing the reaction turnover. In the presence of $A\beta_{16}$ and copper, the competition substrate/oxygen is shifted to higher DA concentration and the quenching of the reactivity shown with *N*-acetylated peptide is not observed. Therefore, the oxidation of dopamine at saturating concentration (4 mM) was studied catalyzed by the two previous complexes both with atmospheric oxygen and upon enrichment of the buffer solution with pure molecular oxygen. The data verify that the slow step of the redox cycle is determined by the possibility to generate the adduct with oxygen. The data shown in Figure 27 could suggest that the amine group of dopamine could influence the reactivity of copper-peptide complexes. Indeed, dopamine could easily interact with the *N*-terminus of amyloid-β peptide, a highly negative-charged domain due to the presence of Asp and Glu residues flanking the main copper binding sites. These electrostatic interactions could direct the substrate toward the metal site with some peculiar coordination that allows or blocks the metal redox cycling.

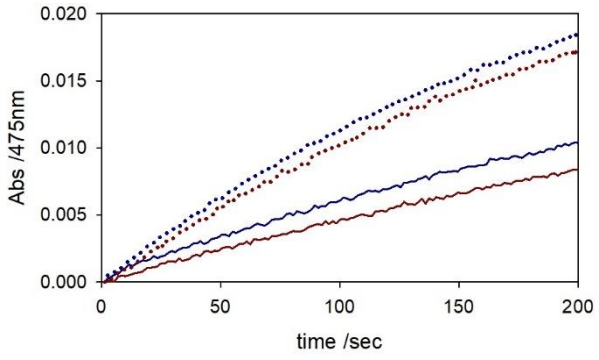

Figure 27. *DA oxidation (4 mM) in the presence of constant [catalyst], Cu-Ac-$A\beta_{16}$ complex (1:1, 25 μM, solid blue trace) or Cu-$A\beta_{16}$ (solid brown trace) in 50 mM HEPES buffer at pH 7.4. Upon saturation of buffer with pure oxygen the same experiment was repeated (dotted blue for Ac-$A\beta_{16}$ and dotted brown for $A\beta_{16}$).*

The addition to the reaction mixture of a not-catecholic substrate showing an amine side group, as 2-phenylethylamine, could mimic the chemical structure of the neurotransmitter, having the same side-chain able to coordinate the metal ion and to stabilize the copper complex. This molecule is totally unreactive and is not directly involved in the oxidative

reaction, but it could influence the redox cycling both affecting the interaction with ascorbate or decreasing the metal availability upon its direct binding. The binding of PEA to the metal site would occur only in the presence of the mono-adduct with catechol, having a modest steric hindrance to allow the interaction with the substrate and then, the oxygenation. If dopamine concentration is sufficient to generate the bis-adduct, the copper interaction with PEA might prevent the binding with dioxygen and the re-oxidation of the complex.

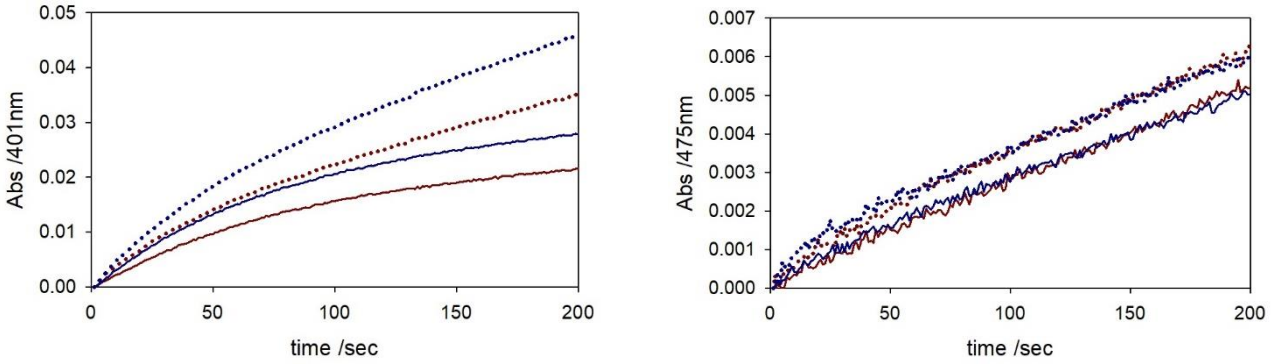

Figure 28. *Kinetic profiles of MC (left panel) and DA (right panel) (3 mM) oxidation with time in 50 mM HEPES buffer at pH 7.4 and 20 °C in the presence of Cu-Aβ16 complex 1:1 (25 μM, solid brown trace) and upon the addition of 2-phenylethylamine (3 mM, dotted brown) or with Cu-Ac-Aβ16 1:1 (solid blue) and upon the addition of the mimicking molecule (dotted blue).*

In Figure 28, the reactivity enhancement promoted by PEA suggests that the presence of primary amine can alter the redox reaction rate, probably coordinating the copper ion bound to the peptide. If 4-methylcatechol would be able to form only the mono-adduct, the addition of a secondary molecule and the binding of the amine to the metal would not influence the reaction rate and the generation of O_2-adduct. On the other hand, the supposed bis-adduct promoted by saturating concentration of dopamine and the further coordination with PEA should quench the reaction, limiting the interaction with oxygen. The kinetic plot obtained at low concentration of dopamine and 10 equiv. of 2-phenylethylamine (Figure 29) excludes the involvement of a bis-adduct in the reaction mechanism, but highlights that the additional coordination of an amine group to the catalytic center enhances the redox activity of copper and promotes the binding with oxygen. It will be interesting to understand if the involvement of a biological amine, such as GABA or other neuronal molecules, could alter the mechanism of catecholamine oxidation and contribute to the oxidative stress.

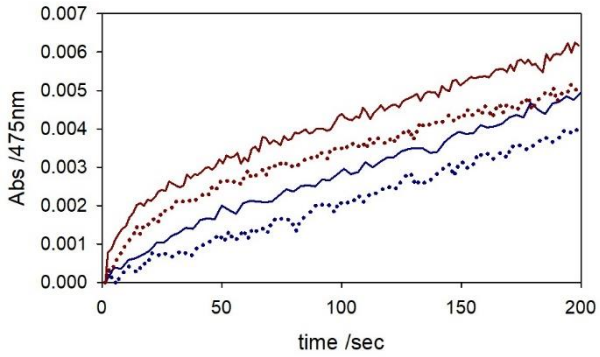

Figure 29. *Kinetic profiles of DA (0.3 mM) oxidation with time in 50 mM HEPES buffer at pH 7.4 and 20 °C in the presence of Cu-Aβ16 complex 1:1 (25 μM, dotted blue trace) and upon the addition of 2-phenylethylamine (3 mM, solid blue) or with Cu-Ac-Aβ16 1:1 (dotted brown) and upon the addition of the mimicking molecule (solid brown).*

Anyway, these data suggest that the presence of an additional amine could direct the substrate toward a more competent catalytic site, probably located at *C*-terminus. Amyloid-β peptide binds copper(II)/(I) ions through several coordination spheres, mainly involving imidazolic side chains. When the *N*-terminus of Aβ is available to bind copper, the metal coordination sphere could involve the terminal free-amine, a *N*-amide group, a *N*-imidazole group and the

carboxylate side chain of Asp1 as axial ligand. The environment around copper ion would not allow to generate an efficient catalytic cycle and the presence of a carboxylate would reduce the metal redox potential. Therefore, 2-phenylethylamine could directly interact with aspartate 1 and shift the substrate toward the *C*-terminal site; thus, the negative-charged residues are hidden and dopamine can interact with copper bound to the His-tandem site, enhancing its reactivity. To study if an electrostatic interaction between carboxylates and dopamine can play some role in the redox mechanism, high amounts of sodium acetate (0.5-3 mM) were added to the reaction mixture containing dopamine (0.3 mM) and copper-peptide complexes (25 μM) in 50 mM HEPES buffer at pH 7.4 (Figure 30). A negligible effect was evidenced upon the addition of acetate, suggesting that some generic acids or bases do not influence the reaction mechanism and these small molecules do not act as amino acid-mimetic system, in which the electrostatic interaction could be governed by a peculiar conformation of the peptide backbone.

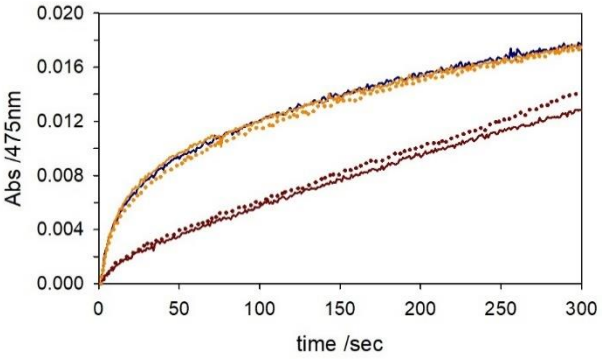

Figure 30. *Kinetic profiles of dopamine (0.3 mM) oxidation with time in 50 mM HEPES buffer at pH 7.4 and 20 °C in the presence of [Cu^{II}-$A\beta_{16}$] (25 μM) (green trace) and [Cu^{II}-Ac-$A\beta_{16}$] (grey). The same experiment was performed in the presence of sodium acetate at 0.5 mM concentration (light blue for [copper-$A\beta_{16}$] and yellow for [copper-Ac-$A\beta_{16}$]) and at 3 mM, only in the presence of the acetylated isoform (orange trace).*

Substrate-dependence kinetics.

The kinetic data were obtained following the oxidation of dopamine and 4-methylcatechol catalyzed by fixed concentration of copper-peptide complex (at 1:1 molar ratio, 25 μM). The substrate-dependence was performed by varying the substrate concentration from 0.3 to 4.0 mM. The initial rates of 4-methylcatechol oxidation were fitted with the Michaelis-Menten-like equation (see the follow equation) to obtain the kinetic parameters. The rate values, obtained as ΔAbs/s, were converted into s^{-1} through the Beer equation. Substrate oxidation promoted by copper(II) was studied at room temperature in 50 mM HEPES buffer at pH 7.4 and the reaction was monitored by UV/vis spectroscopy through the absorption band of 4-methylquinone at 401 nm (epsilon 1550 $M^{-1}cm^{-1}$) or dopaminochrome at 475 nm (epsilon 1500 $M^{-1}cm^{-1}$). For the autoxidation of each substrate it was assumed a hypothetical concentration of catalyst (25 μM) for the conversion of data into sec^{-1}. The equation used to fit the data obtained from 4-MC-dependence is shown below, besides the reaction mechanism.

$$\frac{\text{rate}}{[Cu^{II}\text{-}A\beta]} = \frac{k_r \times K_B \times [MC]}{1 + K_B \times [MC]}$$

1)	Cu^{II}-Aβ + MC	→	Cu^{I}-Aβ + $MC^{+\bullet}$	Fast Reaction
2)	Cu^{I}-Aβ + MC	⇄	Cu^{I}-Aβ-MC	Fast Equilibrium
3)	Cu^{I}-Aβ-MC + O_2	→	Cu-Aβ-MC-O_2*	Slow Reaction
4)	Cu-Aβ-MC-O_2*	→→	Cu^{II}-Aβ + $MC^{+\bullet}$ + ROS	Fast Reactions
5)	2 $MC^{+\bullet}$	→	MC + MQ	Chromophore Formation
6)	MC + MQ	→→	oligomers	Oligomerization

The peptide is indicated as generic Aβ, while $MC^{+\bullet}$ indicates the radical cation of this substrate, K_B is the binding constant for binding between catechol and Cu^I, and k_r is the second order rate constant for O_2 binding to the complex. Cu-Aβ-MC-O_2* corresponds to the active species previously described.

Further investigation of Cu^I-intermediate and ROS production.

Cu^I-adducts were obtained from the addition of 1 equiv. tetrakis(acetonitrile) copper(I) hexafluorophosphate (25 μM) (Figure 31), previously dissolved in acetonitrile and complexed with Ac-$Aβ_{16}$/$Aβ_{16}$ (25 μM), while the reaction was monitored toward catecholic substrates (0.3 mM). To have additional details on the ternary Cu^I-intermediate, Cu^I-Ac-$Aβ_{16}$ adducts (25 μM) were generated in anaerobic conditions at 6 °C, both as previously described or generating copper(I) ions from the direct reaction between copper(II) nitrate and 2 equiv. ascorbate (50 μM).

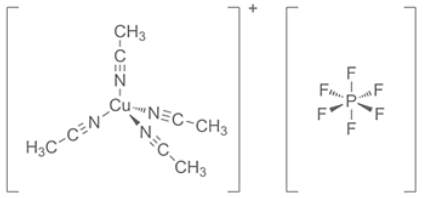

Figure 31. *Chemical structure of tetrakis(acetonitrile) copper(I) hexafluorophosphate $[Cu(CH_3CN)_4]PF_6$ (MW 372.72)*

The reaction was monitored either in anaerobic or dioxygen-saturation conditions upon the addition of several substrates, such as 4-chlorocatechol, 4-methylcatechol and dopamine (0.3 mM). In order to study the involvement of ROS in the oxidative mechanism, the substrate oxidation was followed as previously described but several scavengers, as DMSO (1.25 % v/v), KI or NaN_3 (0.1 mM), SOD and catalase enzymes (500 units/1.6 mL), were added. The denaturation of the enzymes was performed by heating at 100 °C for 1 hour. The participation of H_2O_2 in the reaction was also studied by its addition (0.25 mM) both in the presence of Cu^{II} alone and Cu^{II}-Ac-$Aβ_{16}$ at usual ratio.

Synthesis of N-acetyldopamine (NADA)

The reaction was performed adding NaOAc (0.1442 g, 1.06 mmol) and Ac_2O (0.1004 mL, 1.062 mmol) to the solution of dopamine hydrochloride (0.2 g, 1.06 mmol) in 3-4 ml DMF. The mixture was stirred for about 2-3 hours and then was evaporated. The crude product was purified by flash chromatography on silica using DCM : MeOH 9:1 as elution mixture, upon absorption of the product on silica powder dissolving in pure methanol.[19]

Esterification of the carboxyl-side chain of Aspartate and Glutamate of $Aβ_{16}$

The influence of negative-charged groups of Aβ was studied through the protection of the four carboxyl side chains of the two glutamates and two aspartates with a common esterification procedure.[20] Thionyl chloride (100 μl) was added to the solution of $Aβ_{16}$ (5 mg) dissolved in methanol (1.5 mL) and cooled at 0 °C. After the addition of $SOCl_2$, the reaction was stirred at room temperature for about 4 hours. ESI-MS direct injection confirms the generation of the product: m/z $671^{(3+)}$. The solution was evaporated and powdered with diethylether. At the end, the product was purified with HPLC separation and the pure peptide was controlled thought ^{1}H-NMR and COSY spectra (Figure 32).

The same reaction was performed on the *N*-acetylated $A\beta_{16}$ peptide and the product was controlled by ESI-MS: $685^{(3+)}$, $514^{(4+)}$. The same workout procedure was used for the purification of Ac-$A\beta_{16}$-OMe and the peptide was lyophilized.

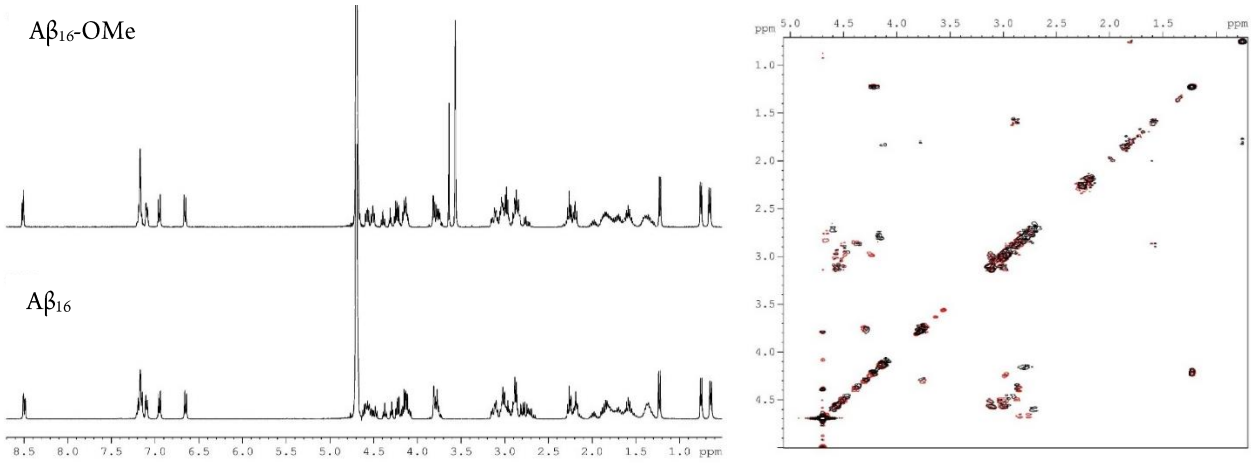

Figure 32. *^1H and COSY spectra of native $A\beta_{16}$ peptide and upon the esterification of carboxyl groups (red spectrum).*

The catalytic activity of copper bound to the esterified peptides was followed and compared to the redox activity of the unmodified complexes. Three substrates, such as dopamine, L-DOPA and L-DOPA methyl ester, at sub-saturating (0.3 mM) or saturating concentrations (3 mM) were selected to this purpose due to the presence of the amine group able to interact with negative-charged residues (Figure 33 and 34).

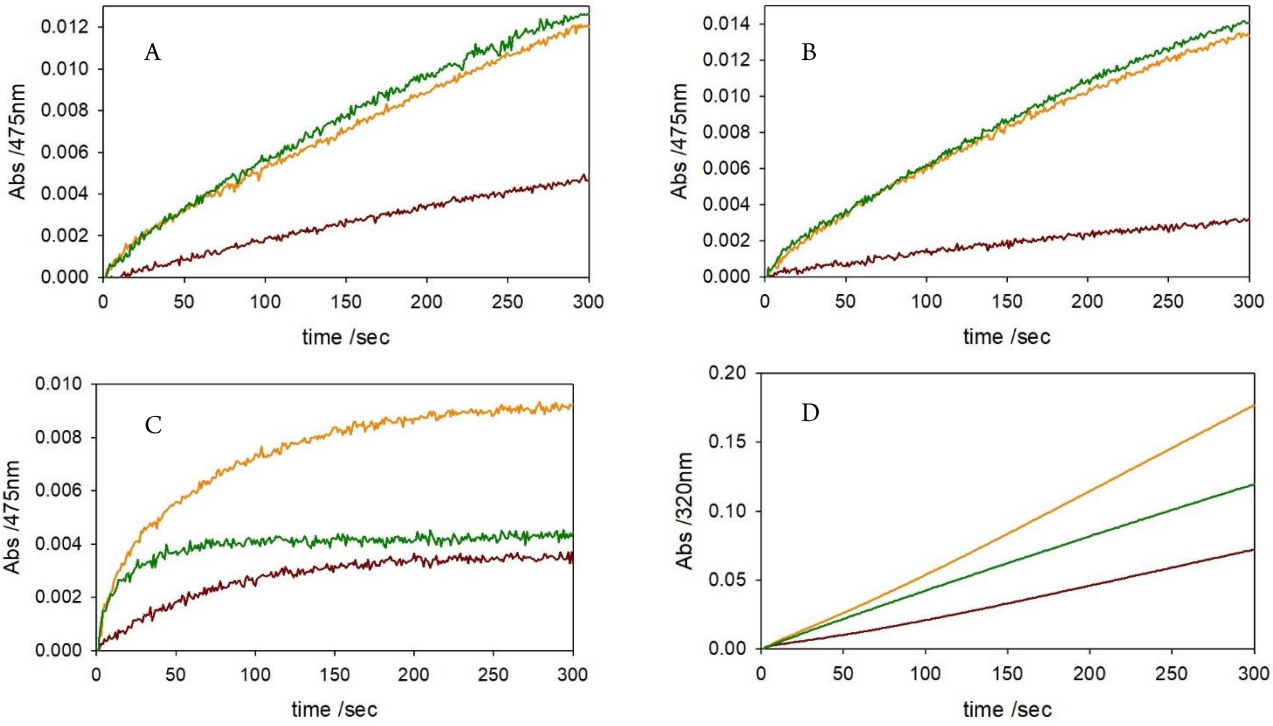

Figure 33. *Kinetic profiles of dopamine (panel A), L-DOPA (panel B) and L-DOPA methyl ester (panel C) (0.3 mM) oxidation with time in 50 mM HEPES buffer at pH 7.4 and 20 °C in the presence of Cu^{II} (25 μM) (brown trace) and the following complexes: [Cu^{II} -$A\beta_{16}$] (25 μM) (orange) and [Cu^{II}-$A\beta_{16}$-OMe] (green). Panel D shows the same kinetic data obtained from the L-DOPA methyl ester oxidation but following its oligomerization at 320 nm.*

Masking the negative side chains of the *N*-terminal region, a random distribution of the substrates between the *N*-terminal copper site and the *C*-terminal His-tandem domain would be allowed. The data suggest that the effect of electrostatic interactions is probably marginal and the absence of negative charges in the *N*-terminal site is not sufficient

alone to induce visible changes in the reactivity. $A\beta_{16}$-OMe shows a slight increase of its oxidative capability if compared to the native isoform but the changes are not sufficient to affirm an involvement of aspartate 1 in the catalytic cycle.

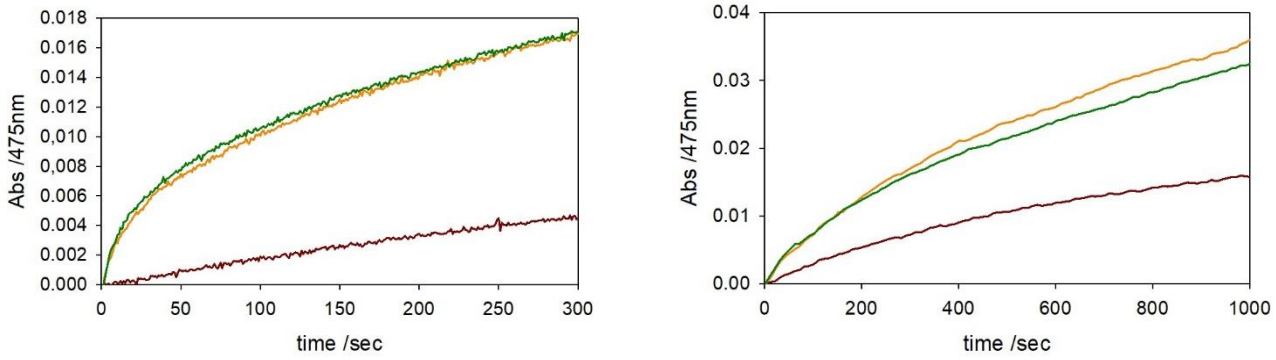

Figure 34. *Kinetic profiles of dopamine (0.3 mM, left panel and 3 mM, right panel) oxidation with time in 50 mM HEPES buffer at pH 7.4 and 20 °C in the presence of Cu^{II} (25 μM) (brown trace) and the following complexes: [Cu^{II} –Ac-Aβ16] (25 μM) (orange trace) and [Cu^{II}-Ac-Aβ16-OMe] (green).*

HPLC quantification of MC consumption.

The oxidation of 4-methylcatechol in 50 mM HEPES buffer at pH 7.4 and 25°C was also evaluated via HPLC separation, performing a 0-50% linear gradient of 0.1% TFA in water to 0.1% TFA in acetonitrile over 40 min (flow rate of 4 ml/min, loop 2 ml), as eluent. Stock solutions of substrate at sub-saturating concentration (0.3 mM) was previously prepared and divided in three aliquots corresponding to the initial condition of reaction (zero point), 5 min and 30 min reaction. The reaction was catalyzed by copper(II) nitrate (25 μM) complexed to following Aβ fragments, NH_2-$A\beta_{16}$, Ac-$A\beta_{16}$, NH_2-$A\beta_{16}[H_6A]$, Ac-$A\beta_{16}[H_6A]$, NH_2-$A\beta_{16}[H_{13}A]$, Ac-$A\beta_{16}[H_{13}A]$ (25 μM).

Table 2. *Qualitative characterization of the oxidative products generated by the reaction of MC with copper(II) alone or complexed with β-amyloid peptides; each peak numbered in the HPLC chromatograms was analyzed through ESI-MS and, when possible, by ^{1}H-NMR.*

Peak Number	Retention time	ESI/MS (m/z)	Oxidative Products
1	16 min	245(+)	MC/MQ-dimer
2	19.5 min	311(+) 328(+)	MC-dimer with 4 H_2O MC-dimer with 5 H_2O
3	23.5 min	439(+) 457(+)	MC-trimer with 3 H_2O + Na^+ MQ-trimer with 6 H_2O
4	29 min	276(+) 371(+)	MC/MQ-dimer with 2 H_2O MC-trimer
5	31 min	246(+) 262(+)	MC-dimer MC-dimer with 1 H_2O
6	31.7 min	416(+) 439(+)	MC-trimer with 3 H_2O MC-trimer with 3 H_2O + Na^+
7	33.5 min	245(+) 262(+)	MC/MQ-dimer MC-dimer with 1 H_2O
8	35.5 min	245(+)	MC/MQ-dimer

Before each injection, kojic acid (0.1 mM) was added to the solutions as internal standard to allow the quantification of MC peak (Figure 34). Moreover, the main oxidative products obtained from HPLC separation were collected and gently evaporated to perform a qualitative characterization of the mixtures. Each pure product is then identified through ESI-MS and eventually, through ^{1}H-NMR. From the data shown in Table 2, the heterogeneity of the oxidative

products generated upon few minutes of reaction can be easily observed although MC is a simpler substrate if compared to the oxidative pathway of dopamine. Dimers and trimers, and more complexed products, are formed upon the intermolecular nucleophilic attack between catecholic and quinonic species and their further re-aromatization; moreover, the resulting adducts are susceptible to the addition of water molecules on the suitable aromatic carbons. The oligomerization of substrates is enhanced by the presence of an oxidative environment and is time-dependent, and leads to the production of highly conjugated products.

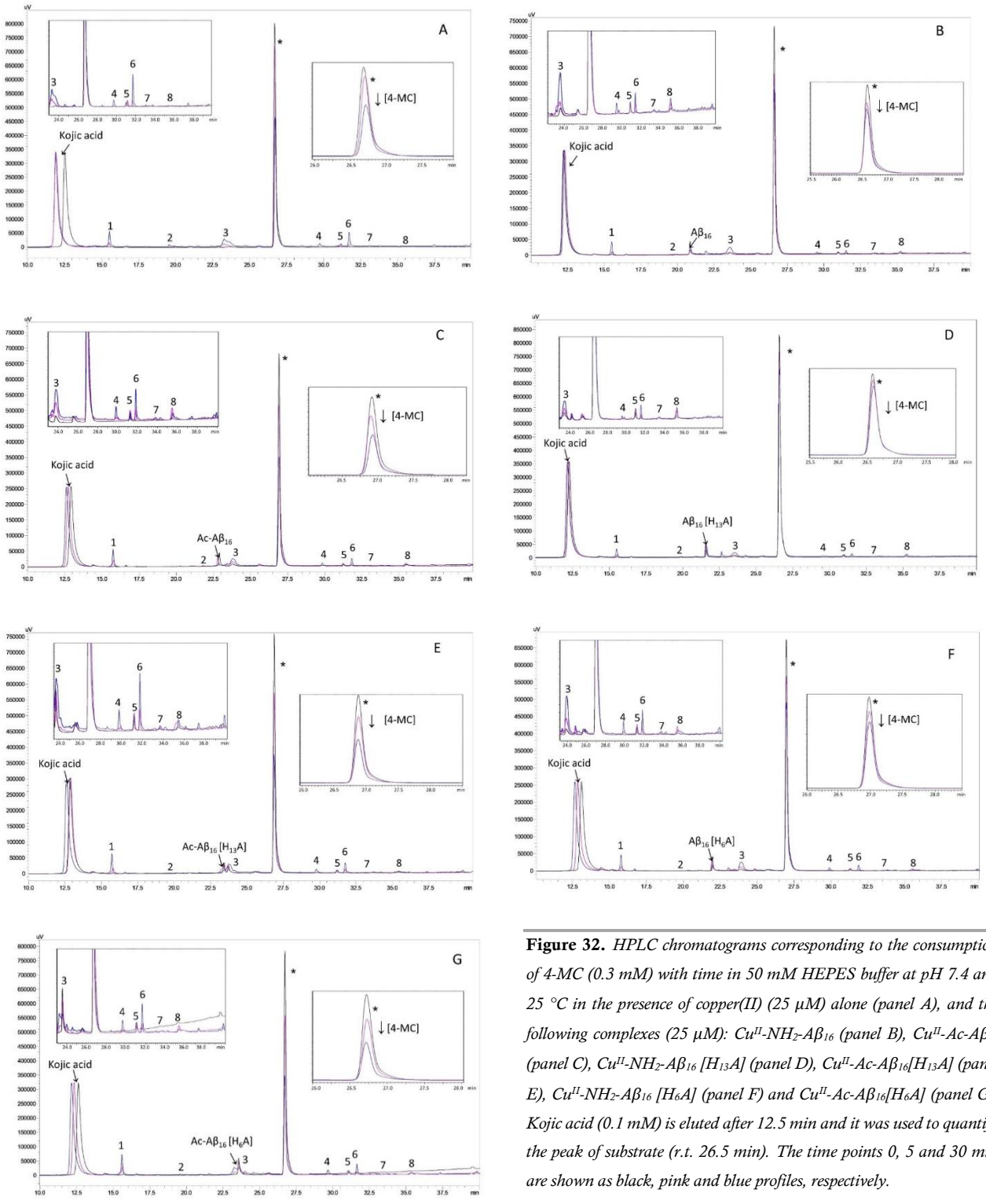

Figure 32. *HPLC chromatograms corresponding to the consumption of 4-MC (0.3 mM) with time in 50 mM HEPES buffer at pH 7.4 and 25 °C in the presence of copper(II) (25 μM) alone (panel A), and the following complexes (25 μM): Cu^{II}-NH_2-$Aβ_{16}$ (panel B), Cu^{II}-Ac-$Aβ_{16}$ (panel C), Cu^{II}-NH_2-$Aβ_{16}$ [$H_{13}A$] (panel D), Cu^{II}-Ac-$Aβ_{16}$[$H_{13}A$] (panel E), Cu^{II}-NH_2-$Aβ_{16}$ [H_6A] (panel F) and Cu^{II}-Ac-$Aβ_{16}$[H_6A] (panel G). Kojic acid (0.1 mM) is eluted after 12.5 min and it was used to quantify the peak of substrate (r.t. 26.5 min). The time points 0, 5 and 30 min are shown as black, pink and blue profiles, respectively.*

References

1. **a**) *Smith D.G., Cappi R. and Barnham K.J., The redox chemistry of the Alzheimer's disease amyloid beta peptide.;* ***Biochimica et Biophysica Acta - Biomembranes,*** 1768, 1976-1990, 2007; **b**) *Squitti R., Simonelli I. Ventriglia M., Siotto M., Pasqualetti P., Rembach A., Doecke J., and Bush A.I., Meta-analysis of serum non-ceruloplasmin copper in Alzheimer's disease,* ***J Alzheimers Dis,*** 38, 809-822, 2014
2. **a**) *Giacovazzi R., Ciofini I., Rao L., Amatorea C. and Adamo C., Copper–amyloid-β complex may catalyze peroxynitrite production in brain: evidence from molecular modeling,* ***Phys Chem Chem Phys,*** 16, 10169-10174, 2014; **b**) *Minati L., Edginton T., Bruzzone M.G. and Giaccone G., Current concepts in Alzheimer's disease: a multidisciplinary review.,* ***Am J Alzheimers Dis Other Demen,*** 24, 95-121, 2009.
3. *Wippold F.J, Cairns N., Vo K., Holtzman D.M. and Morris J.C., Neuropathology for the Neuroradiologist: Plaques and Tangles,* ***American Journal of Neuroradiology,*** 29, 1, 18-22, 2008.
4. **a**) *Alies B., Eury H., Bijani C., Rechignat L., Faller P. and Hureau C., pH-Dependent Cu(II) Coordination to Amyloid-β Peptide: Impact of Sequence Alterations, Including the H6R and D7N Familial Mutations,* ***Inorg Chem,*** 50, 11192-11201, 2011. **b**) *Furlan S., Hureau C., Faller P. and La Penna G., Modeling Copper Binding to the Amyloid-β Peptide at Different pH: Toward a Molecular Mechanism for Cu Reduction,* ***J Phys Chem B,*** 116, 11899-11910, 2012.
5. **a**) *Cheignon C., Tomas M., Bonnefont-Rousselot D., Faller P., Hureau C. and Collin F., Oxidative stress and the amyloid beta peptide in Alzheimer's disease,* ***Redox Biology,*** 14, 450-464, 2018; ***b)*** *Cheignon C., Jones M., Atrián-Blasco E., Kieffer I., Faller P., Collin F., and Hureau C., Identification of key structural features of the elusive Cu–Aβ complex that generates ROS in Alzheimer's,* ***Chem Sci,*** 8, 5107-5118, 2017.
6. **a**) *Cassagnes L.E, Hervé V., Nepveu F., Hureau C., Faller P. Collin F., The catalytically active copper-amyloid-Beta state: coordination site responsible for reactive oxygen species production.,* ***Angew. Chem. Int. Ed.,*** 52, 11110-11113, 2013; **b**) *Monzani E., Nicolis S., Dell'Acqua S., Capucciati A., Bacchella C., Zucca F.A., Mosharov E.V., Sulzer D., Zecca L. and Casella L., Dopamine, Oxidative Stress and Protein-Quinone Modifications in Parkinson's and Other Neurodegenerative Diseases,* ***Angew Chem Int Ed Engl,*** 58, 6512-6527, 2019.
7. **a**) *Abd El Wahed, M. G., Stability constants of Cu^{2+}, Fe^{3+} and Zr^{4+} chelates of ampicillin, dopamine and α-methyl L-dopa in aqueous medium.* ***Anal Lett,*** 17, 205-216, 1984; **b**) *Young, T. R.; Kirchner, A.; Wedd, A. G.; Xiao, Z., An integrated study of the affinities of the Aβ16 peptide for Cu(I) and Cu(II): Implications for the catalytic production of reactive oxygen species.* ***Metallomics*** 6, 505-517, 2014; **c**) *Alies, B.; Bijani, C.; Sayen, S.; Guillon, E.; Faller, P.; Hureau, C., Copper coordination to native N-terminally modified versus full-length amyloid-β: second-sphere effects determine the species present at physiological pH.* ***Inorg Chem,*** 51, 12988-13000, 2012.
8. **a**) *Pirota, V.; Dell'Acqua, S.; Monzani, E.; Nicolis, S.; Casella, L., Copper-Aβ peptides and oxidation of catecholic substrates: Reactivity and endogenous peptide damage.* ***Chem Eur J,*** 22, 16964-16973, 2016; **b**) *Dell'Acqua, S.; Bacchella, C.; Monzani, E.; Nicolis, S.; Di Natale, G.; Rizzarelli, E.; Casella, L., Prion peptides are extremely sensitive to copper induced oxidative stress.* ***Inorg Chem*** *56,* 11317-11325, 2017; c)
9. **a**) *T. R. Young, A. Kirchner, A. G. Wedd and Z. Xiao, An integrated study of the affinities of the Aβ16 peptide for Cu(I) and Cu(II): Implications for the catalytic production of reactive oxygen species.* ***Metallomics,*** 6, 505-517, 2014; **b**) Kowalik-Jankowska T., Ruta-Dolejsz M., Wiśniewska K., Łankiewicz L., *Cu(II) interaction with N-terminal fragments of human and mouse beta-amyloid peptide,* ***J Inorg Biochem,*** 86, 535-545, 2001; **c**) *Hureau C. and Dorlet P., Coordination of redox active metal ions to the amyloid precursor protein and to amyloid-beta peptides involved in Alzheimer disease. Part 2: Dependence of Cu(II) binding sites with Aβ sequences.* ***Coord Chem Rev,*** 25, 2175-2187, 2012.
10. **a**) *Syme C.D., Nadal R.C., Rigby S. E. and Viles J.H., Copper binding to the amyloid-beta (Abeta) peptide associated with Alzheimer's disease: folding, coordination geometry, pH dependence, stoichiometry, and affinity of Abeta-(1-28): insights from a range of complementary spectroscopic techniques.* ***J Biol Chem,*** 279, 18169-18177, 2004; **b**) *Drew S.C., Noble C.J., Masters C.L., Hanson G.R. and Barnham K.J., Pleomorphic copper coordination by Alzheimer's disease amyloid-beta peptide,* ***J Am Chem Soc,*** 131, 1195-1207, 2009.
11. **a**) *Drew S.C., Masters C.L. and Barnham K.J., Alanine-2 Carbonyl is an Oxygen Ligand in Cu^{2+} Coordination of Alzheimer's Disease Amyloid-β Peptide – Relevance to N-Terminally Truncated Forms,* ***J Am Chem Soc,*** 131, 8760-8761, 2009; **b**) *Dong X., Wang X., Lin M., Sun H., Yang X. and Guo Z., Promotive effect of the platinum moiety on the DNA cleavage activity of copper-based artificial nucleases,* ***Inorg Chem,*** 49, 2541-2549, 2010; **c**) *Aruoma O.I., Halliwell B. and Dizdaroglu M., Iron ion-dependent modification of bases in DNA by the superoxide radical-generating system hypoxanthine/xanthine oxidase.* ***J Biol Chem,*** 264, 13024-13028, 1989.
12. *Elwell E.C., Gagnon N.L., Neisen B.D., Dhar D., Spaeth A.D., Yee G.M. and Tolman W.B., Copper-Oxygen Complexes Revisited: Structures, Spectroscopy, and Reactivity,* ***Chem Rev,*** 117, 2059-2107, 2017
13. *Chang C.M., Klema V.J., Johnson B.J, Mure M., Klinman J.P. and Wilmot C.M., Kinetic and Structural Analysis of Substrate Specificity in Two Copper Amine Oxidases from Hansenula polymorpha,* ***Biochemistry,*** 49, 2540-2550, 2010.
14. *Steiner R.A., Kalk K.H. and Dijkstra B.W., Anaerobic enzyme·substrate structures provide insight into the reaction mechanism of the copper-dependent quercetin 2,3-dioxygenase,* ***Structure,*** 10, 259-268, 2002.
15. *Pirota V., Dell'Acqua S., Monzani E., Nicolis S. and Casella L., Copper-Aβ Peptides and Oxidation of Catecholic Substrates:*

Reactivity and Endogenous Peptide Damage, ***Chemistry – A European Journal*, 22**, 16964-16973, 2016

16. *Merrifield R.B., Solid Phase Peptide Synthesis. I. The Synthesis of a Tetrapeptide,* ***Journal of the American Chemical Society,*** 85, 2149-2154, 1963.
17. *Fields G.B. and Noble R.L., Solid phase peptide synthesis utilizing 9-fluorenylmethoxycarbonyl amino acids,* ***Int J Pept Protein Res***, 35, 161-214,1990.
18. *Mach H., Middaugh C.R. and Lewis R.V., Statistical determination of the average values of the extinction coefficients of tryptophan and tyrosine in native proteins,* ***Anal Biochem,*** 200(1), 74-80, 1992
19. *Siopa F., Pereira A.S., Ferreira L.M., Marques M.M. and Branco P.S., Synthesis of catecholamine conjugates with nitrogen-centered bionucleophiles,* ***Bioorg Chem,*** 44, 19-24, 2012
20. *Patila P. and Chaskarb A., An efficient general method for esterification of aromatic carboxylic acids,* ***Tetrahedron Letters***, 37, 35, 6375-6378, 1996.

Chapter 5

N-TERMINAL CLEAVAGE OF AMYLOID-β PEPTIDE: THE EFFECTS ON BINDING STABILITY AND REDOX BEHAVIOR OF COPPER-β-AMYLOID.

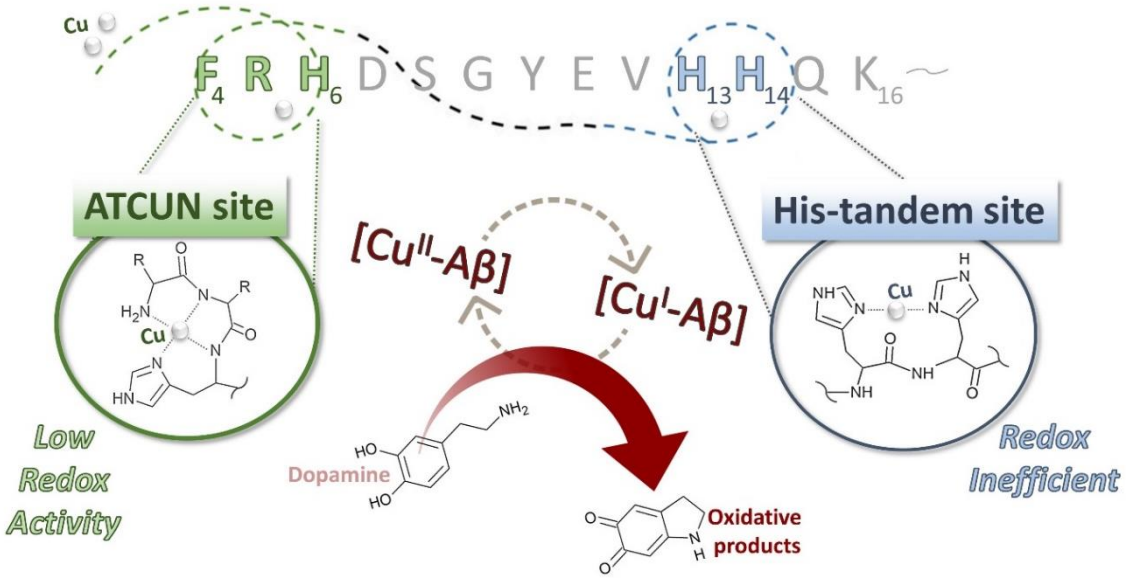

Ref. Int. J. Mol. Sci., 22, 5190, 2021
"Oxidase Reactivity of Cu^{II} Bound to N-Truncated Aβ Peptides Promoted by Dopamine"
C. Bacchella, S. Dell'Acqua, S. Nicolis, E. Monzani and L. Casella

Introduction

Alzheimer's disease is a neurological disorder characterized by the presence of amyloidogenic deposits probably due to the overproduction and the lower degradation or dyscatabolism of Aβ peptide. Amyloid-β peptides represent a wide population commonly generated from the precursor protein, known as APP,[1a] that undergoes the cleavage by some aminopeptidases and it was hypothesized that changes of the proteolytic pathway of these proteins or of the activity of these enzymes would influence the amyloid aggregation and plaque generation.[1b,1c] An abnormal presence of amyloid plaques and fibrils in dopaminergic areas of AD affected brains is usually observed, in which amyloid-β fragments (1-40) and (1-42) are detected as the major constituents. On the other hand, several *N*-truncated fragments that start with alanine 2, glutamate 3, or phenylalanine 4, were also identified, reporting the Aβ(4-x) peptide as one of the main isoforms extracted from hippocampus and cortex of subjects with Alzheimer's and Down syndromes.[2a] Indeed, until 64 percent of the peptides incorporated in the amyloid plaques has the phenylalanine 4 as first amino acid, as reported in literature.[2b]

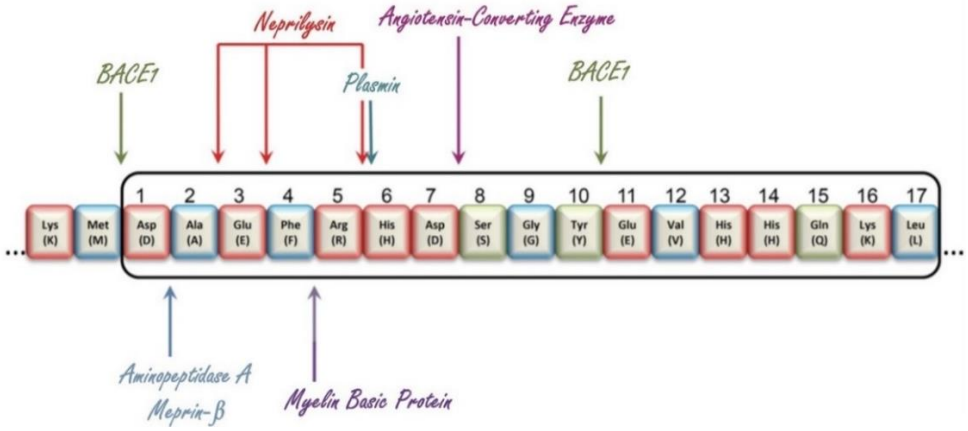

Figure 1. *The main N-truncations as result of some enzymatic activities are shown; NEP is the primary enzyme responsible of the cleavage between Arg-2 and Glu-3 or between Glu-3 and Phe-4, while plasmin prefers a cleavage after basic residues, preferentially cutting after Arg-5. Moreover, the activity of ACE is usually directed at Asp-7, slowing down the aggregation and the deposition of amyloid-β. MBP is another protease able to degrade Aβ peptides cutting between Phe-4 and Arg-5; finally, BACE1, besides its activity required to produce Aβ 1-x, is also able to generate fragments upon the cleavage between Tyr-10 and Glu-11.*

The generation of amino-terminally modified peptides would result from an erroneous proteolytic cleavage mediated by aminopeptidases, where a decrease in the aminopeptidase activity and in the plasma levels, more specifically in the glutamyl aminopeptidase or aminopeptidase A, was observed in AD patients, suggesting the catalytic cleavage as rate-limiting step in the Aβ catabolism in brain.[1b] The modification of the full-length Aβ peptide could change the chemical stability of the peptide and its resistance to the peptidase activity, influencing its aggregation and its endosomic degradation. On the other hand, experimental data obtained upon the incubation of another enzyme known as zinc-metalloprotease neutral endopeptidase or neprilysin (NEP) in the presence of amyloid-β 1-10 peptide have shown high levels of *N*-terminal fragmentation mainly between Arg-2 and Glu-3 or between Glu-3 and Phe-4, suggesting a causative role of this enzymatic activity (Figure 1).[2c] If Aβ *C*-terminal cleavage leads to the generation of more soluble fragments, easily degraded and eliminated from brain, *N*-terminal truncation at position 4 induces the formation of poorly soluble peptides that are highly prone to aggregate, playing a harmful role in the amyloidogenic deposition of fibrils. Immunoreaction experiments through the use of polyclonal antibodies have indicated a prevalent localization of *N*-truncated isoforms at position 4 in the amyloid plaques and an absence of a diffuse pattern, verifying the correspondence between the *N*-terminal modification and the generation of fibrillary lesions.[2d] Moreover, some

differences in the aggregation mechanism of the full-length amyloid-beta peptides and their truncated species have been suggested: while Aβ1-42 is commonly considered as highly fibrillogenic and prone to form β-sheet rich secondary structures and high molecular mass aggregates, *N*-terminal deletion to give Aβ(4-42) species modulates the fibrillary propensity, enhancing the deposition rate of high m.w. oligomers.[3] Therefore, known the low solubility of these *N*-truncated species, a possible role in the amyloidogenic progression as nucleation seeds for the fibrillation was suggested. This section has the aim to investigate the possible implications of the *N*-terminal cleavage on the reactivity and on the interaction with redox-active metals, since these species have been found for more than 50% of the total β-amyloid peptides in the hippocampus and cerebral cortex and 60% in amyloid plaques.[2a,4a,4c] Alzheimer's disease (AD) is a neurological disorder that has been largely associated with the metal dysmetabolism, detecting high levels of zinc, copper and iron ions in amyloid plaques; therefore, the main purpose of this work is to understand the possible biological consequences of the complexation of metals to the *N*-truncated amyloid peptides.

Recent publications indicate that, if compared to the binding stability observed in the presence of Aβ(1-16), copper(II)-Aβ(4-x) complex has higher stability of some magnitude orders at neutral pH, probably due to the presence of a conserved sequence H_2N-Xxx-Zzz-His, called "amino terminal copper and nickel binding motif" (ATCUN), already detected in some biological enzymes (Figure 2).[5] A protein involved in the transport of copper in the circulatory system as the serum albumin is an example of protein showing an amino-terminal Cu and Ni-binding motif; the binding with copper(II) occurs through a square planar geometry mediated by four nitrogen ligands, the *N*-terminal amine, two vicinal amides and an imidazole of histidine in third position. This coordinative environment leads to a dissociation constant at neutral pH for cupric ion comprised in a range of 10^{-12} to 10^{-15} M^{-1}.[6] Electrochemical studies suggest that Cu^{II}-ATCUN complexes show very low tendency to undergo redox reduction of the metal center, since Cu^{II} is stably bound and Cu^{I} is not potentially able to deprotonate amides. The redox reactivity of these complexes is only mediated by the two $Cu^{II/I}$ couple, excluding some Cu^{III}-intermediate, and the generation of radical oxygen species is strongly reduced if compared to the reactivity of full-length peptides bound to copper.[5] The high stability of copper(II) and the low affinity for copper(I) was also verified through experimental data collected in the presence of metallothioneins, some homeostatic proteins showing high density of thiolates to favor the binding with copper(I) and zinc(II) ions. The competition between the binding of copper(I) with amyloid-β fragments 4-16 and MT highlights the possibility to silence the redox activity of the metals in a biological context via the interaction of these proteins with cuprous ions, generally poorly stabilized by this square-planar geometry. This interchange occurs only in the presence of strong reducing agents that are able to promote the conversion from cupric to cuprous ions, shifting the redox reaction toward the reduced species that can be easily trapped by the thiolates.[7] Anyway, studies performed on neuronal cells upon injection of some amyloid-beta species as $Aβ_{4-38}$, $Aβ_{4-40}$, $Aβ_{4-42}$, and $Aβ_{1-42}$ have proposed a tight correlation between the presence of the first three isoforms and the progression of disease, probably correlated with their ability to generate toxic oligomers. The higher aggregation propensity observed on $Aβ_{4-42}$ if compared to the full-length peptide suggests a possible fibrillation mechanism in which the seed of nucleation could correspond to the oligomerization of the truncated species. Moreover, the overexpression of $Aβ_{4-42}$ in transgenic mouse models promotes a massive age-dependent loss of pyramidal neuronal cells and huge deficits of memory and neuronal functions.[2a] Furthermore, if the

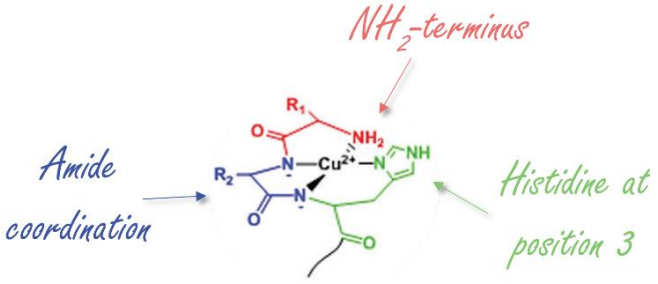

Figure 2. *Schematic structure showing the typical coordination geometry of Cu^{II} bound to ATCUN motif.*

full-length protein is widely expressed both in normal tissues and in AD-affected neuronal cells, the isoforms 4-42 is not expressed under not-pathological conditions, maybe linked to their tendency to form soluble and highly toxic aggregates. A possible protein useful as a target to design a specific immunotherapy would be the *N*-truncated Aβ peptide and therefore, a wide characterization of the mechanism leading to the generation and to the following aggregation of these *N*-truncated isoforms together with the assay of their biochemical properties are fervently required. If the multitude of data focused on the aggregation mechanism followed by these peptides seems to be in agreement with each other, the publications about the reactivity of the peptides when bound to copper are still controversial, partially suggesting, on one side, a totally inert behavior of copper(II)-ATCUN adducts and, on the other, a modest ability to produce ROS.[8a,8b] Moreover, besides the (5,5,6)-membered chelate rings around copper(II) provided by the *N*-terminal domain of $A\beta_{4-x}$ that shows a logK value more than three orders of magnitude higher respect with $A\beta_{1-x}$ and thirty times higher than that of human serum albumin (HSA), an additional binding site for the metal has been detected.[8a] The secondary binding site is independent from the *N*-terminal domain and consists in a His-tandem site, encompassing His-13 and His-14 residues, where the interaction with copper(I) ions can easily occur while the binding affinity for copper(II) is 7 order of magnitude below the values obtained for the ATCUN environment. The simultaneous presence of these two binding domains could indicate the involvement of these species in the trafficking and control of copper levels, given the high homology with the amino acidic sequences of copper transport protein (CTR1), human salivary antimicrobial peptides (AMP) and histatin-5 (Hst5) (Figure 3).[8c,8d]

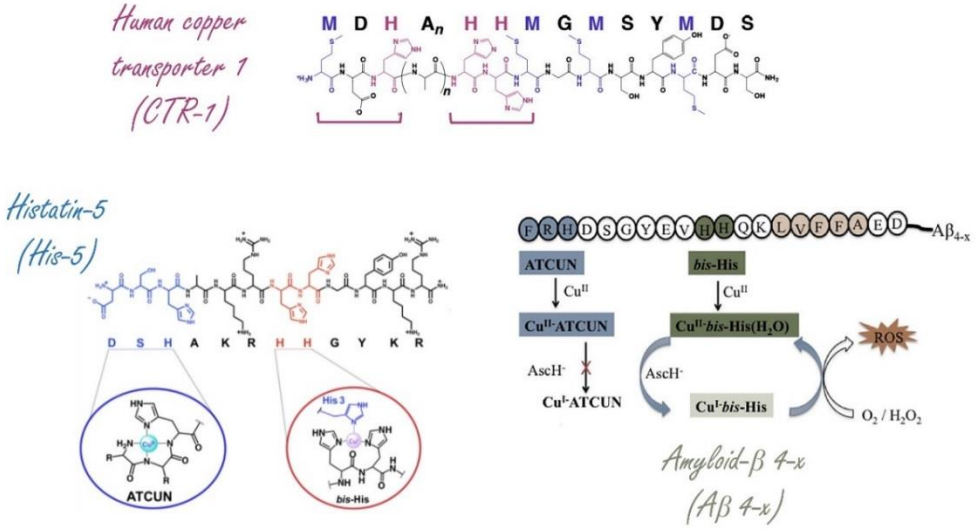

Figure 3. *Similarity between the amino acids sequences of CTR-1, Hst-5 and Aβ(4-x), showing the presence of the N-terminal ATCUN site and the bis-His tandem domain.* [8e, 8f, 8g]

The aim of this section is therefore the assay of the total unreactivity of Cu ions when are trapped in the primary binding site besides the study of the redox ability of the secondary binding domain located in the *C*-terminal region. The redox cycling of the metal alone and bound to *N*-truncated Aβ(4-x) peptide compared with adducts generated by Aβ(1-x) isoforms is herein promoted through the reaction with reducing substrates, as catechols. As previously described, catechols and catecholamines, as dopamine, act as biological messengers of signals in the neuronal compartments and, in the presence of strongly oxidative conditions and dysregulation of their release, these molecules work as substrates for several oxidative reactions that lead to quinonic products and gradually to high m.w. and insoluble aggregates, known as neuromelanins.[9a,9b] Furthermore, catechols and their products are able to unselectively attach and covalently modify structural proteins and enzymes, altering their biological role or their native conformation; we have thus characterized the oxidative vulnerability shown by Aβ(4-x) peptides when in the presence of metals and catechols.

Redox efficiency and oxidative modification of Aβ(4-x) and Aβ(1-x) bound to Cu

The catalytic oxidation of dopamine and 4-methylcatechol promoted by copper was studied at room temperature in 50 mM HEPES buffer at pH 7.4, saturated with atmospheric oxygen. The reaction was monitored as previously described and all kinetic data were collected at sub-saturating concentration of substrate (0.3 mM) and higher ones (3 mM) catalyzed by only molecular oxygen, shown as autoxidation traces, by copper alone (25 μM) and by the adducts generated upon the binding between 1 equiv. copper and 1 or 2 equiv. $A\beta_{1\text{-}16}$ and $A\beta_{4\text{-}16}$ peptides (25-50 μM). The resulting catalysis promoted by the complexes and the stabilization of the metal in the ATCUN site are strongly influenced by the amount and by the reducing capability of the substrate and therefore divergent results were obtained. As shown in Figure 4, the oxidative reaction is only disfavored when it works with saturating amount of catechols and with copper(II) bound to the *N*-truncated peptide while, decreasing the concentration of substrate at sub-saturating values, the redox cycling of Cu bound to $A\beta_{4\text{-}16}$ is almost totally quenched.

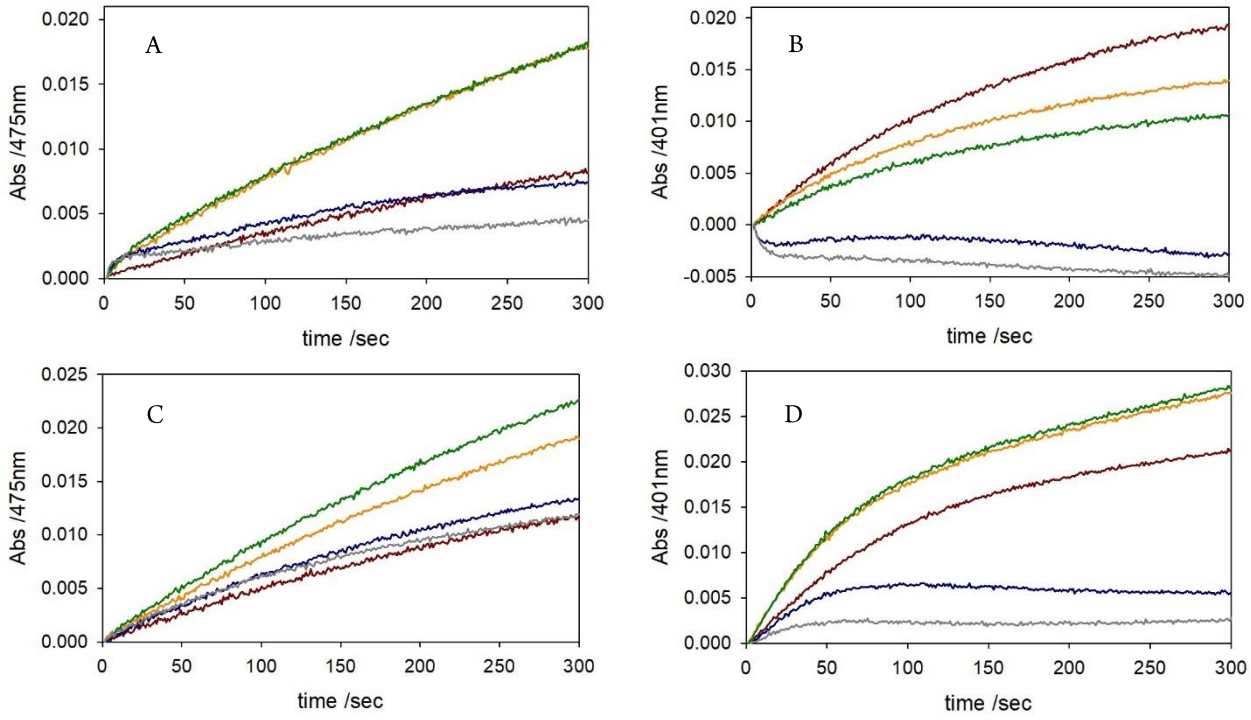

Figure 4. *Kinetic profiles of DA (panel A, 0.3 mM and panel C, 3 mM) and MC (panel B, 0.3 mM and panel D, 3 mM) oxidation with time in 50 mM HEPES buffer at pH 7.4 and 20 °C in the presence of Cu^{II} (25 μM) (brown trace) and with 1 eq. $A\beta_{16}$ (orange), 2 eq. $A\beta_{16}$ (green), or 1 eq. $A\beta_{4\text{-}16}$ (blue) and 2 eq. $A\beta_{4\text{-}16}$ (grey).*

As shown in Figures 5, the catalytic mechanism followed by this complexes views the production of an initial chromophore presenting a high absorption band around 300 nm and probably corresponding to some copper(II) adduct with the substrate. Although an initial binding between metal and catechol occurs and induces a short-time accumulation of oxidative products, the high affinity binding site provided by the *N*-truncated peptide would be able to overcome the modest binding affinity for catechol, shifting the metal coordination to the ATCUN site. The square planar coordination environment, later distorted by the interaction with the substrate, ensures a high stability of copper(II) binding with the peptide, partially quenching the reactivity of the complex if compared to the full-length *N*-terminal isoform. A low extraction of copper(II) from the dopamine-metal adduct is also reflected by the general

slowness of the oxidative mechanism of this substrate respect with the chemically simpler 4-methylcatechol, that is subjected to faster oxidation to give a reduced population of products less prone to aggregate.

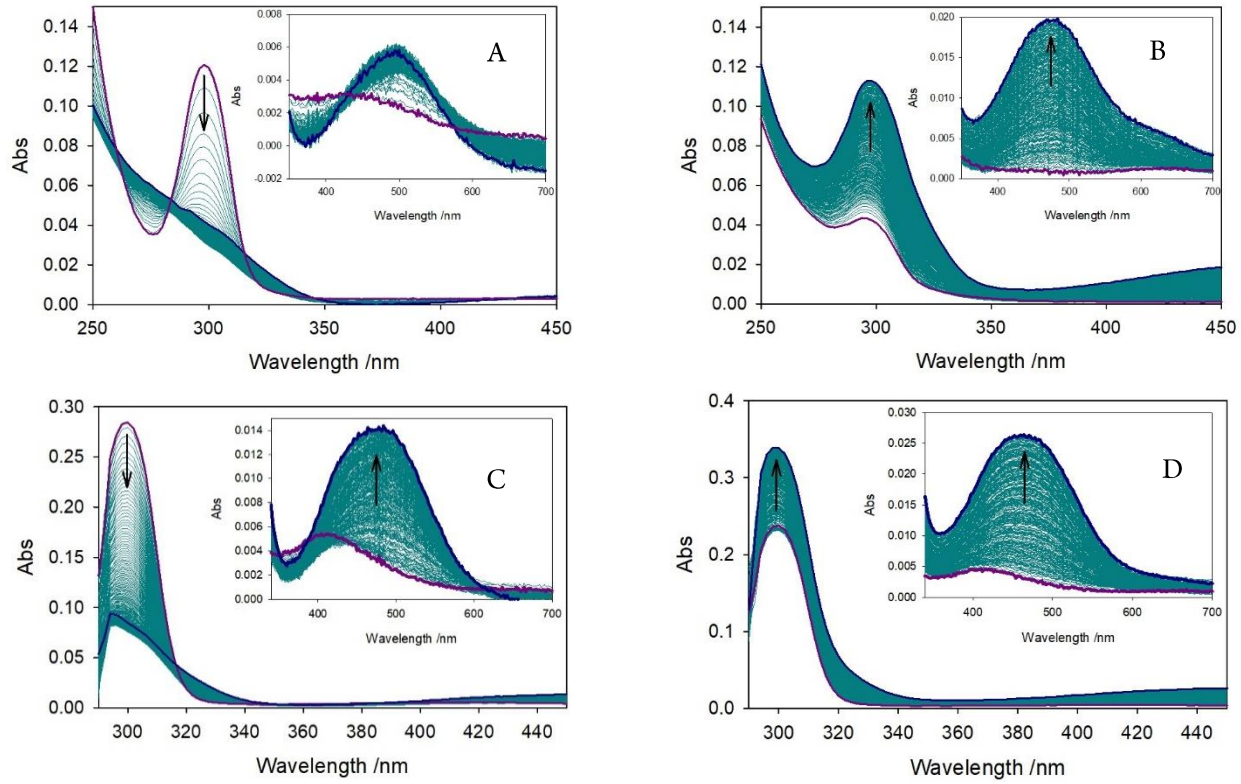

Figure 5. *The spectra show the oxidative reaction toward dopamine (0.3 mM, panel A and B and 3 mM, C and D) in the presence of two equiv. of $A\beta_{4-16}$ (panel A and C) and $A\beta_{1-16}$ (panel B and D).*

In the same conditions, the oxidation of both substrates was followed for longer reaction time to verify the divergences between the catalytic ability of the two complexes (Figure 6). The presence of a quite stable copper(II) adduct upon the metal binding with the *N*-truncated peptide emerges from the partial quenching of the reactivity shown in the presence both of 4-methylcatechol and dopamine, in which the kinetic profiles performed with copper(II) bound to 1 or 2 equiv. of peptide suggest a lower oxidation rate compared with the catalytic ability of the metal alone. On the other hand, the total shutdown of reaction does not occur and, in these conditions, copper(II) trapped by the ATCUN site is not completely inactive.

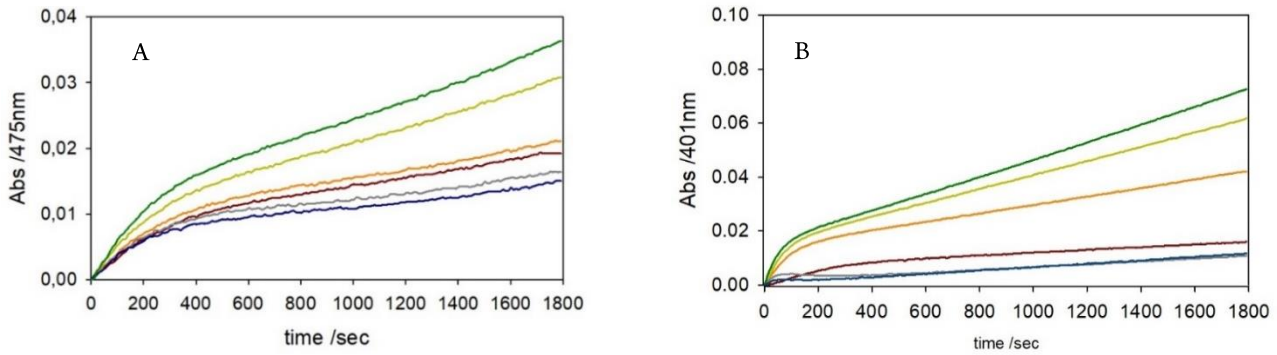

Figure 6. *Kinetic profiles of DA (3 mM, panel A) and MC (3 mM, panel B) oxidation with time in 50 mM HEPES buffer at pH 7.4 and 20 °C (autoxidation, brown trace) in the presence of Cu^{II} (25 μM) (orange) and upon the addition of 1 eq. $A\beta_{16}$ (light green), 2 eq. $A\beta_{16}$ (green), or 1 eq. $A\beta_{4-16}$ (grey) and 2 eq. $A\beta_{4-16}$ (blue).*

Therefore, Cu^{II} alone is stably bound into the planar coordination sphere in the *N*-terminal region but, upon the addition of high amount of catechol, the substrate can partially alter the geometry of the chelate and the structural twist may be sufficient to destabilized the metal interaction, leading to its reduction. Anyway, this reaction slowly occurs and it is influenced by the reduction potential of the substrate. Similar data were also obtained on the longer amyloid fragments 1-28 and 4-28 (Figures 7 and 8), where the *N*-terminal region allows the interaction with the metal while the *C*-terminal tail is modestly hydrophobic and slowly mediates the intermolecular stacking and the aggregation of the peptide. On the other hand, the absence of the region 29-42 increases the solubility of this sequence and therefore, the fibrillation requires the presence of high concentration of peptide together with longer incubation times.[10a,10b,10c] As shown in Figure 7, the *N*-truncated peptide 4-28 shows lower capability to stabilize Cu^{II} ion and to quench the redox cycling of the metal, although an analogous trend can be observed if compared with the previous ones. Moreover, an excess of peptide seems to restore the shutdown of the redox cycling.

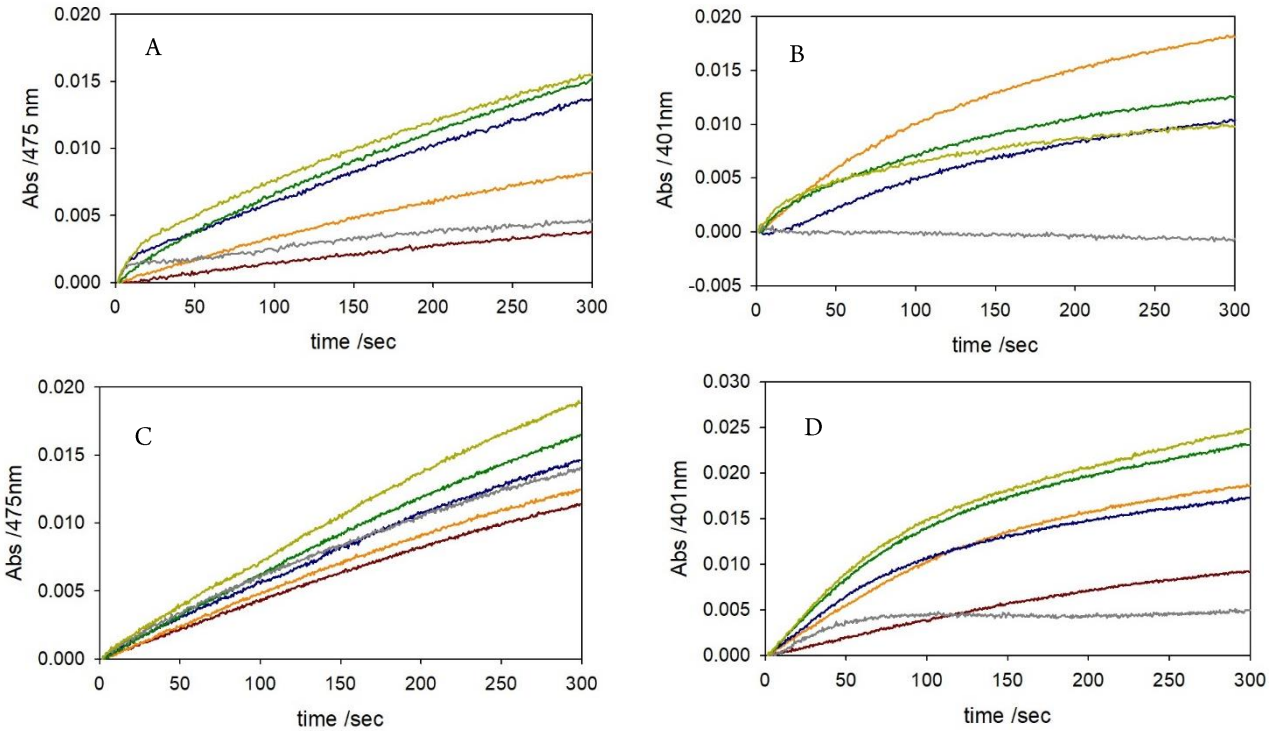

Figure 7. *Kinetic profiles of DA (panel A, 0.3 mM and panel C, 3 mM) and MC (panel B, 0.3 mM and panel D, 3 mM) oxidation with time in 50 mM HEPES buffer at pH 7.4 and 20 °C in the presence of Cu^{II} (25 μM) (orange trace) and with 1 eq. $Aβ_{28}$ (green), 2 eq. $Aβ_{28}$ (light green), or 1 eq. $Aβ_{4-28}$ (blue) and 2 eq. $Aβ_{4-28}$ (grey). The autoxidation of substrate is shown as brown trace.*

These results are probably linked to the presence of an additional tail that can interfere in the metal binding or in the structural rearrangement of the peptide that normally occurs with the metal interaction. The fragment 1-28 in aqueous *medium* shows a bit lower reactivity if compared to the oxidative efficiency of the shorter analogous peptide 1-16 and this trend is ascribable to the higher aggregation rate of the longer peptide that partially decreases the total amount of redox-active species in the reaction *medium*. This effect is more pronounced when the *N*-terminal deletion occurs: Aβ(4-x) peptides are highly prone to generate oligomers and fibrils if compared to the full-length peptides 1-x and therefore, the resulting kinetic profiles reflect the partial aggregation of a small percentage of peptide in solution that does not allow the total Cu^{II} complexation. The treatment of the peptide with hexafluoro-2-propanol (HFIP) to disaggregate the eventual presence of oligomers in solution enhances the effective presence of monomeric species able to interact and stabilize the metal, as suggested by the lower oxidation rate toward the substrate shown in Figure 8 but

it is not sufficient to induce a considerable reaction quenching as observed with Cu-Aβ(4-16) adduct at 1:1 molar ratio. On the other hand, a similar profile can be achieved by working with a small excess of peptide (1.2 equiv.).

The presence of small factions of unbound copper in the reaction mixture can be also motivated by the higher oxidative modification rate of *N*-truncated peptide 4-28 if compared with all previously analyzed fragments (see Chapter 1). The modification patterns shown in Figure 9 were obtained in the same conditions of the kinetics at saturating concentrations of substrate and analyzing the samples at different reaction times through HPLC-MS. Tables 1 and 2 suggest that this oxidative environment promotes the fast oxidation of the most susceptible residues and in particular, only upon 15 min of reaction, almost 15% Aβ(4-28) shows at least one histidine covalently modified though the insertion of an *O*-atom (mass increment +16).

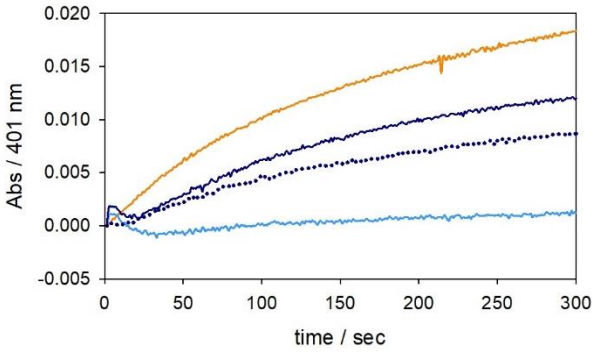

Figure 8. *Kinetic profiles of MC (0.3 mM) oxidation with time in 50 mM HEPES buffer at pH 7.4 and 20 °C in the presence of Cu^{II} alone (25 μM, orange trace) and with the addition of 1 equiv. $Aβ_{4-28}$ dissolved in water (25 μM, solid blue) or 1 equiv. (25 μM, dotted blue) or 1.2 equiv. $Aβ_{4-28}$ (30 μM, light blue) treated with HFIP for 3h to avoid the presence of oligomeric species in solution.*

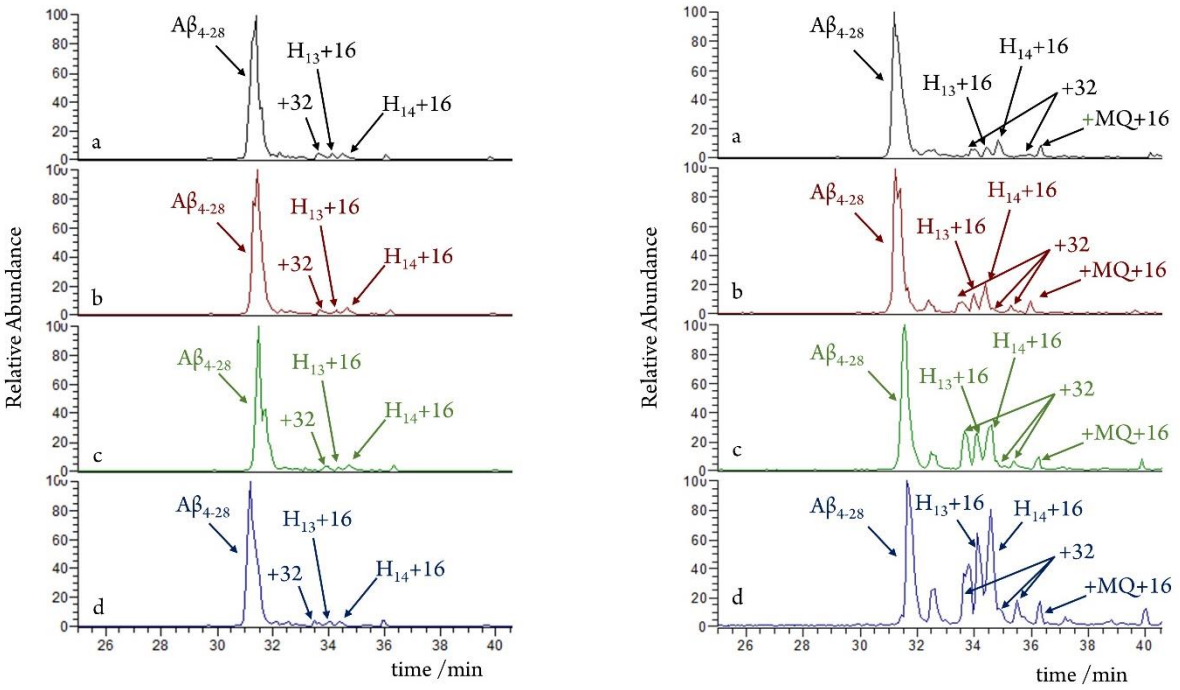

Figure 9. *LC-MS elution profiles of $Aβ_{4-28}$ peptide (25 μM) in 50 mM HEPES buffer at pH 7.4 with DA (3 mM, at left) or MC (3 mM, at right) in the presence of copper (25 μM). The reaction was analyzed at different reaction times: 15 min (panel a), 25 min (panel b), 35 min (panel c) and 60 min (panel d).*

Minor modifications are the multiple insertion of *O*-atoms (mass increment +32 and +48) on the histidines, that are normally involved in the metal binding, besides the covalent modification due to the attack of some amino acidic residues by the catechol or its products. The pattern of fragmentation is negligible, in which the *C*-terminal region seems to be affected by cleavages located between glutamate-11 and valine-12, histidine-13 and histidine-14, aspartate-7 and serine-8, glutamine-15 and lysine-16.

Table 1. *Oxidative modification with time of Aβ4-28 peptide (25 μM) detected by LC/MS analysis upon the reaction with MC (3 mM) and copper (25 μM) in 50 mM HEPES buffer pH 7.4 at 20 °C.*

	Aβ4-28 (not modified)	**Aβ4-28 mono-oxidized** (+16)	**Aβ4-28 bi-oxidized** (+32)	**Aβ4-28 tri-oxidized** (+48)	**Aβ4-28 -dopaminated** (+120, +122)	**Aβ4-28 -oxidized and dopaminated** (+136, +138)
time						
15'	66%	15%	4%	1%	6%	8%
25'	56%	20%	7%	1%	6%	10%
35'	49%	23%	8%	1%	6%	13%
60'	41%	29%	11%	1%	4%	14%

Table 2. *Oxidative modification with time of Aβ4-28 peptide (25 μM) detected by LC/MS analysis upon the reaction with DA (3 mM) and copper (25 μM), in 50 mM HEPES buffer pH 7.4 at 20 °C.*

	Aβ4-28 (not modified)	**Aβ4-28 mono-oxidized** (+16)	**Aβ4-28 bi-oxidized** (+32)	**Aβ4-28 tri-oxidized** (+48)	**Aβ4-28 -dopaminated** (+145, +147, +149, +151)	**Aβ4-28 -fragmented**
time						
15'	78%	14%	4%	1%	3%	-
25'	75%	17%	4%	1%	3%	-
35'	68%	20%	6%	1%	5%	-
60'	62%	17%	6%	2%	9%	4%*

If there are modest differences between the two oxidative traces obtained in the presence of copper adduct (1:1) with the shorter 4-16 and the more hydrophobic 4-28 peptides, both complexes show the same peculiar absorption at 300 nm that is subjected to a visible decay upon few seconds of reaction. On the other hand, the amyloid peptides 1-x upon the addition of copper and catechol give rise the same contribution, that is stable with time as shown in Figure10.

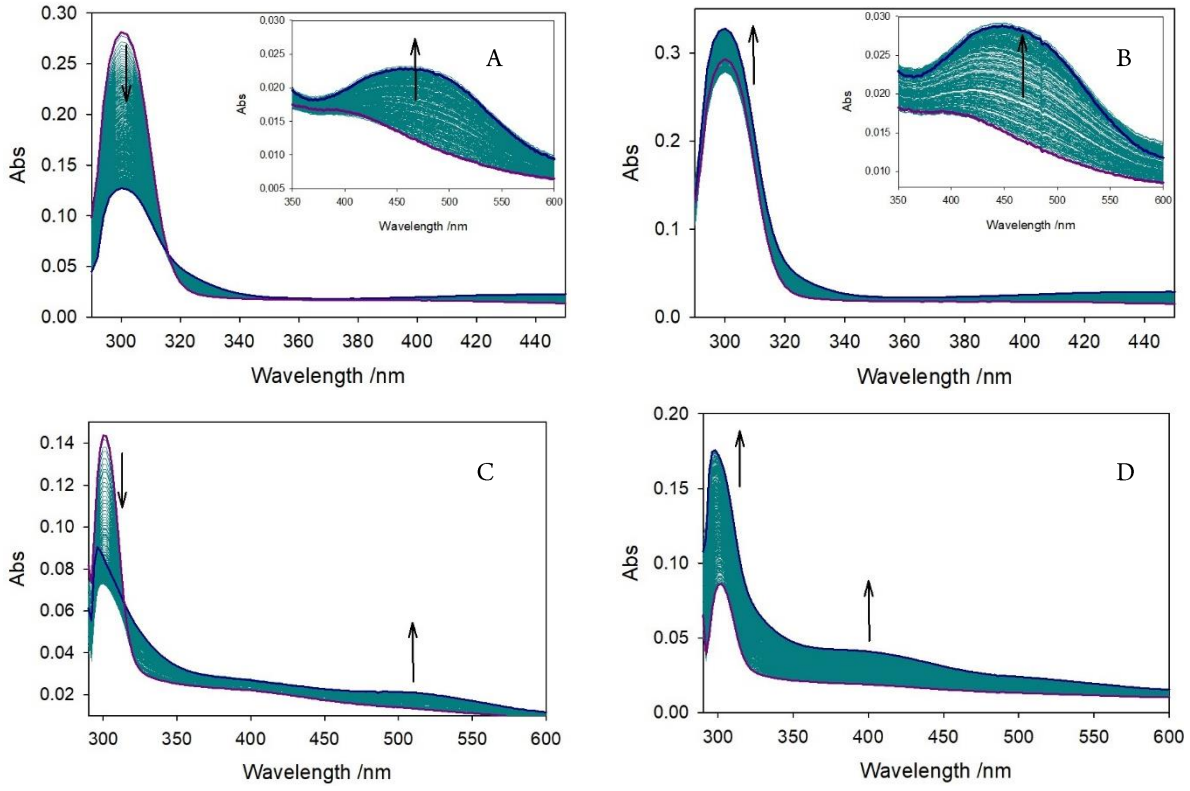

Figure 10. *The spectra show the oxidative reaction toward dopamine (panel A and B) and 4-methylcatechol (panel C and D) in the presence of two equiv. of Aβ4-28 (panel A and C) and Aβ28 (panel B and D).*

In order to verify the effective stabilization of the metal binding provided by the ATCUN sphere and the oxidative capability of Cu-Aβ$_{1-x}$ and Cu-Aβ$_{4-x}$ adducts, the reactivity was studied in terms of oxidative consumption of ascorbate, following the decay of its absorption at 265 nm, induced by the metal alone and upon the binding with 1 and 2 equiv. Aβ$_{16}$ and Aβ$_{4-16}$ (Figure 11).

The unbound metal is the most reactive species and shows the highest consumption of substrate. The redox cycling of copper is promoted by the reaction with the reducing agent and by the lacking of ligands able to stabilize one of the two redox forms. When amyloid-beta 1-16 peptide is added to the reaction mixture, the binding with the metal partially influences the stabilization of one redox species and the rate of $Cu^{II/I}$ cycling and a similar effect is evidenced when the *N*-truncated isoform is added but the higher stabilization of copper(II) binding leads to the further slowdown of the redox cycling, influencing the rate of ascorbate consume.

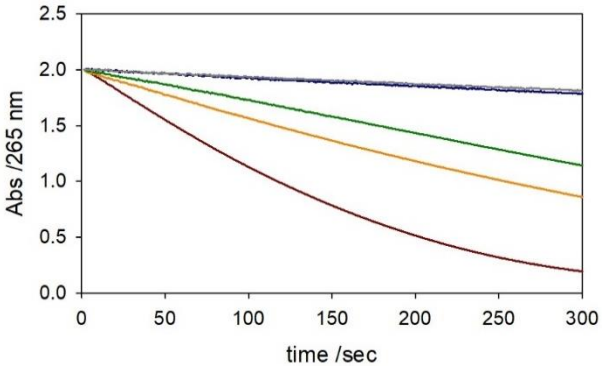

Figure 11. *Kinetic profiles of ascorbate (0.15 mM) consume with time in 50 mM HEPES buffer at pH 7.4 and 20 °C in the presence of Cu^{II} (25 μM) (brown trace) and with 1 eq. Aβ$_{16}$ (orange), 2 eq. Aβ$_{16}$ (green), or 1 eq. Aβ$_{4-16}$ (blue) and 2 eq. Aβ$_{4-16}$ (grey).*

Moreover, in order to characterize the reaction mechanism followed by these metal complexes and to verify the existence of a rate-determining step, previously identified in the metal re-oxidation $Cu^{+}\rightarrow Cu^{2+}$,[11a,11b,11c] oxygen-saturation experiments were performed through previous enrichment of the buffer solution with pure dioxygen (1 atm).

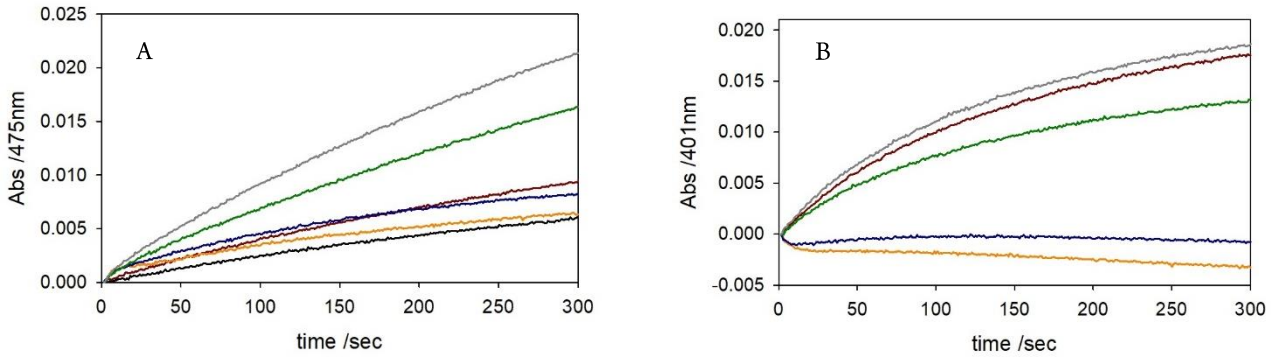

Figure 12. *Kinetic profiles of DA (0.3 mM, panel A) and MC (0.3 mM, panel B) oxidation with time in 50 mM HEPES buffer at pH 7.4 and 20 °C in the presence of only Cu^{II} (25 μM, brown trace) and upon the addition of [Cu-Aβ$_{4-16}$] at 1:1 molar ratio (25 μM) exposed to the air (orange) and after saturation with pure dioxygen (blue) and [Cu-Aβ$_{16}$] at 1:1 molar ratio (green) and with O_2-enrinchment (grey). The autoxidation of substrate is shown as black trace.*

Both in the presence of atmospheric amounts of oxygen and upon saturation with the pure gas, the first 10 seconds of the kinetics obtained with Cu-Aβ(4-16) adduct as catalyst are not affected by the changes of experimental conditions and dioxygen does not influence the decay of the transient species absorbing at ~300 nm. After few second of reaction, oxygen-saturation affects the redox efficiency of the second step of the catalysis, suggesting that the slow-step of the full mechanism coincides with the conversion from copper(I) to copper(II) (Figure 12). These results suggest that, in the first seconds of the reaction, a ternary complex with specific optical properties is generated by the interaction between copper, catechol and the amyloid fragment.

This species is not influenced by the order of addition of the reaction partners and the pre-incubation of metal-peptide adduct then added to the substrate does not induce any significant changes if compared with the generation of the complex directly in cell, which excludes the participation of some binary complex [metal-substrate] linked with the absorption at 300 nm (Figure 13). The nature of the ternary adduct was also verified by the addition of a further reducing agent, such as ascorbate, in the reaction *medium* previously described (Figure 14), determining a fast decay of the absorption at 300 nm that corresponds to the metal reduction.

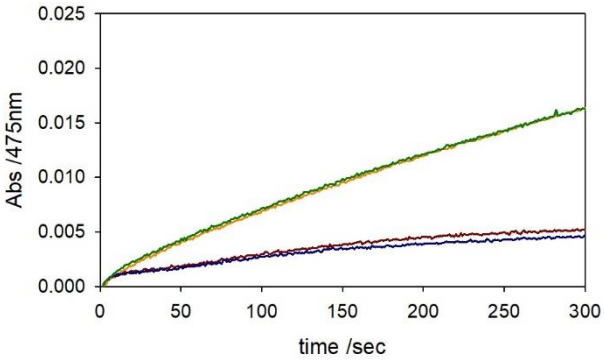

Figure 13. *Kinetic profiles of DA (0.3 mM) oxidation with time in 50 mM HEPES buffer at pH 7.4 and 20 °C in the presence of [Cu-Aβ4-16] (brown trace) and [Cu-Aβ16] (orange) adducts at 1:1 molar ratio (25 μM) generated by the direct addition in the reaction medium, or after the pre-incubation of peptide with Cu, [Cu-Aβ4-16] (blue) and [Cu-Aβ16] (green).*

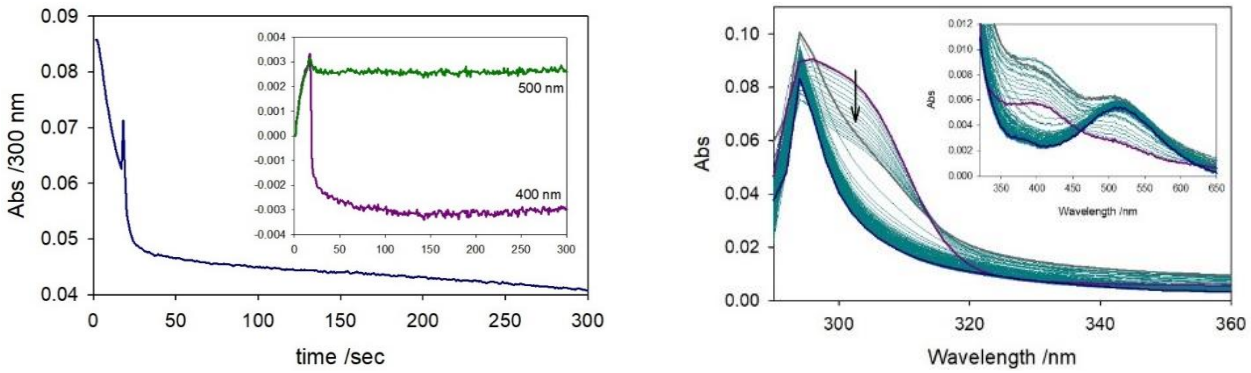

Figure 14. *Abs changes with time of a solution of 4-methylcatechol (3 mM) in 50 mM HEPES buffer at pH 7.4 in the presence of the N-truncated peptide (4-16) and copper(II), at 1:1 molar ratio (25 μM) (violet spectrum). Upon few seconds of oxidation, ascorbate (50 μM) was added to the reaction mixture (grey spectrum) and the kinetics was followed for 300 sec (final spectrum- blue). At left, the kinetic profiles obtained at 300 nm (blue trace), 400 nm (violet), and 500 nm (green) are shown before and after the addition of ascorbate.*

In order to assay if the band at 300 nm is ascribable to some charge transfer transition from catecholato bound to Cu^{II}, a further substrate as 4-chlorocatechol was used. The choice of substituents on the aromatic ring of catechols strongly affects the rate of substrate oxidation, where methyl or ethyl groups are electron donating substituents that favor the catechol oxidation via dioxygen, while electron withdrawing groups, as chloro- and carboxyl groups, reduce the susceptibility of the catechol toward oxidation. Therefore, the use of an electron-rich substrate was chosen to verify the dependence of the band at 300 nm from the binding with catechol and to follow the changes in its decay if the redox potential of the substrate is lower (Figure 15). As shown by the decay of the band at 300 nm, this chromophore corresponds to some Cu^{II}-species that undergoes the reduction to Cu^{I}-adduct and it is evidenced by the gradual vanishing of this absorption; moreover, the decrease of the absorption intensity is strongly determined by the presence of substrate and by its reducing potential. When the oxidation of 4-chlorocatechol is catalyzed by Cu^{II}-*N*-truncated peptide complex, the reduction of the metal is less efficient and therefore, the contribution at 300 nm is more stable with a slower rate of its decay. Furthermore, in order to verify that the slow step of the oxidative mechanism is the oxidation of cuprous ions upon the interaction with dioxygen, the pre-saturation with oxygen of buffer solution was performed and the data suggest that the decay of Cu^{II}-ternary complex at 300 nm is again independent from the amount of dioxygen in the reaction *medium* (Figure 16).

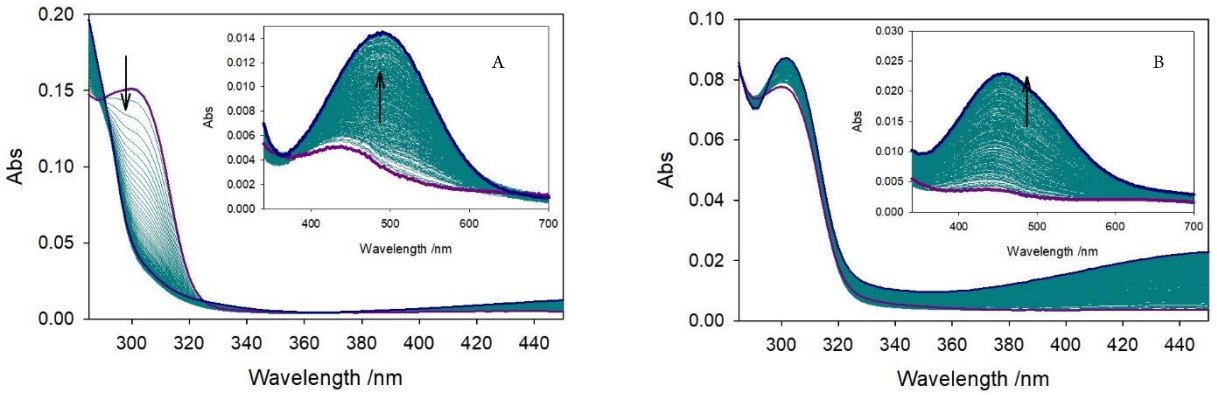

Figure 15. *Abs spectra of 4-clorocatechol (0.3 mM) oxidation with time in 50 mM HEPES buffer at pH 7.4 and 20 °C in the presence of [Cu-Aβ4-16] (25 μM, panel A) and [Cu-Aβ16] (25 μM, panel B).*

The modest redox potential of this substrate leads to slow reduction of copper(II), but, at the same time, the oxygenation and re-oxidation of the metal is limited by a less flexible (as suggested by the following sections) linear coordination geometry given by the *N*-truncated species, not allowing an efficient interaction with oxygen independently from its availability in solution. As previously described, the reaction mechanism views the first stoichiometric step corresponding to the reduction of the metal through the reaction with substrate and a second limiting step in which the metal is re-oxidized via interaction with oxygen. As shown in Figure 16, the two reactions when in the presence of hardly oxidizable substrates become comparable with similar slopes.

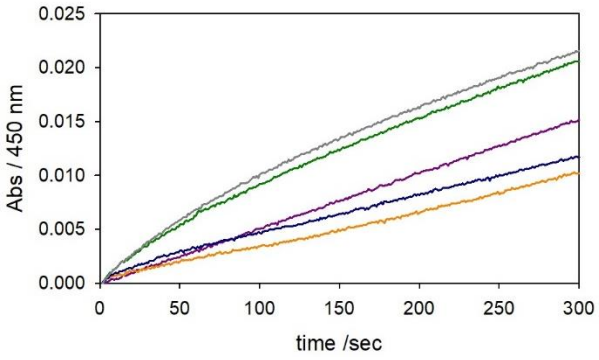

Figure 16. *Kinetic profiles of 4-ClCat (0.3 mM) oxidation with time in 50 mM HEPES buffer at pH 7.4 and 20 °C in the presence of only Cu^{II} (25 μM, violet trace) and upon the addition of [Cu-Aβ4-16] at 1:1 molar ratio (25 μM) exposed to the air (orange) and after saturation with pure dioxygen (blue) and [Cu-Aβ16] at 1:1 molar ratio (green) and with O_2-enrinchment (grey).*

Anyway, a transient species that disappears upon few seconds of reaction can be detected in the presence of copper bound both to amyloid fragments 1-x and 4-x and their further interaction with all substrates previously shown. When the *N*-truncated peptide is complexed with the metal, copper(II) is strongly stabilized via the *N*-terminal high-affinity binding site and the reduction of the metal is partially limited; the slow reduction also influenced by the redox potential of substrate allows to observe the decay of the ternary complex to generate the reduced one, which is slowly re-oxidized. When copper interacts with the amyloid peptide 1-16, the metal is not trapped in a preferential binding site with so high affinity constant, and therefore, the redox cycling of the adducts results more efficient, leading to higher generation of oxidative products that mask this region because of their absorption around 300 and resulting in an apparent stabilization of this contribution.

Characterization of the secondary His-tandem binding site

The binding between Cu^{II} ions and amyloid-β peptides 4-x, such as Aβ 4-40/42 or shorter peptides as the sequence 4-16 usually selected as model to study the metal coordination, is still debated. If the stoichiometric interaction between 1 equiv. Cu^{II} and 1 equiv. peptide is well-characterized and shows a high affinity constant around $10^{13.5}$ M^{-1} at neutral pH,[12a] the interaction with a further copper ion is controversial, probably due to the weaker binding affinity

approximately five orders of magnitude lower.[12b,13,14a] Copper is normally involved in the neuronal signaling and its local concentration in the synaptic clefts can fluctuate from 3 μM to 0.10-0.25 mM while amyloid peptides can be normally detected around μM/ nM levels; therefore, the generation of multinuclear adducts could occur.[14b] Recently, two distinct coordinative environments were suggested for the metal coordination in the *N*-truncated species, highlighting the redox silencing of the first equivalent of copper(II) trapped by the squared planar geometry provided by the ATCUN site, while the second ion is directed toward a low-affinity site in which the redox cycling of the metal is probably allowed and the coordinative sphere is mediated by two vicinal histidines, His-13 and His-14. Therefore, the reactivity was also assayed in the presence of 2 equivalents of copper(II) to promote the redox activation of the "secondary site" (Figures 17); in this way, while the first equiv. of metal is quenched by the *N*-terminal site, a modest fraction of cupric ions can be chelated by the His-tandem site.

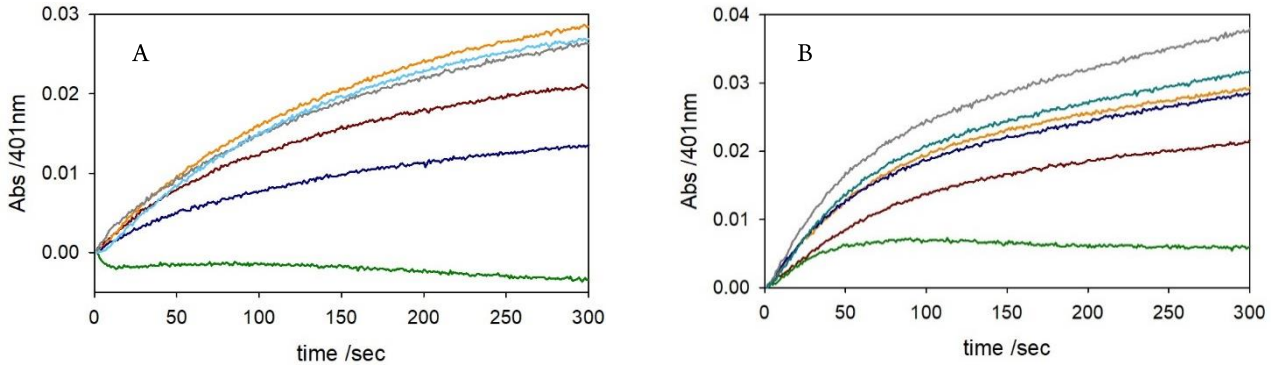

Figure 17. *Kinetic profiles of MC (panel A, 0.3 mM and panel B, 3 mM) oxidation with time in 50 mM HEPES buffer at pH 7.4 and 20 °C in the presence of only Cu^{II} (25 μM, brown trace or 50 μM, orange) and with the following complexes: [Cu-Aβ$_{16}$] at 1:1 molar ratio (25 μM, blue), [Cu-Aβ$_{16}$] at 2:1 molar ratio (grey), [Cu-Aβ$_{4\text{-}16}$] at 1:1 molar ratio (green) and [Cu-Aβ$_{4\text{-}16}$] at 2:1 molar ratio (light blue).*

The reactivity promoted by 2 equiv. of metals vs. 1 equiv. of *N*-truncated fragment 4-16 views an enhancement on the initial slopes of the kinetic profiles if compared with the reaction catalyzed by the stoichiometric complex. On the other hand, this increase does not exclude the presence of additional activity of a modest fraction of metal only bound to the substrate. Indeed, when the reaction is promoted by catechols, the metal binding to the peptide is competitive toward the interaction with the substrate and, in these conditions, the affinity constant for copper by the His-tandem site, that is around $10^{6.7}$ M^{-1}, is similar to the values shown for the interaction between the metal and substrate (K_a $5x10^6$ M^{-1}).[14c] Therefore, the secondary site does not allow to overpass the competition with the substrate at saturating concentrations and, together with the low redox activity of this adducts, the data reflect the involvement of a metal-peptide adduct with 1:1 molar ratio besides the simple oxidation of substrate that proceeds through the binary complex [metal-substrate]. To isolate the catalytic efficiency of the *C*-terminal redox-active site, the ATCUN site was masked by the interaction with Zn^{II} ions and then by Ni^{II} ions, as suggested by Pushie et all.[15a] When the *N*-terminally truncated peptide is previously incubated in the presence of Zn^{II} ions, a metal adduct could be

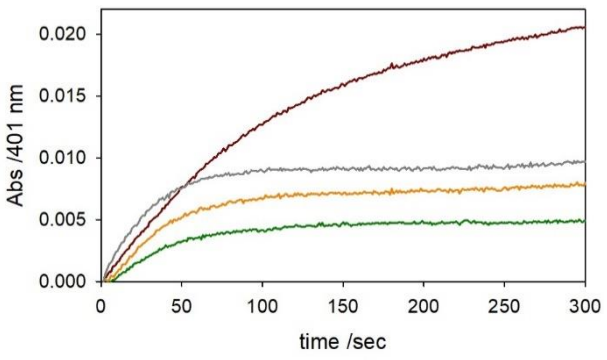

Figure 18. *Kinetic profiles of MC (3 mM) oxidation with time in 50 mM HEPES buffer at pH 7.4 and 20 °C in the presence of only Cu^{II} (25 μM, brown trace) and upon the addition of Aβ$_{4\text{-}16}$: [Cu-Aβ$_{4\text{-}16}$] at 1:1 molar ratio (25 μM, green), [Cu-Zn-Aβ$_{4\text{-}16}$] at 1:1:1 molar ratio (orange) generated in cell or after*

pre-generated and, upon the further addition of 1 equiv. copper(II), the His-tandem site would be available for the generation of the binuclear complex. As shown in Figure 18, the substrate oxidation promoted by this complex seems to be influenced by the incubation time of the adduct and by the order of reagent addition. Anyway, zinc ion is usually detected in tetrahedral coordination sphere and bound by at least three imidazolic ligands, as observed in some metalloenzymes such as carbonic anhydrase.[15b] The squared-planar geometry provided by the ATCUN site does not allow an efficient stabilization of the metal, while other cations, as nickel(II), are more appropriate for this type of accommodation.

incubation of Zn^{II} with the peptide followed by the addition of copper before the analysis (grey).

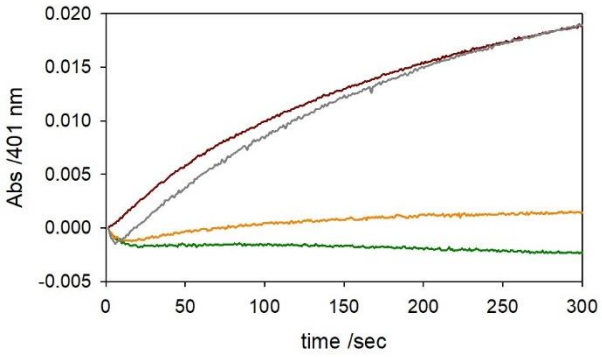

Figure 19. *Kinetic profiles of MC (0.3 mM) oxidation with time in 50 mM HEPES buffer at pH 7.4 and 20 °C in the presence of only Cu^{II} (25 μM, brown trace) and upon the addition of $A\beta_{4\text{-}16}$: [Cu-$A\beta_{4\text{-}16}$] at 1:1 molar ratio (25 μM, green), [Cu-Ni-$A\beta_{4\text{-}16}$] at 1:1:1 molar ratio (orange) and [Cu-Ni-$A\beta_{4\text{-}16}$] at 2:1:1 molar ratio (grey).*

Therefore, the same experiment was performed hiding the *N*-terminal binding site of Aβ(4-16) with 1 equiv. of Ni^{II}, only assaying the redox activity of the *N*-truncated fragment because of the presence of two independent binding sites; in the amyloid-β (1-16) sequence, the absence of a predominant binding site and the easy exchange between several coordination modes for copper do not allow to determine any relevant change in the redox ability associated to a specific coordination sphere. As suggested by the Figure 19, the reactivity of Cu-Ni-$A\beta_{4\text{-}16}$ adduct (1:1:1) ratio is almost totally quenched, which could verify the absence of free copper in solution. If Ni^{II} is trapped by the *N*-terminal site, the resulting reactivity of free copper will correspond to an efficient redox cycling of the metal promoted by the interaction with substrate; as shown by the orange trace in Figure 19, the catechol oxidation is almost totally absent, suggesting that copper(II) is not free in solution and its binding in the secondary site does not allow an efficient cycling of the metal. The addition of copper in excess (2 equiv.) restores the substrate oxidation, confirming that, while the first equiv. of copper is sequestered by the peptide, the second one is free in solution and is able to promote the reaction. Moreover, it may propose that this secondary site does not involve the participation of histidine-6, that probably mediates the *N*-terminal interaction with Ni^{II}, and that the resulting coordination sphere for copper is mainly represented by the two vicinal histidines. This coordination sphere together with the low flexibility of *C*-terminal domain, particularly when the *N*-terminus is occupied by an additional cation as Ni^{II}, lead to a resulting complex that is totally inefficient in the catechol oxidation.

In order to verify the independent binding of two metals, a competitive titration of the Ni^{II}-Aβ(4-16) complex (0.5 mM) against copper(II) (0-0.55 mM) in phosphate buffer solution at pH 7.4 was performed (Figure 20). Ni^{II}-adduct shows a specific contribution at 423 nm that is unaffected by the following addition of copper and seems to be stable with time. Another contribution at higher wavelengths around 570 nm appears upon the addition of Cu^{II} that does not match neither with the absorption usually observed with Cu-ATCUN adducts, characterized by an Abs maximum at 525 nm,[15c,15d] nor with the unbound metal in phosphate *medium*, that shows

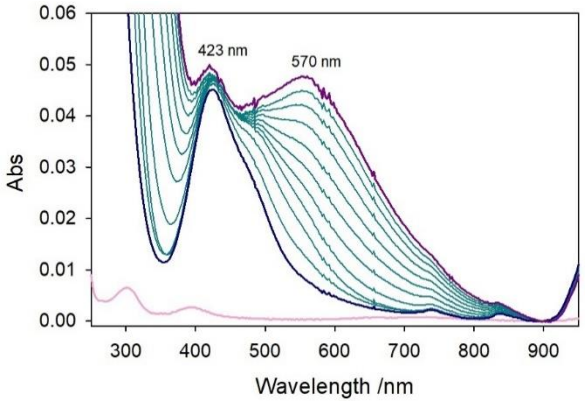

Figure 20. *Competitive titration of Ni^{II}-$A\beta_{4\text{-}16}$ adduct at 1:1 ratio (0.5 mM, blue spectrum) by the addition of 0-0.50 mM Cu^{II} (final point as*

an absorption around 750-800 nm. The data also indicate that the two binding sites works as independent and the coordination of Cu^{II} in the *C*-terminus does not affect the coordination sphere of Ni^{II}, as shown by the stability of blue spectrum. Furthermore, when the retro-titration is performed starting from Cu^{II}-Aβ(4-16) adduct (0.5 mM) against nickel(II) (0-0.5 mM), copper is trapped in the ATCUN site and shows a stable contribution at 525 nm that is not affected by the addition of nickel (Figure 21). The high stability of *N*-terminal Ni^{II} and Cu^{II} coordination is also verified with time: when nickel or copper are stably inserted in the *N*-terminal binding site, the addition of a further equivalent of metals does not result in an equilibrium for the *N*-terminal binding and any competition or coordination changes can be detected.

violet spectrum) in 5 mM phosphate buffer solution at pH 7.4. The pink spectrum corresponds to the absorption of Ni^{II} alone.

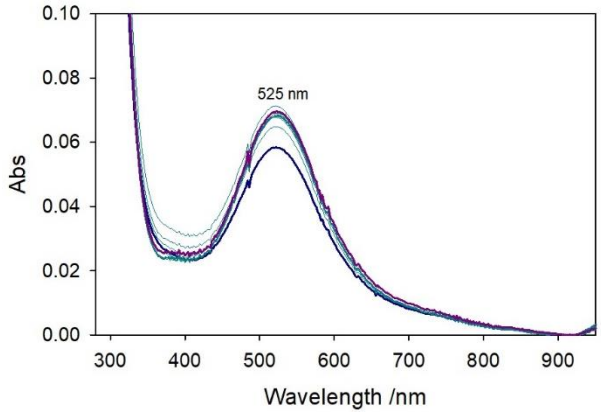

Figure 21. *Titration of Cu^{II}-$A\beta_{4\text{-}16}$ adduct at 1:1 molar ratio (0.5 mM, blue spectrum) by the addition of Ni^{II} (0-0.5 mM, final point as violet spectrum) in 5 mM phosphate buffer solution at pH 7.4.*

As shown in Figure 22, the stabilization of the *N*-terminal binding both for copper and nickel also occurs after 24h of incubation of each complex in the presence of a further equiv. of metal but the main difference between the two metals can be evidenced in the metal binding in the primary site. When copper(II) is added to the *N*-truncated peptide, the strong interaction in the ATCUN site immediately occurs without any relevant changes with time, while more time is required for a stable binding of nickel(II) in the same coordination sphere.

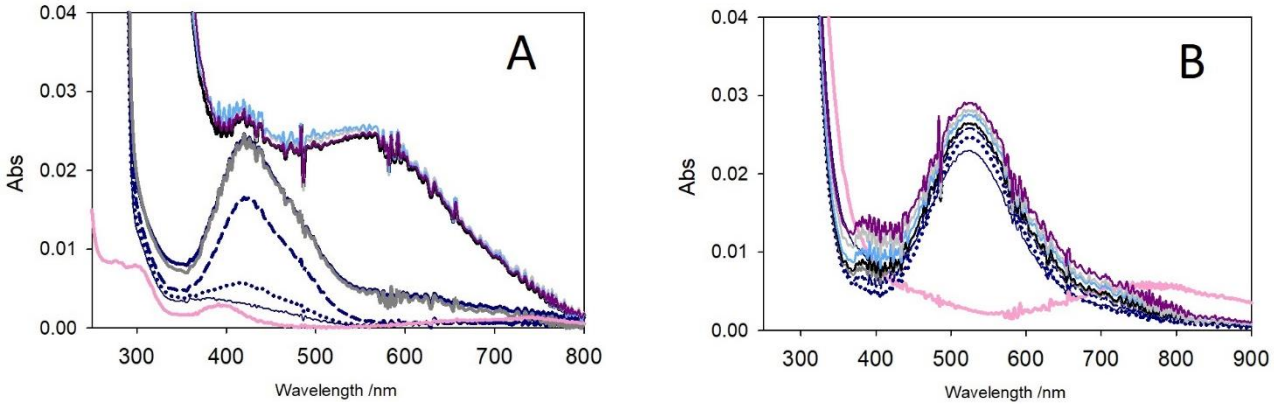

Figure 22. *Abs spectra with time of: A) Ni-$A\beta_{4\text{-}16}$ adduct (1:1, 0.24 mM) at time 0 (thin blue spectrum), 1 min (dotted blue), 5 min (dashed blue), 30min (solid blue) and 1h (dark grey); the effect of the addition of 1 equiv. Cu^{II} (black) was followed after 30 min (light blue), 3h (light grey) and 24h (violet). Ni^{II} alone is shown as pink trace. B) Cu-$A\beta_{4\text{-}16}$ adduct (1:1, 0.20 mM) at time 0 (thin blue spectrum), 5 min (dotted blue), 30 min (dashed blue), and 1h (dark grey); the effect of the addition of 1 equiv. Ni^{II} (black) was followed after 30 min (light blue), 3h (light grey) and 24h (violet). Cu^{II} alone is shown as pink trace.*

Moreover, in order to verify the involvement of copper(II) in the binding of the secondary binding site and to exclude the participation of some Cu^{I} species, stoichiometric ascorbate (0.55 mM) was added at the end of titration of Ni-adduct against copper and the data confirm the reduction of coordinated copper(II) followed by the decay of its band around 580 nm. The spectrum acquired upon 2h on the same solution also evidences a higher contribution at 425 nm that is probably linked to the generation of several oxidative and reactive species that are able to modify some amino acidic residues, as tyrosine-10, adding further contributions in the final UV-vis spectrum of the mixture. To reinforce the previous data, a deep investigation of the metal binding was also associated with other spectroscopic techniques,

such as circular dichroism (CD) both to acquire structural details about the conformation of the peptides upon the metal interaction and to study the metal coordination in the visible spectral region, and nuclear magnetic resonance (NMR), to detect which residues contribute to the coordination sphere for each metal.

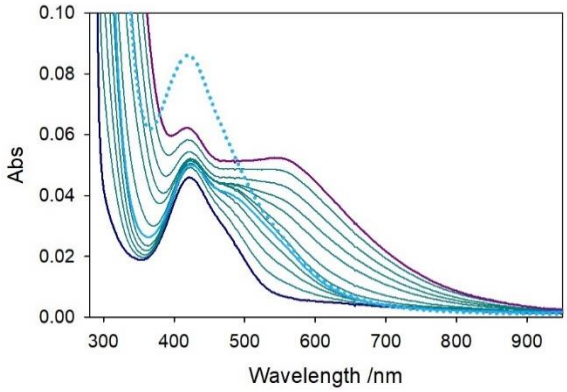

Figure 23. *Titration of Ni^{II}-Aβ$_{4-16}$ complex at 1:1 ratio (blue spectrum, 0.5 mM) by the addition of copper (0-0.5 mM) in 5 mM phosphate buffer solution at pH 7.4. The solid light blue spectrum shows the effect of the addition of 0.55 mM ascorbate and the dotted one corresponds to the acquisition after 2h of the same reaction mixture.*

CD and NMR characterization of metal binding in the N-truncated fragments

The conformational study on the folding of each peptide free in phosphate buffer solution and after the addition of the metals was performed through circular dichroism. In particular, the effect of the presence of 1 equiv. Cu^{II} bound to Aβ(4-x) peptides and the further interaction with the substrate by the resulting complex were compared to the structural conformations adopted by the amyloid fragment 1-x. The data shown in Figures 23 and 24 indicate that all fragments used in this section are characterized by a random and unstructured conformation when are dissolved in an aqueous *medium*, as previously observed in Chapter 1.[10c] On the other hand, copper(II) interaction differently affects the folding of the peptides, where the binding of 1 equiv. Cu^{II} to Aβ(4-x) peptide strongly alters the peptide structure and enhances the β-sheet content, while in the presence of fragments 1-x, the metal binding does not significantly modify the overall folding of the peptide backbones, only leading to a modest stiffening of the structure, as suggested by the decreased intensity of the signals around 198 nm. The interaction with the catechol does not lead to significant conformational changes toward all analyzed fragments.

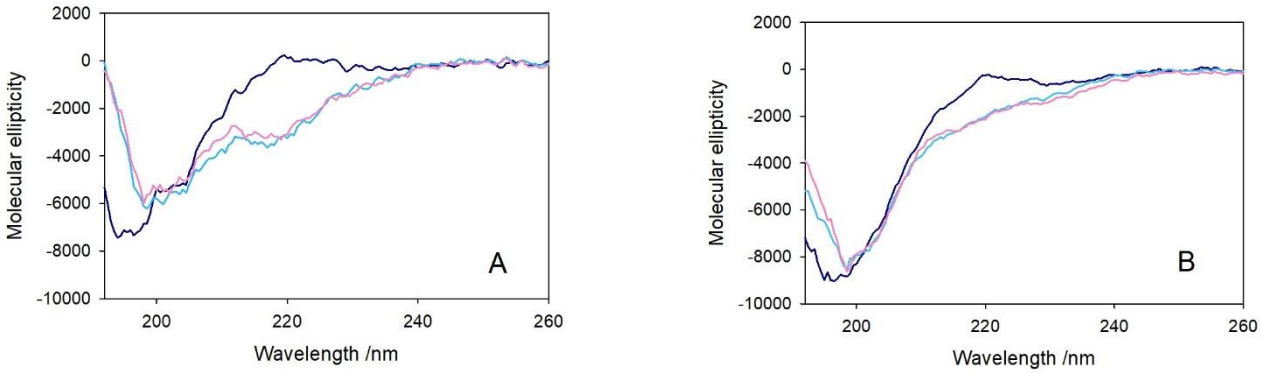

Figure 23. *Far-UV CD spectra of Aβ$_{4-16}$ (1.1 equiv., 10 μM, panel A) and of Aβ$_{4-28}$ sequences (1.1 equiv., 5.5 μM, panel B) in 5 mM phosphate buffer solution at pH 7.4 (blue spectrum) and with the addition of 1 equiv. copper (light blue) and of 1 equiv. dopamine (pink).*

Similar results were also obtained when the structure of Ni-Aβ(4-16) complex was investigated, as shown in Figure 25. As previously proposed, the stable binding between nickel ion and the *N*-terminal coordination sphere does not immediately occur and requires more time if compared with the addition of copper(II), which is instantly trapped by the ATCUN site (Figure 26); therefore, upon the addition of Ni^{II} to the peptide solution, the spectrum of the adduct

was also registered upon 15 min of incubation, suggesting that the slower metal binding is reflected by a gradual rearrangement of the peptide structure around the metal center.

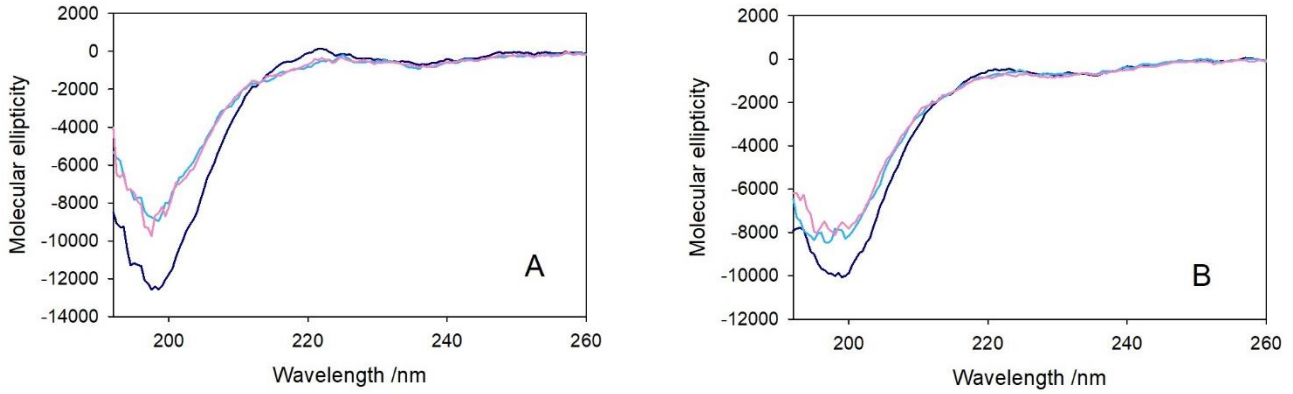

Figure 24. *Far-UV CD spectra of $A\beta_{1\text{-}16}$ (1.1 equiv., 10 μM, panel A) and $A\beta_{1\text{-}28}$ sequences (1.1 equiv., 5.5 μM, panel B) in 5 mM phosphate buffer solution at pH 7.4 (blue spectrum) and with the addition of 1 equiv. copper (light blue) and of 1 equiv. dopamine (pink)*

On the other hand, the final folding observed in the presence of stoichiometric Cu- or Ni-adduct shows similar dichroic signals, characterized by an increase of intensity at 218 nm associated to β-sheet structures. Anyway, these structures are not sufficiently defined to be detected by Thioflavin assay (data not shown). An additional information comes from the pink spectrum in Figure 25 that shows the effect of the presence of 1 equiv. Cu^{II} on the Ni-adduct, suggesting that the resulting spectrum does not match with the data obtained on the binary Cu-Aβ(4-16) complex and therefore it indicates a simultaneous interaction of both metals in two independent coordination sites. While the first equiv. copper(II) appreciably alters the peptide conformation, the additional presence in the previous solution of another equiv. Cu^{II} does not change the folding properties of Aβ(4-16) since this fraction of metal is free in solution and does not interact with the peptide. The CD data of Ni and Cu complexes were also registered in the near-UV and visible region in order to define the nature of the adduct. The binding between 1 equiv. copper(II) and 1 equiv. of *N*-truncated peptide 4-16 (2 mM) was studied in phosphate buffer solution at neutral pH and, upon the stabilization of their interaction (approximately 30 min), 1 equiv. of nickel was added to the adduct. The binary Ni-complex was generated in the same condition, waiting the stabilization of the dichroic signal and following addition of 1 equiv. Cu^{II} (Figure 27).

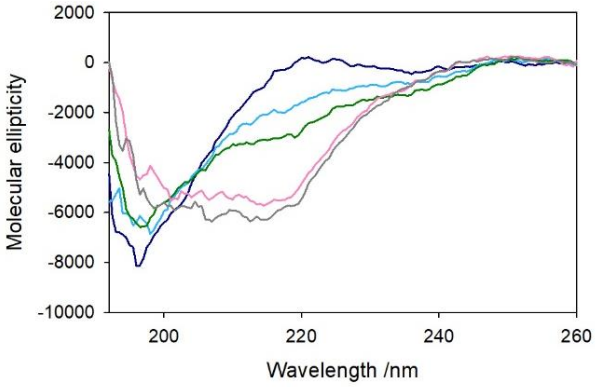

Figure 25. *Far-UV CD spectra of $A\beta_{4\text{-}16}$ sequence (10 μM) in 5 mM phosphate buffer solution at pH 7.4 (blue trace) with the addition of Ni^{II} (9.5 μM), registered upon few seconds of incubation (light blue) and 15 min (green). 1 (pink) and 2 equiv. Cu^{II} (grey) were then added to the Ni-complex.*

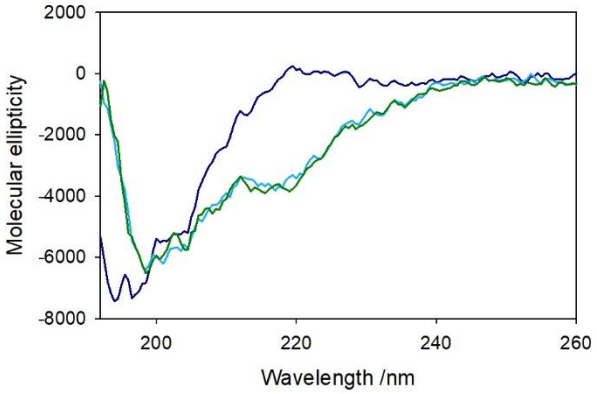

Figure 26. *Far-UV CD spectra of $A\beta_{4\text{-}16}$ sequence (1.1 equiv., 10 μM) in 5 mM phosphate buffer solution at pH 7.4 (blue traces) with the addition of Cu^{II} (1 equiv., light blue) and after 15 min incubation (green).*

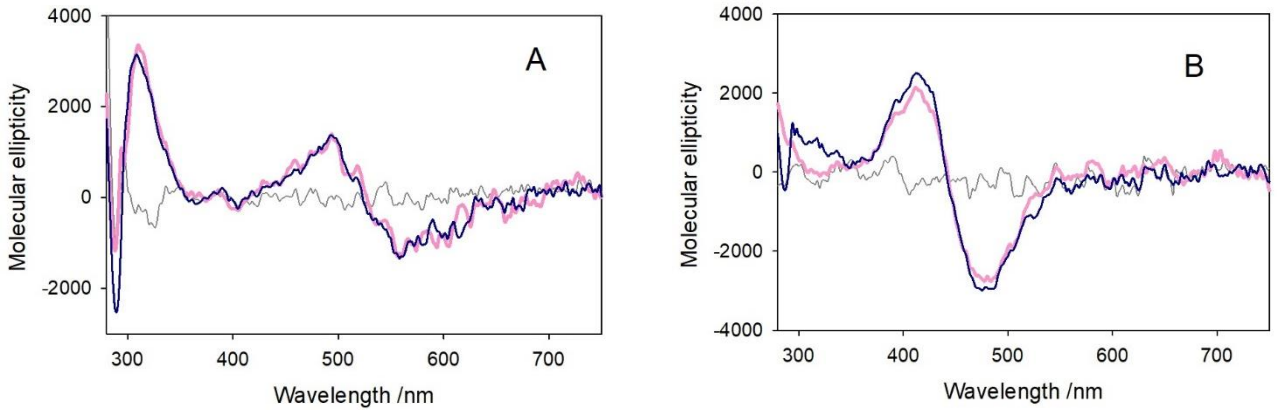

Figure 27. *Panel A) Visible CD spectra of Cu^{II} (2 mM) alone in 5 mM phosphate buffer solution at pH 7.4 (grey trace), with the addition of 1 equiv. $A\beta_{4-16}$ sequence (2 mM, pink) and of 1 equiv. of Ni^{II} to the binary copper-adduct (blue). Panel B) Visible CD spectra of Ni^{II} (2 mM) alone (grey trace) with the addition of 1 equiv. $A\beta_{4-16}$ sequence (2 mM, pink) and of 1 equiv. of copper(II) to the binary Ni-complex (blue).*

As shown by the panel A, Cu-complex is characterized by an intense signal at 310 nm associated with amide-Cu^{II} LMCT[10b] besides two contributions at 490 and 560 nm that indicate the generation of 3N/4N coordination sphere for the metal, accommodated in a squared planar geometry, according with the *N*-terminal binding site.[16a] Ni-complex shown in panel B is identified by two signals at 412 and 478 nm that are usually detected in 4N {NH_2, $2N^-$, N_{Im}} complexes arranged in squared planar spheres.[16b] When 1 equiv. of the other metal is added to these complexes, no spectra changes are observed, suggesting that the two tetradentate complexes are highly stable, no competitions occurs when the *N*-terminal site is occupied and that both metals bind as preferential binding site the ATCUN region via the same coordinative environment. Moreover, circular dichroism signals are strongly correlated with the mobility of the analyzed structure where a loss of rigidity of the molecules induces lower intensity signals; when the ATCUN site is masked by Ni^{II}, copper(II) is trapped by a secondary binding site in which the metal is trapped by a linear coordination sphere via two histidines and probably with a water molecule equatorially bound: these complexes are characterized by high rotation mobility of the imidazole ligands around the binding axis with copper ion, avoiding any additional contribution from the CD analysis.

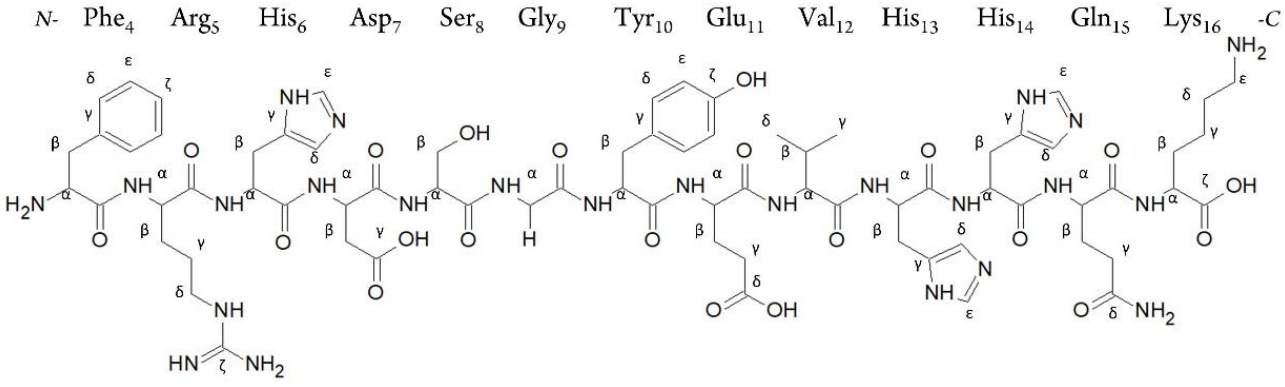

Figure 28. *Chart of the amyloid sequence 4-16 with the assignment of each proton of all amino acids.*

Simple NMR experiment was also associated with the CD characterization in order to determine which residues are involved in Cu^{II} binding when the *N*-terminal region is occupied by nickel. At first, to assign each signal to the related

residue (Figure 28), one dimensional ^{1}H and two dimensional COSY spectra were registered on a solution of Aβ(4-16) peptide (8.6 mM, 1.1 equiv.) in deuterated phosphate buffer solution at neutral pH (Figure 29).

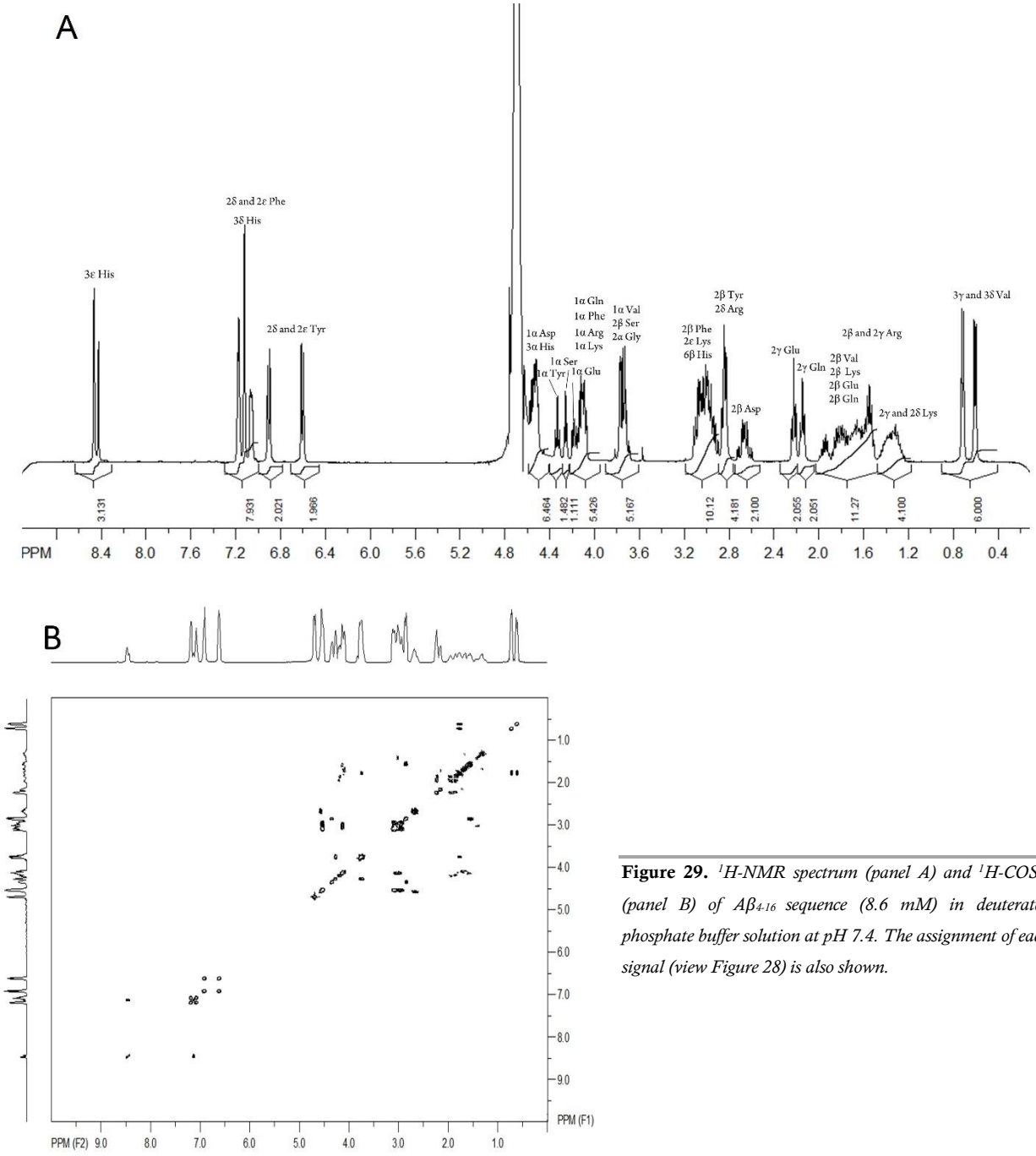

Figure 29. *^{1}H-NMR spectrum (panel A) and ^{1}H-COSY (panel B) of $A\beta_{4\text{-}16}$ sequence (8.6 mM) in deuterated phosphate buffer solution at pH 7.4. The assignment of each signal (view Figure 28) is also shown.*

To the previous solution, 1 equiv. (7.8 mM) Ni^{II} was incubated with the peptide for 30 min to allow a stable interaction and then, a small amount of copper(II) (78 μM) was added to the complex, in order to follow eventual changes in the NMR spectrum avoiding the general broadening of all signals. The NMR data shown in Figure 30 suggest the presence of Ni^{II} as well as Cu^{II} significantly affect the aromatic protons of all three His residues, where His-6 may probably act as binding ligand for Ni^{II} in the primary site while copper(II) is trapped the the *C*-terminal binding site. On the other hand, the protons of Tyr-10 and Phe-4 are not notably affected by the metal binding. Analogously, some aliphatic signals shown in Figure 31 are more perturbed by the addition of the metal and in particular, γ-protons at 2.14 ppm of Gln-15 are strongly broaden besides a modest paramagnetic effect exerted on α-, γ- and δ-protons at respectively ~3.75,

0.72 and 0.60 ppm of Val-12. The two triplets corresponding to the α-protons of serine and tyrosine at 4.3 ppm does not evidence any relevant changes upon the binding with the metals, while the amide protons at 4.12 ppm of Lys-16 and Arg-5 are considerably influenced by both metals but any other details can be obtained because of the overlay of the signals.

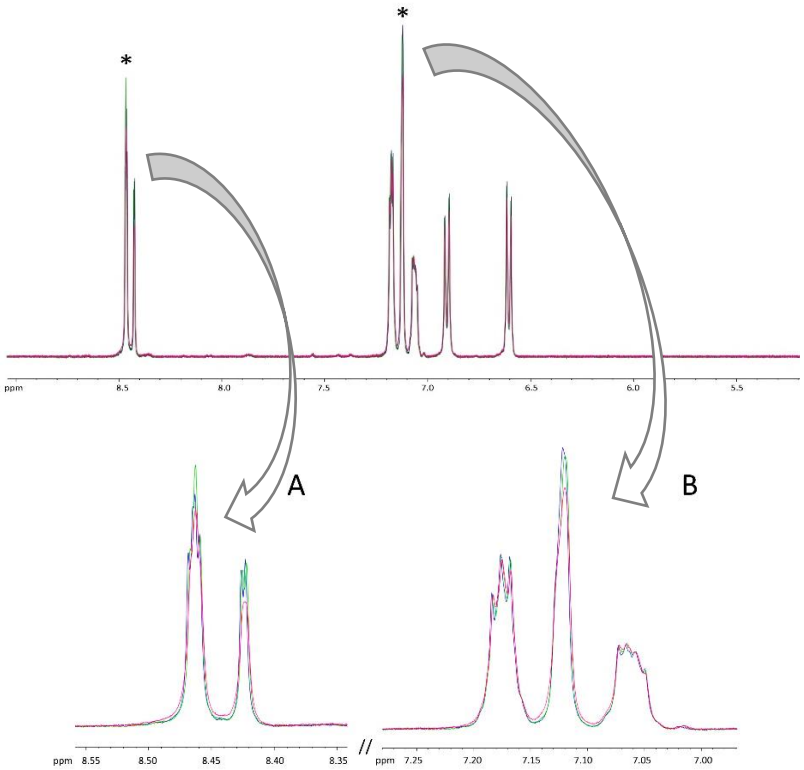

Figure 30. *[1]H-NMR spectrum of the aromatic protons of Aβ4-16 sequence (8.6 mM, 1.1 equiv., blue spectrum) in phosphate buffer solution at pH 7.4 and after the addition of 1 equiv. nickel(II) (green spectrum) and 0.01 equiv. of copper(II) (pink spectrum). Panels A and B show the His signals significantly affected by the presence of metals.*

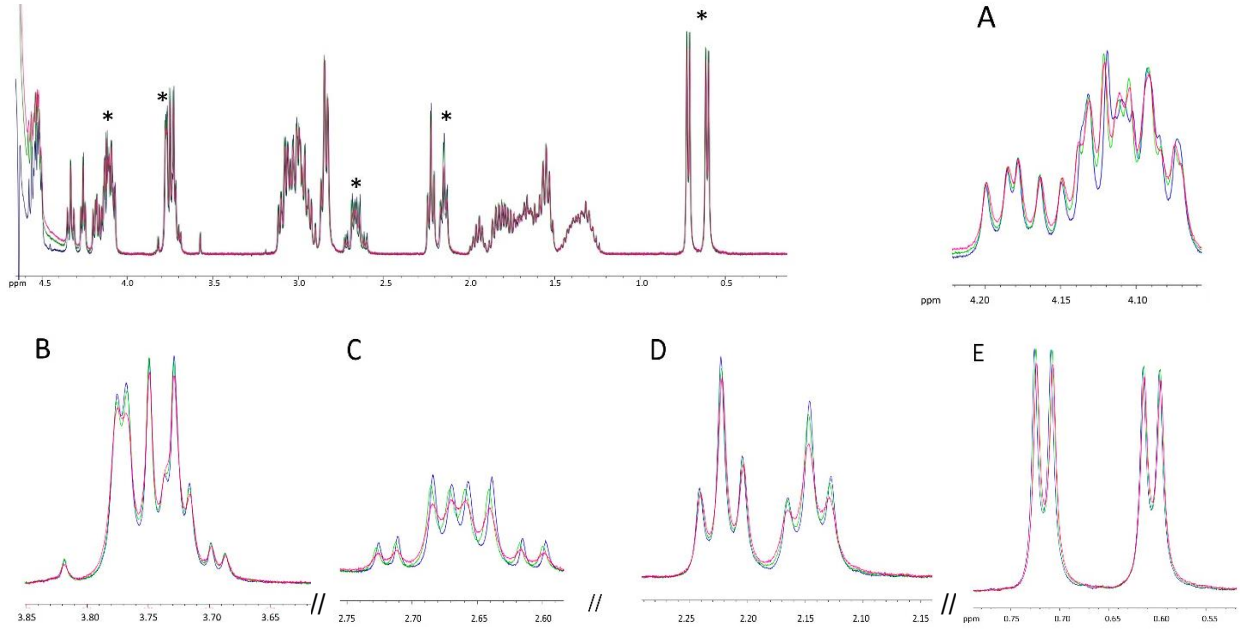

Figure 31. *[1]H-NMR spectrum in the aliphatic protons of $A\beta_{4\text{-}16}$ sequence (8.6 mM, 1.1 equiv., blue spectrum) in phosphate buffer solution at pH 7.4 with the addition of 1 equiv. nickel(II) (green spectrum) and 0.01 equiv. copper(II) (pink spectrum). Panel A, B, C, D and E show the proton signals more perturbed by the metals.*

Not negligible shift of β-protons of Asp-7 at 2.65 ppm can also be detected after the addition of Ni^{II} besides the broaden of the peaks in the presence of copper(II). In conclusion, the NMR data indicate that copper is located in the *C*-terminal domain, mainly affecting the regions confined between Val-12 and Lys-16, once Ni^{II} has occupied the primary binding site, that is further confirmed by the modest changes of signals encompassing Arginine-5, Histidine-6 and Aspartate-7. Moreover, an addition evidence on the stability of the binuclear Ni-adduct is provided by ^{1}H-NMR spectrum registered on the previous solution after 6 and 12 hours of incubation in the presence of Cu^{II} (Figure 32). Although the low concentration of copper, if the binding in the *N*-terminus is competitive between the two metals, marked paramagnetic effects due to the copper coordination will be observable, but any relevant changes in the proton spectrum can be detected with time, suggesting that any exchange between Cu or Ni inside the ATCUN site occurs in this conditions.

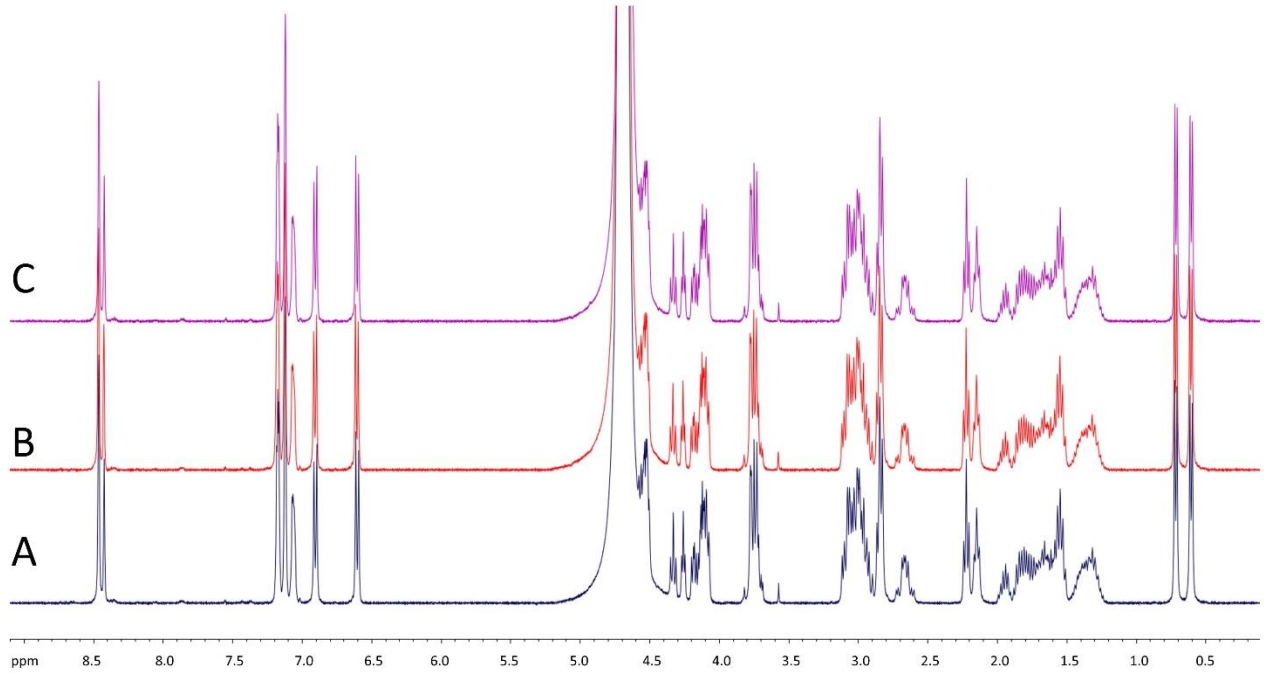

Figure 32. *^{1}H-NMR spectrum of [Ni-Cu-Aβ$_{4-16}$] complex at 1 : 0.01 : 1.1 molar ratio in phosphate buffer solution at pH 7.4 (spectrum A) and after 6 (spectrum B) and 12 hours (spectrum C).*

Conclusions

Amyloid-β aggregates are the main pathological hallmarks of Alzheimer's disease detected both in parenchymal and vascular compartments and generated by the fibrillation of Aβ(1-40) and (1-42) peptides. On the other hand, a high heterogeneity of amyloid-β sequences presenting *N*- or *C*-terminal cleavages has been observed, probably generated by the iterated enzymatic activity of some peptidases. In particular, *N*-terminal truncations alter the solubility of the peptides, enhancing their neurotoxicity and promoting their deposition in amyloid plaques.[17a] In particular, the main *N*-truncated species identified in neuronal tissues of subjects affected by AD and Down syndrome and detected as secretion by astrocytes and microglia starts with Phe-4 as first amino acid.[17b, 17c]

A multitude of details about the localization, the biological origin and the functional role of these fragments is currently unclear; therefore, this section aims to obtain some biochemical insights about the folding, the redox ability and the vulnerability toward modifications when these peptides are in the presence of an oxidative *medium*, enriched with redox metals and reactive catecholamines. Indeed, metals such as copper are transiently located in the synaptic clefts, being involved in neuronal signaling, and their local concentration can reach high values around 100–250 μM.[17d] The binding between copper(II) and Aβ(1-x) peptides has been modestly investigated, in which the interaction with 1 equiv. Cu^{II} characterized by an affinity constant of 10^{10} M^{-1} at neutral pH was determined besides the existence of a weaker site (with an affinity constant 100 times lower) able to bound a second equiv. of the metal.[12b,13] At the same time, two independent sites have been suggested in the *N*-truncated sequence 4-x, in which the first Cu^{II} ion is quickly trapped by the *N*-terminal domain with an affinity constant of $10^{13.5}$ M^{-1}; the resulting complex has low redox activity because of the presence of an ATCUN-like motif that strongly stabilizes the oxidized redox form of the metal. Moreover, besides the *N*-terminal Phe-Arg-His sequence that acts as the "main binding site", a "secondary site" with a K_a value around $10^{6.7}$ M^{-1} has been suggested in which the interaction with the metals occurs via two vicinal histidines, His-13 and His-14.[8a]

The present study is focused on the comparative redox behavior of the full-length peptide 1-x and the *N*-truncated 4-x fragments bound with 1 or 2 equiv. of copper and promoted by catecholic substrates, such as dopamine. At first, the mechanism of the redox reaction was assayed, verifying the existence of two steps, the initial reduction of copper(II) to copper(I) in the presence of catechol and the following oxygen-dependent step that leads to the re-oxidation of the complex. In particular, when the reaction is catalyzed by Cu-Aβ(4-x) adducts, a peculiar band at 300 nm can be observed with a half life of ~ 10 seconds. This absorption reflects the presence of a transient ternary adduct [Cu^{II}-peptide-substrate] that quickly decays for the progressive reduction of the metal center. Indeed, the *N*-truncated peptide highly stabilizes copper(II) via its *N*-terminal coordination site, not allowing an efficient reduction of the metal that is reflected by the easily detectable decrease of the absorption at 300 nm. On the other hand, Aβ(1-x) peptide interacts with copper(II) with a lower stability constant, promoting more efficient reduction of the metal and, at the same time, the following re-oxidation of the adduct is faster because of the better re-oxygenation of the metal center; these aspects result in an apparent stabilization of the contribution at 300 nm, in which a faster production of oligomers and soluble oxidative products that absorb in the same spectral region hides the redox reactions. The change of external substrate and the use of a less reactive catechol, as 4-chlorocatechol, have verified the correspondence between this ternary adduct and the contribution at 300 nm since the decreased metal reduction rate is reflected by the slower kinetic of intensity decay so that the first redox reaction is here comparable with the rate of the limiting step of the reaction mechanism.

The slower interaction with dioxygen by copper(I) bound to *N*-truncated peptides if compared with Aβ(1-x) suggests an involvement of His-13 and His-14 arranged in a linear geometry around the metal and excludes any participation of His-6. More specifically, the possible oxidative mechanism promoted by Cu^{II} binding to amyloid-β (4-16) could be schematized as follows (Figure 33). An initial ternary adduct is generated in which copper(II) is anchored both to the ATCUN site and to the catecholic substrate; this high-affinity binding site limits the reduction of metal and this reaction is highly influenced by the reducing efficiency of the substrate.

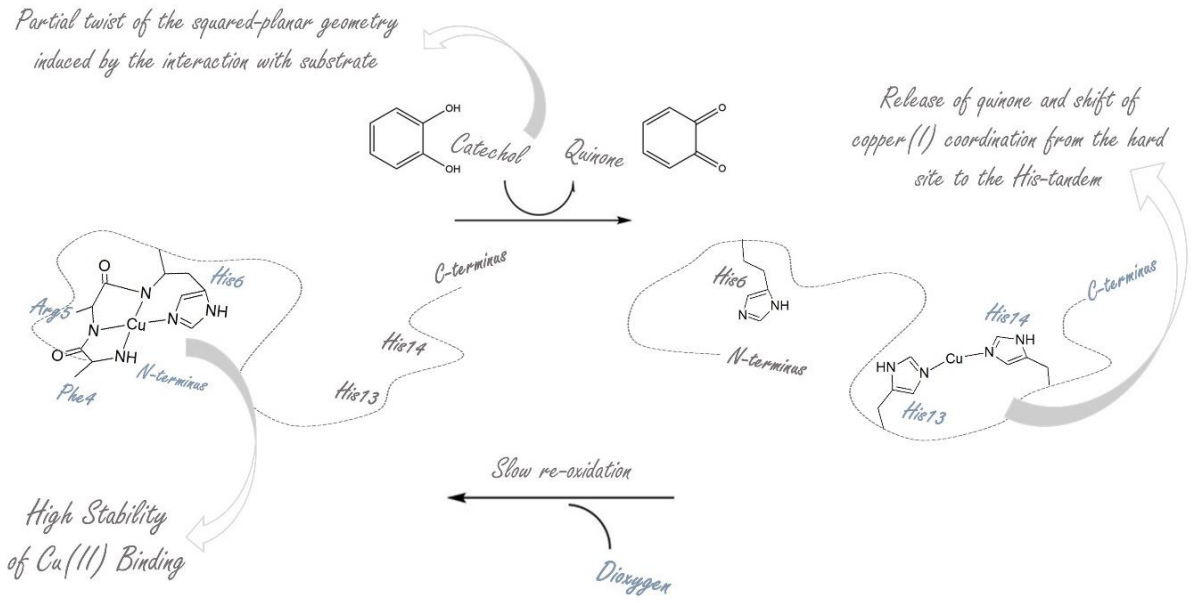

Figure 33. *Schematic representation of the reaction mechanism followed by Cu-Aβ(4-x) peptides in the presence of catechols.*

Therefore, when the harder-oxidizable 4-chlorocatechol is added to the adduct, this reaction is significantly slowed down by enough to become the determining step of the full oxidative process. Since the proposed planar geometry for copper(II) coordination has been determined on binary complexes obtained from the interaction of equimolar amounts of peptide and copper,[8a] the presence of a further species, as the substrate, may partially alter the geometry of the complex. Indeed, catechols have an intrinsic affinity for metals, as copper, and their interaction may induce some distortions of the coordination sphere, resulting in the partial destabilization of bound Cu^{II} and in the modest promotion of its redox cycling. The planar squared coordination suggested for copper(II) in the *N*-terminus is mediated by the binding of one primary amine, one imidazolic group of histidine 6 and some amide groups: this coordination sphere is suitable for copper(II), but it is too hard for the stabilization of copper(I). Therefore, it could be assumed that upon the slow reduction of the metal, Cu^{I} has to be shifted from the *N*-terminal site to the His-tandem site, where the oxidation of copper(I) complex through the interaction with dioxygen seems to be slightly slowed down respect with Aβ(1-16). Anyway, these two vicinal histidines have been extensively proposed as additional site working together with the *N*-terminus in order to allow the stabilization of both redox states of the metal, but they have been poorly studied as secondary and independent binding site. Therefore, the attention of this work was shifted to the redox behavior of the "main" and "secondary" sites seen as two independent binding domains and assaying both the redox potential and the binding affinities for copper. Unlike the high affinity for Cu^{II} shown by the ATCUN motif, the low affinity of the secondary site is in competition with the extraction of the metal from the substrate binding, that shows an affinity constant around $5x10^6$ M^{-1}.[14c] In order to isolate the redox activity of the secondary site, the ATCUN motif was hidden through the interaction with nickel(II), that can be easily accommodated in a similar coordination sphere.

The results suggest that, upon the Ni binding in the *N*-terminal site, any reactivity of free copper has been observed and therefore, copper(II) is chelated by a secondary site in which its reactivity is almost absent. This redox inertia is probably due to the partial rigidity of the peptide backbone in the His-tandem domain when the *N*-terminus is occupied by the Ni^{II} ion. Moreover, when the *N*-terminal site is occupied by one of the two metals, any competition can be established, suggesting the interaction with two metals is not in equilibrium; the same results was obtained both for copper(II) and nickel(II), but showing that two metals are kinetically different in the binding of the ATCUN site: if copper(II) is immediately stabilized by this domain, nickel required more time to be stably internalized. Anyway, the final complexes show similar structural features with a peculiar conformational change to β-sheet of the peptide backbone upon the metal binding in the *N*-terminus. Lastly, CD and NMR data have confirmed the similar coordination sphere for both metals in the primary site with the shift of copper(II) in the *C*-terminal *bis*-His site when the *N*-terminus is not available, as detected by the paramagnetic effect observed on the proton signals of some *C*-terminal residues.

In conclusion, these results clarify that two independent coordinative domains for copper(II) exist in the *N*-terminal truncated peptide 4-x and indicate a possible active role of these amyloid variants in the biological buffering of circulating copper ions. Furthermore, the structural rearrangement of these sequences induced by the metal binding together with their propensity to undergo oxidative modification, detected with the highest percentages of modifications if compared with all peptides previously analyzed (see Chapter 1), reveal an active and potentially dangerous role of the peptides in the progression of these neurological disorders.

Peptide synthesis and purification

The amyloid-β peptides used in this Chapter were synthesized using the previously described Fmoc solid-phase synthesis in DMF. The removal of the protective groups from the amino acid side chains and the peptide release from the resin are performed through a solution of 95% TFA, TIS (2.5 %), and water (2.5 %). Cold diethyl ether was added to allow the peptide precipitation and the powder was then purified by chromatographic separation, using a 0–100% linear gradient of 0.1% TFA in water to 0.1% TFA in CH_3CN over 50 min (flow rate of 4 ml/min, loop 2 ml), as eluent. The product was lyophilized and then characterized by direct injection in mass spectrometry, obtaining the following ESI-MS data:

$A\beta_{16}$	$_1$DAEFRHDSGYEVHHQK$_{16}$-NH_2	m/z 1955 $^{(+)}$; 978 $^{(2+)}$; 652 $^{(3+)}$; 489 $^{(4+)}$
$A\beta_{4\text{-}16}$	$_4$FRHDSGYEVHHQK$_{16}$-NH_2	m/z 1641 $^{(+)}$; 821 $^{(2+)}$; 547.7 $^{(3+)}$; 411 $^{(4+)}$
$A\beta_{28}$	$_1$DAEFRHDSGYEVHHQKLVFFAEDVGSNK$_{28}$-NH_2	m/z 1631 $^{(2+)}$; 1088 $^{(3+)}$; 816 $^{(4+)}$; 653 $^{(5+)}$
$A\beta_{4\text{-}28}$	$_4$FRHDSGYEVHHQKLVFFAEDVGSNK$_{28}$-NH_2	m/z 1474 $^{(2+)}$; 983 $^{(3+)}$; 737.5 $^{(4+)}$; 590.2 $^{(5+)}$

Ascorbate consumption promoted by the redox efficiency of each complex.

The catalytic consumption of sodium ascorbate (1 mM) was studied at room temperature for 1800 or 300 sec in 50 mM HEPES buffer at pH 7.4. The reaction was followed through the decrease of the absorption at 265 nm corresponding to the substrate. The experiments were carried out by adding copper(II) nitrate (25 μM) to 1 or 2 equiv. $A\beta_{16}$ or $A\beta_{4\text{-}16}$ peptides (25-50 μM), preforming the metal-peptide complex and its further addition to the substrate solution as last reagent. To verify the copper(II) involvement in the binding of the secondary site and to verify that the metal is quenched by the two vicinal histidines when the *N*-terminus is not available, the data were also obtained in the presence of 1 equiv. Ni^{II} pre-incubated with the *N*-truncated peptide and further addition of 1 equiv. of copper(II) before the analysis.

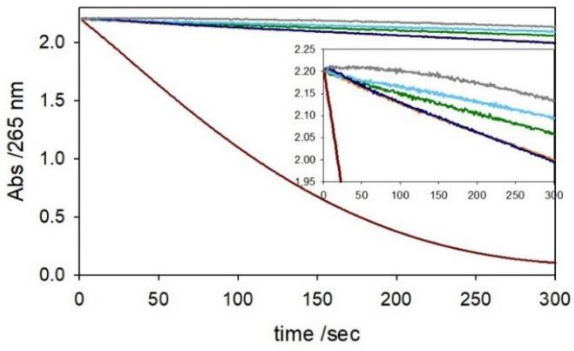

Figure 34. *Ascorbate consumption (in only buffer, grey) promoted by copper(II) (brown) and nickel(II) alone (green), and upon the addition of Cu-$A\beta_{4\text{-}16}$ complex (1:1, orange), Ni-$A\beta_{4\text{-}16}$ complex (1:1, light blue) and further addition of 1 equiv. copper (blue)*

Oxidation of dopamine, 4-methylcatechol and 4-chlorocatechol

The substrate oxidation promoted by copper(II) was studied at room temperature for 300 sec in 50 mM HEPES buffer at pH 7.4. The reaction was monitored by UV-visible spectroscopy following the generation of dopaminochrome at

475 nm for dopamine, of 4-methylquinone at 401 nm for 4-methylcatechol and of 4-chloroquinone at 400 nm for 4-chlorocatechol. The substrate amount was fixed at low concentration (0.3 mM) or at saturating values (3 mM) and the autoxidation was also evaluated. All experiments were carried out by adding copper(II) nitrate (25 μM) and amyloid-β fragments at 1:1/1:2 molar ratios to the substrate solution.

When the secondary site was investigated, copper(II) concentration was also increased to 50 μM. The catalytic profiles were also obtained at longer reaction times (1800 sec) to assay the substrate polymerization rate induced by each catalyst. Quantification of peptide solution was obtained by UV-Visible absorption at 280 nm corresponding to the tyrosine band (epsilon 1480 M^{-1} cm^{-1}). All measurements were performed at least in duplicate. To study the oxygen-dependence and to verify the reaction mechanism, some aliquots of buffered solution were previously saturated with pure oxygen (1 atm) through direct bubbling into the solution for at least 30 min. As shown in Figure 35, the results verify that oxygen-saturation does not affect the first 10 sec of the kinetics that correspond to the reduction of the metal center.

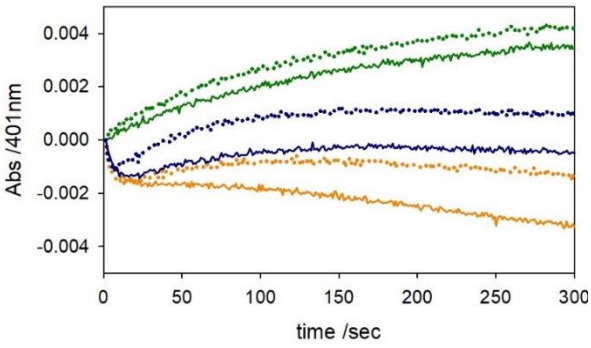

Figure 35. *Kinetic profiles of MC (0.3 mM) oxidation with time in 50 mM HEPES buffer at pH 7.4 and 20 °C with atmospheric oxygen (solid traces) and upon dioxygen saturation (dotted traces) in the presence of [Cu-Aβ4-16] at 1:1 molar ratio (25 μM, orange), [Ni-Aβ4-16] at 1:1 molar ratio (25 μM, green) and upon the addition of copper before the analysis (blue).*

Metal binding titrations

Aβ(4-16) peptide (0.5 mM) was titrated through progressive addition of increasing equiv. of copper(II) nitrate (0-1 mM) and the experiment was performed at room temperature in 5 mM phosphate buffer solution at pH 7.4 in quartz cell of 1 cm path length; copper complexation in the *N*-terminal site was firstly verified by an increasing absorption at 530 nm (ε = 110 M^{-1} cm^{-1}), characteristic of Cu^{II}-bound ATCUN site.[8e]

As suggested in literature, the amyloid peptide has two distinct copper binding sites, particularly evident in the presence of the *N*-terminal truncated isoform: the titration of the peptide against copper(II) starts with a linear slope of the plotted values that suggests the presence of a strong-affinity binding site till 1 equiv. of metal, corresponding to the primary ATCUN domain. The 2 equiv. of copper(II) is involved in an independent binding with the *C*-terminal portion of the peptide 4-16, probably involving the two vicinal histidines, but with lower affinity (Figure 36 and 37). The precipitation of copper(II) at high concentrations when is alone in phosphate buffer solution does not allow to calculate the binding constants.

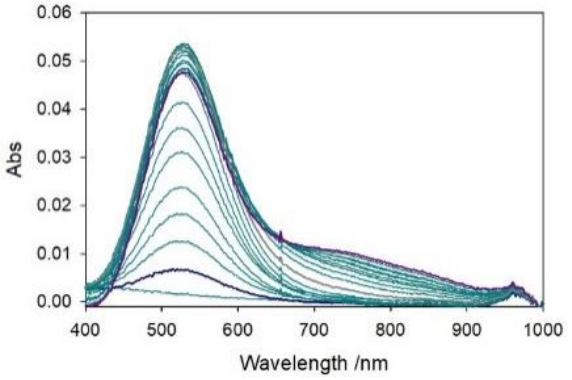

Figure 36. *UV-Vis spectrophotometric titrations in 5 mM phosphate buffer solution at pH 7.4 of Aβ4-16 (0.5 mM) against copper (0-1 mM) in quartz cell of 1 cm path length.*

Competitive titrations were also performed of [Ni-$Aβ_{4-16}$] (1:1, 0.5 mM) at 20 °C in phosphate buffer solution at pH 7.4 in 1 cm path length cell by the addition of copper(II) nitrate (0-0.5 mM); moreover, in order to verify the oxidized

nature of copper(II) adduct in the secondary site, 0.55 mM ascorbate was added to the solution and was followed upon 2h.

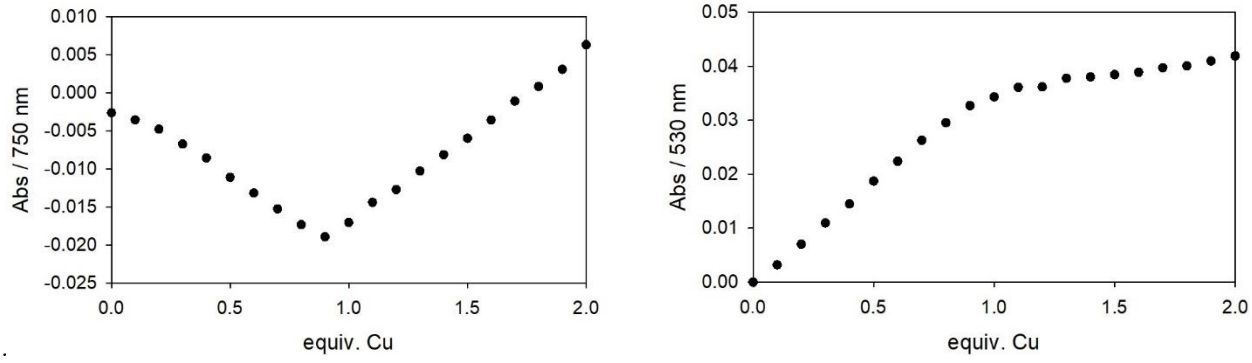

Figure 37. *Plots of the absorbance values registered at 750 nm (left panel, corrected at 466 nm) and 530 nm (right panel, corrected at 466 nm) and obtained from the previous titration, in which Aβ4-16 (0.5 mM) was titrated against copper (0-1 mM) in 5 mM phosphate buffer solution at pH 7.4.*

The retro-titration of Cu^{II}-adduct against nickel was also studied maintaining the same previous conditions. Finally, to study the stability of binary and ternary complexes with metal ions, Ni^{II}- and Cu^{II}-adducts were preformed and followed at different reaction times; then, the addition of the other metal (1 equiv.) was assayed till 24h of incubation.

LC-MS modification pattern of N-truncated Aβ peptides

The peptide modification was studied by HPLC-ESI/MS, using a LCQ ADV MAX ion-trap mass spectrometer. All samples were prepared adding copper(II) nitrate (25 μM), $Aβ_{4-28}$ (25 μM) and MC or DA (3 mM) in 50 mM HEPES buffer at pH 7.4. The oxidative modifications were thus assayed at different reaction times (15, 25, 35, 60 min). The elution of Aβ peptide as described in Chapter 1.

CD and NMR characterization of metal-Aβ complexes

The folding of Aβ(4-x) and Aβ(1-x) peptides was followed in the spectral region encompassing 192-260 nm using Jasco 1500 spectrometer in 1 cm path length cell. Peptide solutions in 5 mM phosphate buffer solution at pH 7.4 were at first investigated in the absence of metals; then, Cu^{II} and Ni^{II} were added to allow the generation of the metal complexes at 1:1 molar ratio. Seven acquisitions of each sample were used to register the spectrum, while al least 30 min was the time required to allow an efficient stabilization of the metal binding. In order to assay the resulting adducts, the visible spectra in the 280-750 nm range were also register, enhancing the amounts of the complexes to 2 mM. The NMR data were obtained from a solution of Aβ(4-16) peptide (8.6 mM) in 5 mM deuterated phosphate buffer solution at pH 7.4. Both one dimensional ^{1}H and two dimensional COSY spectra were performed on the previous sample to define the assignment of each signal with the relative amino acid. Nickel (7.8 mM) was then added to generate the binary complex and, upon 30 min of stabilization, the acquisition of the complex was obtained. At last, a small amount of Cu^{II} (78 μM) was added to the NMR tube to assay the ternary complex without an uncontrolled broadening of all signals. The acquisition was repeated after 6 and 12 hours.

References

1. (a) C. L. Masters and D. J. Selkoe, Biochemistry of amyloid β-protein and amyloid deposits in Alzheimer disease, **Cold Spring Harbor Perspect. Med.**, 2, a006262, 2012; (b) T.C. Saido, Alzheimer's Disease as Proteolytic Disorders: Anabolism and Catabolism of β-Amyloid, **Neurobiology of Aging,** 19, 1S, S69–S75, 1998; (c) D. J. Selkoe, Alzheimer's disease: genes, proteins, and therapy, **Physiol. Rev.**, 81, 741–766, 2001.
2. (a) C.L. Masters, G. Simms, N.A. Weinman, G. Multhaup, B.L. McDonald and K. Beyreuther, Amyloid plaque core protein in Alzheimer disease and Down syndrome, **Proc. Natl. Acad. Sci. U. S. A.**, 82, 4245, 1985; (b) Y. Bouter, K. Dietrich, J.L. Wittnam, N. Rezaei-Ghaleh, T. Pillot, S. Papot-Couturier, T. Lefebvre, F. Sprenger, O. Wirths, M. Zweckstetter and T.A. Bayer, N-truncated amyloid β (Aβ) 4-42 forms stable aggregates and induces acute and long-lasting behavioral deficits, **Acta Neuropathol,** 126, 189–205, 2013; (c) T.A. Bayer and O. Wirths, Focusing the amyloid cascade hypothesis on N-truncated Abeta peptides as drug targets against Alzheimer's disease, **Acta Neuropathol,** 127, 787–801, 2014; (d) O. Wirths, S. Walter, I. Kraus, H.W. Klafki, M. Stazi, T.J. Oberstein, J. Ghiso, J. Wiltfang, T.A. Bayer and Sascha Weggen, N-truncated Aβ4-x peptides in sporadic Alzheimer's disease cases and transgenic Alzheimer mouse models. **Alzheimers Res Ther.**, 9, 1, 80, 2017.
3. E. Cabrera, P. Mathews, E. Mezhericher, T.G. Beach, J. Deng, T.A. Neubert, A. Rostagno and J. Ghiso, Aβ truncated species: Implications for brain clearance mechanisms and amyloid plaque deposition, **BBA - Molecular Basis of Disease**, 1864, 208-225, 2018.
4. (a) C.L. Masters, G. Multhaup, G. Simms, J. Pottgiesser, R.N. Martins and K. Beyreuther, Neuronal origin of a cerebral amyloid: neurofibrillary tangles of Alzheimer's disease contain the same protein as the amyloid of plaque cores and blood vessels, **EMBO J.,** 4, 2757, 1985; (b) E. Portelius, M. Olsson, G. Brinkmalm, U. Rüetschi, N. Mattsson, U. Andreasson, J. Gobom, A. Brinkmalm, M. Hölttä, K. Blennow and H. Zetterberg, Mass spectrometric characterization of amyloid-β species in the 7PA2 cell model of Alzheimer's disease, **J. Alzheimer's Dis.,** 33, 85, 2013.
5. A. Santoro, G. Walke, B. Vileno, P.P. Kulkarni, L. Raibauta and P. Faller, Low catalytic activity of the Cu(II)-binding motif (Xxx-Zzz-His; ATCUN) in reactive oxygen species production and inhibition by the Cu(I)-chelator BCS, **Chem. Commun.,** 54, 11945 - 11948, 2018.
6. P. Gonzalez, K. Bossak, E. Stefaniak, C. Hureau, L. Raibaut, W. Bal and P. Faller, N-Terminal Cu-Binding Motifs (Xxx-Zzz-His, Xxx-His) and Their Derivatives: Chemistry, Biology and Medicinal Applications, **Chem. - Eur. J.,** 24, 32, 8029-8041, 2018.
7. A. Santoro, N.E. Wezynfeld, E. Stefaniak, A. Pomorski, D. Płonka, A. Krężel, W. Bal and P. Faller, Cu transfer from amyloid-β_{4-16} to metallothionein-3: the role of the neurotransmitter glutamate and metallothionein-3 Zn(II)-load states, **Chem Commun.,** 54, 89, 12634-12637, 2018.
8. (a) M. Mital, N.E. Wezynfeld, T. Frączyk, M.Z. Wiloch, U.E. Wawrzyniak, A. Bonna, C. Tumpach, K.J. Barnham, C.L. Haigh, W. Bal and S.C. Drew, A Functional Role for Ab in Metal Homeostasis? N-Truncation and High-Affinity Copper Binding, **Angew. Chem. Int. Ed.,** 54, 10460 -10464, 2015; (b) V. A. Streltsov, R. S. K. Ekanayake, S. C. Drew, C. T. Chantler and S. P. Best, Structural Insight into Redox Dynamics of Copper Bound N-Truncated Amyloid-β Peptides from in Situ X-ray Absorption Spectroscopy, **Inorg. Chem.**, 57, 11422−11435, 2018; (c) M.J. Pushie, K. Shaw, K.J. Franz, J. Shearer and K.L. Haas, Model Peptide Studies Reveal a Mixed Histidine-Methionine Cu(I) Binding Site at the N-Terminus of Human Copper Transporter 1, **Inorg. Chem.**, 54, 17, 8544 - 8551, 2015; (d) W.M. Tay, A.I. Hanafy, A. Angerhofer and L.J. Ming, A plausible role of salivary copper in antimicrobial activity of histatin-5–metal binding and oxidative activity of its copper complex. **Bioorg. Med. Chem. Lett.**, 19, 23, 6709 – 12, 2009; (e) S.E. Conklin, E.C. Bridgman, Q. Su, P. Riggs-Gelasco, K.L. Haas and K.J. Franza, Specific Histidine Residues Confer Histatin Peptides with Copper-Dependent Activity against Candida albicans, **Biochemistry,** 56, 32, 4244-425, 2017; (f) S. Schwab, J. Shearer, S.E. Conklin, B. Alies and K.L. Haas, Sequence proximity between Cu(II) and Cu(I) binding sites of human copper transporter 1 model peptides defines reactivity with ascorbate and O2, **J. Inorg. Biochem.,** 158, 70-76, 2016; (g) B.K. Maiti, N. Govil, T. Kundu and J. J.G. Mourai, Designed Metal-ATCUN Derivatives: Redox and Non-redox-Based Applications Relevant for Chemistry, Biology, and Medicine, i**Science,** 23, 101792, 2020.
9. (a) A. Napolitano, P. Manini and M. d'Ischia, Oxidation chemistry of catecholamines and neuronal degeneration: an update. **Curr Med Chem.,** 18, 12, 1832-45, 2011; (b) E. Ferrari, A. Capucciati, I. Prada, F. A. Zucca, G. D'Arrigo, D. Pontiroli, M. G. Bridelli, M. Sturini, L. Bubacco, E. Monzani, C. Verderio, L. Zecca and L. Casella, Synthesis, structure characterization and evaluation in microglia cultures of neuromelanin analogues suitable for modeling Parkinson Disease, **ACS Chem. Neurosci.,** 8, 3, 501–512, 2017.
10. (a) L. Guilloreau, L. Damian, Y. Coppel, H. Mazarguil, M. Winterhalter and P. Faller, Structural and thermodynamical properties of Cu^{II} amyloid-β16/28 complexes associated with Alzheimer's disease., **J Biol Inorg Chem**, 11, 1024–1038, 2006; (b) C.D. Syme, R.C. Nadal, S.E.J. Rigby, and J.H. Viles, Copper binding to the amyloid-β (Aβ) peptide associated with Alzheimer's disease: Folding, coordination geometry, pH dependence, stoichiometry, and affinity of Aβ-(1−28): Insights from a range of complementary spectroscopic techniques, **J. Biol. Chem.**, 279, 18169– 18177, 2004; (c) C. Bacchella, S. Nicolis, S. Dell'Acqua, E. Rizzarelli, E. Monzani and L. Casella, Membrane Binding Strongly Affecting the Dopamine Reactivity Induced by Copper Prion and Copper/Amyloid-β (Aβ) Peptides. A Ternary Copper/Aβ/Prion Peptide Complex Stabilized and Solubilized in Sodium Dodecyl Sulfate Micelles., **Inorg Chem.**, 59, 1, 900-912, 2020.
11. (a) S. Dell'Acqua, C. Bacchella, E. Monzani, S. Nicolis, G. Di Natale, E. Rizzarelli, L. Casella, Prion Peptides Are Extremely Sensitive to Copper Induced Oxidative Stress, **Inorg Chem.**, 56, 18, 11317-11325, 2017; (b) V. Pirota, S. Dell'Acqua, E. Monzani, S. Nicolis, L. Casella, Copper-Aβ Peptides and Oxidation of Catecholic Substrates: Reactivity and Endogenous Peptide Damage, **Chem. Eur. J.**, 22, 16964 -16973, 2016; (c) C. Bacchella, S. Dell'Acqua, S. Nicolis, E. Monzani and L. Casella, A Cu-bis(imidazole) Substrate Intermediate Is the Catalytically Competent Center for Catechol Oxidase Activity of Copper Amyloid-β, **Inorg. Chem.**, 60, 606−613, 2021.
12. (a) N. E. Wezynfeld, E. Stefaniak, K. Stachucy, A. Drozd, D. Płonka, S. C. Drew, A. Krezel, and W. Bal, Resistance of Cu(Aβ4–16) to Copper Capture by Metallothionein-3 Supports a Function for the Aβ4–42

Peptide as a Synaptic Cu^{II} Scavenger, ***Angew. Chem. Int. Ed.,*** 55, 8235 –8238, 2016; ***(b)*** *B. Alies, E. Renaglia, M. Rózga, W. Bal, P. Faller and C. Hureau, Cu(II) Affinity for the Alzheimer's Peptide: Tyrosine Fluorescence Studies Revisited,* ***Anal. Chem.,*** 85, 1501–1508, 2013.

13. *T.R. Young, A. Kirchner, A.G. Wedd and Z. Xiao, An integrated study of the affinities of the Aβ16 peptide for Cu(I) and Cu(II): implications for the catalytic production of reactive oxygen species,* ***Metallomics,*** 6, 505–517, 2014.
14. ***(a)*** *V. Borghesani, B. Alies and C. Hureaua, Cu(II) binding to various forms of amyloid-β peptides. Are they friends or foes?,* ***Eur J Inorg Chem.,*** 1, 7–15, 2018; ***(b)*** *W. Goch and W. Bal, Numerical Simulations Reveal Randomness of Cu(II) Induced Aβ Peptide Dimerization under Conditions Present in Glutamatergic Synapses.* ***PLOS ONE,*** 12, 1, e0170749, 2017; ***(c)*** *Abd El Wahed, M. G., Stability constants of Cu^{2+}, Fe^{3+} and Zr^{4+} chelates of ampicillin, dopamine and α-methyl L-dopa in aqueous medium.* ***Anal Lett,*** 17, 205-216, 1984;
15. ***(a)*** *M.J. Pushie, E. Stefaniak, M.R. Sendzik, D. Sokaras, T. Kroll and K.L. Haas, Using N-Terminal Coordination of Cu(II) and Ni(II) to isolate the Coordination Environment of Cu(I) and Cu(II) Bound to His13 and His14 in Amyloid-β(4–16),* ***Inorg. Chem.,*** 58, 15138–15154, 2019; ***(b)*** *C.T. Supuran, Structure and function of carbonic anhydrases,* ***Biochem J,*** 473, 14, 2023-2032, 2016; ***(c)*** *C. Harford and B. Sarkar, Terminal Cu(II)- and Ni(II)-Binding (ATCUN) Motif of Proteins and Peptides: Metal Binding, DNA Cleavage, and Other Properties,* ***Acc. Chem. Res.,*** 30, 123-130, 1997; ***(d)*** *S.-J. Lau and B.J. Sarkar, Ternary Coordination Complex between Human Serum Albumin, Copper (II), and L-Histidine,* ***Biol. Chem.,*** 246, 5938-5943, 1971.
16. ***(a)*** *C.E. Jones, S.R. Abdelraheim, D.R. Brown, and J.H. Viles, Preferential Cu^{2+} Coordination by His96 and His111 Induces β-Sheet Formation in the Unstructured Amyloidogenic Region of the Prion Protein,* ***J. Biol. Chem,*** *279, 31, 32018–32027, 2004;* ***(b)*** *M. Mylonas, J.C. Plakatouras and N. Hadjiliadis, Interactions of Ni(II) and Cu(II) ions with the hydrolysis products of the C-terminal -ESHH- motif of histone H2A model peptides. Association of the stability of the complexes formed with the cleavage of the -E–S- bond,* ***Dalton Trans.,*** *4152 – 4160, 2004.*
17. ***(a)*** *C.J. Pike, M.J. Overman and C.W. Cotman, Amino-terminal deletions enhance aggregation of β-amyloid peptides in vitro,* ***J Biol Chem.,*** 270, 23895–23898, 1995; ***(b)*** *D.L. Miller, I.A. Papayannopoulos, J. Styles, S.A. Bobin, Y.Y. Lin, K. Biemann and K. Iqbal, Peptide compositions of the cerebrovascular and senile plaque core amyloid deposits of Alzheimer's disease,* ***Arch Biochem Biophys.,*** 301, 41–52, 1993; ***(c)*** *T.J. Oberstein, P. Spitzer, H-W Klafki, P. Linning, F. Neff, H.J. Knölker, P. Lewczuk, J. Wiltfang, J. Kornhuber and J.M. Maler, Astrocytes and microglia but not neurons preferentially generate N-terminally truncated Aβ peptides,* ***Neurobiol Dis.,*** 73, 24–35, 2015; ***(d)*** *J. Kardos, I. Kovacs, F. Hajos, M. Kalman and M. Simonyi, Nerve endings from rat brain tissue release copper upon depolarization. A possible role in regulating neuronal excitability,* ***Neurosci. Lett.,*** 103, 139–144, 1989.

Chapter 6

CATECHOLAMINE OXIDATION AND AMYLOID-β MODIFICATION IN THE PRESENCE OF HEMIN AND HYDROGEN PEROXIDE.

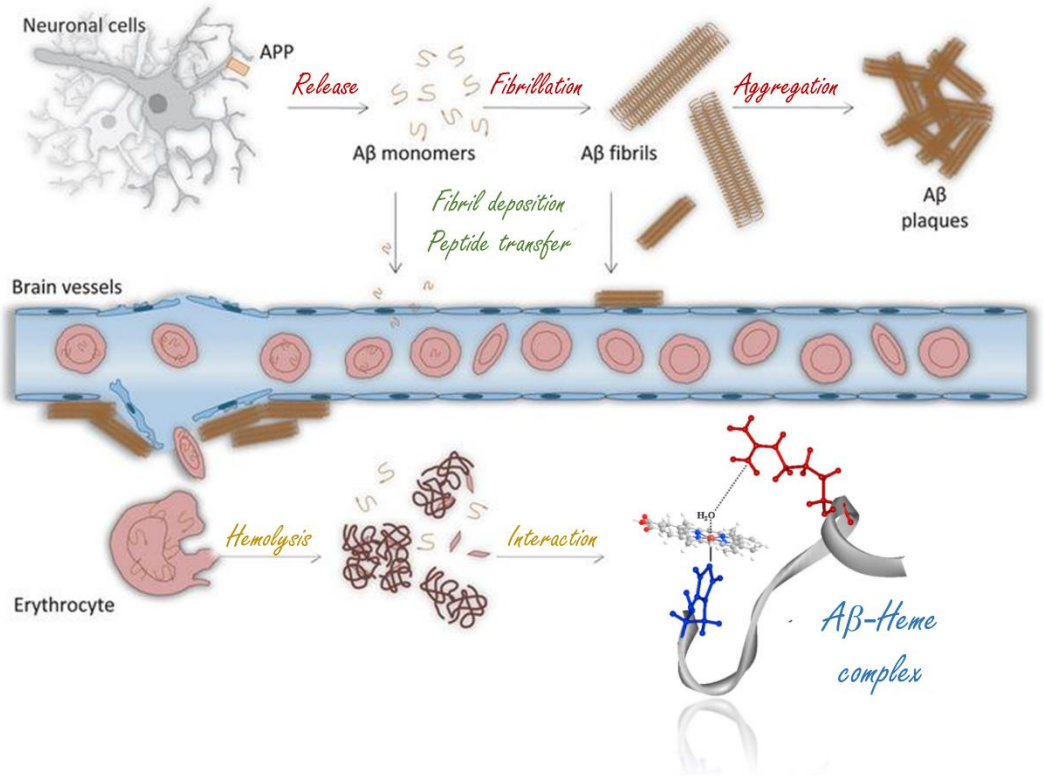

Ref. Molecules **2020**, 25, 5044.
"Condition-Dependent Coordination and Peroxidase Activity of Hemin-Aβ Complexes"
C. Bacchella, J.T. Brewster, S. Bähring, S. Dell'Acqua, H.D. Root, G.D. Thiabaud, J.F. Reuther, E. Monzani, J.L. Sessler and L. Casella

Ferriprotoporphyrin IX is a macrocyclic complex that is generated by the coordination of one central iron ion to a porphyrin ring via tetradentate geometry, while the axial positions are available for biological ligands. Depending on the redox form of the central ion, this prosthetic group is called as hemin, if iron assumes +3 redox state, or heme, in the presence of central iron(II). Several metalloproteins, known as hemoproteins, contain heme, which assumes heterogeneous biological functions, such as binding and transport of molecular oxygen in hemoglobin or electron transfer and chemical catalysis in enzymes, such as catalases, peroxidases and cytochromes (Figure 1).[1a]

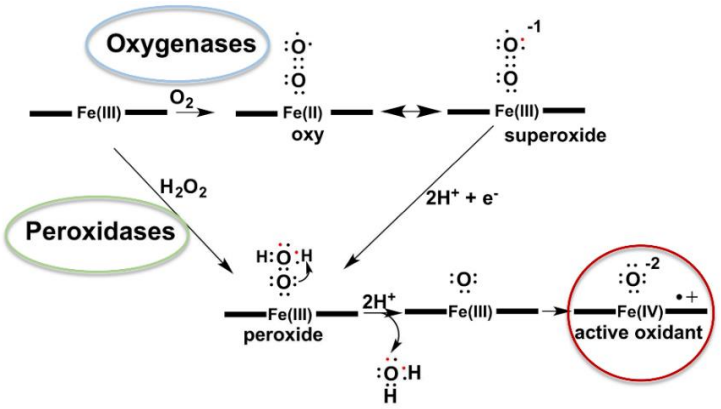

Figure 1. *Oxygenase like cytochrome P450 requires that the central iron ion is in a reduced form as ferrous ion (Fe^{2+}) for the binding with molecular oxygen. Upon the interaction with O_2, the oxy-complex, known as ferric-superoxide ($Fe(III)\text{-}OO^{-}\cdot$) is generated. A second electron transfer results in the reduction of superoxide to peroxide. At this point the P450 and peroxidase mechanisms are similar. The protonation of the distal oxygen atom allows the heterolytic cleavage of the O-O bond with the loss of one water molecule and resulting in the generation of species in which the O-atom presents only 6 valence electrons. An electronic rearrangement leads to the formation of the real oxidant species.*[1b]

Several studies have suggested a correlation between ferric heme and the onset and development of neurodegenerative diseases, such as Alzheimer's.[1c,1d,1e] Alteration in the iron metabolism and an increase in free heme levels, even up micromolar values, are observed during brain injury and neurodegenerative pathologies. Moreover, high levels of iron are observed in both the plaques and tangles in the cortex and hippocampus, leading to the severe progression of the disorder. Other hallmarks besides the dyshomeostasis of the metal are the alterations in the activity of mitochondrial complex IV, heme oxygenase and biliverdin reductase-A.[2a, 2b, 2c,2d] The last enzyme is the key catalyst for the synthesis of bilirubin from its precursor biliverdin: bilirubin works as a scavenger for dangerous species like NO and PROS, protecting neuronal cells from oxidative and nitrative damage.[2e] Heme exists as three main forms: (i) heme-a that is contained in the mitochondrial complex IV, in which works as the rate limiting factor for the structuring of the complex; (ii) heme-b, as the most common form in the biological systems, results from the activity of ferrochelatase in the mitochondrial compartments and is the precursor of other heme groups; (iii) heme-c, that is structurally similar to heme-b, is only found covalently associated to apoproteins, in which an example is the cytochrome c. Alteration in the maturation pathways and endogenous levels of heme are tightly associated with the progression of Alzheimer's, in which too low levels of heme-a have been connected with the dysregulation of complex IV, inefficiency of the mitochondrial electron transport chain and production of reactive radicals.[3a] As the same time, the concentration of heme-b detected in temporal lobe of AD patients is enhanced by 250%, which can promote high oxidative stress damages not only confined into the mitochondrial structures.[3b] Moreover, some observations lead to conclude that the possible interaction between heme and amyloid-β proteins can exacerbate the progression of the disorder. The ferric

heme complex shows high peroxidase activity and, in the presence of hydrogen peroxide, favors the dimerization of peptide, such as $A\beta_{16}$, via dityrosine cross-linking. Hemin-b is coordinated by the amyloid-β peptide both in the six-coordinated and low-spin form, via the binding with two peptide chains, and in the high-spin form, in which the pentacoordinated adduct is obtained by the binding with only one peptide. These two complexes are in equilibrium each other, which is strongly influenced by temperature and peptide concentration.[3c] Moreover, the oxidative and nitrative conditions observed in neuroinflammatory processes usually result in high percentage of amyloid-β modification, such as oxidation, nitration and dimerization; these alterations in the primary sequence promote the misfolding of the protein, enhancing its aggregation and plaque generation.

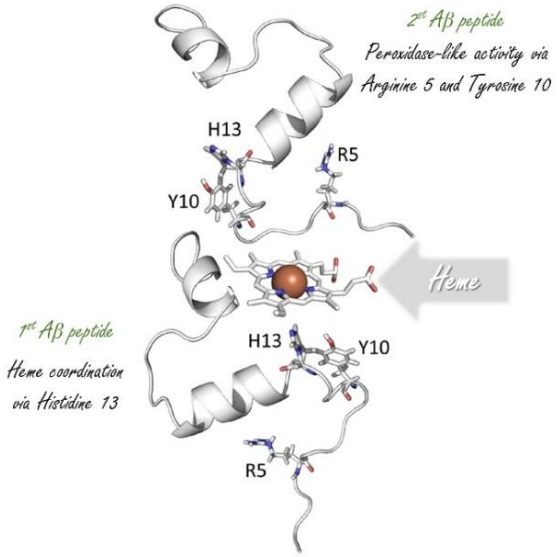

Figure 2. *Cartoon of heme-Aβ complex, showing the interaction between the metal and the N-terminus of the peptide. The catalytic mechanism probably views the involvement in one axial position of one amyloid peptide and the coordination of a second peptide that exposes Arg-5 and Tyr-10 residues to allow the catalysis.*

Amyloid-β peptide can be easily schematized in two main regions, a hydrophilic *N*-terminus and a more hydrophobic and structured domain; each region probably contains one ferric heme binding site, although the first region is mainly involved in the direct binding with ferric center (Figure 2) while the hydrophobic tail could be useful to stabilize the complex via salt bridges to lysine 28 or π-stacking to phenilalanines.[4] In particular, the key ligands for ferric center are His-6, His-13 and His-14, probably in equilibrium between three high-spin species, as suggested by the observed peroxidase-like behavior of these adducts.[5a] The additional stabilization due to the participation of arginine-5 as secondary binding site or the involvement of positively charged amino acids, such as arginine, lysine and the *N*-terminal amino group, in the electrostatic interaction with propylcarboxy groups of heme are still controversial. Moreover, spectroscopic results confirm the simultaneous and independent binding both of copper(I) and Fe(III)-heme, which would be explained through the pseudo-linear coordination of reduced copper via histidines 13 and 14 while heme group is chelated by histidine 6 as axial ligand.[4] Heme bound to β-amyloid peptides exhibits peroxidase activity through the involvement of Fe(III) as reducing agent to give Fe(IV) oxo species, usually indicated as Component I. In addition, the adduct with copper(II) is commonly recognized as peroxidase-like system that, in reducing environment and in the presence of molecular oxygen, enhances the production of hydrogen peroxide, which is further reduced to hydroxyl radical. The imputable ligands responsible of the catalytic activity of these complexes are probably arginine-5 and tyrosine-10 and the key role of these residues is verified by the relationship between the absence of typical hallmarks of neurodegeneration in rats and mouse and the mutations R5G, Y10F and Y13R obtained by the alignment of APP sequences of humans and mouse. The previous coordination sphere for heme is evidenced in several endogenous enzymes, for instance histidine works as binding ligand for heme in hemoglobin, myoglobin and peroxidase while tyrosine was identified as axial ligand in catalase.[5b] Spectroscopic studies have confirmed that the specific binding of

ferric heme occurs in the first *N*-terminal region (1-16), showing a decrease in intensity at 365 nm, a blue shift of the Soret band from 618 nm to 606 nm and the increase of the band at 693 nm. These observations are not evidenced when heme is incubated in the presence of the *C*-terminal fragment (17-40), suggesting that this portion does not directly bind the axial positions of iron. Moreover, mutational studies have shown that the substitution of Tyr at 10 position does not influence the stability of heme-Aβ complex and the cleavage of the sequence encompassing 1-10 residues is not affected by the coordination of metal, suggesting His-13 and His-14 residues as main coordinating ligands. When heme is incubated in the presence of 1 equiv. of beta-amyloid peptide, the high frequency resonance Raman spectrum displays signals at 1374 (ν_4), 1492 (ν_3), 1574 (ν_2), and 1630 (ν_{10}) cm^{-1} that indicate a five-coordinated high-spin iron and a weak signal at 1505 cm^{-1} relieves the low concentration of low-spin species. The high-spin coordination through one axial histidine is also confirmed by EPR studies, suggesting a g-value around 6.0 corresponding to S = 5/2.[2e] Anyway, the more interesting features of these complexes are their peroxidase-like activity and the capability to efficiently oxidize neurotransmitters like serotonin and DOPA in the presence of hydrogen peroxide.[2a] Hence the active site of these adducts is represented by the central heme coordinated with an axial histidine and a distal water molecule weakly bound to the iron ion and hydrogen bonded to the arginine-5 residue, as shown in Figure 3. In this way, the resulting complex resembles the chemical environment of peroxidase enzymes, in which iron assumes the high spin form. Moreover, the second distal position for iron can be occupied by a second molecule of peptide, resulting in the bis-His low-spin form that mimics the active site of cytochrome b.

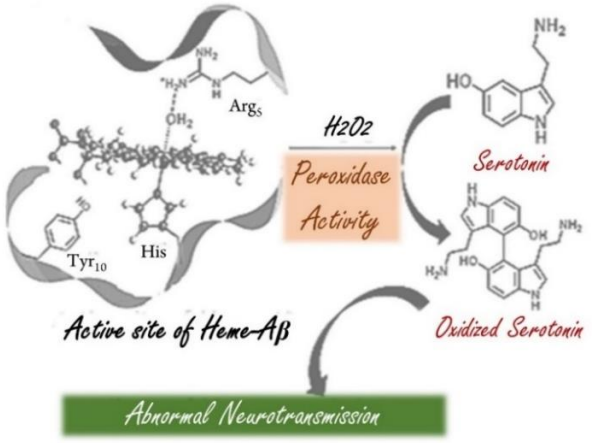

Figure 3. *Schematic representation of the alteration of serotonin levels and neurotransmitter oxidation. The unregulated peroxidase activity of heme-Aβ leads to extensive damage in the neurotransmission pathways.*

Endogenous peroxidases show a conserved primary sequence that allows to assume a peculiar conformation with an acidic arginine residue located in distal position respect with heme core and working as proton source for the heterolytic cleavage of O-O bond. Arginine 5 plays a key role in the second coordination sphere, while tyrosine 10 can provide electron for the reduction of molecular oxygen and further generation of partial radical oxygen species and formation of the tyrosyl radical, enhancing the peptide tendency to the crosslinking.[5c] A defined coordination sphere of heme bound to beta-amyloid sequences and its peroxidase-like activity are still controversial, being highly influenced by the chemical and thermodynamic conditions chosen for the experimental studies. In this chapter, the reactivity of these complexes was assayed working in conditions similar to neuroinflammatory state, such as slightly acid pH, and more equivalents of peptide compared to the amount of heme iron in solution. In these conditions, the activity in term of oxidation of the neurotransmitter dopamine to dopaminochrome and the conversion of 2,2'-azino-bis(3-ethylbenzothiazoline-6-sulfonic acid) (ABTS) into its radical form were performed. The results will mainly indicate that the peroxidase-like activity of heme is evidently enhanced upon its coordination with beta-amyloid peptide, where the amount of peptide plays a key role in the resulting reaction rates, and is further increased performing the kinetics in acidic *medium*, a common feature observed in neurodegenerative conditions.

Reactivity of ferric heme complexed with beta-amyloid peptide

The peroxidase-like activity of hemin bound to β-amyloid peptides can lead to the uncontrolled production of reactive species and to severe damages of neuronal structures. Several factors, such as *medium* pH, ionic strength and temperature are able to influence the catalytic capability of these complexes, altering the equilibrium between low-spin and high-spin states of ferric heme. The effect of the chemical environment is herein assayed in term of oxidative activity of hemin-complex toward ABTS and dopamine as exogenous substrates. The data were collected both in the presence of the *C*-truncated peptide, corresponding to the *N*-terminal sequence ($A\beta_{16}$), and of the full-length peptide that comprises the hydrophobic tail and shows a high tendency to aggregate ($A\beta_{40}$). The kinetics were obtained either using hemin alone as catalyst and increasing the concentration of peptide in solution up to 100 equivalents.

ABTS oxidation in neutral and acid medium

ABTS can be readily oxidized to its free radical cation ($ABTS^{\bullet+}$) when in the presence of oxidizing agent and its product can be easily followed via spectroscopic methods at 660 nm showing an intensely colored, green-blue product. The radical cation can be oxidized via another electronic transfer to obtain the cationic species, $ABTS^{2+}$. A simplified mechanism of the oxidative reaction of substrate is explained below. ABTS can undergo one-electron oxidation to generate the metastable radical cation (II), which is partially unstable and shows great tendency to disproportion to give the starting molecules and the more stable azodication.[6a] This reaction is catalyzed by heme that upon the binding with the imidazole chains of the peptide increases its peroxidase activity. The complex operates like an endogenous peroxidase: it starts from a *resting state* containing ferric heme that reacts with a molecule of hydrogen peroxide to give the first enzyme intermediate, called Component I and presenting a radical [Fe^{IV}=OR^{+}] which formally presents an oxidation state of +5. The interaction with a molecule of substrate promotes the changes from Component I to Component II, the second enzymatic intermediate, through the transfer of one electron to the ferric center to give a formal charge of +4 (Figure 4).[6b]

The peroxidase activity of hemin alone and chelated by beta-amyloid peptide was measured through the oxidation of ABTS in co-presence of hydrogen peroxide and increasing equivalents of peptide respect with the metal. All data were collected in phosphate buffer solution 50 mM at pH 7.4 and mimicking a neuroinflammatory states at pH 6.3, at 37 °C. Moreover, the data confirm that the *N*-terminal region of amyloid-beta peptide is the domain required for the interaction with hemin and for an efficient peroxidase-activity; indeed, the same trend can be observed from the reactions promoted by heme bound to Aβ16 or Aβ40 and only slight differences in the catalytic activities of the hemin complexed to the full-length Aβ are evidenced, probably linked to the onset of an initial aggregation process.

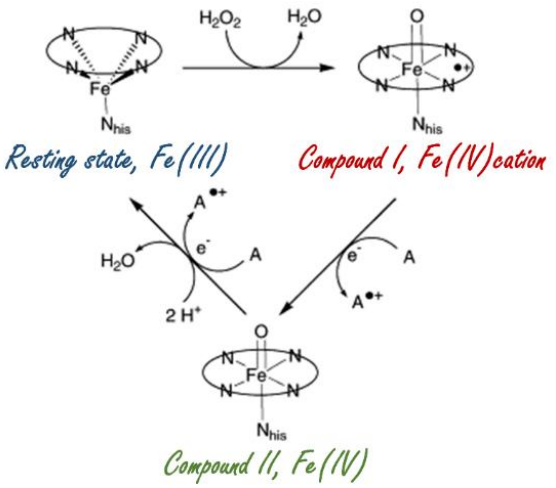

Figure 4. *Simplified reaction mechanism of peroxidase enzyme. A indicates the substrate while $A^{\bullet+}$ corresponds to its radical products.*[7]

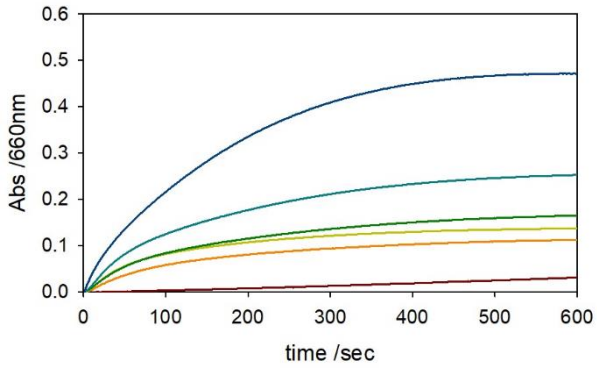

Initial rates (Abs/sec)	
H_2O_2-Hemin	7.9555 E-4
+ 2 μM peptide	1.2961 E-3
+ 10 μM peptide	1.3015 E-3
+ 40 μM peptide	1.8995 E-3
+ 200 μM peptide	3.1484 E-3

Figure 5. *Kinetic profiles of ABTS (3 mM) oxidation with time in 50 mM phosphate buffer solution at pH 7.4 and 37 °C in presence of hydrogen peroxide (2.5 mM) (brown trace) and hemin (2 μM, orange) and upon the addition of 2 μM (light green), 10 μM (green), 40 μM (light blue) and 200 μM $A\beta_{16}$ (blue).*

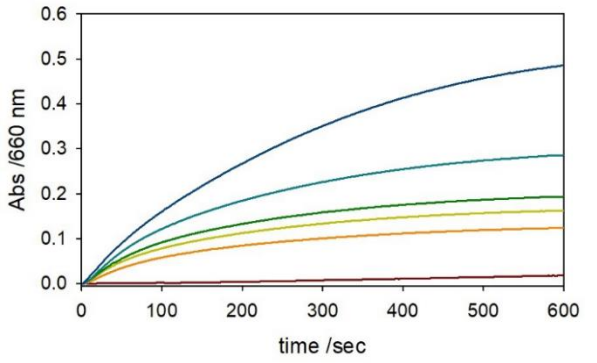

Initial rates (Abs/sec)	
H_2O_2	2.4248 E-5
H_2O_2-Hemin	7.8707 E-4
+ 2 μM peptide	1.0847 E-3
+ 10 μM peptide	1.2283 E-3
+ 40 μM peptide	1.5809 E-3
+ 200 μM peptide	1.8688 E-3

Figure 6. *Kinetic profiles of ABTS (3 mM) oxidation with time in 50 mM phosphate buffer solution at pH 7.4 and 37 °C in presence of hydrogen peroxide (2.5 mM) (brown trace) and hemin (2 μM, orange) and upon the addition of 2 μM (light green), 10 μM (green), 40 μM (light blue) and 200 μM $A\beta_{40}$ (blue).*

A further enhancement of the catalytic activity of hemin alone was observed in the experimental data obtained at slightly acidic conditions and the same effect was shown when the complexing peptide was added (Figures 7, 8 and 9). The catalysis was followed for only 10 minutes to avoid the contribution of hemin degradation with time, that is already visible at neutral pH while in acid conditions the peroxidation of substrate is maintained with a pseudo-constant rate.

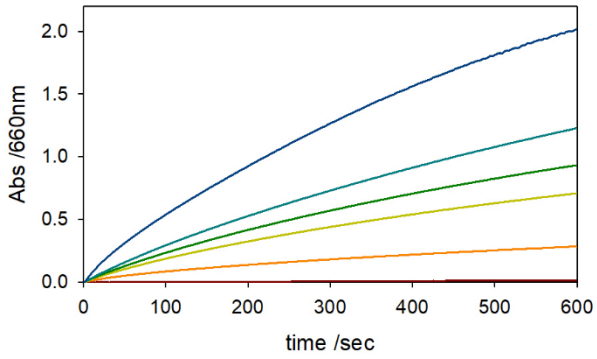

Initial rates (Abs/sec)	
H_2O_2	2.2677 E-5
H_2O_2-Hemin	9.5779 E-4
+ 2 μM peptide	2.0264 E-3
+ 10 μM peptide	2.4914 E-3
+ 40 μM peptide	3.1445 E-3
+ 200 μM peptide	5.3948 E-3

Figure 7. *Kinetic profiles of ABTS (3 mM) oxidation with time in 50 mM phosphate buffer solution at pH 6.3 and 37 °C in presence of hydrogen peroxide (2.5 mM) (brown trace) and hemin (2 μM, orange) and upon the addition of 2 μM (light green), 10 μM (green), 40 μM (light blue) and 200 μM $A\beta_{16}$ (blue).*

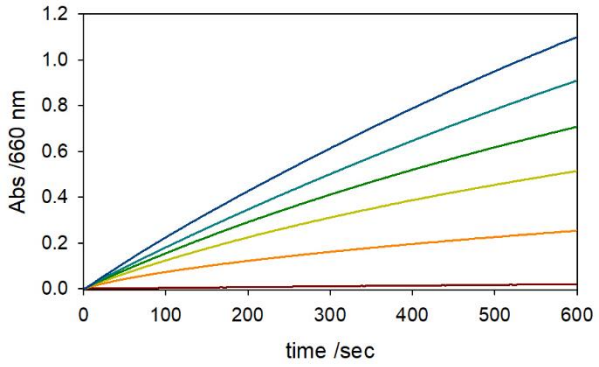

Initial rates (Abs/sec)	
H_2O_2	3.5763 E-5
H_2O_2-Hemin	7.5992 E-4
+ 2 μM peptide	1.2762 E-3
+ 10 μM peptide	1.5792 E-3
+ 40 μM peptide	1.8460 E-3
+ 200 μM peptide	2.3226 E-3

Figure 8. *Kinetic profiles of ABTS (3 mM) oxidation with time in 50 mM phosphate buffer solution at pH 6.3 and 37 °C in presence of hydrogen peroxide (2.5 mM) (brown trace) and hemin (2 μM, orange) and upon the addition of 2 μM (light green), 10 μM (green), 40 μM (light blue) and 200 μM $A\beta_{40}$ (blue).*

Moreover, the effect of temperature was assayed obtaining the kinetic plots both at atmospheric temperature (25 °C) and at biological one (37 °C) in order to assay the redox behavior of these complexes in experimental conditions more similar to the biological environment. As expected, the reaction is partially enhanced by the higher temperatures but without any significant increase in the initial rates of the catalysis (Figure 10).

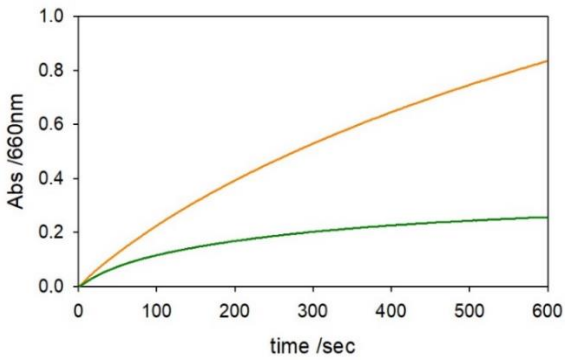

Figure 9. *Kinetic profiles of ABTS (3 mM) oxidation with time in 50 mM phosphate buffer solution at two pH value, 7.4 (green trace) and 6.3 (orange) at 37 °C in presence of hemin (2 μM), hydrogen peroxide (2.5 mM) and 2 μM $A\beta_{16}$.*

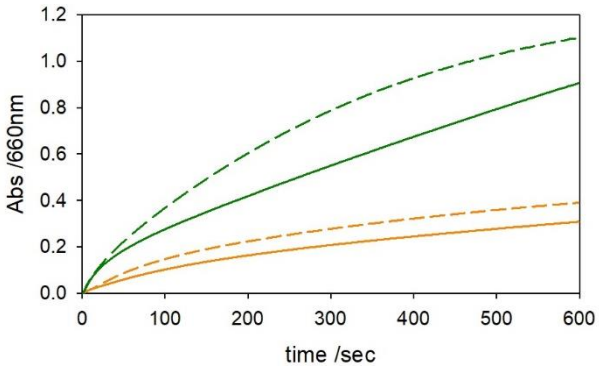

Figure 10. *Kinetic profiles of ABTS (3 mM) oxidation with time in 50 mM phosphate buffer solution at pH 7.4 in the presence of hemin (2 μM), hydrogen peroxide (2.5 mM) and upon the addition of Aβ16 10 μM (orange solid and dashed, at 25°C and 37°C, respectively) and 200 μM (green solid and dashed, at 25°C or 37°C, respectively)*

		Initial rates (Abs/sec): Hemin-H_2O_2-peptide (2 μM)
ABTS	**pH 7.4**	1.8341 E-4
	pH 6.3	2.3367 E-4

Initial rates (Abs/sec)		
	ABTS	
	25°C	37 °C
10 μM peptide	1.1105 E-3	1.7860 E-3
200 μM peptide	4.3492 E-3	4.1043 E-3

Dopamine oxidation in neutral and acid medium

The oxidation of another substrate was assayed to evaluate the effect of the peroxidase activity on an endogenous neurotransmitter. Dopamine is a monoamine involved in the signaling pathway between neuronal cells and it is easily oxidized to give oligomeric products and further melaninic species, playing a role in the progression of neurodegenerative condition. The reaction was monitored at 475 nm following the generation of dopaminochrome

maintaining the experimental conditions of the kinetics performed on ABTS. The resulting oxidative traces do not exhibit a Michaelis-Menten-like function, where the increasing concentrations of substrate induce an inhibition of the reaction rate, as shown in Figure 11. As suggested by the data shown in Figures 12 and 13, the oxidation of substrate is enhanced by the presence of peptide chelated to ferric heme with an increase of the initial rate almost two-fold respect with heme alone. The influence of the temperature was also analyzed maintaining the same reaction conditions but varying the temperature at 25 °C and 37 °C (Figure 14); obviously the dopamine oxidation proceeds more quickly at higher temperature and the lag phase observed at atmosphere temperature disappears showing a prolonged and major accumulation of quinone in solution.

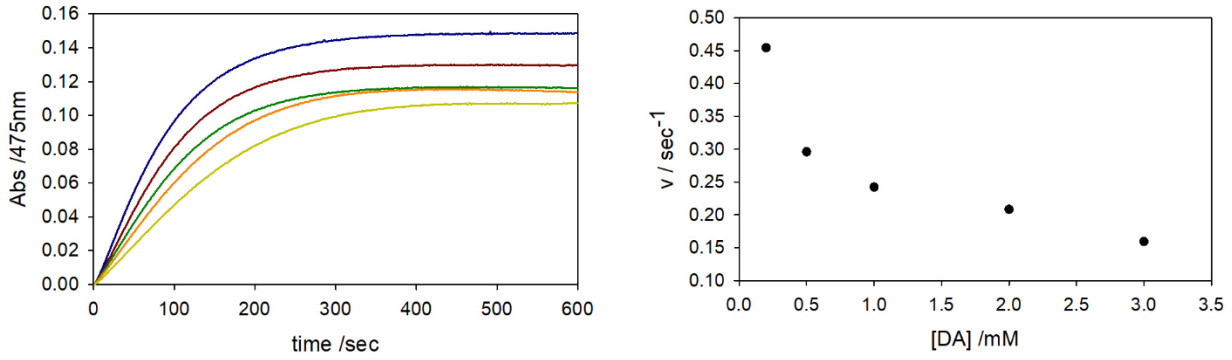

Figure 11. *(Left) Kinetic profiles of DA oxidation with time in 50 mM phosphate buffer solution at pH 7.5 and 37 °C in presence of hemin (2 μM), hydrogen peroxide (2.5 mM), Aβ16 (10 μM), and varying concentration of DA (0.2 mM, blue trace; 0.5 mM, brown; 1 mM, green; 2 mM, orange and 3 mM, light green). (Right) Dependence of the reaction rates of dopaminochrome formation on the concentration of DA.*

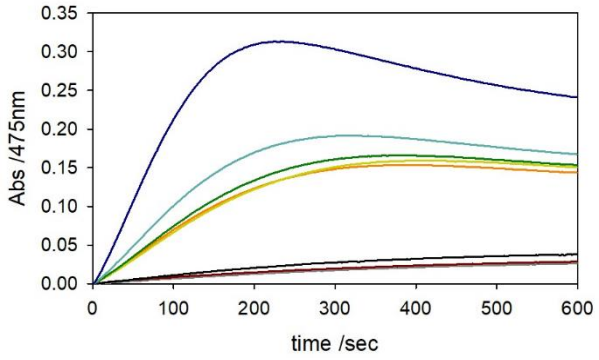

Initial rates (Abs/sec)	
Hemin	7.0023 E-5
H_2O_2	1.0223 E-4
H_2O_2-Hemin	7.0023 E-4
+ 2 μM peptide	6.5902 E-4
+ 10 μM peptide	7.3341 E-4
+ 40 μM peptide	1.0150 E-3
+ 200 μM peptide	2.2519 E-3

Figure 12. *Kinetic profiles of DA (3 mM) oxidation with time in 50 mM phosphate buffer solution at pH 7.4 and 37 °C in presence of hemin (2 μM) (brown trace) or hydrogen peroxide (2.5 mM, black), after the addition of both hemin and peroxide (orange) and upon the addition of 2 μM (light green), 10 μM (green), 40 μM (light blue) and 200 μM Aβ16 (blue). The autoxidation trace is shown as grey curve.*

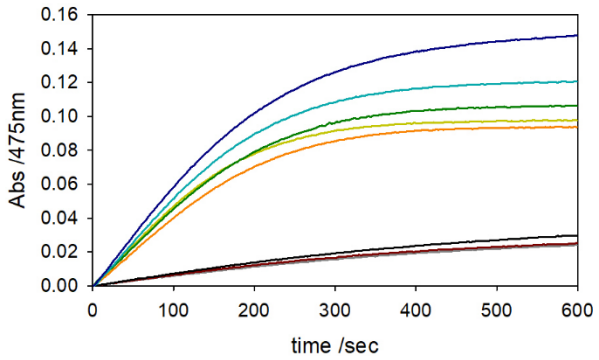

Initial rates (Abs/sec)	
Autoxidation	5.9371 E-5
Hemin	6.1131 E-5
H_2O_2	7.2639 E-5
H_2O_2-Hemin	4.1270 E-4
+ 2 μM peptide	4.6875 E-4
+ 10 μM peptide	4.6333 E-4
+ 40 μM peptide	5.3347 E-4
+ 200 μM peptide	5.9762 E-4

Figure 13. *Kinetic profiles of DA (3 mM) oxidation with time in 50 mM phosphate buffer solution at pH 7.4 and 37 °C in presence of hemin (2 μM) (brown trace) or hydrogen peroxide (2.5 mM, black), after the addition of both hemin and peroxide (orange) and upon the addition of 2 μM (light green), 10 μM (green), 40 μM (light blue) and 200 μM Aβ40 (blue). The autoxidation trace is shown as grey curve*

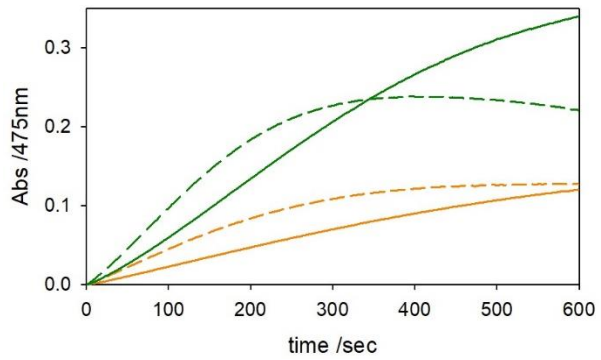

Initial rates (Abs/sec)		
Dopamine		
	25 °C	**37°C**
10 μM peptide	2.3423 E-4	4.6292 E-4
200 μM peptide	6.3030 E-4	1.0118 E-3

Figure 14. *Kinetic profiles of DA (3 mM) oxidation with time in 50 mM phosphate buffer solution at pH 7.4 in the presence of hemin (2 μM), hydrogen peroxide (2.5 mM) and upon the addition of Aβ16 10 μM (orange solid and dashed, at 25°C and 37°C, respectively) and 200 μM (green solid and dashed, at 25°C or 37°C, respectively).*

The effect of *medium* pH is more difficult to explain because the autoxidation of dopamine is partially quenched by the presence of acidic proton in solution. The mechanism of DA autoxidation involves at first the reaction with molecular oxygen to release the quinone products and superoxide anion, which is quickly subjected to decomposition to ROS. The quinone is able to give a Michael addition, therefore a cyclization, to aminochrome and this step is defined as the rate-determining reaction of the full process. Further reactions allow the polymerization into oligomers and then in melaninic structures. The cyclization is favored at pH ≥ 7.0, while at acidic values the quinone is accumulated and the rate of aminochrome formation is massively decreased (Figures 15, 16 and 17).[8]

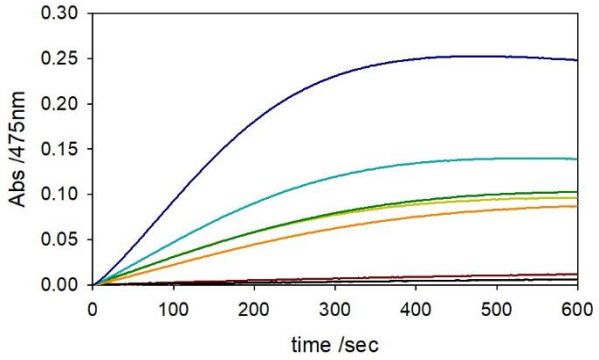

Initial rates (Abs/sec)	
Autoxidation	1.3251 E-5
Hemin	2.6912 E-5
H_2O_2	1.2241 E-4
H_2O_2-Hemin	2.3442 E-4
+ 2 μM peptide	3.1504 E-4
+ 10 μM peptide	3.0449 E-4
+ 40 μM peptide	4.8941 E-4
+ 200 μM peptide	9.9889 E-4

Figure 15. *Kinetic profiles of DA (3 mM) oxidation with time in 50 mM phosphate buffer solution at pH 6.3 and 37 °C in presence of hemin (2 μM) (brown trace) or hydrogen peroxide (2.5 mM, black), after the addition of both hemin and peroxide (orange) and upon the addition of 2 μM (light green), 10 μM (green), 40 μM (light blue) and 200 μM $Aβ_{16}$ (blue). The autoxidation trace is shown as grey curve.*

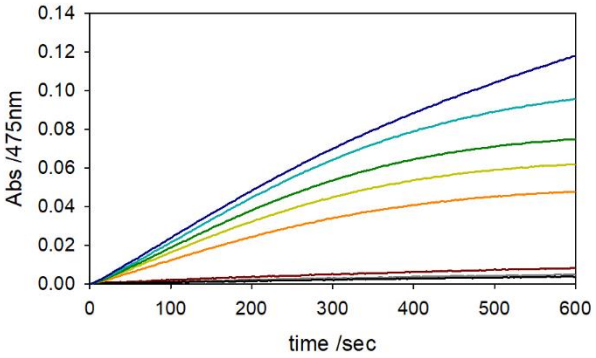

Initial rates (Abs/sec)	
Autoxidation	9.3108 E-6
Hemin	6.2843 E-6
H_2O_2	1.8249 E-5
H_2O_2-Hemin	1.2557 E-4
+ 2 μM peptide	1.6737 E-4
+ 10 μM peptide	1.9878 E-4
+ 40 μM peptide	2.2186 E-4
+ 200 μM peptide	2.4848 E-4

Figure 16. *Kinetic profiles of DA (3 mM) oxidation with time in 50 mM phosphate buffer solution at pH 6.3 and 37 °C in presence of hemin (2 μM) (brown trace) or hydrogen peroxide (2.5 mM, black), after the addition of both hemin and peroxide (orange) and upon the addition of 2 μM (light green), 10 μM (green), 40 μM (light blue) and 200 μM Aβ40 (blue). The autoxidation trace is shown as grey curve.*

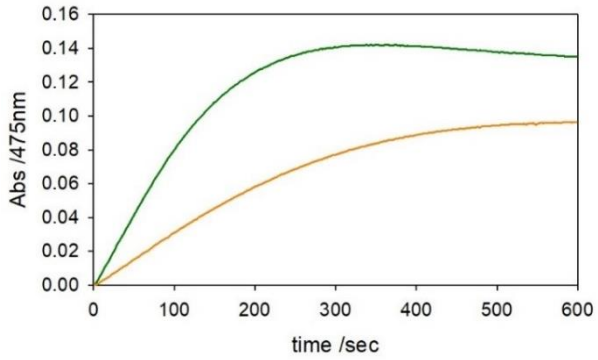

		Initial rates (Abs/sec): Hemin-H_2O_2-peptide (2 μM)
Dopamine	**pH 7.4**	8.4634 E-4
	pH 6.3	3.1504 E-4

Figure 17. *Kinetic profiles of DA (3 mM) oxidation with time in 50 mM phosphate buffer solution at two pH value, 7.4 (green trace) and 6.3 (orange) at 37 °C in presence of hemin (2 μM), hydrogen peroxide (2.5 mM) and 2 μM $A\beta_{16}$.*

The catalysis observed when amyloid-beta peptide is coordinated to heme iron can be explained through multiple factors: the axial coordination of imidazole of histidine residue can activate the iron(III) center of the *resting state* and it could facilitate the heterolytic cleavage of O-O bond and the further release of a water molecule. Moreover, the amino acid side chains and their rearrangement around the catalytic core could promote the interaction with substrate.

Oxidation of Dopamine in the presence of Hemin-Gly-His adduct

To assay the nature of the increase in the reaction rates observed when the peptide is added to the solution containing heme and hydrogen peroxide, the following experimental data were collected maintaining the same conditions of the previous studies but changing the catalyst, from ferric heme to hemin-glycyl-L-histidine methyl ester (hemin-GH).[9a]

Mimicking the active-site structure of heme proteins, it was synthesized a porphyrin complex showing a dipeptide glycine-histidine connected to one of the propionate side chains of the protoporphyrin, which allows the intramolecular coordination between the iron(III) and the imidazole group; the complex views the metal core in five-coordinated form, hence it contains a high-spin iron that enhances the catalytic activity toward the external substrate (Figure 18).

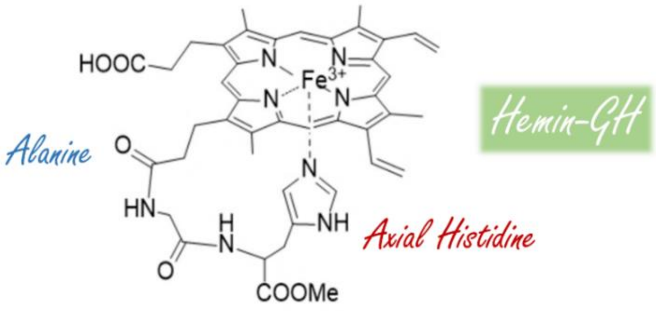

Figure 18. *Structure of Hemin-GH showing the distortion of the synthetic chain and the coordination of histidine to the iron core.*

The reaction performed in the presence of this synthetic adduct occurs with higher oxidation rate showing an order of magnitude higher than the hemin alone, while the axial coordination of peptide does not significantly alter the trend of substrate oxidation. A slight decrease in the initial rate was observed in correlation with the equivalents of β-amyloid added into the solution, where the spatial organization of the peptide around the coordination sphere of the metal enhances the steric hindrance, decreasing the access to the metal. Anyway, these data also suggest that the increased catalysis promoted by the peptide coordinated with ferric hemin is due to the chelation of iron in a distorted axial position, leading to the activation of the catalyst (Figures 19, 20 and 21).

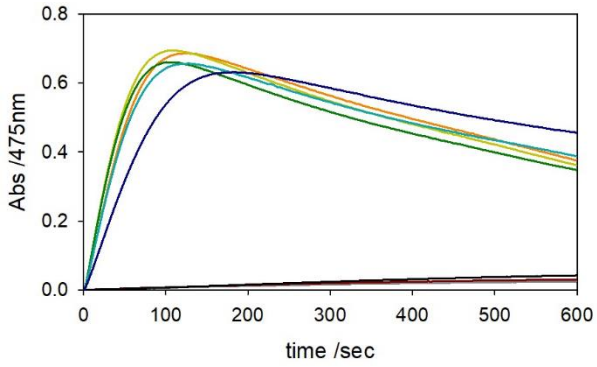

Initial rates (Abs/sec)	
Autoxidation	5.9371 E-5
HGH	6.9220 E-5
H_2O_2	7.2639 E-5
H_2O_2-HGH	1.0359 E-2
+ 2 μM peptide	1.1820 E-2
+ 10 μM peptide	1.1878 E-2
+ 40 μM peptide	1.0204 E-2
+ 200 μM peptide	6.6184 E-3

Figure 19. *Kinetic profiles of DA (3 mM) oxidation with time in 50 mM phosphate buffer solution at pH 6.3 and 37 °C in presence of hemin-GlyHis (2 μM) (brown trace) or hydrogen peroxide (2.5 mM, black), after the addition of both hemin and peroxide (orange) and upon the addition of 2 μM (light green), 10 μM (green), 40 μM (light blue) and 200 μM $Aβ_{16}$ (blue). The autoxidation trace is shown as grey curve.*

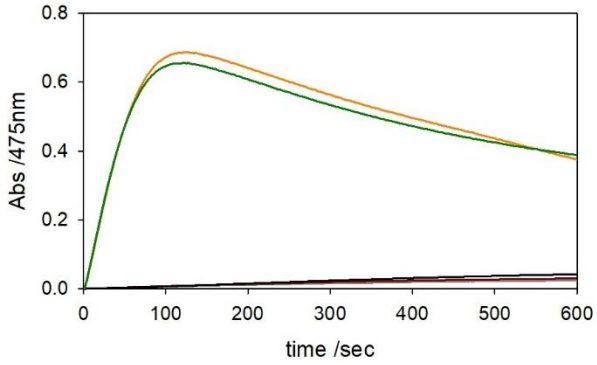

Initial rates (Abs/sec)	
Autoxidation	5.9371 E-5
HGH	6.9220 E-5
H_2O_2	7.2639 E-5
H_2O_2-HGH	1.0359 E-2
+ 10 μM peptide	1.0637 E-2

Figure 20. *Kinetic profiles of DA (3 mM) oxidation with time in 50 mM phosphate buffer solution at pH 6.3 and 37 °C in presence of hemin-GlyHis (2 μM) (brown trace) or hydrogen peroxide (2.5 mM, black), after the addition of both hemin and peroxide (orange) and upon the addition of 10 μM $Aβ_{40}$ (green). The autoxidation trace is shown as grey curve.*

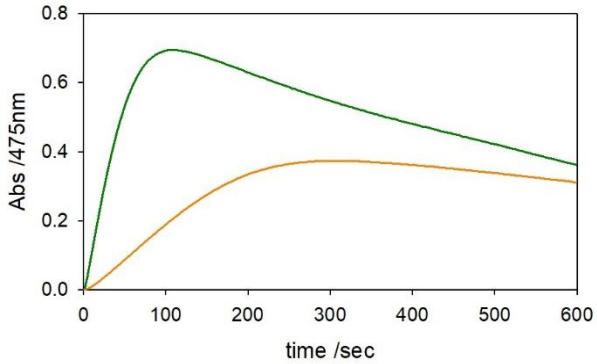

		Initial rates (Abs/sec): HGH-H_2O_2-peptide (2 μM)
Dopamine	pH 7.4	1.1820 E-2
	pH 6.3	2.0456 E-3

Figure 21. *Kinetic profile of DA (3 mM) oxidation with time in 50 mM phosphate buffer solution at pH 7.4 (green trace) and 6.3 (orange trace) and 37 °C. The concentration of catalysts was kept at 2 μM hemin-GlyHis, 2.5 mM hydrogen peroxide and 2 μM $Aβ_{16}$.*

The chart shown in Figure 22 explains the reactivity previously described through a reaction mechanism similar the peroxidase cycle. The enzymatic reaction mechanism for classical peroxidation involves three consecutive enzymatic redox stages and results in the consume of one equivalent of hydrogen peroxide (the most common hydrogen donors, although the enzyme is also able to accept other molecules, as polyphenols) and the oxidation of two equivalents of reducing substrate (AH). The two main steps of this mechanism can be assumed as:

i) $AH_2 + H_2O_2 \rightarrow A + 2H_2O$ and ii) $2AH + H_2O_2 \rightarrow AA + 2H_2O$.

The catalytic behavior of hemin-Aβ complexes is probably linked to the presence of an initial pre-equilibrium between free hemin, hemin coordinated to one peptide with high-spin iron center and ferric heme bound to two peptides that occupy both the axial positions. The hemin is converted in the oxo-form via reaction with hydrogen peroxide, following the pathway previously presented and indicated as pathway A. The mono- and bis-adduct are subjected to the same reaction through the pathways B and C. The bis-complex is easily converted in the mono- species, being in equilibrium with the five-coordinated form and this balance allows to prevent the full quenching of the peroxidase activity of the system. The reversible bond of the second histidine can be displaced by one molecule of H_2O_2 when it is added at saturating concentration in the solution. The coordination of beta-amyloid at 1:1 ratio occurs via only one histidine bound to the iron center in axial position that notably increases the electron density of metal and activates the catalyst toward the substrate.

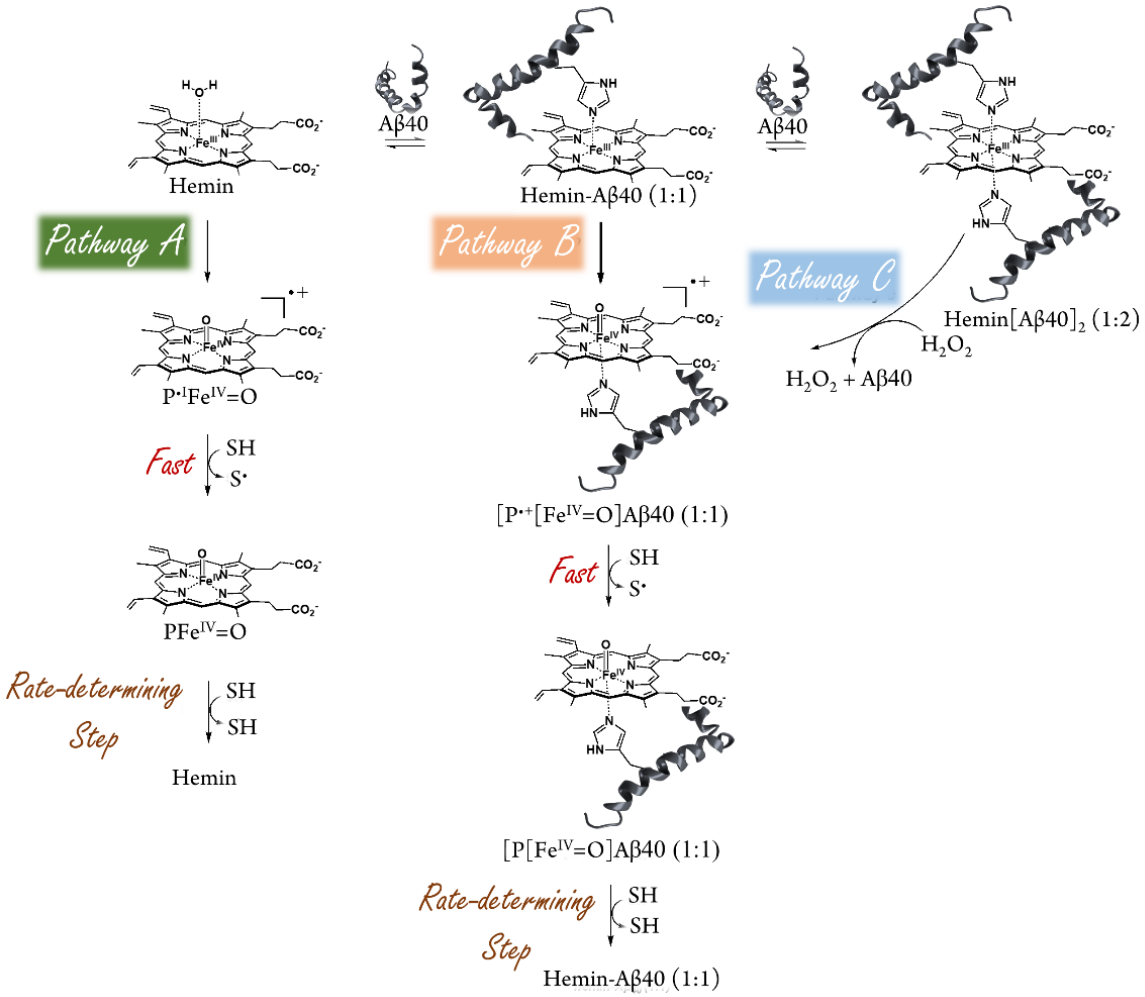

Figure 22. *Reaction mechanism of the catalytic activity of ferric heme-Aβ$_{40}$, probably analogous to the peroxidase pathway assumed by the hemin-Aβ$_{16}$ adducts. SH indicates the substrate molecule, while the three pathway A, B and C show the three mechanisms that lead to the generation of hemin alone, hemin bound to one peptide or chelated in both axial positions by the equivalent of beta-amyloid peptide.*

At the end, the comparative study in the presence of full-length amyloid-β 1-40 and of the smaller fragment 1-16, consisting in the *N*-terminal portion of the peptide and lacking of the hydrophobic and aggregating tail, was performed. Although the binding affinity of heme is higher for the full-length peptide, the catalytic behavior of the hemin-Aβ$_{16}$ complex seems to allow more efficient activity respect with heme coordinated to Aβ$_{40}$ peptide. The *C*-terminal portion of full-length peptide is known to be partially structured and shows several hydrophobic amino acids that are involved

in the peptide stacking and aggregation. The lack of plasticity of this region leads to significant steric hindrance exercised by the peptide around the catalytic center that does no allow the interaction with substrate and the electron transfer reaction. Moreover, high concentration of peptide required to significantly increase the peroxidase activity of hemin are justified through the competition between the activation of the catalyst via hydrogen peroxide binding and the interaction with substrate molecules, which is largely in excess.

Amyloid-β(1-16) modification pattern detected by HPLC-MS

The peroxidase activity of these complexes enhances the production of reactive species and the reaction mechanism has shown the involvement of several radical species that allows the cycling of ferric heme. The high reactivity of these species is directly linked to the higher damage observed toward some biological structures, such as nucleotides and proteins. The competitive modification of the peptide itself was assayed by HPLC-MS spectrometry, incubating amyloid-β fragment (1-16) in the presence of dopamine (1 mM), hydrogen peroxide (1 mM) and hemin (6 μM) at 37 °C for 30 and 120 min. Blank experiment (data not shown) performed in phosphate solution with the addition of dopamine and hydrogen peroxide but lacking of the metal catalyst shows a simple chromatogram characterized by only three main modifications, corresponding to the unmodified peptide (93%), the insertion of one oxygen atom on histidine 13 or 14 (5%) and the modest generation of dimeric species (2%).

Table 1. *Modification with time of $A\beta_{16}$ peptide detected by HPLC-MS upon reaction of hemin (6 μM), $A\beta_{16}$ (30 μM), hydrogen peroxide (1 mM) and DA (3 mM) in phosphate buffer solution (50 mM) pH 7.4 at 37 °C.*

Time (min) (elution)	**$A\beta_{16}$** 20 min	**+16***	**+32**	**+48**	**+147**	**+96**	**+80**	**Dimer**	**Fragments**
30	**79%**	1%	1%	1%	-	6%	4%	2%	6%
120	**79%**	2%	1%	2%	-	8%	4%	2%	2%

Table 2. *Modification over incubation time of $A\beta_{16}$ peptide detected by HPLC-MS upon reaction of hemin (6 μM), $A\beta_{16}$ (30 μM) and hydrogen peroxide (1 mM) in phosphate buffer (50 mM) pH 7.4 at 37 °C.*

Time (min) (elution)	**Aβ16** 20 min	**+16***	**+32**	**+48**	**+96**	**+80**	**Dimer**	**Fragments**
30	**85%**	3%	-	-	1%	9%	2%	-
120	**84%**	3%	2%	1%	3%	3%	3%	1%

**O-atom insertion probably on Y or Histidine 13*

The experimental data show that the peptide has low tendency to undergo modification at short reaction time and the absence of catecholamine seems to slightly affect the pattern of modification, increasing the stability of peptide for longer time. The main modifications detected in all samples are the following: the single insertion of one *O*-atom to a histidine residue or a hydroxylation of the tyrosine side chain (+16), the double oxidation characterized by a mass increase of + 32 units and triple oxidation (+48).

Moreover, fragmentation pathway was analyzed but the cleavage of peptide is not so usual in these reaction conditions; the unspecific fragmentation of the peptides is generally linked to a highly oxidative environment but these conditions are relatively mild to induce massive modifications, as shown by the percentages of oxidation. Therefore, it requires longer reaction times to detect not negligible peaks corresponding to recurrent fragments. Two unknown mass increment (+80, +96) have to be still explored, but control experiment excluded the possible phosphorylation of the peptide due to the presence of phosphate groups in the buffer solution. On the other hand, these increments are

recurring upon manual solid-phase synthesis of peptide sequences, where the addition of TFA is usually associated to the generation of specific adducts detectable via direct injection in mass spectrometer. At the end, the dimerization tendency of the peptide was also investigated. When incubated in the presence of hemin, amyloid-β shows the propensity to form dimers through covalent bond between the two peptide chains and mediated by dityrosine generation. Indeed, the dityrosine cross-linking in amyloid species is usually observed via a covalent ortho-ortho coupling of two tyrosine promoted by the oxidative environment and by high traces of metals.

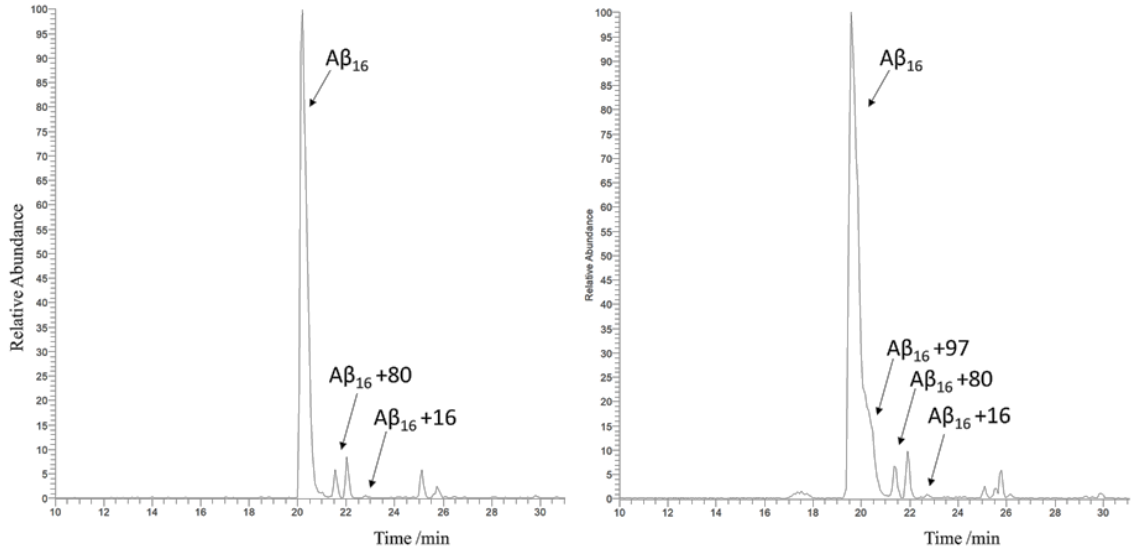

Figure 23. *LC-MS chromatograms showing $A\beta_{16}$ modification percentage upon 30 min (left panel) / 2 h (right panel) of incubation at 37°C in the presence of DA (3 mM), H_2O_2 (1 mM) and hemin (6 μM).*

In the biological context, these modifications can influence the structure and flexibility of the peptide backbone, promoting the aggregation process and making it more resistant to proteolytic cleavage through the stabilization of the fibrils. In particular, the fate of Tyr residue in oxidative *medium* is the generation of several modification products, as dityrosine,[9b] via two possible biochemical mechanisms, as the formation of tyrosyl radical catalyzed by a redox active metal or the cross-linking of tyrosines promoted by peroxidase-like activity.

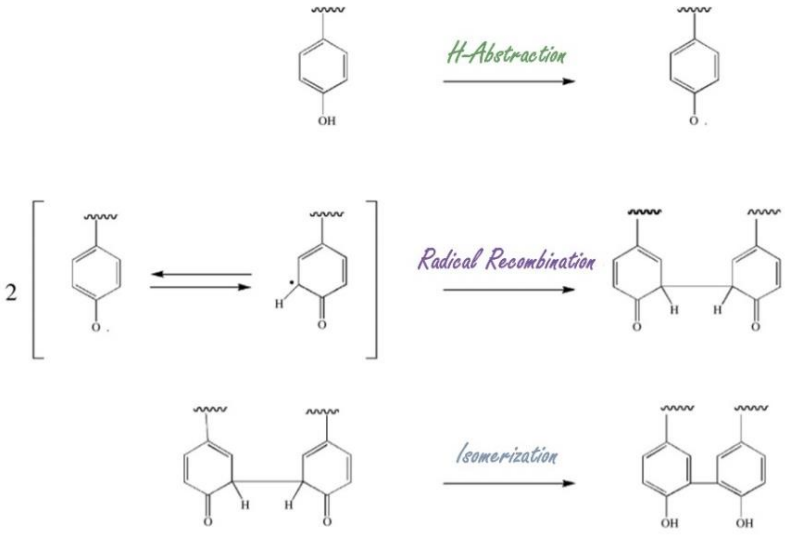

Figure 24. *Oxidative pathway for dityrosine generation.*

The pathway for the intermolecular Tyr cross-links involves the generation of the tyrosyl radical, its isomerization, a diradical reaction and an enolisation, as shown in Figure 24. The reaction thermodynamically requires strong oxidants, such as hydroxyl radical, porphyrin cation radical, peroxynitrite, nitryl cation, nitrogen dioxide etc. and the previous table confirms the production of dimers in these reaction conditions.[9c]

Conclusions

The abnormal regulation of metal ions, such as copper, iron or zinc, in neuronal cells is commonly accepted as causative event of several neurological disorders, enhancing the production of reactive oxygen and nitrogen species and the uncontrolled damage toward several biological structures. Indeed, the presence of elevated levels of metals, as zinc(II) (around 1055 μM), copper(II) (393 μM) and iron(III) (980 μM) has been detected in post-mortem AD brains.[10a,10b] Besides their redox reactivity, the interaction between neuronal proteins and metal ions can alter the protein solubility and their aggregation mechanism, influencing structural folding, promoting the oxidative modification of peptide scaffolds and ending with the deposition of amyloid plaques and insoluble tangles.

Heme group is bound by the *N*-terminal amyloid domain encompassing the region 1-16 via histidine residue, as His-13 or His-14 and the resulting adduct is characterized by a maximum absorption of Soret band at 392 nm and Q-band at 606 nm, when in the presence of 1:1 complex.[10c] The second axial position can be occupied by a water molecule, in which the O-O bond heterolysis can be assisted by the distal arginine-5. This system mimics the coordination environment of peroxidases, a class of heme enzymes able to oxidize the organic substrates in the presence of hydrogen peroxide. The previous catalytic data confirm that hemin-Aβ complex is characterized by a dynamin equilibrium that comprises a low-spin species, corresponding to a five-coordinated iron, and a high-spin form with a six-coordinated metal center (Figure 25). Moreover, peroxidase-like activity of heme bound to amyloid-β peptide can be assayed, verifying the involvement of these complexes in the oxidative damage of neurological structures and in the promotion of neurodegeneration.

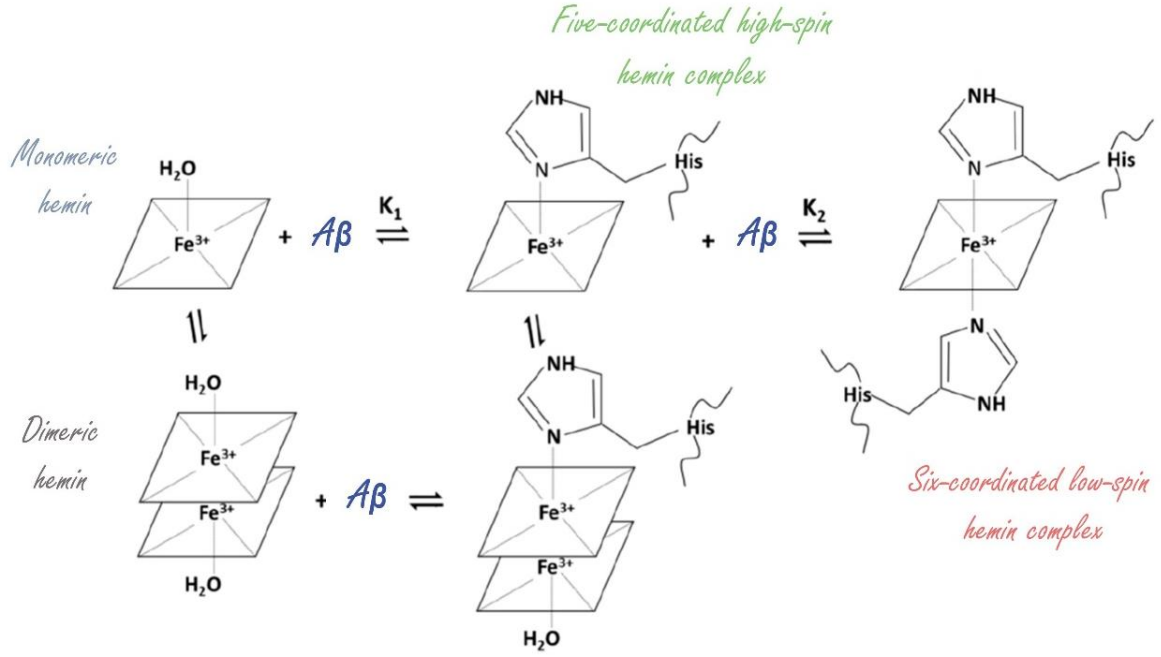

Figure 25. *Chart of the possible forms of hemin when in co-presence of amyloid peptides, in which an initial equilibrium between the monomeric and dimeric forms can occur, while, upon the addition of peptide, the mono-His and bis-His adducts can be generated.*

Herein, elucidations about the reaction mechanism of the peroxidase activity of these complexes were suggested and the catalytic capability of hemin alone and bound to β-amyloid peptides was compared in term of oxidation of two different substrates, ABTS and the neurotransmitter dopamine. The peroxidase-like activity of the adducts was assayed varying the temperature, the ionic strength and the pH *medium*, also working in acidic conditions to mimic the

biological conditions observed in neuronal environments affected by high levels of oxidative stress damages and neurodegenerative processes.[10d,10e]

The kinetic data suggest a strong promotion of the peroxidase activity of hemin once bound to Aβ, although the reactivity evidenced in the presence of [hemin-$A\beta_{16}$] seems to be higher than one promoted by the full-length peptide, probably due to the major aggregation tendency of $A\beta_{40}$ that shows a hydrophobic tail responsible of the intermolecular stacking. The peroxidase-like reactivity follows an oxidative mechanism previously described[11]:

$$\text{(i)} \qquad PFe^{III} + H_2O_2 \rightarrow {}^{\bullet+}PFe^{IV} = O + H_2O$$

$$\text{(ii)} \qquad {}^{\bullet+}PFe^{IV} = O + SH \rightleftarrows [{}^{\bullet+}PFe^{IV} = O/SH] \rightarrow PFe^{IV} = O + S^{\bullet} + H^{+}$$

$$\text{(iii)} \qquad PFe^{IV} = O + SH \rightleftarrows [PFe^{IV} = O/SH] + H^{+} \rightarrow PFe^{III} + S^{\bullet} + H_2O$$

in which he first step views the reaction between iron porphyrin in the resting state and hydrogen peroxide to give the first reactive intermediate called Compound I and corresponding to the porphyrin π cation radical species. The second reaction leads to the generation of the second intermediate, known as Compound II or ferryl heme via the reaction with substrate. In this mechanism, the second sphere residues as Arg-5 and Tyr-10 play an important role as promoter of the peroxidase activity and as electron donor in the production of ROS, respectively.

The results suggest that the binding between Aβ peptide and the metal induces a drastic increase of the initial rate of the peroxidase-like reaction, favoring the axial coordination of an imidazole group to the ferric ion and the activation of the redox reactivity of the complex. Therefore, histidine and arginine located in the distal positions polarize the O-O bond of peroxide ligand, promoting its breaking; the axial coordination of imidazole also influences the reaction rate allowing a minor structural rearrangement of the adduct that is required for the efficient electron transfer between heme intermediate and external substrate.[11] At the end, further investigation of the oxidative modification of peptide backbones was performed, in which each peptide is subjected to the same reaction environment for different incubation times and the results have mainly suggested a modest propensity to undergo oxidation from His residues and dimerization via intermolecular Tyr cross-linking. A higher stability of peptide was evidenced if compared to the modification shown at the same reaction time but with copper ions (see Chapter 1); on the other hand, this modest reactive *medium* is offset by not negligible generation of intermolecular cross-linking via Tyr side chains that could affect the aggregation rate of β-amyloid protein, enhancing the deposition of insoluble plaques and damaging neuronal signaling.

In conclusion, detection of these complexes as well as their related peroxidase-like reactivity should be marked as future parameters useful for the clinical investigation of AD disorder, where studies *in vitro* could provide simplify and ancestral data for the further analysis *in vivo* and for the design of new antibodies and activity assays.

General procedure and Peptide synthesis

Hemin stock solution was prepared by dissolving 2-3 mg of ferric heme in 0.1 M NaOH (1 mL) and sonicating for almost 1 h. The solution was centrifuged to remove the precipitate and the supernatant was quantified at 386 nm. Amyloid-β 1-40 was previously dissolved in HFIP for 3-4 hours to remove eventual aggregated species and then, the solvent was evaporated. The peptide was maintained in monomeric form for longer time solubilizing the peptide in water with 0.02% ammonia. Amyloid-β 1-16 was synthesized as previously described, while $A\beta_{40}$ was sent us by our colleagues (Department of Chemistry, University of Texas at Austin, and Department of Biotechnologies, Chemistry and Pharmacy, University of Siena).

ABTS and Dopamine oxidation

The catalytic oxidation of ABTS and DA by hemin was monitored by UV/Vis spectroscopy through the absorption band at 660 nm or at 475 nm, respectively. The samples were prepared with the addition of the substrate (3 mM), H_2O_2 (2.5 mM) and amyloid-β fragments 1-16 and 1-40 (0-200 μM) to a solution of hemin (3 μM) in 50 mM phosphate solution. The pH was varied at 7.4 and 6.3 and the mixtures were incubated at 25 °C and 37 °C. Each sample was equilibrated at the selected temperature for 5 minutes before the addition of the substrate and peptide; hydrogen peroxide was added to the reaction solution as the last reagent.

Amyloid-β 16 modification detected by LC-MS

LC-MS analysis was performed on samples incubated in the presence of hemin (6 μM), H_2O_2 (1 mM), Aβ (30 μM), and DA (3 mM) in 50 mM phosphate buffer solution at pH 7.4. The modification pattern was analyzed upon 30 and 120 min reaction times. ESI-MS values for the dimeric amyloid species are the following: m/z $977.5^{(4+)}$, $782^{(5+)}$, $652^{(6+)}$, $559^{(7+)}$. HPLC-MS data were obtained by using a LCQ ADV MAX ion-trap mass spectrometer. The elution of $A\beta_{16}$ was carried out by using 0.1% HCOOH in distilled water (solvent A) and 0.1% HCOOH in acetonitrile (solvent B), with a flow rate of 0.2 mL/min; elution started with 98% solvent A for 5 min followed by a linear gradient from 98 to 55% A in 65 min. In the presence of $A\beta_{40}$, elution conditions were optimized with a linear gradient from 98 to 0% A in 65 min.

References

1. (a) J. Liu, S. Chakraborty, P. Hosseinzadeh, Y. Yu, S. Tian, I. Petrik, A. Bhagi and Yi Lu, Metalloproteins Containing Cytochrome, Iron–Sulfur, or Copper Redox Centers, **Chem. Rev.**, 114, 8, 4366–4469, 2014; (b) T.L. Poulos, Heme Enzyme Structure and Function, **Chem. Rev.**, 114, 3919–3962, 2014; (c) H. Atamna and W.H. Frey, A role for heme in Alzheimer's disease: Heme binds amyloid β and has altered metabolism, **Proc Natl Acad Sci U S A.**, 101, 30, 11153–11158, 2004; (c) J. Flemmig, M. Zámocký and A. Alia, Amyloid β and free heme: bloody new insights into the pathogenesis of Alzheimer's disease, **Neural Regen Res.**, 13, 7, 1170–1174, 2018; (d) H. Atamna and W.H. Frey, A role for heme in Alzheimer's disease: heme binds amyloid beta and has altered metabolism. **Proceedings of the National Academy of Sciences of the United States of America**., *101, 30, 11153-11158, 2004.*
2. (a) D. Pramanik, C. Ghosh, S. Mukherjee and S. Ghosh, Interaction of amyloid beta peptides with redox active heme cofactor: Relevance to Alzheimer's disease, **Coordination Chemistry Reviews,** 257, 81– 92, 2013; (b) H.M. Schipper, S. Cissé and E.G. Stopa, Expression of heme oxygenase-1 in the senescent and Alzheimer-diseased brain, **Ann Neurol.,** 37, 6, 758-68, 1995; (c) M.A. Smith, R.K. Kutty, P.L. Richey, S.D. Yan, D. Stern, G.J. Chader, B. Wiggert, R.B Petersen and G. Perry, Heme oxygenase-1 is associated with the neurofibrillary pathology of Alzheimer's disease, **Am J Pathol.,** 145, 1, 42-47, 1994; (d) T. Kimpara, A. Takeda, T. Yamaguchi, H. Arai, N. Okita, S. Takase, H. Sasaki and Y. Itoyama, Increased bilirubins and their derivatives in cerebrospinal fluid in Alzheimer's disease, **Neurobiol Aging**., 21, 4, 551-4, 2000; (e) C. Mancuso, G. Pani and V. Calabrese, Bilirubin: An endogenous scavenger of nitric oxide and reactive nitrogen species, **Redox report: communications in free radical research,** 11, 207-213, 2006.
3. (a) R.S. Sohal, Aging, cytochrome oxidase activity, and hydrogen peroxide release by mitochondria, **Free Radic Biol** Med, 14, 6, 583-8, 1993; (b) K.R. Wagner, F.R. Sharp, T.D. Ardizzone, A. Lu and J.F. Clark, Heme and iron metabolism: role in cerebral hemorrhage, **J Cereb Blood Flow Metab**, 23, 6, 629-52, 2003; (c) G. Thiabaud, S. Pizzocaro, R. Garcia-Serres, J.-M. Latour, E. Monzani and L. Casella, Heme Binding Induces Dimerization and Nitration of Truncated β-Amyloid Peptide Aβ16 Under Oxidative Stress, **Angew. Chem. Int. Ed.,** 52, 8041 –8044, 2013.
4. S. Azimi and A. Rauk, Fe(III)–Heme Complexes with the Amyloid Beta Peptide of Alzheimer's Disease: QM/MM Investigations of Binding and Redox Properties of Heme Bound to the His Residues of Aβ(1–42), **J. Chem. Theory Comput.**, 9, 9, 4233–4242, 2013.
5. (a) R. Khodarahmi and M.R. Ashrafi-Kooshk, 2Is there correlation between Aβ-heme peroxidase activity and the peptide aggregation state? A literature review combined with hypothesis., **Int. J. Biol. Macromol.,** 100, 18-36, 2017; (b) J. Everse, Heme Proteins, **Encyclopedia of Biological Chemistry,** 532-538, 2013; (c) V. Pfanzagl, K. Nys, M. Bellei, H. Michlits, G. Mlynek, G. Battistuzzi, K. Djinovic-Carugo, S. Van Doorslaer, P.G. Furtmüller, S. Hofbauer and C. Obinger, Roles of distal aspartate and arginine of B-class dye-decolorizing peroxidase in heterolytic hydrogen peroxide cleavage, **J Biol Chem.,** 293, 38, 14823–14838, 2018.
6. (a) I.R. Ilyasov, V.L. Beloborodov, I.A. Selivanova and R.P. Terekhov, ABTS/PP Decolorization Assay of Antioxidant Capacity Reaction Pathways, **Int. J. Mol. Sci.**, *21, 1131, 2020;* (b) A.N. Hiner, E.L. Raven, R.N. Thorneley, F. García-Cánovas and J.N. Rodríguez-López, Mechanisms of compound I formation in heme peroxidases, **Journal of Inorganic Biochemistry,** 91, 1, 27-34, 2002.
7. E.N. Kadnikova and N.M. Kostić, Oxidation of ABTS by hydrogen peroxide catalyzed by horseradish peroxidase encapsulated into sol–gel glass.: Effects of glass matrix on reactivity, **Journal of Molecular Catalysis B: Enzymatic**, 18, 1–3, 39-48, 2002.
8. M. Salomäki, L. Marttila, H. Kivelä, T. Ouvinen and J. Lukkari, Effects of pH and Oxidants on the First Steps of Polydopamine Formation: A Thermodynamic Approach, **J Phys Chem B.,** 122(24), 6314–6327, 2018.
9. (a) L. Casella, E. Monzani, P. Fantucci, M. Gullotti, L. De Gioia, A. Strini and F. Chillemi, Axial Imidazole Distortion Effects on the Catalytic and Binding Properties of Chelated Deuterohemin Complexes, **Inorg. Chem.,** 35, 439, 1996; (b) K. Hensley, M.L. Maidt, Z. Yu, H. Sang, W.R. Markesbery and R.A. Floyd, Electrochemical analysis of protein nitrotyrosine and dityrosine in the Alzheimer brain indicates region-specific accumulation, **J Neurosci,** 18, 8126–8132, 1998; (c) C. Giulivi1, N.J. Traaseth and K.J.A. Davies, Tyrosine oxidation products: analysis and biological relevance, Amino Acids, 25, 227–232, 2003.
10. (a) W.-T. Chen, Y.-H. Liao, H.-M. Yu, I.H. Cheng and Y.-R. Chen, Distinct Effects of Zn2+, Cu2+, Fe3+, and Al3+ on Amyloid-Stability, Oligomerization, and Aggregation. AMYLOID-DESTABILIZATION PROMOTES ANNULAR PROTOFIBRIL FORMATION, **J. Biol. Chem.,** 286, 11, 9646 –9656, 2011; (b) M.A. Lovell, A Potential Role for Alterations of Zinc and Zinc Transport Proteins in the Progression of Alzheimer's Disease, **J Alzheimers Dis**., 16, 3, 471–483, 2009; (c) M. Roy, I. Pal, A.K. Nath and S.G. Dey, Peroxidase activity of heme bound amyloidβ peptides associated with Alzheimer's disease, **Chem. Commun.**, 56, 4505, 2020; (d) M. Chesler, Regulation and modulation of pH in the brain., **Physiol. Rev.,** 83(4), 1183-1221, 2003; (e) K.H. Steen, A.E. Steen and P.W. Reeh, A dominant role of acid pH in inflammatory excitation and sensitization of nociceptors in rat skin, in vitro, **Neurosci.,** 15, 3982, 1995.
11. S. Dell'Acqua, E. Massardi, E. Monzani, G. Di Natale, E. Rizzarelli and L. Casella, Interaction between Hemin and Prion Peptides: Binding, Oxidative Reactivity and Aggregation, **Int. J. Mol. Sci.,** 21, 7553, 2020.